UCL SCHOOL OF PHARMACY

Hertie-Institut für klinische Hirnforschung

A direct interaction between the Parkinson's disease protein leucine-rich repeat kinase 2 and specific β-tubulin isoforms regulates tubulin acetylation

Victoria Spain

Doctoral thesis

Supervised by:

Kirsten Harvey University College London
Saskia Biskup University of Tübingen

Declaration

I, Victoria Spain, confirm that the work presented in this thesis is my own, describing research completed between October 2010 and August 2014 under the supervision of Professor Kirsten Harvey and Dr. Saskia Biskup. Where information has been derived from other sources or in collaboration, I confirm that this has been indicated in the thesis. All text was written by me and those parts which have appeared in publication have been indicated by citation.

Victoria Spain

Date

ii Abstract

Mutations in *LRRK2* are a common cause of Parkinson's disease (PD). *LRRK2* encodes leucine-rich repeat kinase 2 (LRRK2), a ROCO protein. It has an enzymatic core consisting of a Ras of complex proteins (Roc) GTPase domain and kinase domain, surrounded by protein-protein interaction regions. Pathogenic LRRK2 mutations modify activity in these enzymatic domains, but how this leads to neurodegeneration is still to be elucidated.

One of the few confirmed LRRK2 interactors is tubulin, the main constituent of microtubules (MTs) and part of the cytoskeletal network. Disease-causing mutations in LRRK2 alter this network, reducing neurite outgrowth and leading to accumulation of hyperphosphorylated MT-associated protein (MAP) tau. Meanwhile changes in post-translational modifications of tubulin and MAPs alter the dynamic instability of MTs, leading to aberrant axonal transport, synaptic dysfunction and axonal degeneration.

I investigated the LRRK2-tubulin interaction. Using yeast two-hybrid I demonstrated that the interaction is conferred by the LRRK2 Roc domain and the C-terminus of the β-tubulin isoforms TUBB, TUBB4 and TUBB6. The interaction requires Lys362 and Ala364 and is blocked in isoforms expressing a serine at these positions. This site is on the luminal face of MT protofibrils, close to the paclitaxel binding site and α-tubulin Lys40 acetylation site, both of which are involved in MT stability. This location is poorly accessible within mature, stabilised MTs but exposed in dynamic MT populations. Consistent with this finding, endogenous LRRK2 located to dynamic growth cone MTs in SH-SY5Y cells. Overexpression and knock-out studies in HEK cells and mouse embryonic fibroblasts showed that LRRK2 is associated with reduced α-tubulin acetylation.

These results demonstrate the specificity of the LRRK2-tubulin interaction, suggesting LRRK2 distribution at the cytoskeleton is determined by the tubulin composition and may vary between cell types. Changes in MT acetylation in the presence of disease-causing LRRK2 mutations could contribute to pathogenic mechanisms, with altered MT stability implicated in PD neurodegeneration.

As mutations affecting the β-tubulin C-terminal residues could disrupt the LRRK2 interaction without compromising MT integration, a cohort of late-onset familial PD cases was also screened for mutations within the cytoskeleton.

iii Acknowledgements

First to my supervisors: Kirsten Harvey and Saskia Biskup for your help, support and patience as I completed this PhD, for giving me the opportunity, encouraging me when it was all going wrong and supporting me throughout the last four years, I thank you.

Für meine Deutschen Freunde und Kollegen: Danke zum Steffi Kleinmichael, Kathrin Hauser, Claudia Schulte, Max Schubach und Anne Winter, die hat alles mit Edelmut und Geduld für mein Deutsche erklärte. Professor Thomas Gasser und Daniela Berg hat mich gehört und beriet uber die Genetische Suche. Auch Sarah Lechner, Chris Wilhelm, Kathrin Peters. Niemand sind mehr verruckt, immer mit spaß und geplänkel! Und, ganz klar, alle Menschen in CeGaT und die Hertie, die immer freundlich und gütig waren. Endlich Stella Avramidou, die wunderbarste Mitbewohnerin, Köchin, Wörterbuch und Smartie in Deutschland!

Back in the UK, enormous thanks go to Dan Berwick for serenely tackling a constant stream of questions, as well as Jonny Nixon-Abell for late-night yeast chats and mega experiments– team LRRK2! Keep up the good work after I leave! Obviously a big thanks goes to my other friends and workmates: Vicky James, Sarah Ramsden, Caroline Anderson, Jennifer Gill, Marian Blanca Ramirez, Veronica Leinster, Philipp Wesche, Phil Long, Kim Wager, Simone Granno, Laura Fedele, Laura Pellegrini, Alex Pepler, Sophie Leacock and Natasha Quereshi, as well as the rest of the students and post-docs of the pharmacy department. You are all brilliant and made my PhD so much easier and more fun!

Special acknowledgements also go to Rob Harvey for the extra support and advice and Bernard Law and Rosa Sancho for your excellent work which was the basis of everything I did. Thanks to the UCL School of Pharmacy and the University of Tübingen for funding the PhD, along with Guarantors of Brain for the travel grant enabling me to attend the World Parkinson's Congress in Canada.

I would like to thank all my friends and my family: Mum, Dad, Roberta and Susie and the Daniels for attempting to understand and always being supportive; especially Mum for your proofreading and motivational speeches.

Final thanks go to Dom. You patiently helped me through Excel tantrums, missed plane panics and Hula Hoop obsessions in Germany, as well as diligently reading a thesis on a topic of which you know nothing. Thank you so very much.

Table of Contents

iv List of figures

Introduction

Materials and Methods

Results 3.1

Results 3.4

v List of tables

Introduction

Materials and Methods

Results 3.1

Results 3.4

vi List of abbreviations

3-AT	3-amino-1,2,4-triazole
AAO	Age at onset
AD	Activation domain
Ala	Alanine
Ank	Ankyrin-rich repeats
ArfGAP1	ADP-ribosylation factor GTPase-activating protein 1
ArhGEF7	Rho guanine nucleotide exchange factor 7
Arm	Armadillo repeats
ATP13A2	ATPase type 13A2
BD	Binding domain
BDNF	Bone-derived neurotrophic factor
C. tepidum	*Chlorobium tepidum*
CADPS2	Calcium-dependent secretion activator 2
cDNA	Complementary DNA
Chr	Chromosome
CL	Cell lysate
Co-IP	Co-immunoprecipitation
COR	C-terminal of Roc
CPRG	Chlorophenol red-β-D-galactopyranoside
D1R (+)	Dopamine receptor 1 (pathway activated by dopamine)
D2R (-)	Dopamine receptor 2 (pathway inhibited by dopamine)
DC	Disease causing
dNTPs	2'deoxynucleotide triphosphates
ddNTPs	2'3'dideoxynucleotide triphosphatases
dH_2O	Deionised water
DMEM	Dulbecco's modified eagle medium
DMF	N,N-dimethylformide
DMT1	Divalent metal transporter 1
EB	Elution buffer
EBC	European brain council
E. coli	*Escherichia coli*
EIF4G1	Eukaryotic translation initiation factor 4 gamma, 1
EOPD	Early-onset Parkinson's disease
ERRC6	Excision repair cross-complementing group 6 protein
ERM	Ezrin-Radixin-Moesin
EVS	Exome variant server
FasL	Fas Ligand
FADD	Fas-associated death-domain
FBXO7	F box protein 7
FUCA1	Fucosidase, alpha-L- 1, tissue enzyme
FZD4	Frizzled family receptor 4
GAD	G-protein activated by nucleotide-dependant dimerisation
GAF	Global allele frequency
GAP	GTPase-activating protein
GBA	Glucocerebrosidase
GDP	Guanosine diphosphate
GEF	Guanosine exchange factor
GIGYF2	Grb10 interacting GYP protein 2
GPe	Globus pallidus externa
GPi	Globus pallidus interna

GTP	Guanosine triphosphate
GWAS	Genome-wide association studies
HBSS	Hanks balanced salt solution
HDAC6	Histone deacetylase 6
HEK293	Human embryonic kidney 293
HRP	Horseradish peroxidase
HTRA2	HtrA serine peptidase 2
HGNC	Human gene nomenclature committee
HLOD	Maximum heterogeneity logarithm of the odds
IGV	Integrated genome viewer
IL-6	Interleukin 6
IP	Immunoprecipitation
IPDGC	Internatial Parkinson's disease genomics consortium
JNK	c-jun N-terminal kinase
LB	Luria Bertrani
LD	Linkage disequilibrium
LiAc	Lithium acetate
LOPD	Late-onset Parkinson's disease
LRR	Leucine-rich repeat
LRRK1	Leucine-rich repeat protein kinase 1
LRRK2	Leucine-rich repeat protein kinase 2
MAP	Microtubule-associated protein
MAPK	Mitogen-associated protein kinase
MEC-17	α-tubulin Lys40 acetyltransferase
MEF	Mouse embryonic fibroblast
MERLIN	Multipoint engine for rapid likelihood inference
MLK	Mixed-lineage kinases
MOPS	3-(N-morpholino) propanesulphonic acid
MT	Microtubule
MTa	Mutation Taster
NFAT1	Nuclear factor of activated T-cells 1
NFkB	Nuclear factor kappa-light-chain-enhancer of activated B cells
NGS	Next generation sequencing
NPL	Non-parametric linkage
NS	Nutritional selection
NT-3	Neurotrophin-3
OMIM	Online Mendelian inheritance in man
PARK	Parkinson's disease gene locus
PBS	Phosphate buffered saline
PBST	Phosphate buffered saline containing 0.1% Tween-20
PCR	Polymerase chain reaction
PD	Parkinson's disease
PDB	Protein database
PEG	Piluethylene-glycol
PINK1	Phosphatase and tensin-homolog-induced putative kinase 1
PLA2G6	Phospholipase A2-G6
PVDF	Polyvinyldiene fluoride
Roc	Ras of complex proteins
ROS	Reactive oxygen species
SDS-PAGE	Sodium dodecyl sulphate-polyacrylamide gel electrophoresis
SEZ6L	Seizure-related 6 homolog (mouse)-like

SIFT	Sorts intolerant from tolerant
SIRT2	Sirtuin2
SN	Substantia nigra
SNc	Substania nigra pars compacta
SNr	Substantia nigra pars reticulata
SNP	Single nucleotide polymorphism
SOLiD	Sequencing by oligonucleotide detection
STK4	Serine/threonine kinase 4
STN	Subthalamic nucleus
SV2C	Synaptic vesicle glycoprotein 2C
TAE	Tris-acetate ethyenediaminetetra-acetic acid
TC	Transformation control
Tm	Primer melting temperature
TNF-α	Tumor necrosis factor alpha
TUB	Tubulin. Followed by alpha numerical indicator to indicate isoform
UAS	Upstream activation site
UCHL1	Ubiquitin carboxyl-terminal esterase L1
VPS35	Vacuolar protein sorting 35
WTCCC2	Wellcome Trust case control consortia 2
X-gal	5-bromo-4-chloro-3-indolyl-β-D-galactopyranoside
YPD	Yeast extract/peptone/dextrose

1. Introduction

1.1 Parkinson's Disease

Parkinson's disease (PD) is a progressive neurodegenerative disorder of the central nervous system, characterised by loss of movement control due to death of dopaminergic neurons. It is the second most common neurodegenerative disorder after Alzheimer's disease. According to the European Brain Council there are over 6.3 million sufferers worldwide, with 1.2 million of these in Europe (EBC PD fact sheet, 2011). Incidence is gender, ethnicity and age related. Men are 1.5 times more likely to develop the disease than women and the average age of onset is two years earlier (Wooten et al., 2004; Haaxma et al., 2006), possibly due to a protective effect of estrogen (Behl et al., 2000; Liu and Dulzen, 2007; Ragonese et al., 2006; Lyons et al., 1998; de Riik et al., 2000; Van Den Eeden et al., 2003).

PD is the most common of the Parkinsonisms. The others are known as 'atypical PD' or 'Parkinson's plus' diseases. They show similar symptoms and clinical features to classical PD but with additional features which do not respond to dopaminergic therapies. These include multiple systems atrophy, progressive supranuclear palsy and corticobasal degeneration. All Parkinsonisms are commonly considered to be a spectrum of disorders, with severity and symptoms differing between cases (Loy-English and Feldman, 2004; Dugger et al., 2014).

1.1.1 Pathology

PD is characterised by degeneration of dopaminergic neurons in the substantia nigra (SN), often accompanied by dystrophic neurites and Lewy bodies. The SN is part of the basal ganglia network, involved in movement control, mood and reward. It consists of two regions, the pars compacta (SNc) and the pars reticulata (SNr). Degeneration in PD predominantly affects the SNc; over 90% of cells in the ventral SNc and 50% in the dorsal SNc are lost in PD patients in the first decade. This compares to a 2-7% loss experienced as part of the normal aging process (Fearnley and Lees, 1991).

The SNc provides dopaminergic input to the striatum, enabling fine motor control by adjusting the levels of inhibition from the basal ganglia via direct and indirect pathways. Under normal conditions, the direct pathway decreases inhibition from the thalamus to the cortex, leading to an increase in motor activity. Meanwhile the indirect pathway decreases excitatory thalamic input to the cortex, decreasing motor activity. Dopamine has an excitatory affect on the direct pathway (via dopamine 1 receptors) and an inhibitory affect on the indirect pathway (via dopamine 2 receptors); i.e. dopaminergic inputs increase motor activity. Cholinergic

interneurons projecting from the cortex have the opposite effect. These neurotransmitters and pathways acting in synergy enable controlled, steady movements (Figure 1A). Without dopamine, reduced activity in the direct pathway and increased activity in the indirect pathway is combined with a lack of opposition to cholinergic interneurons, leading to an overall reduction in motor control (Figure 1B) (DeLong, 1990; Guridi et al., 2012).

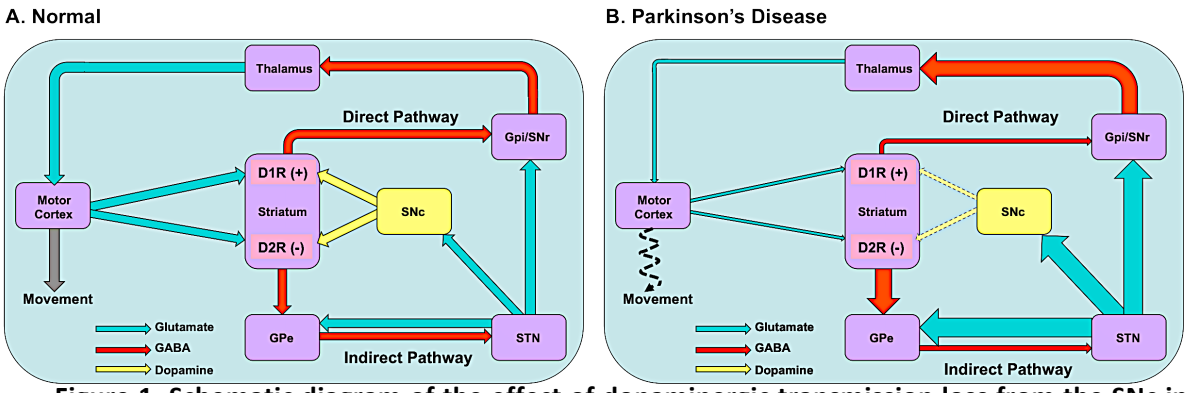

Figure 1. Schematic diagram of the effect of dopaminergic transmission loss from the SNc in the direct and indirect pathways of basal ganglia motor circuits. **A.** Normal motor circuit activity. Conscious movement is controlled via input from the direct and indirect pathways between the striatum and the thalamus. **B.** Altered motor circuit activity in PD patients following decreased dopaminergic inputs. Increased activity is indicated by larger arrows, decreased activity by smaller arrows. Additional interconnections have been purposely omitted from this diagram to ensure clarity. Acronyms: D1R (+) dopamine receptor 1 (pathway activated by dopamine), D2R (-) dopamine receptor 2 (pathway inhibited by dopamine), GPe - globus pallidus externa, GPi - globus pallidus interna, SNc - substantia nigra pars compacta, SNr - substantia nigra pars reticulate, STN - subthalamic nucleus.

However degeneration is not as simple as depicted here, with lesioning of the SNc producing deficits in learning and memory but not motor impairments and no Lewy bodies (Da Cunha et al., 2002; Braga et al., 2014). Brain autopsies comparing individuals with and without PD identified SN pathology as the third stage in a six-stage pattern of degeneration which begins in the medulla oblongata and olfactory regions then progresses to the midbrain and SN, eventually incorporating the neocortex and prefrontal lobes (Braak et al., 2003).

Lewy bodies are insoluble protein aggregates within aging and diseased neurons. They consist of a dense α-synuclein core surrounded by a halo of fibrils and additional proteins such as ubiquitin, tubulin, microtubule-associated proteins (MAPs), cell stress proteins, enzymes, synaptic vesicle proteins and fatty acids (Spillantini et al., 1997). Lewy neurites are elongated, spindle-like structures that also contain α-synuclein (Spillanti et al., 1997; Braak et al., 1994). They are not PD specific, occurring in other disorders as well as part of normal aging, where they can be present for decades without affecting cell survival. It is unclear if Lewy bodies are a

cause of the disease or a protective mechanism by the cell to sequester toxic proteins (Braak and Braak 1990; Braak et al., 1994; Alim et al., 2002).

There are many toxic insults and mechanisms implicated in PD pathogenesis, including Lewy bodies, altered metal homeostasis, oxidative stress, mitochondrial dysfunction and neuroinflammation (reviewed by Tolleson and Fang, 2013). The challenge for researchers is to identify which pathways cause neurodegeneration and which are triggered as part of the degenerative process.

1.1.2 Symptoms

The classical motor symptoms include resting tremor, bradykinesia, rigidity and postural instability. They result from damage to motor pathway control (figure 1) (reviewed in Korczyn and Gurevich, 2010; Parkinson, 1817) and become apparent only when 60-80% of dopaminergic neurons have died (Bernheimer et al., 1973; Cheng et al., 2010). However, as mentioned previously, lesions in PD patients' follow a specific pattern in which motor decline occurs in the third stage. Therefore premotor sensory, autonomic and neuropsychiatric symptoms precede cardinal motor decline. These include reduced cognitive function, insomnia, impotence, incontinence, depression, apathy, lack of impulse control and delusions (Todorova et al., 2014). Gender affects the manifestation of the disease, with females more likely to experience emotional disturbances and levodopa-induced dyskinesia and males an increased risk of sleep disturbances and severe motor features (Lyons et al., 1998).

1.1.3 Causes

It is not yet known what the exact pathological mechanisms behind PD are, as 70-95% of disease sufferers exhibit no identifiable genetic cause (Cookson et al., 2005). Mendelian forms of PD provide insights into the molecular mechanisms involved, accelerating understanding and the identification of new therapeutic targets for both idiopathic and familial PD. However, these genes do not always show complete penetrance, meaning genetic predisposition toward the disease also requires environmental, epigenetic factors or additional genetic risk factors for the illness to develop (reviewed by Lesage and Brice, 2009).

1.1.3.1 Environmental Risk factors

Age and sex are the main PD risk factors, with only 5% of cases occurring before the age of 60 (Van Den Eeden et al., 2003; Reeve et al., 2014). Individuals with over 20 years of occupational exposure to certain metals, including copper and manganese, have up to tenfold higher odds of developing PD (Gorell et al., 1997). Meanwhile rural living and pesticides have been shown

to play a causative role in PD, resulting in a 1.3-3 times increased likelihood of developing the disease (Tanner et al., 2011; Costello et al., 2009; Priyadarshi et al., 2000). Pesticides are thought to inhibit complex I, part of the mitochondrial electron transfer chain, leading to mitochondrial dysfunction and oxidative stress, as well as increasing α-synuclein aggregation (Tanner et al., 2011; Costello et al., 2009; Priyadarshi et al., 2000; 2001; Silva et al., 2013). Finally, both number of brain injuries and time spent unconscious are associated with an upto double PD risk, possibly due to the activation of long-term inflammatory cascades or mitochondrial dysfunction (Goldman et al., 2006).

1.1.3.2 Protective factors

It is well documented that caffeine and nicotine consumption inversely relate to risk of PD (Grandinetti et al., 1994; Hellenbrand et al., 1996; Nefzger et al., 1968; Jimenez-Jimenenez et al., 1992). However, recent studies have found these effects are allele specific, with nicotine intake actually causing a 200% increased risk in those with rare homozygous synaptic vesicle glycoprotein 2c *(SV2C)* alleles but a 56% risk reduction in most individuals (Hill-Burns et al., 2013). Similarly, in caffeine neuroprotection, mitogen-activated protein kinase 10 *(MAPK10)* alleles provide a 0-80% increase in protection (Conference presentation, Haydeh Payami, WPC 2013). Exercise is associated with both a decreased risk of PD and amelioration of symptoms after onset of PD (Xu et al., 2010; Thacker et al., 2008; Ciucci et al., 2013; Fisher et al., 2013). Diet can also be protective; a Mediterranean diet halves the risk of PD (Gao et al., 2007; Shen and Ji, 2013).

1.1.3.3 Genetic

PD was long thought to be an entirely sporadic disease. Despite mentions in the literature as far back as the 12th century BC and James Parkinson's seminal 1817 essay (Parkinson, 1817), it was not until 1994 that a familial component to PD was described (Payami et al, 1994; Lazzarini et al, 1994). The first gene identified was *SNCA*, coding for α-synuclein (Polymeropoulos et al, 1997). Since then, many genetic links to PD have been found. With dominant genes, recessive genes, risk factors and varying levels of penetrance, heritable PD is complex. This is discussed further in section 1.2.

1.1.4 Treatment

PD is currently incurable, with only palliative treatments available. This is unlikely to change until understanding of the mechanisms behind the disease improves. Treatments aim to increase dopamine levels in the brain, reduce the effect of dopamine overload in the rest of the body and treat the accompanying non-motor symptoms. Levodopa has been the main

treatment since the 1960s. It is a dopamine precursor, used as dopamine is unable to cross the blood-brain barrier. Side-effects of these drugs (such as dyskinesias and compulsions) are also treated (Parkinson's society 'Drug treatments for PD' 2012 booklet). Deep brain stimulation is increasingly used in cases which cannot be controlled by medication or in patients that experience severe side-effects. Patients who underwent deep brain stimulation found significant improvements in quality of life, with a 70% reduction in dyskinesias and a 60% decrease in L-dopa dose (Kleiner-Fisman et al., 2006). There is also ongoing investment and clinical trials into the possibilities of treatment using gene therapy. A recent preliminary trial introducing three enzymes involved in dopamine synthesis to the striatum found all patients experienced persistent improvements in motor control, without dyskinesias or immune responses (Palfi et al, 2014; clinical trial NCT00627588).

1.2 Genetics of PD

Although the selective degeneration of dopaminergic neurons and the exact pathological mechanisms behind PD are unknown, genetic analyses and genome-wide association studies (GWAS) have identified multiple genes and regions of the genome that are linked with PD. The PD loci each have a 'PARK' identifier, according to the order in which they were identified. There are currently 18 accepted loci (table 1) although the genes associated with these loci have not all been identified or confirmed.

PARK Locus	Approved Symbol	Protein	Location	Inheritance	Initial study
PARK1/4	***SNCA***	**α-synuclein,**	**4q21.3-q22**	**D**	**Polymeropoulos, 1996**
PARK2	***PARK2***	**parkin**	**6q25.2-q27**	**R**	**Matsumine, 1997**
PARK3	*PARK3*	?	2p13	D	Gasser, 1998
PARK5	*UCHL1*	ubiquitin carboxyl-terminal esterase L1	4p13	D	Leroy, 1998
PARK6	***PINK1***	**PTEN-induced kinase 1**	**1p36.12**	**R**	**Valente, 2001**
PARK7	***PARK7***	**DJ-1**	**1p36.23**	**R**	**van Duijn, 2001**
PARK8	***LRRK2***	**leucine-rich repeat kinase 2**	**12q12**	**D**	**Funayama, 2002**
PARK9	***ATP13A2***	**ATPase type 13A2**	**1p36**	**R**	**Hampshire, 2001**
PARK10	***PARK10***	**?**	**1p32**	**R**	**Hicks, 2002**
PARK11	*PARK11*	?	2q36-q37	D	Pankratz, 2003b
PARK12	***PARK12***	**?**	**Xq21-q25**	**X**	**Pankratz, 2003a**
PARK13	*HTRA2*	HtrA Serine Peptidase 2	2p13.1	D	Strauss, 2005
PARK14	***PLA2G6***	**phospholipase A2, Group VI**	**22q13.1**	**R**	**Paisan-Ruiz, 2009**
PARK15	***FBXO7***	**F-box protein 7**	**22q12.3**	**R**	**Shojaee, 2008**
PARK16	***PARK16***	**?**	**1q32**	**?**	**Satake, 2009**
PARK 17	***VPS35***	**vacuolar protein sorting 35 homolog**	**16q12**	**D**	**Vilarino-Guell, 2011**
PARK18	*EIF4G1*	eukaryotic translation initiation factor 4 gamma, 1	3q27.1	D	Chartier-Harlin, 2011

Table 1. Genetic locations linked to PD through linkage and association studies. The 'Parkinson's gene family' as determined by the Human gene organisation gene nomenclature committee (HGMC). Loci in bold have been independently confirmed since they were first reported, those not in bold are currently unconfirmed (Klein and Westenberger 2012). Inheritance modes are dominant (D), recessive (R), X-linked (X) or unknown (?). HGNC database, HGMC.

The variety of proteins encoded by these genes has improved our understanding of the causal pathogenic mechanisms of the disease, indicating multiple pathways that contribute to pathogenicity in PD. These include lysosomal function (ATP13A2, GBA), lipid biosynthesis (PLA2G6), protein translation (EIF4G1, LRRK2), vesicle trafficking (VPS35, LRRK2), ubiquitination (UCHL1, Parkin, FBXO7), mitochondrial function (Parkin, PINK1, DJ1, FBXO7, HTRA2) and autophagy (LRRK2).

Inheritance can follow an autosomal dominant or recessive pattern and the type of inheritance often alters the age of onset, the speed of progression and disease severity.

1.2.1 Autosomal dominant

Variants of *SNCA, LRRK2* and *VPS35* have been found to cause PD following dominant inheritance in multiple families (reviewed in Dachsel and Farrer 2010; Philstrøm and Toft, 2011; Strauss et al., 2005; Vilarino-Guell et al., 2011; Zimprich et al., 2011). The characteristics

associated with confirmed genes causing late-onset PD are summarised in table 2 while the unconfirmed genes are discussed briefly below (section 1.2.1.4).

PARK Locus	Gene name	Frequency -familial	Frequency -sporadic	AAO	No. of mutations identified	Disease features
PARK2/4	*SNCA*	2%	<1%	30-40	4, plus duplications + triplication	Rapid progression, Lewy bodies, cognitive and autonomic changes
PARK8	*LRRK2*	2-40% (population dependent)	1-2%	50-60	>40 unconfirmed, 7 confirmed, 2 risk variants	Slow progression, ± Lewy bodies and neurofibrillary tangles
PARK17	*VPS35*	<1%	<1%	~50	1	Currently little data

Table 2. A summary of characteristics of confirmed autosomal dominant PD cases. The frequency in heritable and sporadic cases, usual age of onset (AAO), number of pathogenic mutations currently identified and any additional features associated with the disease phenotype (Klein and Westenberger 2012; Berg et al., 2005; Ahn et al., 2008; Puschmann et al., 2009, OMIM pages, accessed 140414).

1.2.1.1 *SNCA* (PARK1/4)

SNCA was the first gene in which PD-causing mutations were found (Polymeropoulos et al., 1997). It encodes the protein α-synuclein, the major component of Lewy bodies (Baba et al., 1998). Later, disease-causing duplications and triplications were also identified, demonstrating that increased protein dose is pathogenic (Singleton et al., 2003). Natively soluble and unfolded, α-synuclein adopts a secondary structure only when bound to interaction partners. Pathogenic *SNCA* mutations cause an increased tendency of the protein to form stable, insoluble β-sheets which aggregate into toxic oligomers and fibrils. It is not known if fibrils and Lewy bodies are themselves toxic or an attempt by the cell to sequester damaging species, thereby reducing toxicity. α-synuclein is widely expressed throughout the brain and enriched at pre-synaptic terminals. Its role is uncharacterised but it is thought to be involved in neurotransmitter release (Klein and Westenberger 2012; Bekris et al., 2010).

1.2.1.2 LRRK2 (PARK8)

Mutations in leucine-rich repeat kinase 2 (*LRRK2),* sometimes referred to as 'Dardarin', are relatively common, causing upto 2% of idiopathic (*de novo*) PD cases. Mutations are inherited dominantly with incomplete penetrance (Latourelle et al., 2008). It is a large, multi-domain protein and over 40 putatively pathogenic mutations have been located, seven of which convincingly segregate with the disease (figure 2, section 1.3.1) (Lesage and Brice, 2009). The most common, the *LRRK2* G2019S mutant, is implicated in 10-40% of North African Arab and Ashkenazi Jewish PD cases, though is rarer in European and Asian populations (Ozelius et al, 2006). There are six additional causative mutations and two risk variants. (Aasly et al., 2010).

With the exception of one risk variant, these mutations are all located in the enzymatic RocCOR and Kinase domains.

LRRK2 is of particular interest as familial forms of the disease resulting from mutations in *LRRK2* present with the same late-onset clinical phenotype as idiopathic PD (Healy et al., 2008) and it is hoped that understanding the changes mediated by *LRRK2* mutations may provide clues to the underlying causes of idiopathic PD.

LRRK2 is discussed in detail in section 1.3.

1.2.1.3 VPS35 (PARK17)

Vacuolar protein sorting 35 (*VPS35*) gene encodes a subunit of the retromer complex, a protein complex involved in retrograde transport of receptors from endosomes to the endoplasmic reticulum (Popoff et al., 2007). The VPS35 protein binds specific cargo including the wnt signalling receptor wntless, divalent metal transporter 1 (DMT1) and the lysosomal protease cathepsin D (Belenkaya et al., 2008; Tabuchi et al., 2010; Follet et al., 2014). Mutated VPS35 may alter binding affinity to these interaction partners. Impaired wntless transport would inhibit wnt signalling, known to be important in development of dopamine neurons and impaired in PD (Deng et al., 2013; Berwick and Harvey, 2012b), α-synuclein degradation could be disrupted by mislocalised cathepsin D (Follett et al., 2014) and inhibited recycling of DMT1 would alter iron transport (Tabuchi et al., 2010). Any of these variations could lead to neurodegeneration in PD.

1.2.1.4 Unconfirmed genes

There are several genes within the risk loci in which putative causative mutations have been found, but the pathogenicity of the proteins they encode is not confirmed. Ubiquitin carboxyl-terminal esterase L1 (UCHL1) de-ubiquitinates proteins before associating with the ubiquitinase monomers, preventing their degradation. Possible pathogenic mechanisms are reduced ligase activity or conferral of a novel antioxidant role (Liu et al., 2002; Carmine Belin et al., 2007; Kyratzi et al., 2008). Eukaryotic translation initiation factor 4G (EIF4G1) forms part of a recruitment complex, facilitating mRNA transfer to initiate protein synthesis. By preventing formation of the translation initiation complex, pathogenic mutations may reduce the stress response of cells (Chartier-Harline et al., 2011). HTRA serine peptidase 2 (HTRA2), like PINK1 (linked to autosomal recessive PD), is involved in mitochondrial quality control and pathogenic mutations would be expected to alter damaged mitochondrial proteolysis (Moisoi et al., 2009).

GRB10 Interacting GYF Protein 2 (*GIGYF2*) has been identified as *PARK11*, although follow-up studies have not been able to confirm a PD-GIGYF2 link. It regulates trypsin kinase receptor signalling (Lautier et al., 2008; Lesage et al., 2010; Bras et al., 2009).

1.2.2 Autosomal recessive

There are multiple recessive forms of PD. Most result in loss of function due to an inactive or absent protein and cause an early disease onset (EOPD). Interestingly, many of these are involved in mitochondrial function, making this a likely disease mechanism for EOPD. Parkin, PINK1, DJ1 and FBXO7 are all linked to mitochondrial stress responses (Burchell et al., 2013; Jendrach et al., 2009; Irrcher et al., 2010). Post-mortem examinations of PD patients often reveal altered mitochondrial morphology, although again, it is not clear if this damage is causative or a consequence of the disease. EOPD is very different to idiopathic PD, not only in age at onset (AAO) but with additional features to the cardinal ones described above, such as psychiatric symptoms and gaze palsy (Schulte and Gasser, 2010; Klein and Westenberger 2012; Lesage and Brice, 2012).

The characteristics associated with each confirmed early-onset gene implicated in PD are summarised in table 3.

PARK locus	Name	frequency -familial	frequency -sporadic	AAO	No. of mutations identified	Additional disease features
PARK2	*PARK2* (parkin)	77%	20%	Childhood – 40s	>100 mutations, deletions, duplications	No LBs. Slow progression
PARK6	*PINK1*	1-15%	1-4%	30s-40s	>50 mutations and deletions	Slow progression
PARK7	*PARK7* (DJ-1)	1%	<1%	20s-30s	4	bradydactyly, psychiatric symptoms, short stature
PARK9	*ATP13A2*	<1%	<1%	Teenage	7	Dementia supranuclear gaze palsy. Aggressive onset
PARK14	*PLA2G6*	<1%	<1%	Teenage-20s	6	Dystonia, dementia, frontotemporal atrophy
PARK15	*FBXO7*	<1%	<1%	Childhood - teenage	4	Pyramidal system involvement

Table 3. A summary of characteristics of early-onset, recessive PD cases. The frequency in heritable and sporadic cases, usual age of onset (AAO), number of pathogenic mutations currently identified and any additional features associated with the disease phenotype (Schulte and Gasser, 2010; Klein and Westenberger 2012; Lesage and Brice, 2012; Online Mendelian Inheritance in Man (OMIM) pages, accessed 140414).

1.2.2.1 EOPD and the mitophagy pathway *(PARK2, PARK6, PARK7* and *PARK15)*

Several of the proteins linked with EOPD are involved in neuroprotection and mitophagy initiation: parkin (*PARK2*), PINK1 (*PARK6*), DJ-1 (*PARK7*) and FBXO7 (*PARK15*).

Under normal conditions, the serine/threonine kinase PINK1 is rapidly degraded at mitochondria (Lin and Kang, 2008). Damaged mitochondria undergo membrane depolarisation which inhibits PINK1 degradation. The subsequent accumulation of PINK1 leads to parkin recruitment to the mitochondria and phosphorylation (Matsuda et al., 2010a; 2010b; Kondapalli et al., 2012). Recruitment is mediated by an E3 ubiquitin ligase complex that contains the PD-implicated FBXO7 (Burchell et al., 2013). Parkin, also an E3 ubiquitin ligase, then catalyses polyubiquitination of substrates, including mitofusins and voltage-dependant anion channels which enable apoptotic factors to enter the organelle, triggering mitochondrial fragmentation and mitophagy (Glauser et al., 2011; Ziviani and Whiltworth, 2010; Gegg et al., 2010; Tsujimoto and Shimizu, 2002). Overexpression of PINK1 or parkin is neuroprotective, shielding neurons from insults including α-synuclein toxicity, proteasomal dysfunction and oxidative stress (Feany and Pallanck, 2003; Todd and Staveley, 2008).

DJ-1 is an antioxidant, protecting against reactive oxygen species (ROS)-induced oxidative stress by auto-oxidation at specific cysteine residues (Irrcher et al., 2010; Ariga et al., 2013). Not only does the high rate of ATP metabolism compared to the rest of the body mean the brain is particularly vulnerable to stress, but dopamine metabolism releases ROS, resulting in increased exposure of nigral dopamine neurons (Spina and Cohen, 1989). As well as regulating expression of genes involved in dopamine synthesis to protect neurons from damage induced by excess dopamine oxidation (Ishikawa et al., 2009; 2012), DJ-1 also maintains mitochondrial complex I function during oxidative stress, protecting against mitophagy (Waak et al., 2009; Mullett et al., 2011; Hayashi et al., 2009).

1.2.2.2 ATP13A2 (PARK9)

Mutations in ATPase, type 13A2 (*ATP13A2*) lead to Kufor-Rakeb syndrome, a parkinsonism associated with dementia and supranuclear gaze palsy. ATP13A2 is a lysosomal membrane protein, involved in heavy metal ion membrane transport (Schmidt et al., 2009). ATP13A2 regulates neuronal integrity and protects against mitochondrial fragmentation; a possible link to other pathogenic mechanisms associated with EOPD. Indeed, it is dramatically upregulated in the remaining dopamine neurons of PD brains (Ramirez et al., 2006; Ramonet et al., 2012).

1.2.2.3 PLA2G6 (PARK14)

Phospholipase A2, group VI (*PLA2G6*) encodes iPLA$_2$-VI, a calcium independent phospholipase, important for maintaining membrane integrity by regulating phosphatidylcholine, a major cell membrane component. In addition to PD, *PLA2G6* mutations are also implicated in infantile neuroaxonal dystrophy and neurodegeneration with brain iron accumulation, both disorders in which changes in iron homeostasis is implicated (Morgan et al., 2006; Gregory et al., 2009; Khateeb et al., 2006). Mateos and colleagues (2008) identified iron build-up as an oxidative stress trigger, leading to phosphatidylcholine breakdown. It is possible that mutated iPLA$_2$-VI inhibits a protective response to reduced membrane integrity in the presence of oxidative stress.

1.2.3 Risk loci

PD rarely shows monogenetic inheritance (Klein and Westenberger, 2012). Complex interactions between genetics and the environment are able to impact on both the presence and progression of the disease. Multiple risk genes have been identified using GWAS. This powerful tool uses large cohorts of people to detect low penetrance alleles which cannot be detected within families. Confirmed risk-enhancing genes include *SNCA, LRRK2, MAPT* and *GBA*.

1.2.3.1 *GBA*

Mutations in the lysosomal enzyme glucocerebrosidase (GBA) cause Gaucher disease, a glycolipid storage disorder. *GBA* was identified as a PD risk gene after the increased rate of PD in sufferers and relatives of Gaucher patients was spotted by physicians (Goker-Alpan et al., 2004). There is a 3-fold higher risk of PD in Gaucher patients (Mata et al., 2008). Mutated forms of the GBA protein may reduce lysosomal function: impairing degradation of α-synuclein or glucocerebroside, altering the composition of membranes and leading to cytosolic aggregation of α-synuclein (Brockmann et al., 2012; Mazzulli et al., 2011; Nichols et al., 2009b).

1.2.3.2 *MAPT*

MAPT encodes Tau, a microtubule associated protein (MAP) involved in maintaining the organization and integrity of the cytoskeleton. *MAPT* risk variants for PD have been indentified by GWAS. (Pastor et al., 2001; Healy et al., 2004). Tau is not only implicated in PD, but inclusions are also found in multiple neurodegenerative diseases and tauopathies including Alzheimer's disease, sporadic corticobasal degeneration, progressive supranuclear palsy, and Pick's disease (reviewed by Lee et al., 2001). Hyperphosphorylated forms of the protein aggregate to form neurofibrillary tangles leading to destabilisation of microtubules (MTs)

(Haggerty et al., 2011; Duka et al., 2006; Alonso et al., 1996; Lindwall et al., 1984). Guo and colleagues showed that α-synuclein is able to seed tau fibrilisation, while other studies have found the converse also true, with tau able to enhance α-synuclein aggregation (Guo et al., 2013; Badioal et al., 2011), suggesting there may be a toxic feedback loop.

1.2.4 Additional locations

There are many additional genes implicated in PD. However their incidence is so rare that they are difficult to detect and confirm. International consortia including the 'Wellcome trust case control consortia 2' (Saad et al., 2012; WTCCC2 studies) and the 'International Parkinson's Disease genomics consortium' (International Parkinson's Disease Genomics Consortium (IPDGC) et al., 2011) collect genetic data from large groups of individuals which are then tested by GWAS for association with PD, with the aim of identifying new risk factors. These data have been combined into the publicly available 'PDGene' database (Lill et al., 2012), containing over 3000 variants in 900 genes which may be involved in PD development. However, despite this international effort to identify new causative factors for the disease, 70-95% of PD patients exhibit no identifiable genetic cause (Cookson et al., 2005; Lesage and Brice, 2012).

1.3 Leucine-rich repeat kinase 2 (LRRK2)

LRRK2 is a large, 280 KDa, ubiquitiously expressed protein encoded by *LRRK2*. Expression is highest in the kidneys and lungs, low throughout most brain regions but slightly higher in the putamen and SN (Zimprich et al., 2004; Higashi et al., 2007). LRRK2 has a paralogue, LRRK1. This is also widely expressed and has an almost identical domain organization, with 70% similarity to LRRK2 in the Roc, COR and Kinase domains and 48% similarity overall (Taymans, 2012). Differences predominate in the shorter N-terminus, however genetic analyses of *LRRK1* have not identified a role in PD (Haugarvoll et al., 2007) and cellular expression of equivalent pathogenic *LRRK2* mutations do not show the same toxicity when introduced into *LRRK1* (Greggio et al., 2007).

1.3.1 LRRK2 - Structure

The LRRK2 protein is composed of several distinct domains. A catalytic core of RocCOR and kinase domains is surrounded by structural and protein-protein interaction motifs of armadillo, ankyrin, leucine-rich and WD40 repeats (see figure 2). It exists natively as a dimer (Sen et al., 2009). Over 40 mutations linking *LRRK2* to PD have been published, but only 7 are confirmed

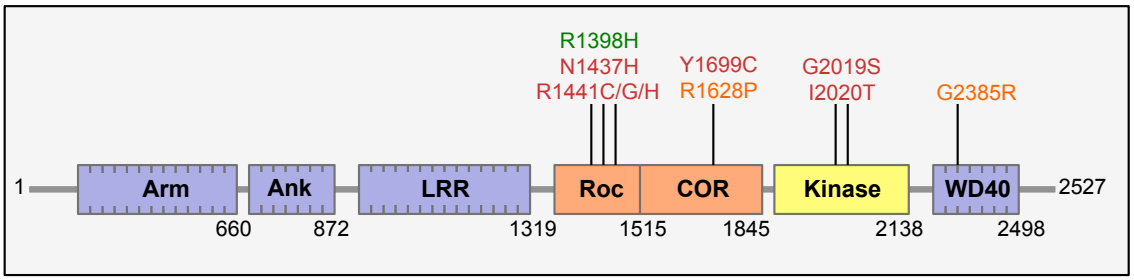

as pathogenic with two established risk factors and one protective variant (figure 2) (Mata et al., 2006; Fu et al., 2013; Chen et al., 2011; Lesage et al., 2009).

Figure 2. The structure of LRRK2. Schematic diagram of the LRRK2 functional domains: Armadillo repeats (Arm), Ankyrin-rich repeats (Ank), Leucine-rich repeats (LRR), Ras of complex proteins (Roc), C-terminal of Roc (COR), Kinase domain and a WD40 domain. Pathogenic mutations found in each domain are listed above in red, risk factors in orange and a protective variant in green. Amino acid residues at domain boundaries are labelled.

1.3.1.1 RocCOR tandem GTPase domain

The Ras of complex proteins (Roc) domain is a GTPase. It is always expressed with a subsequent C-terminal of Roc (COR) domain which is thought to facilitate dimerisation (Gotthart et al., 2008; Sen et al., 2009). This RocCOR tandem domain indicates LRRK2 is part of the ROCO subfamily of Ras-GTPase proteins (Lewis, 2009; Taymans, 2012; Bosgraaf and Van Haastert, 2003), all members of which contain both the Roc and COR domains, often accompanied by a kinase and/or a WD40 domain. Their dual enzymatic function and protein-protein interaction sites suggest involvement in signalling cascade modulation (Lewis, 2009).

Canonical small GTPases, such as those in the Ras superfamily, act as a 'molecular switch', cycling between a GDP-bound (inactive) and GTP-bound (active), conformation. The active form of a GTPase signals to downstream effectors, activating signalling cascades (Taymans, 2012). Due to their high guanosine nucleotide affinity, these conventional small GTPases require accessory GEFs (guanine nucleotide exchange factors) and GAPs (GTPase activating proteins) to catalyse the GDP/GTP exchange. Some evidence points to putative LRRK2-interacting GAPs and GEFs; *ARHGEF7, ARHGEF9* and *ARHGEF12* are upregulated in LRRK2 knockdown neuroblastoma cells (Haebig et al., 2010). These encode Rho-GEFs, with Rho-GEF7 activating LRRK2 GTPase activity, though the interaction occurs with both wild-type and GTP-binding deficient mutants (Haebig et al., 2010). Also, ADP-ribosylation factor GTPase-activating

protein 1 (ArfGAP1) binds LRRK2 and enhances LRRK2 GTP hydrolysis, increasing kinase activity. Surprisingly the interaction occurs via the WD40 and kinase domains (Stafa et al., 2012; Xiong et al., 2012). These data suggest that the LRRK2 Roc domain is not a typical small GTPase.

An alternative proposal is that the LRRK2 RocCOR tandem domain acts as a GAD (G proteins activated by nucleotide-dependant dimerisation). GADs are not regulated by GAPs and GEFs, effecting GTPase activity by dimerisation (Gasper et al., 2009). GADs have a low guanosine nucleotide affinity, therefore the involvement of GAPs and GEFs are not required. Instead, these proteins undergo nucleotide-dependent dimerisation, with guanosine nucleotide binding bringing the effector regions into proximity and assembling the active site (Gasper et al., 2009; Wittinghofer and Vetter, 2011).

Cellular LRRK2 predominantly exists in a dimeric GTP-bound 'active' state (Ito et al., 2007; Greggio et al., 2008; Sen et al., 2009), however dimerisation has not been proven to be guanosine nucleotide-dependent (Biosa et al., 2013; Taymans et al., 2011) and although crystalisation of the *C. tepidum* Roco RocCOR homologue does support COR-mediated dimerisation (figure 3), this has not yet been shown for LRRK2 itself (Gotthardt et al., 2008; Deng et al., 2008). Elucidation of the mechanism is hindered by the low levels of intrinsic GTPase activity (Ito et al., 2007; Xiong et al., 2010).

There are several confirmed pathogenic mutations located within the RocCOR tandem domain; R1441C, R1441G, R1441H and N1437H in the Roc domain, and Y1699C and the R1628P risk variant in the COR domain (figure 2). Each of these locates to the hydrophobic interaction region between the Roc and COR domains (figure 3). Tyr1699 is fully conserved and forms a hydrogen bond with the nearby Roc domain Asn1437 residue, whereas mutations in Arg1441 alter the charge or remove the aliphatic side-chain, altering the interaction strength and structural stability between the two regions (Gotthardt et al., 2008; Daniels et al., 2011). Thus it is postulated that altered Roc-COR positioning reduces intra-RocCOR dimerisation, leading to reduced GTPase function (Daniels et al., 2011; Mata et al., 2006; Greggio and Cookson, 2009; Li et al., 2007). Although LRRK2-induced neurodegeneration has been suggested to be mediated by the kinase domain, toxicity in yeast has been shown to be mediated by GTPase activity (Xiong et al., 2010) as indicated by reduced growth compared with controls. Meanwhile, the protective R1398H mutation also extends into this hydrophobic cleft between the Roc and COR

domains, where it is located in the 'switch II' region. It is at a site considered critical for GTPase

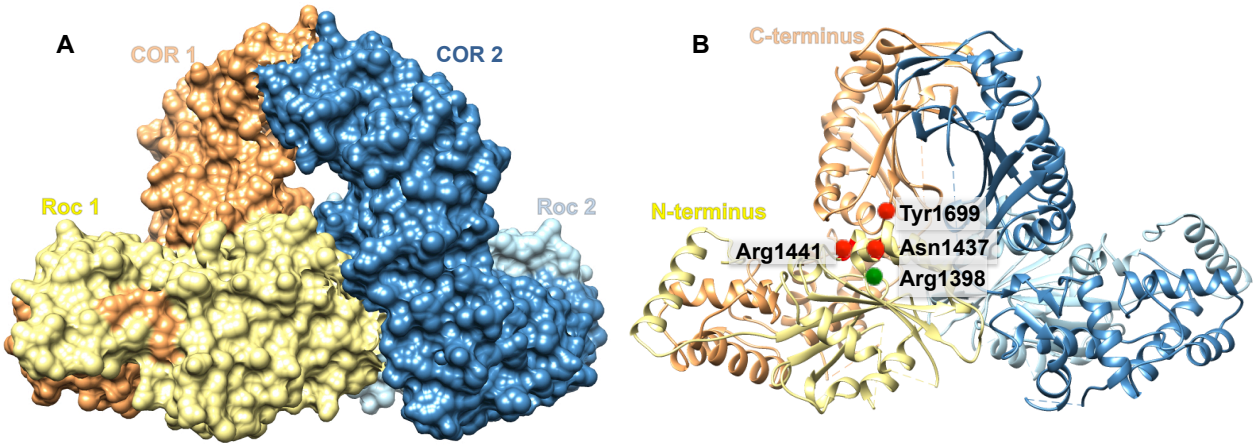

activity in many small GTPases (Tsika and Moore 2012) and may facilitate GTPase function.

Figure 3. Homology model of the RocCOR domain dimer. A. Homology model of the RocCOR surface, demonstrating the predicted dimer structure of LRRK2 functioning as a G-protein activated by nucleotide-dependant dimerisation (GAD). **B.** Ribbon model of the internal structure with the equivalent location of the Roc and COR Asn1437, Arg1441 and Tyr1699 pathogenic mutation sites and the protective R1398 site highlighted, all of which cluster to the Roc-COR interface. Modelled using *C. tepidum* Rab RocCOR structure, publicly available from the Protein Data Bank (model 3DPU) (Gotthardt et al., 2008).

RocCOR domain interactors, identified by yeast two-hybrid screens and further characterised to date, include dishevelled proteins 1-3 (Sancho et al., 2009), tubulins (Gillardon, 2009; Law et al., 2014) and snapin (Yun et al., 2013). As regulators of wnt signalling, dishevelled proteins are involved in diverse signalling pathways including synaptic formation and plasticity, MT stability and diabetes susceptibility (Avila et al., 2010; Grant et al., 2006; Berwick and Harvey 2012b; Ciani et al., 2004). Wnt signalling modulation is a compelling pathogenesis candidate, being already linked with Alzheimer's disease neurodegeneration. LRRK2 has been shown to regulate canonical wnt signalling and, importantly, *Lrrk2* mutants reduce the ability of Lrrk2 to increase wnt signalling activity (Berwick and Harvey, 2012b). The LRRK2 Roc domain has been shown to interact with MTs in a GTPase independent fashion (Gillardon, 2009; Gandhi et al., 2008; Law et al., 2014). This is discussed later in section 1.3.4. The Roc domain has also been found to regulate neurotransmitter release via an interaction with Snapin in a manner unaffected by pathogenic mutations (Yun et al., 2013).

For reasons of clarity and because they only exist together, the Roc and COR domains will subsequently be referred to as one 'RocCOR' domain, except where it is important to emphasise which region of the RocCOR domain is being referred to, in which case they will be separately named.

1.3.1.2 Kinase domain

Based on protein homologues, the kinase domain appears to be related to MLK (mixed-lineage-kinases). MLKs are involved in programmed cell death via the JNK and c-jun apoptosis regulation pathway (Gallo and Johnson, 2002; West et al., 2005). They contain two lobes linked by a hinge region and flexible activation loop. Phosphorylation of the activation loop triggers the change between the 'active' and 'inactive' conformations, altering substrate accessibility. ATP and substrates bind between the lobes in the active site (Luzon-Toro et al., 2007). These features are visible in figure 4, a homology model of the LRRK2 kinase domain.

There are two pathogenic mutations in this domain; G2019S and I2020T. G2019S is the only *LRRK2* mutation to cause a reproducible increase in kinase activity. It was also shown to result in tau positive inclusions and decreased neurite length *in vitro* (Greggio et al., 2006; Jaleel et al., 2007; Luzon-Toro et al., 2007; West et al., 2005; 2007), while work on *Lrrk2* G2019S transgenic mice suggests increased activation of the MKK4-JNK-c-Jun pathway, leading to specific degeneration of dopaminergic neurons in the SNc (Chen et al., 2012a). Meanwhile I2020T was found to modestly enhance *in-vitro* kinase activity by some groups (Gloekner et al., 2006; Greggio et al., 2006) but the opposite, or no effect, was seen by others (Jaleel et al., 2007; Anand et al., 2009). Both mutations are located between the two lobes; Gly2019 in the hinge region, immediately followed by Ile2020 in the flexible activation loop. G2019S and I2020T have been predicted to form additional hydrogen bonds, stabilising the activation loop in an active conformation, while the *LRRK2* G2019S mutation also introduces an additional autophosphorylation site (Gilsbach et al., 2012; Ray et al., 2014; Luzon-Toro et al., 2007).

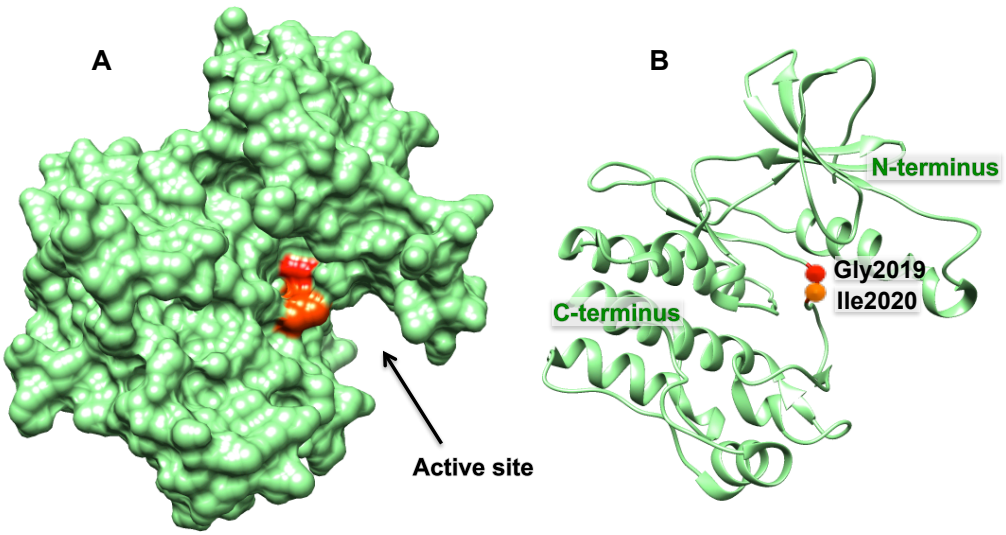

Figure 4. Homology model of the LRRK2 kinase domain. A. The inactive kinase domain surface, demonstrating the external equivalent location of the pathogenic PD mutations. **B.**

Ribbon model of the internal structure with the equivalent location of the pathogenic G2019S and I2020T mutations highlighted in red and orange respectively. Modelled using *D. dusiudeum* Roco4 kinase structure, publicly available from the Protein Data Bank model 4F0G (Gilsbach et al., 2012).

Currently the only confirmed substrate of the LRRK2 kinase is considered to be the LRRK2 protein, containing multiple autophosphorylation sites. However, kinase activity in both wild-type LRRK2 and mutant LRRK2 are very low. This may be due to the absence of important cofactors, or missing chaperones that ensure LRRK2 is correctly folded, resulting in low levels of functional LRRK2. Alternately this may be due to the lack of genuine substrates (Greggio and Cookson, 2009; Mata et al., 2006; West et al., 2005; Gloekner et al., 2006; Guo et al., 2007).

The kinase domain has been the focus of much of the interest in LRRK2 after it was shown that pathogenic PD mutants alter kinase activity (Chen et al., 2012b; West et al., 2005; Smith et al., 2006). Artificially reducing or blocking LRRK2 kinase activity concordantly reduced the toxicity of the pathogenic mutations (Greggio et al., 2006; Greggio and Singleton, 2007). Pharmacological inhibition of the LRRK2 kinase domain is therefore considered a plausible method of treating PD. Early LRRK2 kinase domain inhibitors were non-specific or unable to cross the blood-brain-barrier, though recent inhibitors such as HG-10-102-01 and GNE7915-18 can cross the blood-brain-barrier and are highly selective, with limited off-target effects (Chen et al., 2012b; Choi et al., 2012a; Estrada et al., 2012). They were the first inhibitors to induce endogenous LRRK2 dephosphorylation at Ser910 and Ser935 in transgenic mouse brains and are currently in pre-clinical trials in primates (Estrada et al., 2012; Kavanagh et al., 2013). However, LRRK2 is also highly expressed in lungs and kidneys. Indeed, the strongest degenerative phenotype in *Lrrk2* knock-out mice develops in these organs. The ambiguous function of LRRK2 as well as high expression outside the CNS makes it unclear if LRRK2 kinase inhibitors are a viable clinical prospect, though interestingly some have shown a greater affinity for the *LRRK2* G2019S mutant. This potential for selectivity intimates that the mutant LRRK2 species could be preferentially targeted (Nichols et al., 2009a; Reichling and Riddle, 2009).

Intriguingly, treatment of *LRRK2* overexpressing HEK cells with the H-1152 non-selective LRRK2 kinase inhibitor not only dephosphorylated LRRK2 residues Ser910 and Ser935, but it caused a relocation of the protein from a diffuse cytoplasmic distribution to the MTs, suggesting one role of autophosphorylation may be to mediate LRRK2 cellular location (Dzamco et al., 2010). Kett and colleagues (2012) were unable to repeat this result and it has not been reported with

more specific kinase inhibitors but demonstrates a possible kinase-mediated mechanism to control cellular LRRK2 location (Nichols et al., 2010).

The interplay between the RocCOR and kinase domains is described in section 1.3.1.4.

1.3.1.3 Non-enzymatic domains

The N-terminus of LRRK2 contains 13 armadillo repeats preceding 7 ankyrin repeats. These repeats are usually found in cytoskeletal proteins, transcription factors and signalling proteins (Mosavi et al., 2004; Mills et al., 2012). Following these are the 14 leucine-rich repeats (LRR) for which the protein is named. They assemble in an arch-like formation of β-strands and α-helices and are often involved in protein interactions, mediating diverse cellular functions (Vancraenenbroeck et al., 2012; Kobe and Kajava, 2001). Mills and colleagues (2012) propose that this region acts as a flexible 'solenoid'-like structure, able to anchor the protein to membranes, bind cytoskeletal proteins and as-yet-unidentified functional ligands.

The WD40 domain has a circular 7-bladed propeller-like structure, which acts as a surface for protein or lipid interactions. It is one of the most common protein domains and may provide the location for interactions with cellular and organelle membranes (Mata et al., 2006), in addition to playing an autoregulatory role within LRRK2 (see section 1.3.1.4).

The LRR and WD40 regions are highly positively charged, providing surfaces to bind negatively charged structures such as nucleic acids and phospholipids. This charge is not found in LRRK1 and suggests an area of clear divergence between the two proteins (Mata et al., 2006). There are putative pathogenic PD mutations in each domain but the only confirmed site is the G2385R risk factor on the surface of the WD40 domain (Tan et al., 2006), the large arginine side-chain and positive charge possibly hindering the protein-protein interactions. This is discussed further in section 1.2.

It has been proposed that these non-enzymatic domains combine to make LRRK2 a central signalling hub, in which the outer protein binding domains provide a surface for substrates and their partners to bind, facilitating access to the catalytic domains. Not only do the variety of protein-protein interaction domains enable LRRK2 to play a role in many different signalling cascades, but they also regulate the enzymatic domains.

1.3.1.4 LRRK2 autoregulation

In addition to LRRK2 autoregulation occurring between the enzymatic domains, it also happens between regions throughout the protein.

The majority of autophosphorylation sites are located near the GTPase nucleotide binding pocket. LRRK2 containing the G2019S mutation, a kinase activity enhancer, also enhances autophosphorylation compared with wild-type LRRK2, suggesting that the kinase domain affects GTP-GDP hydrolysis. Conversely, mutations altering GTP binding alter kinase activity. Mutating autophosphorylation sites prevents GTP binding and leads to a reduction in kinase activity whereas the binding of unhydrolysable GTP analogues increases kinase activity (West et al., 2005; 2007; Smith et al., 2006; Webber et al., 2011). Therefore neither domain clearly functions upstream. Instead there seems to be intrinsic regulation between the two, with each influencing the other.

In addition to regulation between the enzymatic domains, the full-length protein also affects the catalytic domain outputs. GTPase activity is reduced in the full-length LRRK2 protein compared to the Roc domain alone in *E. coli* and mammalian cells (Deng et al., 2008; Li et al., 2007). Meanwhile LRRK2 with an N-terminal truncation has increased autophosphorylation, while the LRRK2 central catalytic domains (RocCOR-Kinase) were stable but did not undergo autophosphorylation in the absence of the C-terminus (Jaleel et al., 2007; Greggio et al., 2008; 2009; Jorgensen et al., 2009). The WD40 domain plays an interesting role; Jorgensen and colleagues (2009) found that the loss of the LRRK2 WD40 domain not only abrogated autophosphorylation but also all PD mutation-induced neurotoxicity in zebrafish, while Iaccarino and colleages (2007) showed that LRRK2-ΔWD40 mutants reduce downstream caspase activation by known pathogenic LRRK2 mutants in SH-SY5Y cells. Additionally it was shown that the LRRK2 G2385S mutation decreases kinase activity and autophosphorylation in vivo (Rudenko et al., 2010). Therefore LRRK2 catalytic activity is modulated by both the N- and C-termini.

1.3.2 LRRK2 - Expression and function

LRRK2 expression is greatest in the lungs and kidneys but also occurs in the brain. Expression in mouse and rat brains is highest in the striatum, cortex and hippocampus but weak in the hypothalamus, olfactory bulb and SN (Taymans et al., 2006). Additional studies of the murine brain demonstrate *Lrrk2* expression in neurons (particularly dopaminergic), and more weakly in microglia and astrocytes. Within murine cells it is located both in the cytoplasm and at MTs and membranes (Giesert et al., 2013; Galter et al., 2006; Miklossy et al., 2006). Interestingly, in

HEK cells and human lymphoblasts the membrane-bound LRRK2 has increased dimerization levels, kinase activity and GTP binding but reduced levels of phosphorylation when compared with cytosolic LRRK2, again suggesting regional divergent functional effects (Berger et al., 2010; Li et al., 2011; Sen et al., 2009; Zimprich et al., 2004).

LRRK2 is implicated in many biological functions of the cell, including protein degradation, synaptic transmission, inflammatory response and cytoskeletal integrity. Dysregulation of any of these could lead to cellular dysfunction and trigger degeneration.

Under normal conditions LRRK2 regulates autophagy, inducing increased autophagosome production (Gomez-Suaga and Hilfiker, 2012). These autophagosomes fuse with lysosomes where their contents are degraded. Mice with the *Lrrk2* G2019S mutation feature autophagic and mitochondrial abnormalities, with an accumulation of autophagic vacuoles, swollen lysosomes, multivesicular bodies and distended mitochondria, accompanied by hyperphosphorylated tau (MacLeod et al., 2006; Ramonet et al, 2011). PD brains show impairments in lysosomal membrane stability, lysosome acidification, lysosomal enzyme processing, substrate degradation and clearance of autophagosomes (Dehay et al., 2013). These impairments, further impeded by trafficking defects, may lead to accumulation of faulty organelles and toxic proteins (such as α-synuclein), causing neurodegeneration.

Synaptic changes are also associated with *LRRK2* mutations. *LRK-1* knockout in *C. elegans* leads to changed synaptic vesicle location in dendrites (Sakaguchi-Nakashime, 2007) while Matta and colleagues suggest LRRK2 regulates synaptic vesicle function by phosphorylation of Endophillin A, vital for synaptic membrane curvature and fission (Matta et al., 2012; Guichet et al., 2002). An inability to release synaptic vesicles may explain why *Lrrk2* R1441C transgenic mice feature reduced cortical catecholamines and synaptic dysfunction (Ramonet et al., 2011).

Additionally, GWAS have linked *LRRK2* variants with Crohn's disease and leprosy (Barrett et al., 2008; Zhang et al., 2009). These diseases all share an inflammatory phenotype, indicating an involvement of LRRK2 in immune response. LRRK2 regulates several proteins involved in modulation of immune response, including the transcription factor NFAT1 (nuclear factor of activated T-cells), interferon-γ and nuclear factor kappa-light-chain-enhancer of activated B cells (NFκB), suggesting a role orchestrating immune response cascades (Moehle et al., 2012; Greggio et al., 2012).

Finally, LRRK2 is linked to cytoskeleton function. Associations with F-actin, the most dynamic

form of microfilament, and phosphorylation of actin-associated ERM (ezrin-radixin-moesin) proteins, which anchor microfilaments to the cell membrane, were increased by the G2019S mutation, leading to disrupted neurite outgrowth in *Lrrk2* G2019S transgenic mice (Meixner et al., 2011; Parisiadou et al., 2009; Parisiadou and Cai, 2010; Ramonet 2011; Macleod et al., 2006). The mutation also leads to tau hyperphosphorylation, further destabilising MTs and therefore cellular transport (Parisiadou and Cai, 2010; Melrose et al., 2010). Meanwhile the loss of LRRK2 function leads to increased neurite length and branching in rat primary neuron cultures and reduced tau phosphorylation (Macleod et al., 2006; Gillardon 2009). This interaction is discussed further in section 1.3.4.

1.3.3 LRRK2 - Signalling pathways

It is possible for a single protein to be implicated in so many functions via upstream regulation of multiple signalling pathways. This could be facilitated by the various protein-protein interaction domains and by a location dependent divergence in function, as suggested by the dephosphorylation-mediated relocation to MTs described in section 1.3.1.2. Indeed, LRRK2 has already been linked to multiple signalling cascades including mitogen-activated kinase (MAPK) pathways, tumor necrosis factor-α (TNF-α)/Fas ligand (FasL) and wnt signalling. MAPK pathways show increased activation in PD brains. They direct multiple cellular processes in response to external stimuli, including proliferation, apoptosis, cell division and inflammation (Berwick and Harvey, 2011; Ferrer et al., 2001). *Lrrk2* G2019S transgenic mice have increased activation of the MKK4-JNK-c-Jun pathway (a MAPK pathway), leading to specific degeneration of dopaminergic neurons in the SNc (Chen et al., 2012a). TNF-α and FasL signalling are part of an apoptotic pathway, triggering cell death and neurodegeneration. Ho and colleagues (2009) found that pathogenic mutants strengthened LRRK2 association with FADD (Fas-associated protein with death domain). Meanwhile, LRRK2 links membrane and cytosolic components of wnt signalling and canonical wnt signalling activity is reduced by pathogenic mutations (Berwick and Harvey, 2012a). As mentioned previously, wnt signalling is involved in dopaminergic development, synaptic formation and plasticity, MT stability and also implicated in Alzheimer's disease (Sancho et al, 2009; Min et al., 2011; Berwick and Harvey, 2011).

These data support a role for LRRK2 as an upstream modulator of several signalling cascades which could lead to the activation of the multiple downstream networks in which LRRK2 has been implicated. Small signalling impairments caused by LRRK2 mutants combined with age-related decline in ability of dopaminergic cells to maintain cellular homeostasis and functioning axonal transport under sustained pressure from oxidative stress, is a plausible

pathogenic mechanism for the neurodegeneration observed in PD patients.

1.3.4 LRRK2 and the cytoskeleton

1.3.4.1 Microtubules

Microtubules (MTs) are a network of tubulin polymers which, along with actin microfilaments and intermediate filaments, form the cytoskeleton. In addition to providing structural support to cells, they are required for protein transport, cell division, cell signalling, cell migration and the structure of cilia and flagella. They are polarised, with the minus end toward the cell body and the plus end toward the axon tip (Löwe et al., 2001).

MTs are able to rapidly elongate and shrink, and also to 'treadmill', where dimers are added to one end and removed from the other. This is known as 'dynamic instability' and is important both for chromosome alignment during mitosis and for reacting to guidance cues during neural development (Löwe et al., 2001).

MT arrangements differ between cell types and within cells. While MTs in the majority of cell-types are dynamic, in neurons they are capped and stabilised by MAPs (Dehmelt and Halpain, 2005; Sanchez et al., 2000). Within neurons, axonal MTs are continuous, parallel and uninterrupted bundles whereas dendritic MT arrangements are antiparallel, interrupted and of mixed polarity (Craddock et al., 2012b).

1.3.4.1.1 MAPs

MAPs are defined by their direct interaction with MTs. Their functions include stabilisation and destabilisation of MTs, cross-linking between filaments and mediating MT interactions with other proteins (Olmsted 1986; Chen et al., 1992; Janke and Bulinksi, 2011).

Common examples include type I and type II MAPs. Type I (MAP1A and MAP1B) form bridges between MTs to modulate spacing. Type II (MAP2, MAP4 and tau) stabilise MTs. MAP2 and tau are predominantly neuronal, with MAP2 associated with dendritic MTs and tau axonal MTs, whereas *MAP4* is ubiquitously expressed (Kosik and Finch, 1987; Janke and Kneussel, 2010). The binding of these MAPs to MTs is regulated by MT-affinity-regulating kinases which detach MAPs from MTs by phosphorylation (Drewes, 1997; Drewes et al., 2004), regulating MT stability. Additional MAPs bind to the MT plus end (clasps), sever (spastin and katanin) and destabilise (catastrophin) MTs (Zhang et al., 2011). Chan and colleagues recently reported an interaction between the LRRK2 kinase domain and MAP1B in yeast two-hybrid studies (Chan et al., 2014).

1.3.4.1.2 Tubulin

MTs are composed of α- and β-tubulin dimers, while δ-, ε-, and γ- tubulin isoforms are involved in MT formation and organisation in the centrosome (Dutcher, 2001; Bryan and Wilson, 1971).

There has been no specific naming convention regarding tubulin isoforms and as such, it is often unclear which isoform is being referred to within papers. To avoid confusion and inconsistencies in naming, this thesis refers to both the gene and the protein product using the HUGO gene nomenclature committee (HGNC) gene names.

According to the HGNC, the different human tubulin genes are listed in the table below:

α	β	δ	ε	γ
TUBA1A	*TUBB*	*TUBD1*	*TUBE1*	*TUBG1*
TUBA1B	*TUBB1*			*TUBG2*
TUBA1C	*TUBB2A*			
TUBA3D	*TUBB2B*			
TUBA3E	*TUBB2C/4B*			
TUBA4A	*TUBB3*			
TUBA8	*TUBB4*			
	TUBB6			

Table 4. The human tubulin genes as found in the HUGO gene nomenclature committee database. There are also additional putative genes, pseudogenes and genes for tubulin-like proteins not listed here. HGNC Database, HUGO Gene Nomenclature Committee (HGNC).

Tubulin isoforms show discrete expression. There is high expression of TUBB2A, TUBB2B, TUBB3 and TUBB4 in the brain; TUBB3 is a neuron-specific isoform and often used as a neuronal marker (Burgoyne et al., 1988), while TUBB4 is also found in ciliary structures (Raff et al., 1997). TUBB, TUBB2C and TUBB6 are ubiquitously expressed. TUBB and TUBB2C are the major β-tubulin isoforms outside the brain. TUBB6 expression is consistently of a low level but includes the SN, while TUBB1 is expressed only in leukocytes and hematopoietic tissue (Sullivan et al., 1986; Wang et al., 1986; Cleveland, 1987; Lopata and Cleveland, 1987; Banerjee and Kasmala, 1998; Verdier-Pinard et al., 2005; Leandro-Garcia et al., 2010; Cantuti-Castelvetri et al., 2007).

1.3.4.1.3 Tubulin - MTs

MTs are composed of alternating dimers of α- and β-tubulin, which associate to form protofilaments (Lopata and Cleveland, 1987). Lateral connections between these filaments form the MT. Although MTs predominantly contain 13 protofilaments, they can be different sizes and have different structures, depending on whether intra-protofilament bonds form

between α-α, β-β tubulins (more stable) or α-β tubulins (prone to destabilisation) (Katsuki et al., 2014; Sirajuddin et al., 2014).

Humans have 7 α- and 8 β-tubulin isoforms and members of each group are almost identical. Excepting the diverse C-terminal tail, α-tubulin isoforms are 97% conserved and β-tubulin isoforms 95%. The C-termini vary from 10 amino acids in α-tubulin up to 20 amino acids in β-tubulin and are the site of most tubulin post-translational modifications (Janke and Kneussel, 2010). They contain many aspartic acid and glutamic acid residues, resulting in a negatively charged MT surface. Molecular dynamics modelling predicts that the tubulin C-terminal tails can move between the protruding 'up-state' and the prostrate 'down-state', in which the tail interacts with an adjacent tubulin hetero-isoform (figure 5) (Freedman et al., 2011; Craddock et al., 2012b).

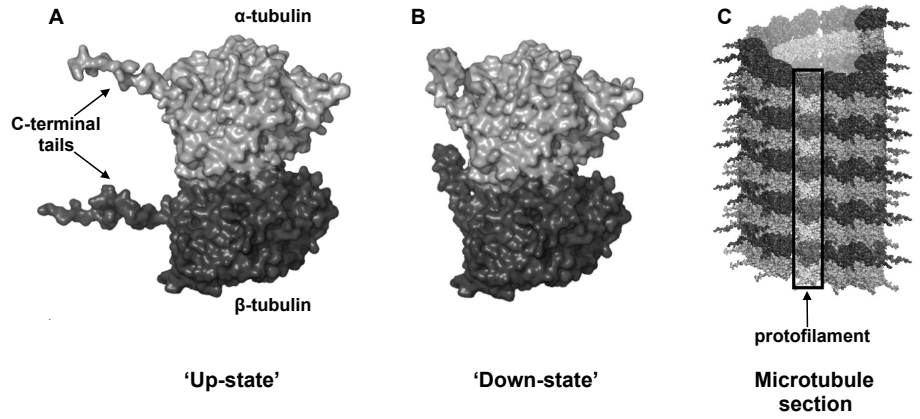

Figure 5. The C-terminal tail protrusions of tubulin. A TUBA1A and TUBB3 dimer with projecting C-termini (TUBB3 residues Ala428-Lys450, TUBA1A residues Val440-Tyr451) in their 'up-state'. **B.** Tubulin dimer with C-termini in their 'down-state' **C.** MT section showing multiple C-terminal tails in the up-state. Figure adjusted from Craddock et al., 2012a and 2012b (PLoS open access).

MTs undergo many post-translational modifications, the majority of which occur on the C-terminus. Newly polymerised MTs are tyrosinated (Webster et al., 1987a), α-tubulins of stable MTs often have the final tyrosine residue irreversibly cleaved (detyrosination) (Webster et al., 1987a; 1987b; 1990). Glycylation and varying levels of polyglutamylation – up to 20 amyl groups – are important for MAP-MT interactions (Audebert et al., 1993; Boucher et al., 1994; Larcher et al., 1996; Rosenbaum, 2000; Bonnet et al., 2001; Sirajuddin et al., 2014). However there is one exception to this C-terminus post-translational modification hot-spot. Stable MTs are also acetylated on the lumenal α-tubulin L40 residue (L'Hernault and Rosenbaum 1985; Schulze et al., 1987).

The 'tubulin code' hypothesis suggests that combinations of tubulin isoform and post-

translational modifications of MTs can generate a system of encoding information (Verhey and Gaertig 2007; Hammond et al., 2008; 2010; Janke and Kneussel, 2010). This proposes that tubulin isoforms and/or post-translational modifications not only alter MT dynamics but also when and where MAP-MT interactions occur. For example, TUBB3 has long been associated with taxol chemotherapy resistance in tumors (Derry et al., 1997). Meanwhile individuals who naturally express higher *TUBB6* levels have reduced MT stability along with reduced pyroptosis (inflammatory programmed cell death) (Salinas et al., 2014; Battacharya and Cabral 2004; 2009). A recent paper elegantly identified multiple motor-protein characteristics which are governed by tubulin isoform and post-translational modification, including increased kinesin-1 motility on polyglutamylated TUBB3 and a requirement for detyrosinated α-tubulin for kinesin-2 transport (Sirajuddin et al., 2014). Finally, the MAP1B, MAP2 and tau affinity for MTs is greatest in regions with tubulin polyglutamylation of 1-3 units, whereas MAP1A affinity increases with increasing polyglutamylation (Boucher et al., 1994; Larcher et al., 1996; Bonnet et al., 2001). These data emphasise the highly complex and dynamic regulation of MTs of which LRRK2 plays a part.

1.3.4.1.4 Tubulin - centrosome

The δ-, ε-, and γ- tubulin isoforms do not dimerise to form MTs, instead playing important roles in MT formation and organisation. They localise to the centrosome where they are involved in the assembly and function of centrioles and basal bodies. This is the main organising centre of MTs and cell cycle progression. δ-tubulin is found at basal bodies and involved in spermatogenesis (Dutcher, 2001; Smrzka et al., 2000). ε-tubulin is connected to centrosomal maturation localisation, associating initially with the older centrosome of a newly divided pair, then later with both (Chang and Stearns 2000; Chang et al., 2002). γ-tubulin forms a MT nucleation base as part of the MT-organising centre (Dutcher, 2001).

1.3.4.1.5 Tubulin in disease

The 'tubulinopathies' are unsurprisingly caused by defects in neuronal migration, axon growth and guidance. They involve multiple tubulin isoforms such as TUBA1A, TUBB, TUBB2A, TUBB2B, TUBB3, TUBB4 and TUBG1 (Kumar et al., 2010; Hikita et al., 2014; Keays et al., 2007; Breuss et al., 2012; Cushion et al., 2014; Jaglin et al., 2009; Poirier et al., 2010; 2013; Hersheson et al., 2012; Simons et al., 2013). Mutations have been linked with malformations in development, including lissencephaly, polymicrogyria and microcephaly. These developmental phenotypes are accompanied by diverse associated defects including intellectual disability, language difficulties, optic atrophy and epilepsy.

This large variation in phenotypes highlights the complex roles, expression patterns and cellular distribution of tubulin. Although demonstrably crucial for correct neurodevelopment, a functioning cytoskeletal network is also required during adulthood. Impaired axonal transport has been linked to degenerative disorders including Alzheimer's disease and other tauopathies (hyperphosphorylation of tau), Huntington's disease (impaired vesicular transport) and amyotrophic lateral sclerosis (loss of kinesin motors), in addition to PD (discussed in 1.3.4.2).

The decline in MT stability and altered MAP-MT association in these diseases prevents precise trafficking, maintenance of cell structure and synapse formation. The long axons of neuronal cells make them particularly vulnerable to defects in the cytoskeletal network and impaired protein transport (McMurray, 2000; Morfini et al., 2009; Parisiadou and Cai 2010).

1.3.4.2 MTs and PD

As mentioned previously, PD is characterised by progressive degeneration of dopamine neurons in the SN. The SN of PD patients show altered expression of several genes involved in MT-dependent transport, interestingly including the tubulin genes *TUBB2, TUBD1, TUBG1* and *TUBG2* (Grunblatt et al., 2004; Noureddine et al., 2005; Cantuti-Castelvetri et al., 2007). The MT depolymerising pesticide Rotenone was significantly more toxic to midbrain dopaminergic neurons than to other types of neuron (Ren et al., 2005) and long-term exposure to rotenone causes PD-like locomotor problems in rats (Betarbet et al., 2000). Thus it is vital that the MT network be maintained. Small changes in stability could have long-term ramifications, with increased vulnerability in neurons and particularly dopaminergic neurons.

1.3.4.3 MTs and LRRK2

There are several lines of evidence implicating LRRK2 involvement with MT function. The Roc domain of LRRK2 interacts with the C-terminus of β-tubulin (Gandhi et al., 2008; Law et al., 2014). Additionally, LRRK2 colocalises with β-tubulin in HEK cells (Gloekner et al., 2006; Gillardon, 2009). Caesar and colleagues found that incubating LRRK2 with MTs in a cell-free assay leads to an increase in LRRK2 GTPase activity and that destabilisation of MTs was associated with reduced kinase activity (Caesar et al., 2013) suggesting an influence of MT binding on LRRK2 function.

These data suggest there may be a pathogenic link between LRRK2 and MT stability and integrity, affecting neuronal viability and contributing to the development of PD.

1.4 Thesis aims

Pathogenic *LRRK2* mutations have been identified in both familial and sporadic PD, causing a

disease onset of similar age and duration as idiopathic forms of the disease. LRRK2 and downstream pathways are therefore attractive therapeutic targets. Although the LRRK2 Roc domain has been shown to interact with tubulin, the role of this LRRK2-tubulin association is as yet unknown. However, cytoskeletal alterations have been observed in PD models harbouring *LRRK2* mutations, with pathogenic *LRRK2* mutation expression reducing neurite outgrowth and promoting the accumulation of hyperphosphorylated tau.

1.4.1 Hypothesis

That novel insight into the functional relevance of the LRRK2-tubulin association can be gained by delineation of the sites of interaction between the two proteins.

1.4.2 Aims

- To characterise the LRRK2 association with tubulin
- To identify and model the interaction site in both tubulin and LRRK2
- To gain understanding of the function of LRRK2 at the cytoskeleton.
- To search for cytoskeletal-related protein mutations in a cohort of PD patients with no known pathogenic PD mutations.

1.4.3 Objectives

- To use yeast two-hybrid to test for an association between LRRK2 and tubulin isoforms with altered expression levels in the PD SN.
- To use yeast two-hybrid to isolate the specific residues conferring the association in each protein:
    - By alanine scanning the LRRK2 Roc domain
    - By testing for association between the LRRK2 homologue LRRK1 and tubulin, and comparing sequences to identify conserved/differring sites between the two and using this to inform the identification of interaction sites.
    - By comparing highly homologous tubulin sequences to identify potential residues which differ between interacting and non-interacting isoforms
    - By mutating the individual residues predicted above to introduce/prevent associations
- To use freely-available tubulin and LRRK2 homologue models to model the interaction sites revealed by yeast two-hybrid.
- To use a cytoskeleton-specific fixation technique and confocal imaging to identify where LRRK2 binds MTs in vitro.
- To use immunocytochemical techniques, antibodies specific to post-translational modification of MTs and agents altering MT stability to determine the role of LRRK2 at MTs in vitro, informed by the site of the interaction identified previously.
- To use NGS and chain-termination sequencing to identify novel mutations in familial PD patient DNA.

2. Materials and Methods

2.1 Generation of plasmid constructs

To create plasmid constructs, the complementary DNA (cDNA) sequence of interest was amplified by polymerase chain reaction (PCR) and inserted into the desired vector. The plasmid construct was cloned by transformation into *E. coli* competent cells, grown overnight and extracted following cell lysis. After purification, the cDNA was sequenced to confirm it was in-frame.

All biochemical reagents are from Sigma unless otherwise stated

2.1.1 Polymerase chain reaction (PCR)

PCR enables the selection and amplification of regions of cDNA. This process uses temperature change to anneal forward and reverse primers to specific cDNA sequences and amplify the fragment between. First the cDNA is denatured using high temperature, breaking the hydrogen bonds between complementary base pairs and separating the two strands into single cDNA strands. These are then used as a template for the DNA polymerase. Lowering the temperature to 5°C below the primer Tm (melting temperature) anneals the primers to the template cDNA. If the temperature is too low, non-specific binding can occur, too high and the primers do not bind. The temperature is then raised to the optimal temperature for the polymerase, which extends the nucleotide sequence from the 3' end of the primer, complementary to the template cDNA.

Primers were designed using NCBI gene consensus sequences in table 5, with the addition of restriction enzyme cut sites. These enabled the DNA fragment to be digested and inserted into a vector multiple cloning site. The template cDNA was either human brain cDNA or plasmid constructs. The primers and restriction enzymes used are listed in section 2.1.1.1.

Gene	Consensus Sequence	Gene	Consensus Sequence
LRRK2	NM_198578	***TUBB2C***	NM_006088
LRRK1	NM_024652.3	***TUBB3***	NM_006086
TUBA1A	NM_006009.2	***TUBB4***	NM_006087
TUBA1B	NM_006082.2	***TUBB6***	NM_032525
TUBA1C	NM_032704.3	***TUBD1***	NM_016261.3
TUBA4A	NM_006000	***TUBE1***	NM_016262.4
TUBB	NM_178014	***TUBG1***	NM_001070
TUBB1	NM_030773.3	***TUBG2***	NM_016437.2
TUBB2A	NM_001069	***ACTB***	NM_001101.3
TUBB2B	NM_178012	***ACTG1***	NM_001614.2

Table 5. Protein consensus sequences. These are the sequences used for DNA construct design and sequence alignment. Sequences are available from the NCBI website http://www.ncbi.nlm.nih.gov/gene/.

The lyophilised primers were dissolved in deionised water (dH_2O), using the volume indicated by the manufacturer synthesis report, to a final concentration of 100 pmol/µl.

The PCR conditions were as described by the manufacturer. A standard reaction combined 22 µl of AccuPrime *Pfx* (22 U/ml *t. kodakaraensis* thermostable DNA polymerase in complex with anti-KOD antibodies, 66 mM Tris-SO_4 (pH 8.4), 30.8 mM $(NH_4)_2SO_4$, 11 mM KCl, 1.1 mM $MgSO_4$, 330 µM dNTPs, AccuPrime proteins, stabilisers-Invitrogen), 10 pM forward and reverse primers and cDNA, totalling 25 µl.

The standard PCR settings are shown in table 6, below:

Stage	Temperature	Time	Cycles
1	95°C	5 minutes	1
2	95°C	30 seconds	25
	60°C	30 seconds	
	68°C	2 min/kilobase	

Table 6. Typical PCR parameters.

2.1.1.1 Plasmid constructs and primers

The primers used to amplify cDNA and the restriction enzyme sites incorporated are listed below. Table 7 contains LRRK1 and LRRK2 constructs while table 8 lists the cytoskeletal protein constructs.

Vector	cDNA Insert	Primer direction	Primer (5'-3')	Restriction site
pDS	LRRK2	Forward Reverse	CAGCCCGGGCCATGGCTAGTGGCAGCTGTCAG ATTCTCGAGTTACTCAACAGATGTTCGTCTCA	XmaI XhoI-SalI
pDS	LRRK2 RocCOR	Forward Reverse	TCCCCCGGGAATGGGGAAATTAAGCAAAATATGGG AGCGTCGACTCATTCCAACTCATCATTATTC	XmaI SalI
pDS	LRRK1 RocCOR	Forward Reverse	GCTCCCGGGACTGGGCAACCTCTGGCAGCTG GTCCTCGAGTCACTCCAGCTTGCTGTTCTCCAGG	XmaI XhoI
pACT2	LRRK2 RocCOR	Forward Reverse	AAAGGATCCTGCCTTATAACCGAATGAAACTTA CCTCTCGAGTCATGGATTTACTAAGAGATCTCC	BamHI XhoI
pACT2	LRRK2 RocCOR 1-3	Forward Reverse	AAAGGATCCTGCCTTATAACCGAATGAAACTTA TTCGTCGACCTATGCAAAATCCCACACATTTAGG	BamHI SalI
pACT2	LRRK2 RocCOR 2-5	Forward Reverse	ACTCCATGGTCCAAATAAGAGACAAAAG CTTTGTCGACCTACTCATCAGAAACATCCAAAT	NcoI SalI
pACT2	LRRK2 RocCOR 4-6	Forward Reverse	CTTCCATGGCCCCTGTGATTCTCCGTTGG AACGTCGACCTATCGGATCTTGAAATTAAGGC	NcoI SalI
pRK5	myc LRRK2	Forward Reverse	AGCGGATCCGCCACCATGGAGCAAAAGCTCATTTCTG AGGAAGATCTCATGGCTAGTGGCAGCTGTCAG ATTCTCGAGTTACTCAACAGATGTTCGTCTCATTTT	BamHI XhoI
pRK5	myc LRRK2 N-terminus	Forward Reverse	AGCGGATCCGCCACCATGGAGCAAAAGCTCATTTCTG AGGAAGATCTCATGGCTAGTGGCAGCTGTCAG ATCGTCGACTTAGCTTAATTTCCCCATTTC	BamHI SalI
pRK5	myc LRRK2 RocCOR	Forward Reverse	TCTGGATCCGCCACCATGGAGCAAAAGCTCATTTCTG AGGAAGATCTCATGGGGAAATTAAGCAAAATA AGCGTCGACTCATTCCAACTCATCATTATTC	BamHI SalI

Table 7. LRRK2 and LRRK1 construct information. The consensus sequences and primers used to clone LRRK1 and LRRK2 constructs, incorporating full-length, individual domains and deletion constructs.

Vector	cDNA Insert	Primer direction	Primer (5'-3')	Restriction site
pACT2	ACTB	Forward Reverse	GCCGGATCCCCATGGATGATGATATCGCCG ATACTCGAGGTAGAATCATTTGCGGTGGAC	BamHI XhoI
pACT2	ACTG1	Forward Reverse	TGCGGATCCCAATGGAAGAAGAGATCGCCG TGACTCGAGTTAGAAGCATTTGCGGTGGAC	BamHI XhoI
pACT2	C-TUBA1A	Forward Reverse	GCTGGATCCTGTACCGTGGTGACGTGGTTC CAGCTCGAGCTTCCCTGTAAAAGCAGCACC	BamHI XhoI
pACT2	C-TUBA1B	Forward Reverse	GCTGGATCCTGTACCGTGGTGACGTGGTTC TGGCTCGAGGACATGCTGCAGGGCCAAAAG	BamHI XhoI
pACT2	C-TUBA1C	Forward Reverse	GCTGGATCCTATACCGTGGTGACGTGGTTC CCACTCGAGAGGAGTGTAAAAGTACAGCAC	BamHI XhoI
pACT2	C-TUBA4A	Forward Reverse	GCTGGATCCTGTACCGTGGAGATGTGGTGC GCACTCGAGATAGTGAATAGGCTCCAGGCA	BamHI XhoI
pACT2	C-TUBB	Forward Reverse	CTGAGATCTTCCGTGGTCGGATGTCCATGA GAACTCGAGAGTTGAGTAAGACGGCTAAGG	BglII XhoI
pACT2	C-TUBB1	Forward Reverse	CCTGGATCCTCCGGGGCAAGATGTCCACCA CTACTCGAGAACTGTTCTGTAAGCGACTCC	BamHI XhoI
pACT2	C-TUBB2A	Forward Reverse	CTGAGATCTTCCGGGGCCGCATGTCCATGA GAACTCGAGTAAGGATGCACGATTGATCTG	BglII XhoI
pACT2	C-TUBB2B	Forward Reverse	CTGAGATCTTCCGGGGCCGCATGTCCATGA TCCCTCGAGGCTTTCCCTAACCCGTCTCGC	BglII XhoI
pACT2	C-TUBB2C	Forward Reverse	CCGAGATCTTCAGGGGCCGCATGTCCATGA TGGCTCGAGATAAAGAGTTCACACTGCTTC	BglII XhoI
pACT2	C-TUBB3	Forward Reverse	CCAAGATCTTCCGGGGCCGCATGTCCATGA CGGGTCGACCCTGCCTCTCACTCCAGCTGC	BglII SalI
pACT2	C-TUBB4 A430	Forward Reverse	CCGAGATCTTCCGGGGCCGCATGTCCATGA GCCCTCGAGGGCCGTGGCGTCCTGGTACTG	BglII-BamHI XhoI

	truncation			
pACT2	C-TUBB6	Forward Reverse	CCAAGATCTTCCGCGGGCCCATGTCCATGA GGACTCGAGGTGTTGTAGGATCTGAGTTGG	BglII-BamHI XhoI
pACT2	C-TUBB6 A430 truncation	Forward Reverse	CCAAGATCTTCCGCGGGCCCATGTCCATGA CCCCTCGAGGGCGGTGGCATCCTGGTACTG	BglII-BamHI XhoI
pACT2	TUBD1	Forward Reverse	TGTGGATCCGCATGTCAATTGTAACAGTGC TGTCTCGAGTCAGAGATTACAGTAACTGGC	BamHI XhoI
pACT2	C-TUBD1	Forward Reverse	TTAGGATCCCCATTGCTAACTTGGTCATTC TGTCTCGAGTCAGAGATTACAGTAACTGGC	BamHI XhoI
pACT2	TUBE1	Forward Reverse	GGCGGATCCCCATGACCCAGTCGGTGG GAGGGTTCTCGAGTCACATAGCTATGC	BamHI XhoI
pACT2	C-TUBE1	Forward Reverse	GTGGGATCCTGGTTAGAGGAAATGTAC GAGGGTTCTCGAGTCACATAGCTATGC	BamHI XhoI
pACT2	TUBG1	Forward Reverse	CCTGAATTCCGATGCCGAGGGAAATCATCA TGTCTCGAGGGACTCACTGCTCCTGG	EcoRI XhoI
pACT2	C-TUBG1	Forward Reverse	TCCGAATTCTCATCCAGGGAGAGGTG TGTCTCGAGGGACTCACTGCTCCTGG	EcoRI XhoI
pACT2	TUBG2	Forward Reverse	TCTCCATGGCGATGCCCCGGGAGATCATC GGAAGATCTGGGAGGGAAATCACTGCTCC	NcoI BglII-BamHI
pACT2	C-TUBG2	Forward Reverse	CTCCCATGGATCCAGGGAGAGGTGGACCC GGAAGATCTGGGAGGGAAATCACTGCTCC	NcoI BglII-BamHI
pRK5	FLAG-TUBB	Forward Reverse	CCAGAATTCGCCACCATGGACTACAAGGACGA TGACGATAAGATGAGGGAAATCGTGCACATG TGACTCGAGTGAGGTGATGGGGGCTCTGCC	EcoRI XhoI
pRK5	FLAG-C-TUBB1	Forward Reverse	GCCGGATCCTTCCGGGGCAAGATGTCCACC TCTCCTAGGGTTAATGTCCCTTATCTTCTG	BamHI AvrII
pRK5	FLAG-TUBB1	Forward Reverse	AGAGGATCCATGCGTGAAATTGTCCATATT TCTCCTAGGGTTAATGTCCCTTATCTTCTG	BamHI AvrII
pRK5	FLAG-TUBB2A	Forward Reverse	ACCGAATTCGCCACCATGGACTACAAGGACGA TGACGATAAGATGCGCGAGATCGTGCACATC CTACTCGAGCACGATTGATCTGAGAAGTTT	EcoRI XhoI
pRK5	FLAG-TUBB2B	Forward Reverse	ACCGAATTCGCCACCATGGACTACAAGGACGA TGACGATAAGATGCGCGAGATCGTGCACATC CTACTCGAGCACGATTGATCTGAGAAGTTT	EcoRI XhoI
pRK5	FLAG-TUBB2C	Forward Reverse	ACCGAATTCGCCACCATGGACTACAAGGACGA TGACGATAAGATGCGCGAGATCGTGCACATC CTACTCGAGCACGATTGATCTGAGAAGTTT	EcoRI XhoI
pRK5	FLAG-TUBB4	Forward Reverse	GCTGAATTCGCCACCATGGACTACAAGGACGA TGACGATAAGATGCGGGAGATCGTGCACCTG TCGAAGCTTCAGGTGGGAAGCGATGGGAGC	EcoRI HindIII
pRK5	FLAG-TUBB6	Forward Reverse	GCGGGATCCATGAGGGAGATCGTGCACATC CTCGAATTCGACTATCCATCGATCTCCTCT	BamHI EcoRI

Table 8. Cytoskeletal construct information. Primer oligonucleotides used in the cloning of plasmid constructs**.** C- indicates C terminus. Protein is full-length unless indicated.

2.1.2 Electrophoresis and gel extraction

Post PCR, the size of the cDNA fragment was confirmed by agarose gel alectrophoresis alongside a protein ladder. If correct, the PCR band was extracted and purified.

Depending on the size, PCR products were run on a 1-2% (w/v) agarose gel composed of UltraPURE electrophoresis grade agarose (Invitrogen) in 1 x TAE buffer (40 mM Tris-base, 20 mM acetic acid, 1 mM EDTA, pH 8). The solution was heated at 600 W for 2 minutes and allowed to cool before 10 µl of SYBR Safe DNA Gel Stain (Invitrogen) was added. This dye binds

the minor groove of double stranded DNA, absorbs blue fluorescent light and emits green light, enabling visualisation of the PCR product. The solution was added to a gel frame, containing a comb to form the wells, and allowed to set for 30 minutes.

The samples were combined with a loading buffer (0.25% (w/v) bromophenol blue, 40% (w/v) sucrose) and run alongside a 1 kb molecular weight marker (Invitrogen) at 100 V for 30-45 minutes. An Ingenius 3 bio-imaging system and Genesnap software (Syngene) were used to visualise the cDNA. A successful PCR revealed a band at the expected molecular weight. This band was excised from the gel using a scalpel and a Safe Imager blue light transilluminator (Invitrogen).

The gel fragment containing the PCR product was purified using the Qiaquick gel extraction kit (Qiagen) according to the manufacturers instructions. Briefly: the agarose was dissolved in three gel volumes of buffer QG (high salt solubilisation and binding buffer) for 10 minutes at 50°C. One gel volume of isopropanol was added to precipitate the DNA and the solution applied to a QiaQuick spin column matrix. The DNA bound the column during centrifugation (16100 x g for 1 minute) and residual agarose and impurities were removed during the subsequent centrifugations with 500 µl buffer QG and 750 µl buffer PE ethanol wash. A final spin ensured all ethanol was removed before the cDNA was eluted in 25 µl of EB (elution buffer) during a final centrifugation step.

2.1.3 Restriction digest of the purified PCR product

Restriction endonucleases were used to insert the amplified cDNA into the relevant vector. They are listed in tables 7 and 8, alongside their respective primers. These 'cut' the cDNA at specific sites inserted into the primer and the vector multiple cloning site, leaving exposed compatible ends.

A standard digest included 25 µl of purified PCR product, 1 µl of each restriction enzyme, 3 µl of enzyme buffer (determined by the enzymes used), totalling 30 µl. To 2 µl of 0.5 µg/µl cloning vector, 1 µl of each restriction enzyme, 2 µl enzyme buffer and 14 µl dH_2O were added, totalling 20 µl. The tubes were incubated at 37°C for 2 hours.

2.1.4 Phenol chloroform extraction and ligation

Phenol chloroform extraction is used to purify the cDNA/vector. A DNA ligase then anneals the 'sticky ends' of the insert and vector by catalysing the formation of a covalent bond between

the 5' phosphate and 3' hydroxyl groups of the insert and vector DNA, forming a recombinant vector.

dH_2O was added to the digests to a total of 100 µl. 100 µl phenol chloroform isoamyl alcohol (Invitrogen) was then added, dividing the digests into aqueous (DNA) and organic phases (enzymes, buffers and impurities). Following a 10 minute centrifugation at 16100 x g, the upper aqueous phase was added to new tubes containing 250 µl 96% ethanol, 10 µl 3M sodium acetate and 1 µl 20 µg/µl glycogen. This mixture precipitated the DNA. The tubes were mixed and kept on dry ice for 30 minutes. After a 10 minute centrifugation at 16100 x g, the supernatant was discarded and the pellets washed in 250 µl 80% ethanol. After ensuring all the ethanol was removed, the vector was eluted in 50 µl EB and the insert eluted in 14 µl EB.

7 µl of insert and 1 µl of vector were combined with 1 µl of ligation buffer (200 mM Tris-HCl, 50 mM MgCl, 50 mM dithiothreitol, 500 µg/ml BSA-Invitrogen) and 1 µl of T4 DNA ligase (Invitrogen). The solution was incubated overnight at 4°C.

2.1.5 Competent cell preparation and transformation

E.coli cells are described as competent when calcium chloride and heat shock enables a transient DNA uptake. The calcium chloride neutralises the repulsion between the negatively charged DNA and cell membrane, while the heat shock induces a thermal gradient, inducting the plasmid DNA into the cell. This is utilised to insert the recombinant vector into *E.coli* cells. The vector contains an antibiotic resistance gene, conferring resistance on those cells which have been transformed. The cells are grown on an antibiotic selection plate overnight, forming colonies.

One Shot Top 10 *E. coli* cells (Invitrogen) were thawed and streaked on Luria-Bertrani (LB-Invitrogen) agar plates and incubated at 37°C overnight. A single colony was added to 2.5ml LB medium and shaken overnight at 37°C. This culture was then transferred to 200ml LB and shaken at 37°C until an OD_{600} of 0.95 AU was reached. The culture was centrifuged for 5 minutes at 4°C and the pellet resuspended in 10 ml 80 mM $CaCl_2$/50 mM $MgCl_2$ solution thrice. Following a final centrifuge step, the cells were suspended in 5.5 ml 0.1 M $CaCl_2$ and 5.5 ml 50% glycerol and frozen in liquid nitrogen before long-term storage at -80°C.

To transform the competent cells, 5 µl of recombinant vector were combined with 100 µl of competent cells and incubated on ice. A 45 second heat shock at 42°C permitted the vector to enter the cells before the cells were returned to ice for 2 minutes. The bacteria were then

combined with 250 µl preheated LB medium and incubated for 1 hour at 37°C, enabling expression of the antibiotic resistance gene, before transferral to an agar plate containing the appropriate selective antibiotic and an overnight incubation at 37°C.

2.1.6 Low-quantity plasmid DNA extraction (miniprep)

A single colony was 'picked' and grown overnight in a small-scale overnight bacterial culture before being lysed to extract the plasmid DNA. The plasmid extraction, or 'miniprep' involved lysing the cell using a strongly alkaline buffer, releasing the plasmid DNA, selectively binding it to a spin column silica membrane then eluting the purified plasmid DNA.

An individual bacterial colony from an agar plate was added to 3ml of selective LB medium containing 100 µg/ml ampicillin or 50 µg/ml kanomycin (depending on the antibiotic resistance of the plasmid). This was shaken at 37°C overnight. The plasmid DNA was extracted from the bacteria using a QIAprep miniprep kit (Qiagen) according to the manufacturers instructions. Briefly: 2 ml of the culture was centrifuged at 16100 x g for 3 minutes and the pellet resuspended in 250 µl resuspension buffer P1 (10 mM EDTA, 100 µg/ml RNase A, 50 mM Tris-HCl, pH 8.0) then combined with 250 µl lysis buffer P2 (200 mM NaOH, 1% SDS), followed by 350 µl neutralisation buffer N3 (3M CH_3CO_2K, pH 5.5). After mixing, the solutions were centrifuged for 10 minutes at 16100 x g. The supernatant was decanted into a QIAprep spin column, washed with 750 µl buffer PE, residual wash buffer removed and the recombinant vector eluted into a clean microcentrifuge tube with 50 µl EB.

2.1.7 Analysis and sequencing

A final diagnostic digest using the appropriate restriction enzymes confirmed that the plasmid DNA contained the correct-sized insert. Sequencing of this DNA then confirmed that the sequence was correct and in-frame.

For the diagnostic digest, 5 µl of miniprep product was added to 3 µl dH_2O, 0.5 µl of each restriction enzyme and 1 µl of the appropriate enzyme buffer. Following a 1.5 hour incubation, the solution was run on an agarose gel and the size detected as described previously. The concentration of minipreps with the correct sized insert was confirmed using a nanodrop spectrophotometer (Thermo Scientific) and 30 µl of 20 ng/µl plasmid DNA was sent for sequencing.

Sequencing of the DNA was performed by DNA Sequencing & Services (MRCPPU, College of

Life Sciences, University of Dundee, Scotland, (www.dnaseq.co.uk) using Applied Biosystems Big-Dye version 3.1 on an Applied Biosystems model 3730 automated capillary DNA sequencer (www.dnaseq.co.uk). The sequencing primers are listed in table 9.

Vector	Direction	Primer name	Primer
pACT2	Forward	Gal4 AD	AATACCACTACAATGGATGATGTAT
	Reverse	pACT2 Rev	GAGGTTACATGGCCAAGAT
pDS	Forward	LexA	CAGCAGAGCTTCACCATTGAAGGG
	Reverse	pDS Rev	CGGAATTAGCTTGGCTGCAAG
pRK5	Forward	SP6	CAGCGAGCTCTAGCATTTAGG
	Reverse	pRK5 Rev	GGACAAACCACAACTAGAATGC

Table 9. Sequencing primers. The primers used to sequence plasmid DNA. They are nucleotide sequences adjacent to the multiple cloning site.

The sequences were compared with reference sequences using Sequencher® (version 5.0 sequence analysis software, Gene Codes Corporation, http://www.genecodes.com).

2.1.8 Large-quantity plasmid DNA extraction (maxiprep)

The QIAprep maxiprep kit (Qiagen) was used to produce large-quantity DNA stocks of plasmid constructs containing the correct insert, following manufacturers instructions. Briefly: 200 µl of the small-scale overnight culture was added to a flask containing 200 ml LB/200 µl antibiotic (concentrations as described in section 2.1.7) and shaken at 37°C overnight. The culture was centrifuged at 4°C, 2880 x g for 15 minutes. The pellet was resuspended in 10 ml pre-chilled buffer P1 (50 mM Tris-HCl pH 8.0, 10 mM EDTA, 100 µg/ml RNase A), 10 ml lysis buffer P2 (200 mM NaOH, 1% (w/v) SDS) and 10 ml neutralisation buffer P3 (3 mM CH_3CO_2K pH 5.5). The lysate was incubated for 10 minutes in a QIAfilter cartridge to allow the DNA and bacterial debris to separate while the HiSpeed maxi tip was equilibrated in 10 ml buffer QBT (750 mM NaCl, 50 mM MOPS pH 7.0, 15% (v/v) isopropanol, 0.15% (v/v) Triton X-100). The DNA solution from the lysate was added to the maxi tip, where the DNA bound to the resin before being washed by 60 ml buffer QC (1.0 M NaCl, 50 mM MOPS (pH 7.0), 15% (v/v) isopropanol). The DNA was eluted in 15 ml buffer QF (1.25 M NaCl, 50 mM Tris-HCl (pH 8.5), 15% (v/v) isopropanol) and precipitated with 10.5ml isopropanol. After a 5 minute incubation, it was poured into a 30ml syringe and pushed through a QIAprecipitator maxi module, binding the DNA to the precipitator. Following a 70% ethanol wash and two plunger insertions to clear the ethanol from the maxi module, the DNA eluted with 300 µl EB.

2.1.9 Site-directed mutagenesis

Site-directed mutagenesis is the alteration of a specific residue or region within a circular plasmid cDNA sequence using a standard PCR protocol. A pair of forward and reverse primers, identical to the template sequence except at the codon(s) undergoing mutagenesis anneal to the cDNA sequence and are amplified using PCR. The polymerase extends the sequence from the primers, incorporating the changed residues into the new DNA sequence.

The mutagenesis PCR set-up was as described under section 2.1.1, but with a lower annealing temperature as the Tm was reduced due to the introduction of unpaired nucleotides. This was typically 50°C, though could be as low as 35°C during mutagenesis of multiple residues, such as the LRRK2 RocCOR alanine block scan.

Following the PCR reaction, the template cDNA was digested using Dpn1 (New England Biolabs). This selectively digests methylated DNA. As methylation occurs *in vivo*, only the template cDNA which was previously amplified using bacterial competent cells was digested, preventing the unmutated template DNA being transformed.

1 µl of Dpn1 was added to the PCR product and incubated at 37°C for 2 hours. The presence of a plasmid at the correct size was confirmed in an agarose gel (described in section 2.1.2)
The mutagenesis primers used are listed below:

Vector	Gene variant	Primer direction	Primer (5'-3')
pACT2	C-TUBA1A ΔB9-10 loop	Forward Reverse	AACTACCAGCCTCCCGCCAAGGTGCAGCGT ACGCTGCACCTTGGCGGGAGGCTGGTAGTT
pACT2	C-TUBB A364D	Forward Reverse	GGCCTCAAGATGGACGTCACCTTCATT AATGAAGGTGACGTCCATCTTGAGGCC
pACT2	C-TUBB A364E	Forward Reverse	GGCCTCAAGATGGAAGTCACCTTCATT AATGAAGGTGACTTCCATCTTGAGGCC
pACT2	C-TUBB A364S	Forward Reverse	GGCCTCAAGATGTCAGTCACCTTCATT AATGAAGGTGACTGACATCTTGAGGCC
pACT2	C-TUBB K362S	Forward Reverse	CCTCGTGGCCTCTCGATGGCAGTCACC GGTGACTGCCATCGAGAGGCCACGAGG
pACT2	C-TUBB-K362R	Forward Reverse	CCTCGTGGCCTCAGGATGGCAGTCACC GGTGACTGCCATCCTGAGGCCACGAGG
pACT2	C-TUBB1 S362K	Forward Reverse	CCCCGGGGGCTGAAGATGGCCGCCACC GGTGGCGGCCATCTTCAGCCCCCGGGG
pACT2	C-TUBB1 S362R	Forward Reverse	CCCCGGGGGCTGAGGATGGCCGCCACC GGTGGCGGCCATCCTCAGCCCCCGGGG
pACT2	C-TUBB1 N371S	Forward Reverse	TTCATTGGCAACAGCACGGCCATCCAA TTGGATGGCCGTGCTGTTGCCAATGAA
pACT2	C-TUBB4 A364D	Forward Reverse	GGCCTGAAGATGGACGCGACCTTCATC GATGAAGGTCGCGTCCATCTTCAGGCC
pACT2	C-TUBB4 A364E	Forward Reverse	GGCCTGAAGATGGAAGCGACCTTCATC GATGAAGGTCGCTTCCATCTTCAGGCC
pACT2	C-TUBB4 A364S	Forward Reverse	GGCCTGAAGATGTCCGCGACCTTCATC GATGAAGGTCGCGGACATCTTCAGGCC
pACT2	C-TUBB4 K362S	Forward Reverse	CCCCGCGGCCTGTCGATGGCCGCGACC GGTCGCGGCCATCGACAGGCCGCGGGG
pACT2	C-TUBB4-K362R	Forward Reverse	CCCCGCGGCCTGAGGATGGCCGCGACC GGTCGCGGCCATCCTCAGGCCGCGGGG
pACT2	C-TUBB4 B9-10 loop insert	Forward Reverse	GTGCGACATCCCGCCCACTGTGGTGCC TGGTGGAGACCTGCGCGGCCTGAAGATG CATCTTCAGGCCGCGCAGGTCTCCACC AGGCACCACAGTGGGCGGGATGTCGCAC
pACT2	C-TUBB6 A364D	Forward Reverse	GGCCTGAAGATGGACTCCACCTTCATC GATGAAGGTGGAGTCCATCTTCAGGCC
pACT2	C-TUBB6 A364E	Forward Reverse	GGCCTGAAGATGGAATCCACCTTCATC GATGAAGGTGGATTCCATCTTCAGGCC
pACT2	C-TUBB6 A364S	Forward Reverse	GGCCTGAAGATGTCCTCCACCTTCATC GATGAAGGTGGAGGACATCTTCAGGCC
pACT2	C-TUBB6 S365A	Forward Reverse	CTGAAGATGGCCGCCACCTTCATCGGC GCCGATGAAGGTGGCGGCCATCTTCAG
pACT2	C-TUBB6 F398Y	Forward Reverse	TTCCTGCACTGGTACACGGGTGAGGGC GCCCTCACCCGTGTACCAGTGCAGGAA
pACT2	C-TUBB6 P320R	Forward Reverse	GATCTTCCGCGGGCGCATGTCCATGAAG CTTCATGGACATGCGCCCGCGGAAGATC
pACT2	C-TUBB6 B9-10 loop insert	Forward Reverse	GTGCGACATCCCGCCCACTGTGGTGCCT GGTGGAGACCTGCGCGGCCTGAAGATG CATCTTCAGGCCGCGCAGGTCTCCACCA GGCACCACAGTGGGCGGGATGTCGCAC
pACT2	C-TUBB6 K362S	Forward Reverse	CCCCGCGGCCTGTCGATGGCCTCCACC GGTGGAGGCCATCGACAGGCCGCGGGG
pACT2	C-TUBB6-K362R	Forward Reverse	CCCCGCGGCCTGAGGATGGCCTCCACC GGTGGAGGCCATCCTCAGGCCGCGGGG

Table 10. Site-directed mutagenesis primers.

An alanine block scan was performed, in which blocks of five amino acids were replaced with alanines, sequentially throughout the region of interest within the RocCOR domain. This is a common technique to identify regions involved in protein-protein interactions. The primers used are listed in table 11.

pDS LRRK2 RocCOR alanine scan residues		Primer direction	Primer (5'-3')
1	**1328-1332**	Forward Reverse	CAACAGCGATTAAAAGCTGCAGCTGCAGCTAACCGAATGAAACTT AAGTTTCATTCGGTTAGCTGCAGCTGCAGCTTTTAATCGCTGTTG
2	**1333-1337**	Forward Reverse	AAGGCTGTGCCTTATGCTGCAGCTGCAGCTATGATTGTGGGAAAT ATTTCCCACAATCATAGCTGCAGCTGCAGCATAAGGCACAGCCTT
3	**1338-1342**	Forward Reverse	AACCGAATGAAACTTGCTGCAGCTGCAGCTACTGGGAGTGGTAAA TTTACCACTCCCAGTAGCTGCAGCTGCAGCAAGTTTCATTCGGTT
4	**1343-1347**	Forward Reverse	ATGATTGTGGGAAATGCTGCAGCTGCAGCTACCACCTTATTGCAG CTGCAATAAGGTGGTAGCTGCAGCTGCAGCATTTCCCACAATCAT
5	**1348-1352**	Forward Reverse	ACTGGGAGTGGTAAAGCTGCAGCTGCAGCTCAATTAATGAAAACC GGTTTTCATTAATTGAGCTGCAGCTGCAGCTTTACCACTCCCAGT
6	**1353-1357**	Forward Reverse	ACCACCTTATTGCAGGCTGCAGCTGCAGCTAAGAAATCAGATCTT AAGATCTGATTTCTTAGCTGCAGCTGCAGCCTGCAATAAGGTGGT
7	**1358-1362**	Forward Reverse	CAATTAATGAAAACCGCTGCAGCTGCAGCTGGAATGCAAAGTGCC GGCACTTTGCATTCCAGCTGCAGCTGCAGCGGTTTTCATTAATTG
8	**1363-1367**	Forward Reverse	AAGAAATCAGATCTTGCTGCAGCTGCAGCTACAGTTGGCATAGAT ATCTATGCCAACTGTAGCTGCAGCTGCAGCAAGATCTGATTTCTT
9	**1368-1372**	Forward Reverse	GGAATGCAAAGTGCCGCTGCAGCTGCAGCTGTGAAAGACTGGCCT AGGCCAGTCTTTCACAGCTGCAGCTGCAGCGGCACTTTGCATTCC
10	**1373-1377**	Forward Reverse	ACAGTTGGCATAGATGCTGCAGCTGCAGCTATCCAAATAAGAGAC GTCTCTTATTTGGATAGCTGCAGCTGCAGCATCTATGCCAACTGT
11	**1378-1382**	Forward Reverse	GTGAAAGACTGGCCTGCTGCAGCTGCAGCTAAAAGAAAGAGAGAT ATCTCTCTTTCTTTTAGCTGCAGCTGCAGCAGGCCAGTCTTTCAC
12	**1383-1387**	Forward Reverse	ATCCAAATAAGAGACGCTGCAGCTGCAGCTCTCGTCCTAAATGTG CACATTTAGGACGAGAGCTGCAGCTGCAGCGTCTCTTATTTGGAT
13	**1388-1392**	Forward Reverse	AAAAGAAAGAGAGATGCTGCAGCTGCAGCTTGGGATTTTGCAGGT ACCTGCAAAATCCCAAGCTGCAGCTGCAGCATCTCTCTTTCTTTT
14	**1393-1397**	Forward Reverse	CTCGTCCTAAATGTGGCTGCAGCTGCAGCTCGTGAGGAATTCTAT ATAGAATTCCTCACGAGCTGCAGCTGCAGCCACATTTAGGACGAG
15	**1398-1402**	Forward Reverse	TGGGATTTTGCAGGTGCTGCAGCTGCAGCTAGTACTCATCCCCAT ATGGGGATGAGTACTAGCTGCAGCTGCAGCACCTGCAAAATCCCA

Table 11. Primers used in the LRRK2 RocCOR alanine scan.

2.2 Yeast two-hybrid

The yeast two-hybrid assay detects protein-protein interactions. It is a system that can be used to screen libraries for interactors to known proteins and does not require the full-length protein, thus it can be used for functional characterisation of subdomains or identification of residues crucial to interactions. The use of a reporter gene system enables detection of weak or transient interactions which may not otherwise be detectable (Fields and Song, 1989; Van Criekinge and Beyaert 1999).

Transcription of a gene is initiated following activation of an upstream activation site (UAS) by a transcription factor. Transcription factors comprise an activation domain and a binding domain and both must be present to initiate transcription, however some are interchangeable. The *S. cerevisiae* Gal4 binding domain combined with an *E. coli* LexA activation domain are able to initiate transcription of the *LacZ* gene. This *E. coli* gene has been inserted into the yeast DNA immediately after the Gal4 promotor and is used as a reporter gene. It encodes β-galactosidase, an enzyme that cleaves X-gal into galactose and 5-bromo-4-chloro-3-hydroxyindole which rapidly oxidises into the blue, insoluble 5,5'-dibromo-4,4'-dichloro-indigo. Yeast colonies incubated in a solution containing X-gal will turn blue if *LacZ* transcription occurs.

In addition to this, a second reporter gene under control of the Gal4 promotor is used; *HIS3*. This encodes imidazole glycerol-phosphate dehydratase, which catalyses the sixth step in histidine biosynthesis, an essential amino acid. However expression of *HIS3* is leaky, some background activation occurs. Thus the inhibitor 3-amino-1,2,4-triazole (3-AT) is also used. The amount varies depending on the strain and is balanced; too much hides weak interactions whereas too little leads to false positives.

Yeast two-hybrid experiments fuse one protein of interest to the LexA binding domain (the 'bait') and the other to the Gal4 activation domain (the 'prey'). If these two proteins interact, they bring the binding and activation domains into close proximity, initiating transcription of the reporter genes (figure 6). Each interaction is tested twice per experiment. The transfection control (TC) plates contain histidine; growth occurs on all plates but only interactors change colour in the X-gal assay. Nutritional selection (NS) plates do not contain histidine, growth occurs only if the *HIS3* gene is expressed, i.e. the proteins interact. The yeast is under greater pressure but this can lead to clearer results as the yeast is forced to express enough *HIS3* to survive.

In semi-quantitative experiments, the colour change is not measured but a visual comparison can indicate differences in binding strength. In quantitative yeast two-hybrid, colour change, and therefore interaction strength, is measured.

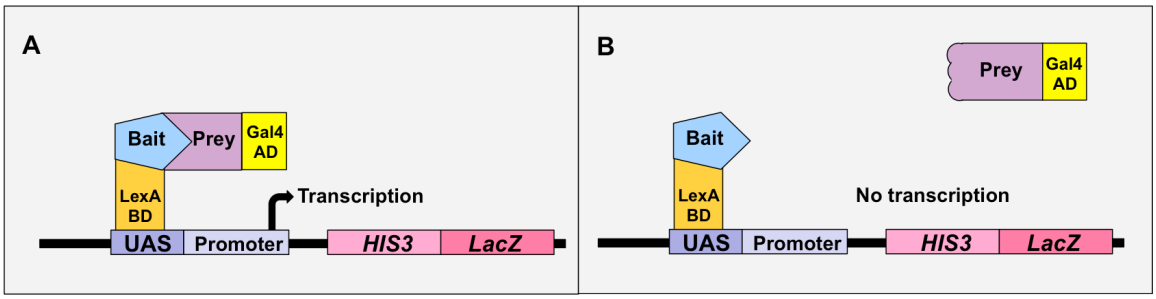

Figure 6. The yeast two-hybrid system. A. The protein of interest is fused to the DNA binding domain (BD). The potential interactor is fused to the AD activation domain (AD). If the two proteins of interest bind, the activation domain is bought into proximity of the promoter and a polymerase is recruited, leading to transcription of the reporter genes. **B.** If they do not associate, transcription is not initiated**.**

2.2.1 Semi-quantitative yeast two-hybrid

L40 yeast was used. This strain of *S. cerevisiae* is missing functional genes encoding leucine (*LEU2*) and tryptophan (*TRP1*). The *LEU2* and *TRP1* genes are each encoded by a different vector, one on the bait and one on the prey; only yeast cells successfully transformed with both vectors are able to grow on transformation control plates lacking leucine and tryptophan (-LT). Where growth occurrs, both transformants have been successfully inserted into the yeast. Nutritional selection plates also lack histidine (–LTH) as described above.

Colonies were grown and transferred to filter paper, freeze-fractured in liquid nitrogen then tested for β-galactosidase activity. Colour change of the colonies from white to blue, where the negative controls were still unchanged, indicated an interaction.

Recombinant pDS and pACT2 plasmids were constructed containing various LRRK2 domains and tubulin C-termini (see table 8 for the cytoskeletal construct primer list). LRRK2 RocCOR domain cDNA was cloned into the bait vector pDS, which contains the *LexA* and *TRP1* genes while tubulin cDNA was cloned into the prey vector pACT2, which includes the *GAL4* and *LEU2* genes.

2.2.1.1 L40 cell line maintenance

A frozen stock of L40 yeast (kept at -80°C) was thawed and streaked onto fresh agar plates using an innoculation loop. The agar plates were made using YPD agar medium (2% (w/v) agar, 1% (w/v) yeast extract, 2% (w/v) peptone and 2% (w/v) dextrose-Clontech), supplemented with 0.4 mM adenine. The plates were incubated at 30°C for 3 days, until there were individual yeast colonies of approximately 2 mm in diameter. The plates were then sealed and stored at 4°C. A single colony of yeast was re-streaked once per fortnight onto a fresh YPD/adenine plate.

2.2.1.2 Preparing and plating the yeast

The yeast two-hybrid protocol is based on the original method described by Gietz et al (Gietz et al., 1995). A single L40 yeast colony was shaken at 30°C overnight in 100 ml YPD. The following morning enough yeast was transferred to a fresh YPD/adenine culture (10 ml yeast per transformation) to give an OD_{600} of 0.25 AU. This was grown at 30°C until it reached an OD_{600} of 0.6 AU, i.e., growth was occurring exponentially. The yeast was harvested by centrifugation at 1620x g for 3 minutes and the pellets resuspended into a single suspension in 25 ml dH_2O. This was centrifuged in the same way and followed by two resuspension/centrifugations in 25 ml 1x Lithium Acetate/Tris-EDTA (LiAC/TE) (10 mM Tris-HCL, 1 mM EDTA, 100 mM LiAC). Finally the pellet was resuspended in LiAC/TE at 1% of the original YPD/adenine culture volume, giving a cell density of approximately $1x10^9$ cells/ml. 100 µl of the yeast suspension was combined with 1 µg of bait, 1 µg of prey and 5 µg herring sperm carrier DNA. The herring sperm had previously been denatured by boiling at 99°C for 5 minutes and cooling to 4°C for 5 minutes, twice in succession. Next, 600 µl of polyethylene glycol (PEG) in LiAC/TE solution (50% (v/v) PEG, 1x LiAC, 1x TE) was added. PEG acted as a spacer, forcing the DNA and yeast cells into close proximity. The solutions were shaken for 30 minutes at 30°C before a 20 minute heat shock enabled the DNA to cross the cell membranes. The yeast was pelleted by a short centrifugation, the PEG/LiAC/TE removed and the pellet resuspended in 100 µl dH_2O. 60 µl of this yeast solution was plated on NS plates (46.7 g/L minimal selective drop-out base, 0.62 g/L -leucine/-tryptophan/-histidine dropout supplement-Clontech), 40 µl onto TC plates (46.7 g/L minimal selective drop-out base, 0.64 g/L -leucine/-tryptophan dropout supplement, Clontech). The plates were incubated at 30°C until the yeast showed sufficient growth, usually 3 days for the TC plates and 5 days for the NS plates.

2.2.1.3 The β-galactosidase assay

Growth on all TC plates indicated that both the bait and prey constructs were successfully transformed into the yeast cells. When there was sufficient growth, the yeast colonies were transferred to a circle of 54-Whatman filter paper (Fisher) and freeze-fractured twice in liquid nitrogen to force open the cells and release β-galactosidase. X-gal solution was prepared and stored wrapped in tin foil to protect it from light exposure. Each plate required 2 ml X-gal solution (2 mg X-gal (5-Bromo-4-chloro-3-indolyl-B-D-galactopyranoside), 20 µl N,N-dimethylformadine, 2 ml Z-buffer (60 mM Na_2HPO_4, 40 mM $NaH_2PO_4.H_2O$, 10 mM KCl and 0.1 mM $MgSO_4.7H_2O$) and 5.4 µl β-mercaptoethanol). The filter-paper/yeast colonies were incubated at 37°C in X-gal solution until the yeast colonies had turned blue, then left to dry in a fume hood.

2.2.2 Quantitative yeast two-hybrid

Quantitative yeast two-hybrid uses chlorophenol red-β-D-galactopyranoside (CPRG) hydrolysis, another β-galactosidase substrate, to measure the intensity of protein-protein interactions. The rate at which CPRG hydrolysis turns the solution from yellow to red indicates LacZ expression; meaning colour change is proportionate to interaction strength.

2.2.2.1 Cell preparation

The protocol is adapted from that described by Ramamoorthy and colleagues (1997). The yeast was transformed and plated as described under section 2.2.1, excepting that only TC agar plates were made. A single colony was shaken overnight in 10 ml selective medium (26.7 g/L minimal SD base, 0.64 –leucine/–tryptophan drop-out supplement and 0.4 mM adenine). The next morning the OD_{600} of each suspension was measured and the yeast transferred to 10ml fresh medium with an OD_{600} of 0.25 AU. This was grown until the concentration reached 0.4-0.6 AU, when the solutions were pelleted by a 3 minute centrifugation at 1620 x g and resuspended in 1 ml resuspension buffer. This contained 50 ml Z-buffer (as previously), one complete mini protease inhibitor cocktail tablet and 40 mM β-mercaptoethanol. Resuspended yeast was then added to resuspension buffer to a final OD_{600} of 0.035 AU in 1 ml buffer. 12 µl 0.1% SDS (w/v) and 15 µl 99% chloroform were added to each tube and the solutions shaken at 30°C for 15 minutes. The SDS and chloroform broke down the cell walls and permeabilised the cells to release the β-galactosidase. 10 µl CPRG was added to each tube, shaken well and 200 µl added in triplicate to a 96 well flat-bottomed transparent plate.

2.2.2.2 Quantification and analysis

The absorbance at OD_{540} (colour intensity, indicating interaction strength) and OD_{620} (optical density, indicating number of yeast cells) of each well were measured using a Multiskan MULTISOFT 220V microplate photometer (Labsystems). After dividing the OD_{540} by the $OD_{620,}$ subtracting the negative controls (yeast transformed with the bait but an empty prey vector), gave the sample interaction strength per unit of yeast cells. The LRRK2-mutant interaction strength was then expressed as a percentage of the LRRK2-wild-type interaction strength and significance assessed using either the two-sample equal variance or paired Student's paired t-test for statistical significance. Combined data from a minimum of three independent experiments was used. p values are indicated (*, $p < 0.05$; **, $p < 0.01$; ***, $p<0.001$). Error bars represent the standard error of the mean (SEM).

2.3 Mammalian cell culture

Human embryonic kidney 293 (HEK293) and human neuroblastoma SH-SY5Y cells were

purchased from the European collection of cell cultures. The SH-SY5Y cells overexpressing LRRK2 were a gift from Jean-Marc Taymans (KU Leuven) and made by lentiviral transduction, while the *Lrrk2* knock out and wild-type mouse embryonic fibroblasts (MEFs) were a gift from Huaibin Cai (NIH). They were derived from the dorsal skin of postnatal day 0 (P0) *Lrrk2* wild-type or knock-out mouse pups and immortalised by transduction using the SV40 T antigen. The HEK and MEF cells were cultured in Dulbecco's modified eagle medium (DMEM) (4.5g/L glucose, L-glutamine, pyruvate (Invitrogen)) supplemented with 10% (v/v) foetal bovine serum (FBS-PAA) and 1% (v/v) penicillin-streptomycin (10000U/ml penicillin, 10mg/ml streptomycin, Invitrogen. This will henceforth be referred to as DMEM+). The SH-SY5Y cells were cultured in DMEM supplemented with 1x non-essential amino acids (Gibco), 15% (v/v) FBS and 1% (v/v) gentamycin. All cell handling occurred in a class II laminar flow hood using sterile technique. Cells were incubated at 5% CO_2, 37°C in a Sanyo CO_2 incubator.

2.3.1 Cell line maintenance

All cell lines were cultured in 75 cm^2 flasks. When the cells were fully confluent, they were passaged, usually every 72 hours. The medium was removed and the cells washed in 10 ml HBSS before the addition of 500 µl trypsin/EDTA. The enzyme trypsin cleaves the peptide bonds, causing cells to dissociate from the flask whereas the calcium/magnesium chelator EDTA inhibits cell adhesion. After ensuring all cells were covered, they were left for a few minutes to detach from the base of the flask. 9.5ml of the appropriate medium was then added to neutralise the trypsin. The cells were diluted 1:3 (SH-SY5Y and MEF cells) or 1:10 (HEK cells) into a new flask with fresh medium.

2.3.2 Cell seeding and transfection

Cells were detached as described under section 2.3.1. They were then centrifuged at 140 x g for 2.5 minutes. The resulting pellet was resuspended in 1 ml of medium, 10 µl of which was further diluted 10-fold. A cover slip was placed on the Neubauer haemocytometer (Hawksley) and 10 µl of the diluted cell suspension was loaded into the space between the cover slip and haemocytometer. The cells in a 1 mm^2 square were counted and multiplied by 10^5 to account for the dilution steps. 10 cm culture dishes were seeded with 2 x 10^6 cells (used in immunoprecipitations). Cells were seeded as in table 12.

Dish size	Cells seeded	DNA transfected	Fugene	OptiMEM
10 cm	2 x 10^6	8 µg	16 µl	400 µl

6 cm	7.2 x 10^5	2 µg	4 µl	100 µl

Table 12. Typical experimental conditions for transfection of 10 cm and 6 cm dishes.

Dishes were transfected when cell confluency reached 60-70%. Fugene HD transfection reagent (Promega) was used to transiently transfect the cells. This is a non-liposomal transfection reagent which complexes with the plasmid to form micelles which transport it across cell membranes. The transfected DNA is then expressed by the cell.

Eight µg DNA was transfected into 10 cm dishes. For co-transfections, this was split between the plasmids. LRRK2 is difficult to transfect due to its large size, therefore 5 µg of the LRRK2 construct was co-transfected with 3 µg of the tubulin construct. The DNA was diluted in 600 µl OptiMEM reduced serum medium (Invitrogen), then 2 µl Fugene transfection reagent was added per 1 µg DNA as per the manufacturers instructions (table 12).

The DNA-Fugene-OptiMEM mixture was incubated for 15 minutes to allow DNA:fugene complexes to form, then gently added to the plate and mixed well. The plates were then returned to the incubator.

2.3.3 Protein extraction

Cells were harvested 24-48 hours post transfection. The medium was removed and the cells washed twice with 2ml ice-cold phosphate buffered saline (PBS) to remove any remaining medium. 600 µl of lysis buffer (HEK cells: 150 mM NaCl, 50 mM Tris-pH 7.5, 5mM EDTA-pH 8.0, 0.25% (v/v) NP-40 and complete mini protease inhibitor cocktail (1 tablet per 10ml), MEF cells: (100 mM NaCl, 50 mM Tris, pH 7.5, 1% (v/v) Triton X-100, 1× complete protease inhibitor mixture (Roche), and 1× Halt phosphatase inhibitor mixture (Pierce)) was added to each plate. Cells were detached using a pre-chilled cell scraper and they were transferred to a pre-chilled eppendorf tube and kept on ice for 20 minutes. A 10 minute, 16100 x g centrifuge at 4°C pelleted the cell debris and the lysate was transferred to a fresh eppendorf tube.

2.3.4 Immunoprecipitation

Immunoprecipitations (IPs) purify target proteins from cell homogenates using specific antibodies. Electrophoretic separation, transfer to a membrane and probing with antibodies enables these proteins to be identified. Co-IPs further identify proteins which bound the target protein and were extracted and purified alongside. Both those interacting directly and as part of a complex are immunoprecipitated.

Constructs to be transfected contained a FLAG or myc sequence tag to aid immunoprecipitation and detection of the proteins. Beads with purified murine IgG_1 monoclonal antibodies covalently attached to the FLAG-tag (NYKNNNNK) of the transfected protein. Proteins not attached to the beads were removed and the target protein and interactors dissociated from the beads before detection by Western blot.

First the cells were harvested as described in section 2.3.3. 50 µl of cell lysate was removed and stored, to be run on the gel alongside the immunoprecipitated proteins. The rest of the lysate was used for the IP.

2.3.4.1 Protein immunoprecipitation

To prepare the anti-FLAG M2 affinity gel beads, 40 µl of gel (per plate) was washed in wash buffer (150 mM NaCl, 50 mM Tris-pH 7.5, 5mM EDTA-pH 8.0, 0.05% (v/v) NP-40). 1 ml PBS was added and the mixture placed on a turning disk at 4°C for 5 minutes. After a 3 minute, 16100 x g centrifugation, the supernatant was removed and replaced with fresh wash buffer. This was repeated twice. Following the final centrifugation and supernatant removal step, cell lysate containing 700 µg of protein was added to the beads. They were then mixed overnight on a turning disk at 4°C. The next day the beads were centrifuged and washed thrice with wash buffer (as described previously). The FLAG-tagged proteins were then dissociated from the beads by competitive elution with 3x FLAG peptide. 100 µl of 150ng/µl peptide was added to the beads and the mixture was shaken at room temperature for 30 minutes. After a final 1 minute, 16100 x g centrifuge, the supernatant collected and the protein concentration determined via a Bradford assay.

2.3.4.2 Bradford Assay

Bradford assays determine protein concentration in a sample by comparing the OD_{600} of the sample against that of a standard curve (Bradford, 1976). The brown Bradford reagent changes to blue when bound to protein due to a change in pH.

10 µl concentrations of bovine serum albumin (New England Biolabs), ranging from 0.1mg/ml to 1mg/ml, were diluted in lysis buffer to plot the standard curve. Meanwhile 1 µl of each cell lysate was diluted 10-fold in lysis buffer. 990 µl of Quickstart Bradford dye reagent (Biorad) was added to each tube and incubated for 15 minutes away from light exposure. The cell lysate OD_{600}s were then compared against the serum albumin dilutions.

One the concentrations were identified, approximately equal protein amounts were run on an SDS-PAGE gel, with their respective cell lysates, as described in section 2.4.

2.3.5 Immunocytochemistry

2.3.5.1 Poly-D-lysine coverslip coat

Prior to beginning the differentiation process, coverslips were autoclaved and coated with 1x Poly-D-lysine. This coating provided a uniform positive charge across the base of the coverslip which enabled the cells to attach and grow.

Pre-autoclaved coverslips were added to each well of a 6-well plate. They were then coated in ~500 µl 0.1 µg/µl poly-D-lysine (enough to cover the coverslip) and left for 1 hour. The poly-D-lysine was removed and the coverslips washed twice in sterile water and left in the hood while the water evaporated.

2.3.5.2 Cell seeding and SH-SY5Y differentiation

MEF and SH-SY5Y cells were detached as in section 2.3.1 and diluted in DMEM+ (MEF) and differentiation medium (SH-SY5Y-DMEM containing 1x non-essential amino acids, 5% (v/v) FBS, 1% (v/v) gentamycin and 10 µM retinoic acid) to a total of 2 x 10^5 cells per well in 2 ml medium. The cell suspension was added to the wells containing the pre-coated coverslips. The SH-SY5Y differentiation took place over 5 days, with the media replaced every 2 days. The MEF cells were lysed/fixed following a 24 hour incubation.

2.3.5.3 Fixation

This method of fixation was optimized for visualisation of the cytoskeleton and associated proteins (Ciani and Salinas, 2007). First the medium was removed and two quick washes made using PBS. Fixation solution (3% (w/v) formaldehyde, 0.2% (v/v) glutaraldehyde, 0.2% (v/v) Triton x 100, 10mM EGTA) was added to each well and the cells incubated at 37°C for 10 minutes.

After being washed twice in PBS (5 minutes each), the cells were quenched with 50 mM NH_4Cl in PBS for 10 minutes to neutralise the formaldehyde. The cells again underwent two PBS washes before permeabilisation by incubation in 0.1% Triton X-100 in PBS for 10 minutes. This allowed the antibodies to penetrate the cell membrane. After two more PBS washes, the cells were blocked in 1% (w/v) BSA in PBS and washed again.

2.3.5.4 Antibody labelling

Primary antibodies were diluted to the concentrations suggested by the manufacturer (table 13) in 1% BSA (w/v)/PBS. The cells were incubated in 100 µl of the relevant primary antibodies (see table 13 for antibodies and dilutions) for 2 hours at room temperature.

Antibody	Supplier	Host	Dilution
LRRK2	Epitomics Neuromab N139/6	Rabbit Mouse	1:100 1:50
Acetylated tubulin	Cell signalling Sigma 611-B1	Rabbit Mouse	1:100 1:100

Table 13. The primary antibodies used in Immunofluorescence. Immuno-tagged secondary antibodies raised against the relevant host (Invitrogen) along with phalloidin (F-actin) and DAPI (nuclei) were also used in cell labelling.

The solutions were added to a sheet of Parafilm, onto which the coverslips were upturned. After the incubation, coverslips were returned to the 6-well plate and washed twice in PBS. Next the cells were incubated in 100 µl of secondary antibodies, again being overturned onto Parafilm. The alexa 488, alexa 546, alexa 633 and phalloidin conjugated secondary antibodies (Invitrogen) were diluted in 1% BSA 1:600, phalloidin 1:40, ensuring that each matched the primary antibody species and had a different associated fluorophore. They were incubated for 1 hour at room temperature in the dark. The coverslips were again returned to the 6 well plate and protected from light exposure. The cells were washed four times in PBS before 300nM DAPI (Invitrogen) was added to the wells. DAPI binds strongly to the minor groove of DNA and is thus used as a nuclear stain. The plate was incubated for 10 minutes before a final 3 PBS washes were performed.

2.3.5.5 Microscopy

Glycerol jelly was incubated at 60°C to reduce the viscosity, then 8 µl was added to a labelled microscope slide. The coverslip was turned, cells down, onto the jelly. These slides were kept in the dark overnight at room temperature then at 4°C long term. Images were captured using a LSM 710 META confocal microscope, with a Plan-Apochromat 63x/1.4 lens (Zeiss). The 488 nm, 543 nm and 633 nm light emitted by the argon and helium/neon lasers excited the secondary antibody fluorophores, which then fluoresced at their specific wavelength. This light was captured and recorded by a computer (Fujitsu). Fluorescence emitted following excitation by each laser was detected separately using the multitrack function. Images were analysed using ZEN software.

2.4 Protein analysis

Proteins were separated by their molecular weight using Sodium dodecyl sulphate-polyacrylamide gel electrophoresis (SDS-PAGE). They were then transferred onto a membrane and bound by specific primary antibodies which were in turn bound by secondary antibodies with chemiluminescent tags.

2.4.1 Sample preparation and electrophoresis

Protein concentrations were determined by Bradford Assay (section 2.3.4.2). Approximately 20 µg of protein was combined with 4x lithium dodecyl sulphate, sample loading buffer (106 mM Tris-HCl, 141 mM Tris base, 2% LDS, 10% glycerol, 0,51 mM EDTA, 0.22 mM Coomassie blue G-250, 0.175 mM phenol red, pH8-Invitrogen) and 10x NuPAGE reducing agent (500 mM dithiothreitol). The LDS sample buffer linearised the proteins by denaturing secondary and tertiary protein structures and bound the length of the protein, imparting a negative charge proportional to the size. This sample mix was then heated to 99°C for 10 minutes to promote denaturation. Meanwhile the gel apparatus was prepared: 10 well or 20 well 4-12% pre-cast Bis-Tris gels (Invitrogen) were loaded into either an Xcell surelock mini cell or Xcell surelock midi cell (both Invitrogen) buffer core. The inner core was filled with 1x MOPS running buffer (20 nM MOPS pH 7.0, 8 mM sodium acetate, 1 mM EDTA pH 8.0-Invitrogen) and antioxidant added (500 µl to the mini cell, 1 ml to the midi cell). This maintained the protein denaturation during the electrophoresis. The outer chamber was then also filled with 1x MOPS running buffer and the samples loaded into the gel, alongside 5 µl of rainbow molecular weight marker (Amersham biosciences). A constant voltage of 150V was applied across the tank for 90 minutes, until the ladder had run the length of the tank.

2.4.2 PVDF membrane transfer

The proteins were next transferred onto a 0.45 µm pore hydrophobic polyvinyldiene fluoride (PVDF) membrane (Amersham Biosciences). PVDF binds proteins non-specifically and is resistant to solvent, thus it can be repeatedly stripped and re-probed.

Eight pieces of Whatman 3MM paper were cut to the size of the gel and soaked in transfer buffer (25 mM Trizma base, 192 mM glycine, 20% (v/v) methanol). Four of these were placed on the anode platform of the trans-blot semi-dry transfer cell (Biorad) and four kept aside to place on top. The PVDF membrane was then 'activated' by immersion in methanol. This enabled the hydrophobic membrane to be wetted. The membrane was next incubated in water for 1 minute to elute the methanol and equilibrated in transfer buffer. This was then placed on top of the blotting paper and the gel removed from the cassette, trimmed to size and placed on top of the membrane. The final pieces of blotting paper were added to the top of the pile and the stack was rolled over to remove any air bubbles. The cathode platform was placed on top and the transfer run at 20 V for 1 hour.

2.4.3 Blocking and antibody incubation

After transfer of the proteins, the membrane was blocked in 5% (w/v) non-fat dried milk (Marvel)/PBS for one hour with gentle rocking. This step attached proteins from the milk to the areas of the membrane not bound by proteins, reducing non-specific antibody binding. The membrane was then incubated in primary antibody solution at 4°C overnight. The antibodies used and their appropriate dilutions are shown in table 14. The membrane subsequently underwent three 10 minute washes in PBS containing 0.1% (v/v) tween (PBS-T), before the secondary antibody incubation. The secondary antibody was conjugated to horseradish peroxidase (HRP-Santa Cruz biotechnology) and raised against the host species of the primary antibody. This was diluted 1:2000 in 5% milk (w/v)/PBS and rocked at room temperature for one hour. The membrane was then washed in PBS-T as described previously.

Membranes were probed first for acetyl tubulin, incubated for 30 min in stripping buffer (1.5% (w/v) glycine, 1% Tween 20 and 1% SDS, adjusted to pH 2.2), and then re-probed for total tubulin.

Antibody	Supplier	Host	Dilution
Myc	Sigma	Rabbit	1:2000
FLAG	Sigma	Rabbit	1:2500
Acetylated tubulin (611-B1)	Sigma	Mouse	1:2000
α/β tubulin	Pierce	Rabbit	1:2000
Actin (AC-15)	Sigma	Mouse	1:2000

Table 14. The primary antibodies used in Western Blotting. HRP-tagged secondary antibodies raised against the relevant host were subsequently used for chemiluminescence detection.

2.4.4 Chemiluminescence detection

The antibodies were detected via the HRP-bound secondary antibody. This enzyme catalyses the oxidation of luminol to 3-aminophthalate in the presence of hydrogen peroxide, emitting light at 428 nm.

The membrane was incubated in SuperSignal west pico chemiluminescence substrate (Pierce) containing luminol and stable peroxide buffer. The light emitted was proportionate to the amount of secondary antibody. A suitable amount of each substrate was combined and added to a piece of Clingfilm onto which the membrane was overturned. Following a 2 minute incubation, the membrane was gently blotted on absorbent paper, wrapped in fresh cling-film and placed into the GeneGnome chemiluminescence bioimaging system (Syngene). After a suitable exposure time (from 20 seconds to 20 minutes), pixel intensity was quantified. Imaging and quantification used Genetools software (Syngene). Tubulin acetylation was calculated as a proportion of total tubulin. Statistical analyses were performed as described in each figure.

2.4.5 Molecular Modelling and sequence alignment

The molecular models used freely available protein structures from the protein database (PDB) (table 15).

Protein	PDB model number	Source	Original reference
α-β tubulin dimer (paclitaxel unbound)	1TUB	*S. scrofa*	Nogales et al., 1998
α-β tubulin dimer (paclitaxel bound)	1JFF	*B. taurus*	Löwe et al., 2001
Rab RocCOR	3DPU	*C. tepidium*	Gotthardt et al., 2008
Roco4 kinase	4F0G	*D. dusiudeium*	Gilsbach et al., 2012

Table 15. The PDB structures used in molecular modelling figures. These are available from the PDB website (http://www.rcsb.org/pdb/home/home.do).

These models were visualised and manipulated using Chimera (Pettersen et al., 2004). Amino acid substitutions were made by the 'Rotamer' function, which uses the Dunbrack backbone-dependent rotamer library (Dunbrack, 2002) to select the option with the highest probability based on lowest clash score and highest number of hydrogen bonds. Hydrogen bond prediction was performed by the 'Find H Bond' function using the default tolerance criteria (0.4 angstroms, 20.0 degrees).

The α-β tubulin dimer model based on protein crystallisation in the absence of paclitaxel (1TUB) was used in the majority of tubulin models as bound paclitaxel altered the surface conformation in the region surrounding the paclitaxel binding site. This included the LRRK2 binding site. The model used in each figure is stated in the legend beneath.

Sequences were aligned using the BLAST NCBI sequence alignment tool (Altschul et al., 1990) and exported to Chimera for visualisation (Pettersen et al., 2004). Colours accord to standard CLUSTAL amino acid physicochemical property groupings; red indicates small and hydrophobic, blue indicates acidic.

Conservation between residues is indicated by a symbol above the grouping: * indicates single conserved residue, : indicates conservation between groups with strongly similar properties (scoring > 0.5 in the Gonnet PAM 250 matrix), . indicates conservation between groups with weakly similar properties (scoring =< 0.5 in the Gonnet PAM 250 matrix).

2.5 Next generation sequencing (NGS) and analysis

2.5.1 Subjects

Parkinson's disease patients of Professor Thomas Gasser (Hertie Institute, University of Tübingen and the Ludwig-Maximilians-University, München) and Professor Alexis Brice (Centre de Recherché de l'Institut du Cerveau et de la Moelle Epiniere, Paris) were genetically screened for known pathogenic SNPs and deletions in Parkin, PINK1, DJ1 and LRRK2. Screening for mutations in additional known PD-related genes was completed later.

From this screening, a cohort of 26 late-onset, probable autosomal dominant PD index cases without known mutations in the genes mentioned above were recruited, along with their families. The cohort is described in table 16.

Age at onset (years)	55.6 ± 14.2
Sex ratio (Male/Female)	1:1
Samples - total	138
- affected	71
- unaffected	21
- at risk	46

Table 16. A description of the cohort used in linkage analysis. 26 families with late-onset PD, recruited in both France and Germany.

The 26 families underwent a linkage analysis, then the 13 index cases of German background were exome sequenced and their DNA screened for pathogenic variants. Initial screening was for cytoskeletal mutations but then extended to other likely PD candidates. Confirmation and segregation analyses were performed using traditional chain-termination sequencing.

2.5.1.1 Family pedigrees and clinical data

The pedigrees of the 13 families recruited in Germany are shown in table 17. The probands, marked with an arrow, were exome sequenced by SOLiD sequencing.

The clinical data summary in figure 7 show (where known) the mean age of disease onset and variance from the mean in each family, as well as any associated disorders. These parameters were used as part of the gene selection process. This is described further under section 2.5.4.1.

Family	Mean AAO	St. Dev. AAO	Associated disorders
1	70.3	6.03	-
2	65.3	8.42	Type 2 diabetes, psoriasis
3	55.5	4.95	-
4	53.5	6.36	-
5	57.5	6.36	-
6	55	7.07	-
7	-	-	-
8	-	-	-
9	-	-	-
10	71.5	6.36	-
11	47	4.24	-
12	55	10.3	-
13	55.7	11.08	-

Table 17. The clinical data for each of the PD families. There is no information regarding age of onset (AAO) for families 7-9.

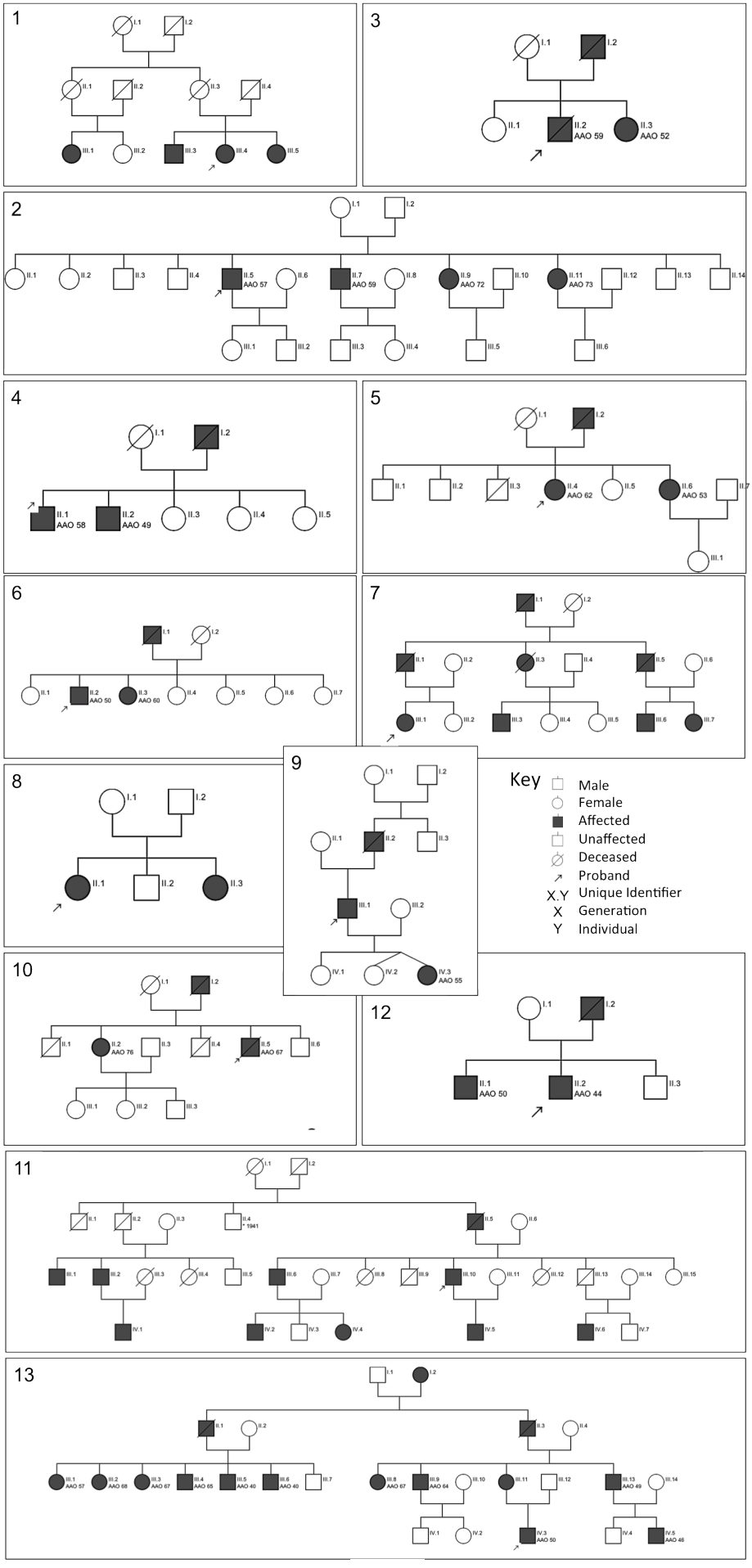
1
I.1
I.2
II.1
II.2
II.3
II.4
III.1
III.2
III.3
III.4
III.5
3
I.1
I.2
II.1
II.2
AAO 59
II.3
AAO 52
2
I.1
I.2
II.1
II.2
II.3
II.4
II.5
AAO 57
II.6
II.7
AAO 59
II.8
II.9
AAO 72
II.10
II.11
AAO 73
II.12
II.13
II.14
III.1
III.2
III.3
III.4
III.5
III.6
4
I.1
I.2
II.1
AAO 58
II.2
AAO 49
II.3
II.4
II.5
5
I.1
I.2
II.1
II.2
II.3
II.4
AAO 62
II.5
II.6
AAO 53
II.7
III.1
6
I.1
I.2
II.1
II.2
AAO 50
II.3
AAO 60
II.4
II.5
II.6
II.7
7
I.1
I.2
II.1
II.2
II.3
II.4
II.5
II.6
III.1
III.2
III.3
III.4
III.5
III.6
III.7
8
I.1
I.2
II.1
II.2
II.3
9
I.1
I.2
II.1
II.2
II.3
III.1
III.2
IV.1
IV.2
IV.3
AAO 55
Key
Male
Female
Affected
Unaffected
Deceased
Proband
X.Y Unique Identifier
X Generation
Y Individual
10
I.1
I.2
II.1
II.2
AAO 76
II.3
II.4
II.5
AAO 67
II.6
III.1
III.2
III.3
12
I.1
I.2
II.1
AAO 50
II.2
AAO 44
II.3
11
I.1
I.2
II.1
II.2
II.3
II.4
- 1941
II.5
II.6
III.1
III.2
III.3
III.4
III.5
III.6
III.7
III.8
III.9
III.10
III.11
III.12
III.13
III.14
III.15
IV.1
IV.2
IV.3
IV.4
IV.5
IV.6
IV.7
13
I.1
I.2
II.1
II.2
II.3
II.4
III.1
AAO 57
III.2
AAO 68
III.3
AAO 67
III.4
AAO 65
III.5
AAO 40
III.6
AAO 40
III.7
III.8
AAO 67
III.9
AAO 64
III.10
III.11
III.12
III.13
AAO 49
III.14
IV.1
IV.2
IV.3
AAO 50
IV.4
IV.5
AAO 46

72

Figure 7. The pedigrees of the PD cohort. Age of disease onset (AAO), where known, is stated beneath the affected individual and probands are indicated with an arrow. Pedigrees made using CeGaT pedigree designer (2014).

2.5.2 SOLiD sequencing

The exomes were sequenced by SOLiD (Sequencing by Oligonucleotide Ligation and Detection) at CeGaT (Centre for Genomics and Transcriptomics) in Tübingen, Germany. An overview of the principles behind the sequencing and the method is given below:

SOLiD sequencing uses a di-base pairs system. There are sixteen possible pairings of the adenine, thymine, cytosine and guanine bases. Each is part of a probe with one of four fluorescence tags (see figure 8A). If the first base is known, it is possible to determine the second base by the colour. The probes contain 5 bases. Bases 1 and 2 match the DNA fragment and bases 3 to 5 are degenerate.

Amplified DNA fragments are attached to a slide where the di-base probes compete to bind the DNA. The sequence extension starts from a known primer. There are 5 reads; in each, the primer is offset by one base; therefore every subsequent base in the sequence is detected by two different starting primers (figure 8B). Polymorphisms must be present in both sequencing reads to be considered valid.

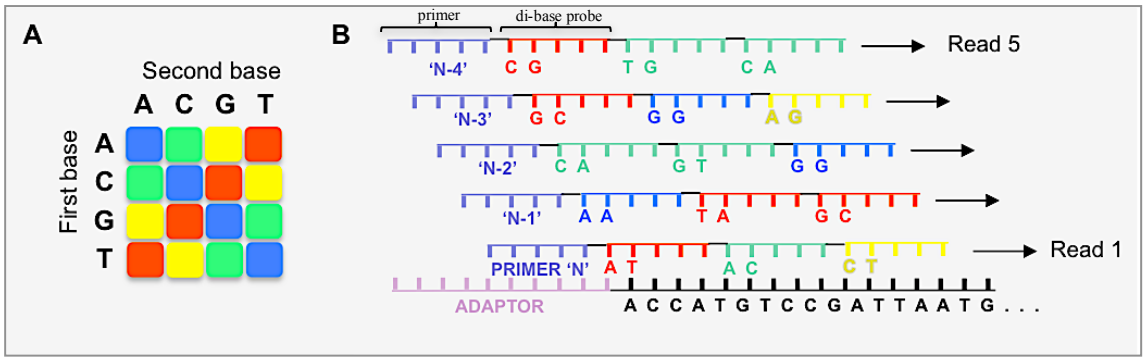

Figure 8. The theory of SOLiD sequencing. A. The fluorescent tag base-pair possibilities. The final base of the primer is always a threonine, allowing the sequence to be tracked by the colour pattern starting with a 'T'. **B.** Dibase probe and primer binding. Each probe contains 5 bases followed by a fluorescent tag; the first two bases bind the DNA fragment, the third to fifth are degenerate. Each read starts with a new universal sequencing primer, offset by one base. Over the 5 reads each base is identified by two different universal sequencing primers.

2.5.2.1 DNA extraction and quantification

3-5 ml of patient blood was taken and stored at 4°C. The Qiagen DNA blood Midi/Maxi kit was used to extract the DNA, following the manufacturer recommended protocol. This involved lysing the cells, denaturing the proteins, binding the DNA to a column then eluting the DNA.

2.5.2.2 Library preparation, amplification and enrichment

The DNA was sheared into fragments by sonication. Fragments of 180-190bp were selected using the AMPure XP kit (Beckman Coulter). This kit was used to selectively bind DNA fragments of specific length to paramagnetic beads by adjusting the bead:DNA ratio and thus the charge per molecule.

The DNA length was analysed for confirmation that the correct length DNA was extracted, before any 5' and 3’ overhangs were 'filled' to create blunt-ended fragments. Each DNA fragment then had an adenine attached to the 3'-end to produce an ‘A’ overhang for IA adapter ligation, and a P1 adaptor attached to the 5' end. The adaptors were 20 bp long and provided known ends, which were bound by amplification primers and the template between amplified by PCR.

Target enrichment then ensured only the coding DNA of interest was further analysed. In this process, the DNA was bound to a biotin-coupled SureSelect (Agilent) RNA probe library (baits); 100 bp stretches of exome sequence. These RNA-DNA complexes were then anchored to Streptavidin coated magnetic beads via the biotin tag and a magnet used to separate the target DNA sequences from the remainder. The DNA was then detached from the baits and beads.

Next, barcodes for identification and P2 adaptors were attached for use in a later purification step. P1 beads bound the P1 primers previously attached to the DNA. This DNA-P1 bead mixture was then stirred in with oil droplets, ensuring the majority of oil droplets contained one DNA fragment and one bead. Multiple fragments per oil droplet result in poor sequencing results. Each DNA-bead complex then underwent an emulsion PCR, where multiple copies of the fragment were created, bound to the bead within the oil droplet (figure 9A).

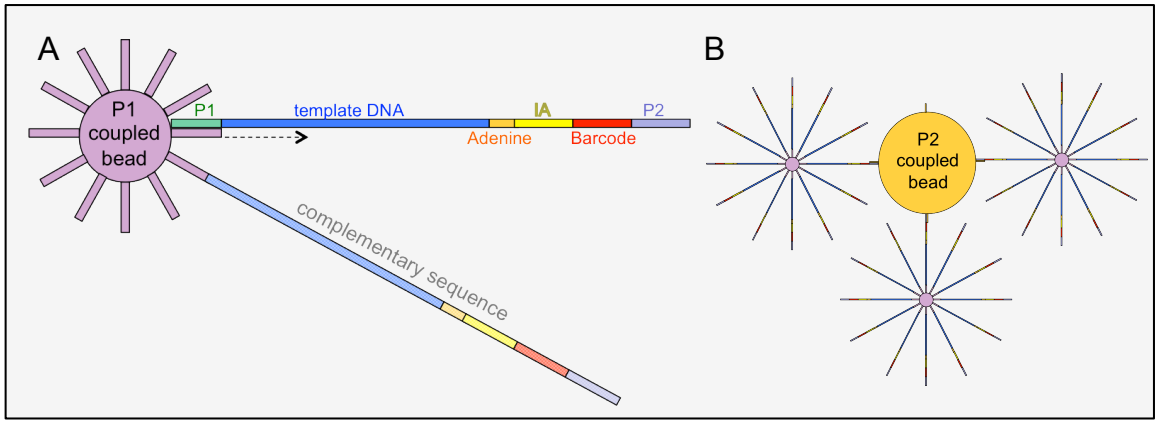

Figure 9. SOLiD sequencing emulsion PCR and enrichment. A. An individual P1 bead with attached DNA-adaptor complex undergoing emulsion PCR. The template DNA and individual adaptors are shown. The P1-coated bead binds the complementary P1 adaptor attached to the template DNA. The single template DNA sequence is amplified by emulsion PCR. **B.** Post-emulsion PCR. The P1-coupled beads with amplified product attached are bound to P2 coupled beads and separated from un-bound beads by a glycerol gradient.

Butanol broke down the oil droplets, then the P1 beads with templates attached were captured using P2 enrichment polystyrene beads (figure 9B), while those without were removed. Finally the DNA was detached from the beads and bound to the glass surface of a flow chip by a final linker attached to the 3' end of the DNA.

2.5.2.3 Sequencing

The sequencing occurred in cycles, as described above under section 2.5.2. For each read length of 75bp, 15 ligation cycles occurred per primer. After each set of cycles, a new primer was used, binding one nucleotide earlier than the previous primer. These were designated 'Universal Primers A-E'.

2.5.2.4 Data processing

The sequences were then computed and aligned to the correct region of the genome. All sequences initially underwent an error correction step using the SOLiD accuracy enhancement tool. This corrected mismatches present only in low quality reads, increasing read length and reducing the error rate. The reads were then mapped to the UCSC hg19 reference genome using Lifescope (sequences 1-10) and Bioscope (sequences 11-13) mapping software from Applied Biosystems. These programs mapped the reads using a hash table algorithm, in which both the reads and the reference sequence were given a unique sequence. The algorithm then matched these at multiple bases to find the correct alignment. When several mapping points aligned, the sequence was extended.

After the reads were mapped, the sequence was compared to the reference genome (UCSC Hg19). The software detected SNPs, insertions/deletions and copy number variants by analysis of the dicolour call, quality and location, in an attempt to remove false positives. Two different 'calling' steps to detect polymorphisms were used, each with slightly different criteria, to prevent SNPs being missed. Finally genomic annotations were added. The allele frequency was annotated according to dbSNP137 and the Exome Variant Server (EVS), the class of variant detected using NGS-SNP**.** Where there was more than one transcript of a gene available, the program selected the most deleterious option, such as a non-synonymous variant over a synonymous one.

2.5.2 Chain termination sequencing (Sanger sequencing)

Chain termination sequencing was used as an independent method to verify SNPs identified by the NGS. It was the first automated sequencing method and is therefore thought of as 'First generation sequencing' (Sanger et al., 1977). It was used to sequence the first human genome (1990-2001). It uses a standard PCR reaction into which fluorescently labelled 2'3'dideoxynucleotide triphosphatases (ddNTPs) are incorporated into the PCR product at random. These lack a 3'hydroxyl group, thus their incorporation into the sequence prevents further elongation. Over many cycles, every base in the chain will become a termination site. Following size separation, excitation with an Argon laser allows the sequence to be read. This method allows the sequencing of up to 2000 nucleotides at a time. It is not cost or time-effective to sequence a whole genome by this method but it is still commonly used in smaller sequence verification.

2.5.2.1 Primer design

Primers were designed to have a Tm of 69°C – 70°C and length 20-26 bp using 'Primer3' (Untergrasser et al., 2007). They were confirmed to be specific only to one binding site throughout the whole genome using the NCBI basic local alignment tool 'BLAT' (Kent, 2002). They were then checked in the Ensembl genome browser (Flicek et al., 2013) to ensure there were no known polymorphisms within the primers, which might affect binding specificity.

Primers were ordered from Metabion and prepared as described in section 2.1.1. The primers are listed in Appendix 1.

2.5.2.2 PCR and purification

The principle of PCR is described in section 2.1.1. The primers and PCR temperatures were checked by a test PCR using spare DNA. The PCR was then repeated with the DNA of the patient under investigation.

The contents of a standard 20µl reaction were: 4 µl 5x Green GoTaq reaction buffer (Promega M830B) 0.4 µl dNTPs (Thermoscientific R0181) 1.2 µl magnesium chloride solution (Promega A3511) 13.5µl dH_2O, 0.1 µl GoTaq DNA Polymerase (Promega M830B) 0.8 µl primer (0.4 µl of 5pg/µl forward and 0.4 µl reverse) DNA (10pg/µl).

The following PCR program (table 18) was run on an ABI 96er fast cycler.

Stage	Temperature (°C)	Time	Cycles
1	94	5 minutes	1
2	94	30 seconds	35
	60	30 seconds	
	72	30 seconds	
3	72	10 minutes	1

Table 18. The amplification PCR conditions.

The product was loaded into a gel and run alongside a GeneRuler Fermentas 1Kb ladder at 90V for 45 minutes in a 1-2% TAE/0.005% ethidium bromide gel. Where bands of the expected size were present only in the probe lane, the PCR was considered successful.

Pelleting the DNA and removing the remaining solution containing the waste products purified the product. 25 ml of 96% EtOH, 2% 3M sodium acetate (pH 4.8) was added to the PCR product. Following a 45 minute centrifuge at 1620 x g the contents were flipped onto a tissue then re-centrifuged twice with 100 µl 70% ethanol for 15 minutes.

A final centrifugation step to remove all ethanol was performed at 50 x g for 1 min, with the plate upside down. The pellet was then dissolved in 15 ml dH_2O and shaken for 15 min.

2.5.2.3 Chain termination PCR and sequencing

The purified PCR products were then prepared for sequencing. The sequencing mix included 1.5 µl Big Dye terminator V3.1 (dNTPs, ddNTPs, buffer and Taq DNA polymerase, $MgCl_2$, Tris-HCL buffer pH 9.0-Applied Biosystems), 1 µl 5x sequencing buffer (Applied Biosystems), 4 µl PCR product, 0.5 µl primer (either forward or reverse), 3 µl dH_2O. The conditions used for the PCR are detailed in table 19.

Stage	Temperature (°C)	Time	Cycles
1	95	1 minutes	1
2	95	10 seconds	30
	60	4 minutes	

Table 19. The chain termination sequencing conditions.

The products were cleaned as described above, before being loaded with HiDi formamide into a new, transparent plate. 10ul formamide (Applied Biosystems 4311320) was added to 7ul of PCR product. The highly deionized formamide improved sample stability and reduced evaporation. They were loaded into the ABI 3100 genetic analyser (16 capillary sequencer) and programmed using the Foundation data collection V2.3 analysis software. The polymer POP-7 was used, as described by Detwiler and colleagues (2004), with a run temperature of 60°C, voltage of 8.5 kV and a run time of 6200 seconds. The sequencing results were visualised using Sequencher® as described in section 2.1.7.

2.5.3 Linkage analysis

GWAS and linkage analyses statistically locate a disease locus by detecting which known markers segregate with the disease phenotype.

Linked genes segregate more often than by chance (i.e. more often than 50%) following crossover events in meiosis. Crossover events are tracked using 'markers'- common polymorphic SNPs or tandem repeats whose locations are known. Finding a marker that co-segregates with disease expression indicates the chromosomal region in which the disease-causing variance is located. Linkage analyses compare polymorphisms in family members with and without the disease. They are useful in detection of Mendelian disorders but do not identify common variants with a modest effect. They require large families with sufficient affected relatives to be fully effective in identifying the pathogenic change(s). Meanwhile association studies do not use a pedigree, instead requiring a large number of individuals (often thousands) with and without the disease phenotype. They are useful for the detection

of lower penetrance phenotypes such as risk factors. Due to the high volume of data created using microarrays, modern analyses are typically done using analysis software such as Merlin (Abecasis et al., 2002).

The linkage analysis was carried out by Claudia Schulte of the Hertie Institute, Tübingen.

2.5.3.1 Data preparation

The DNA of the 26 families, totalling 138 affected family members (see table 16 for further information), was genotyped using Affymetrix 250K DNA microarrays by Michael Bonin of the IZKF Tübingen Microarray Facility.

Prior to performing the linkage analysis, a series of quality control steps were performed. First, individuals with known pathogenic mutations and low individual call rates were excluded. An ancestry analysis confirmed the given genetic origin of the individuals involved by comparing SNP of the families with those of individuals from Nigeria, Japan, China and northern/western Europe from Hapmap (The International HapMap3 consortium, 2010), which contains over 12 million SNPs from 11 populations worldwide. Parental and offspring SNPs were then compared and any individuals likely to introduce error to the data were removed. Finally SNPs with a high linkage disequilibrium (LD) or non-random association of alleles between different loci were excluded as these can falsely increase linkage scores.

2.5.3.2 Linkage analysis

The linkage analysis was performed using Merlin (multipoint engine for rapid likelihood inference), a program designed specifically for analysis of sparse inheritance trees. As data from multiple families with likely different genes and SNPs were being analysed together, multiple models were used. Merlin classic dominance inheritance HLOD scores and non-parametric linkage scores were calculated at each marker.

2.5.4 SOLiD data analysis

2.5.4.1 Variant selection

The patients were initially screened for mutations within the cytoskeletal network. This analysis was then extended to screen for all potential pathogenic mutations. The sequence of screening steps is described below.

2.5.4.1.1 Primary filtering stages

The variation databases of all 13 probands were combined into a single file prior to the removal of variants which were unlikely to be disease causing. First, only SNPs causing a non-synonymous change within coding regions or essential splice sites were kept. A population filter step then removed variations with a global allele frequency (GAF) of over 0.5% according to the 1000 genomes project (The 1000 genomes project consortium, 2012); i.e., over 0.5% of the populace carry this variant, greater than the 0.2% PD frequency. Next 'neighbour pairs' were removed, a common sequencing artefact in which two neighbouring SNPs of low quality were mutated in identical reads. Then the allele frequencies were compared against an internal CeGaT allele frequency database, of which 1.5% were Parkinson's disease patients. Any variants with a frequency of over 2% in this database were removed. Finally homozygous mutations were removed in the cases where the mode of inheritance was clearly dominant. A final filtering step involved performing batch queries within the mutation prediction programs Mutation Taster, SIFT, Polyphen and Provean (section 2.5.4.3.2), removing any mutations which were considered benign in all programs. This left 12977 variants for further analysis, 3.3% of the original total (table 20).

	# SNPS	% drop from previous	% of total
Raw data	389521	0	100
Relevant coding regions only	92476	76.3	23.5
GMAF <0.5	31182	66.3	8.0
EVS MAF <0.5	24775	20.6	6.4
Removal of neighbour pairs	21318	14.0	5.4
Local GAF file	19518	8.4	5.0
Predicted benign by all software	12977	33.5	3.3

Table 20. Reduction in potential pathogenic SNPs following each primary filtering stage. The initial 389,521 candidates SNPs from the late-onset PD sufferer probands were reduced to less than 13000 candidate SNPs remained following sorting.

In order to select only variants relevant to Parkinson's disease, a series of strategic approaches were devised as described below. The bioinformatics resources mentioned are discussed further in section 2.5.4.3.

2.5.4.1.2 Cytoskeletal proteins

Due to the strong likelihood that cytoskeletal dysfunction is involved in neurodegeneration (described in section 1), variants in proteins related to the cytoskeleton were investigated for pathogenic mutations within the cohort. Initially all the tubulin, common MAPs and actin genes were checked. Next all SNP-containing genes in the cohort were entered into the literature mining software 'Gene Distiller' (Seelow et al., 2008), along with any previous or alternative names for these genes. Gene Distiller searched the 'OMIM' and 'GeneCards' entries for the words 'cytoskeleton', 'microtubule', 'tubulin' or 'microfilament' in the genes specified. Those whose entries contained one or more of these words were investigated further.

2.5.4.1.3 Known neurodegenerative genes

Next, genes that have already been linked to neurodegeneration in some way were investigated using those included in the CeGaT 'neurodegenerative diseases panel'. This panel includes genes associated with a broad spectrum of diseases and undergoes regular updates with input from clinicians with primary research interests in neurodegenerative disease. The genes are listed in Appendix 2. In addition, regular literature searches ensured genes which were newly implicated in PD pathogenesis during the investigation were also included in the analysis.

2.5.4.1.4 Linkage analysis

Chromosomes in the region of peaks identified in the linkage analysis were investigated for variants in the same gene in 3 or more individuals. This limit was set lower than the number of families suggested by the linkage analysis as half of the families involved in the analysis were from a separate research group. In addition, genes in these regions with higher frequencies than 0.5% were checked for an incidence in the patients greater than in the general populace, as an indicator for risk alleles. Some genes in these regions had also previously been checked for segregation by Claudia Schulte.

2.5.4.1.5 SN expression

Genes with altered expression in the PD SN were taken from the database 'PDBase', containing almost 2700 genes implicated in PD. The genes were selected by comparing expressed sequence tag efficiencies between cDNA libraries of control and PD patient SN. These data were then integrated with further information from multiple online sources to produce the PDbase gene list (Yang et al., 2009, Kim et al., 2006).

2.5.4.1.6 Dopamine processing genes

Genes involved in both upstream and downstream dopamine processing were investigated, along with neurotrophic factors known to influence dopamine production and maintenance. In addition to genes selected by literature review, gene entries mentioning 'dopamine' in OMIM were mined using Gene Distiller.

2.5.4.1.7 Clinical data

The clinical data was analysed for similar phenotypes between the families. Families in which all the sufferers were male were grouped together, as were those with a similar age at onset and similar spread of ages between sufferers. Patients in family two also suffered from type 2 diabetes and psoriasis. Genes involved in these conditions were investigated using the same research techniques described above. The literature mining involved the words 'psoriasis', 'tubulin' and 'diabetes'.

2.5.4.1.8 Multiple occurrences within the cohort

Genes which contained variants in three or more of the index cases were analysed as a way of selecting between the large number of potential SNPs. Finding variant segregation in multiple families would increase the likelihood that a true pathogenic variant was found.

Each of the strategic approaches described above involved data sorting in Excel using the formulae below:

=IF(logical test [value if true],[value if false])

=COUNTIF (range, criteria)

=VLOOKUP (lookup value, table array, column index number, [range, lookup])

=INDEX (array, row number, [column number])

=MATCH (lookup value, lookup array, [match type])

2.5.4.2 Integrative Genomics Viewer (IGV)

Screening of the reduced variant lists occurred using the Integrative Genomics Viewer (IGV) visualisation tool (Robinson et al., 2011 Integrative Genomics Viewer, Nature Biotechnology). This enabled multiple exomes to be viewed and compared (figure 10). Each index sequence was compared with two control exomes. To reduce time invested in false positives, each variant was required to meet specific controls before being included in the list for consideration of confirmation using chain-termination sequencing. These were:

- The variant was not present in either of the control exomes
- The location was covered by a minimum of ten sequence reads*.

- The variant was present in over 30% of the reads
- The variant did not show the same variant:wild-type read structure as another within 5 bases (this indicates an artefact).

*Where there were less than 10 sequence reads, the variant did not need to be present in over 30% of the reads, instead it was highlighted as a low read variant and kept in the selection process. This is because the allele to be sequenced during each read is chosen at random and so an uneven selection could prevent a heterozygous variant meeting the 30% of reads criterion.

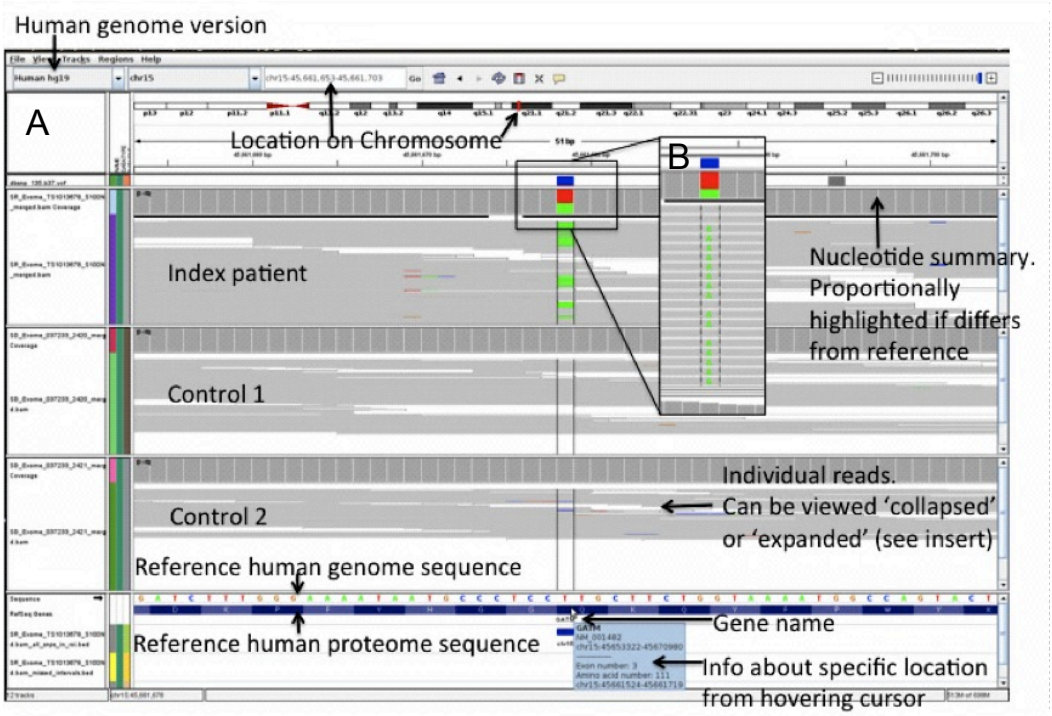

Figure 10. An annotated example of an IGV DNA sequence as read by the SOLiD4 platform. A. The structure or the chromosome is depicted, with a red bar indicating the particular location of the current gene, along with the numerical location in the search bar. The size of the region shown is 52 bp. The individual grey lines in each of the three analyses show a compressed view of single reads of the sequence. These are combined to give the nucleotide at each position over many reads. When a different nucleotide to the reference sequence occurs, the position is highlighted by the program using the colour assigned to each nucleotide: thymine, guanine, cytosine, adenine. Both the protein and nucleotide reference sequences are visible at the bottom of the image and resting the cursor over a particular amino acid provides further information about the transcript and precise location. In this example the patient is heterozygous for adenine at chr 15 position 45,661,682 in the GATM gene; whereas each of the control DNA sequences are homozygous for the thymine found in the reference sequence. **B.** An uncompressed view of the reads.

2.5.4.3 Bioinformatic resources

There are many online tools that are useful in analysing the large volume of data created by NGS. Variant and disease databases collate information about known variants, prediction software uses algorithms to analyse the phenotypic effect of an amino acid change, literature mining software enables quick access to relevant information. After filtering, all variants were checked using these resources as a final validation step before confirmation by chain-termination sequencing. The resources are listed in table 21 with a brief description.

Database name	Function	Reference
Online Mendelian inheritance in man (OMIM)	Database listing known heritable diseases and their clinical characteristics, structure, mapping and function of the genes involved, along with causative allelic variants.	(McKusick-Nathans Institute of Genetic Medicine)
Exome variant server (EVS)	Database comprising known allelic variants including their frequency in over 200,000 individuals. A cautious approach to this data meant the inclusion of variants with a frequency of under 0.5%, based on a general incidence of Parkinson's disease of 0.2% of the population.	(NHLBI GO Exome Sequencing Project; Van den Eeden et al., 2003)
Human gene mutation database (HGMD) -academic access	Database of known, heritable pathogenic mutations, HGMD is updated regularly from over 250 journals. The academic access contains data on 97797 variants (as of 19.02.2013).	(Stenson et al., 2003)
NCBI single nucleotide polymorphism database (dbSNP)	Database containing all known SNPs, their clinical significance where known, and links to relevant journal articles. Build 137 (Feb 2013) includes over 187,000,000 Homo sapien SNPs.	(Sherry et al., 2001)
Gene distiller	Extracts information about genes in a location or list from multiple user specified locations, including synonyms, OMIM, KEGG pathways, interactions, protein domains, families and paralogs	(Seelow et al., 2008).

Table 21. Databases and literature mining software used to select variants for further analysis.

2.5.4.3.1 Pathogenicity prediction software

There are many pathogenicity prediction programs available on the Internet. They take one of two forms, a constraint based predictor or trained classifier. Constraint based prediction software classifies variants according to a principle, such as evolutionary conservation, and tend to provide simple interpretation that is unaffected by contaminated data. However they only model a finite number of factors. Trained classifiers identify combinations of potentially relevant properties to develop predictions. They are able to integrate information from different sources and be adapted for different tasks. Programs which are able to offer different

analysis approaches, perform differing tasks (such as modelling changes in a splice site), are regularly updated and have been cited in many different research papers were selected. A comparison of the accuracy of each of the programs in 2200 test cases found all were correct in between 83.8% (Provean) and 88% (Mutation taster) of cases (Schwarz et al., 2014). A summary of the programs and their prediction methods are listed in table 22.

Program	Type	Prediction method	Reference
Mutation taster -version 2	Trained classifier	Incorporates information from multiple databases as well as external analysis tools to provide information on changes in regions of conservation, splice site effects, polyadenylation, Kozak sequence, protein features, length and mRNA transcription changes. Analyses of these features are combined to predict likely pathogenicity of variants. Is able to analyse variants in coding and non-coding regions, as well as insertions/deletions, stop codon and splice site changes.	Schwarz et al., 2010.
Polymorphism phenotyping -version 2.1.0 (PolyPhen2)	Trained classifier	Analyses multiple sequence and structural properties of the mutant and wild-type alleles to predict functional significance. Output is classified into HumVar and HumDiv predictions. The HumVar model trained for Mendelian diseases with drastic effects. The HumDiv model is trained for rare alleles which may be involved in complex phenotypes, where a lower threshold is used to predict damaging variants. Polyphen2 analyses coding SNPs only.	Adzhubei et al., 2010.
Sorts intolerant from tolerant (SIFT)	Constraint based predictor	Uses sequence homology between similar proteins and throughout evolution to predict functional significance. It analyses coding SNPs only but can predict pathogenicity across multiple species.	Kumar et al., 2009.
Protein variation effect analyzer -version 1.1 (Provean)	Constraint based predictor	Also uses sequence homology to compare WT and mutated sequences. It is able to analyse SNPs, indels and multiple amino acid substitutions.	Choi et al., 2012b.
Mutation predictor -version 1.2 (MutPred)	Trained classifier	Not only classifies substitutions but predicts the molecular cause of deleterious substitutions. Based on the SIFT method but additionally analyses changes in 14 structural and functional properties, such as alteration of a post-translational modification site or gain of helical propensity. It analyses coding SNPs.	Li et al., 2009.

Table 22. Software predicting SNP pathogenicity used as part of the PD variant identification process.

Variants were run through the 'bulk analysis' options of these programs according to the method described on their websites, with the exception of Mutpred, which was used only to analyse the final filtered variants. Ten variants of different predicted outcomes were confirmed by hand on each of the websites as a quality control measure.

Once a list of SNPs was identified by the methods above, each was checked visually in IGV, using the criteria described above, before their expression and role within the cell was researched. The most likely candidate SNPs were confirmed by chain-termination sequencing both the index patient and the available DNA from family members to determine if the SNP segregated with the disease.

The analysis methods are summarised in figure 11.

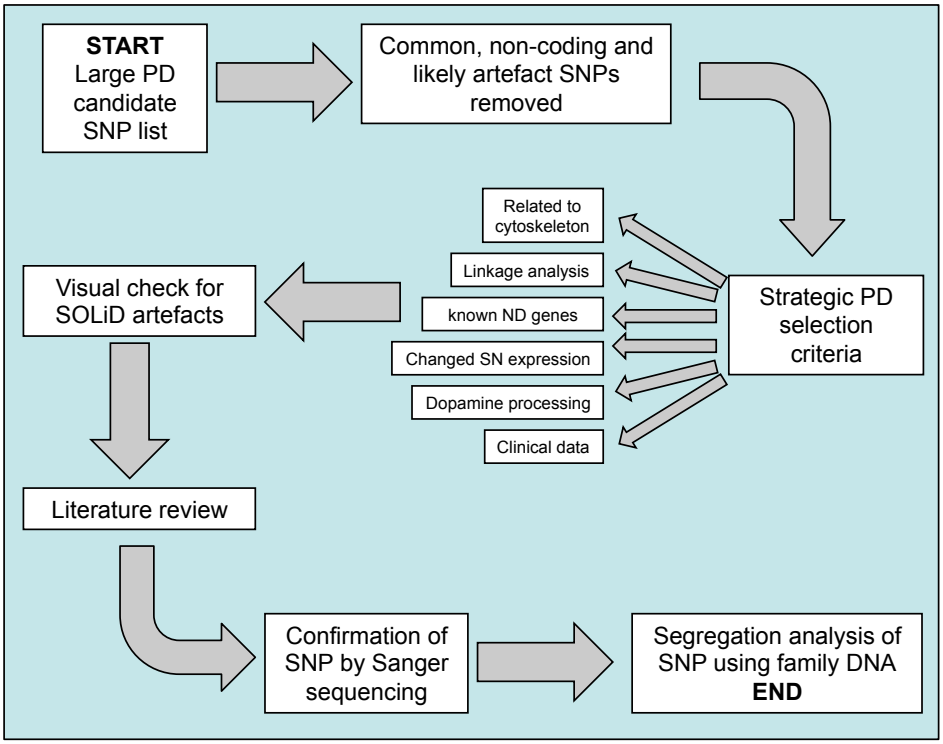

Figure 11. A pipeline diagram of the PD cohort SNP analysis. The initial large candidate SNP list was reduced by removal of artefacts, non-coding and non-synonymous SNPs before being filtered by strategic selection criteria. Likely SNPs were checked in both the proband and family members for segregation with the disease. ND = neurodegenerative.

3. Results

3.1 Characterisation of LRRK2-tubulin binding: Tubulin

3.1.1 The tubulin-LRRK2 binding site: starting point

Characterisation of the LRRK2-tubulin association was begun previously by Rosa Sancho and Bernard Law. A yeast two-hybrid library screen testing for interactions between a LRRK2 RocCOR bait and a human whole-brain cDNA library, revealed the LRRK2 RocCOR domain interacts with the TUBB4 C-terminus (Phe317 – Ala444) (Sancho et al, 2009). The interaction was verified in co-IP assays and TUBB, a second β-tubulin isoform, was also shown to interact (Law et al., 2014).

In each case, the Roc domain bound β-tubulin more strongly than the RocCOR tandem domain, while there was no interaction between tubulin and the COR domain. Introducing a K1347A mutation preventing guanine nucleotide binding of the LRRK2 Roc GTPase domain (Taymans et al., 2011), prevented the interaction and weakened dimerisation (Law et al., 2014).

3.1.2 LRRK2 does not bind additional members of the tubulin superfamily

There are over 21 human tubulin isoforms, the most common of which are the seven α- and eight β-tubulin isoforms, sharing 41% homology. Dimers of α- and β-tubulin form MTs. Additional members of the tubulin superfamily are involved in organisation of the MTs at the centrosome. γ-tubulin forms a base for MT nucleation and orientation, δ- and ε-tubulins are involved in the assembly and function of centrioles and basal bodies. (Oakley, 2000; Inclan and Nogales, 2001; Dutcher, 2001, Ross 2013). A rooted phylogram demonstrates the separate tubulin families, suggests ε-tubulin is most similar to α-and β-tubulins of the centrosomal tubulins and shows that the megakaryocyte and platelet specific TUBB1 is divergent from the other β-tubulin isoforms (figure 12A). A sequence alignment of tubulin C-termini is shown in figure 12B, containing a representative α- and β-tubulin due to the high conservation between isoforms. It is possible to see regions of amino acids containing similar physicochemical properties, although there are few highly conserved residues across the isoforms. All protein sequence alignments were performed using the NCBI basic local alignment search tool (BLAST) (Altschul et al., 1990).

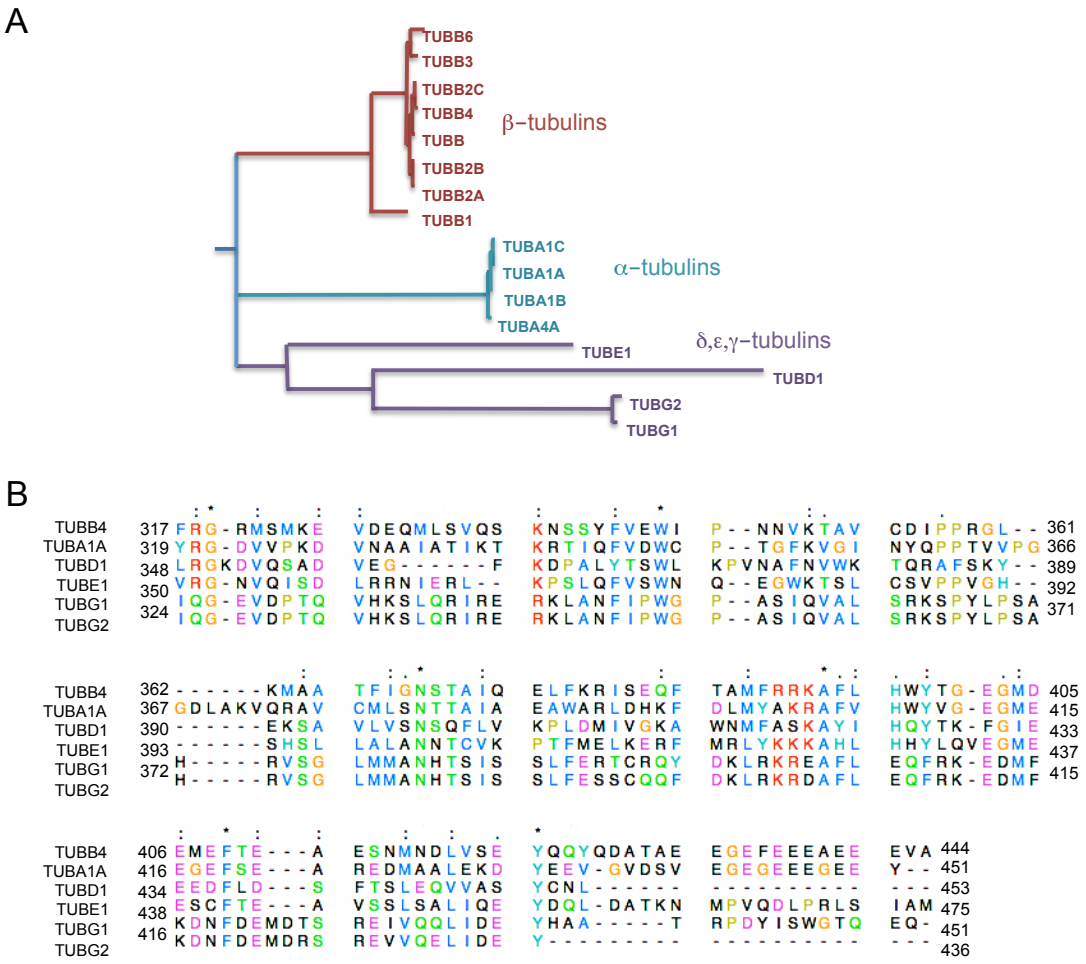

Figure 12. Conservation between different tubulin isoforms. A. Rooted phylogram of full-length tubulin protein sequences demonstrates grouping of families and similarity of isoforms. Sequence aligned using NCBI BLAST protein alignment tool (Altschul et al., 1990). Phylogenetic distances and tree calculated using phylogeny.fr (Dereeper et al., 2008) **B.** Multiple sequence alignment of representative tubulin C-termini shows conserved amino acids between isoform types.

Mass spectrometric analysis of GST-tagged Roc domain immunoprecipitates from whole brain lysates and HEK293 cells identified multiple additional α- and β-tubulin-LRRK2 interactors (table 23) (Law et al., 2014). Therefore semi-quantitative yeast-two hybrid assays were used to determine if any additional tubulin isoforms bind directly to LRRK2. Due to the high homology between α- and β-tubulins, it was hypothesised that an interaction with LRRK2 would occur in the same region in both α- and β-tubulins.

Brain	HEK293
TUBA1(A/B/C)	TUBA1(A/B/C)
TUBA4A	
TUBB	TUBB
TUBB2(A/C)	
TUBB3	TUBB3
TUBB4	TUBB4

Table 23. Roc IP tubulin interactors. Mass spectrometry of a GST-Roc domain IP from brain and HEK293 lysates identified multiple α- and β tubulins as LRRK2 interactors (Law et al., 2013).

The C-termini of the TUBA1 and TUBA4A α-tubulin isoforms (table 23) (using the equivalent residues to β-tubulin) were cloned into yeast two-hybrid vectors.

The centrosome is the MT organising centre and also associates with golgi cisternal stacks, disruption of which has been described following paclitaxel treatment (Wehland et al., 1983) but also in LRRK2-overexpressing mice (Lin et al., 2009). Disrupted golgi could also lead to the impaired vesicle trafficking associated with MT dysfunction. For this reason the tubulins associated with the centrosome (TUBD1, TUBE1, TUBG1 and TUBG2) were also tested for an interaction with the LRRK2 RocCOR domain.

No interactions between any additional tubulin isoforms and RocCOR or full-length LRRK2 were observed in our system (figure 13).

The weaker interaction with full length LRRK2 and the LRRK2 RocCOR domain, compared with the RocCOR-RocCOR association may be due to problems expressing larger proteins within the yeast, the greater distance between the activation domain and the binding domain within the cell nucleus or it may relate to toxicity of LRRK2 regions to the yeast. Xiong and colleagues (2010) found increased toxicity in Roc-COR-kinase and Roc-COR-kinase-C-terminal constructs compared with the GTPase or kinase alone, supporting interaction between the domains.

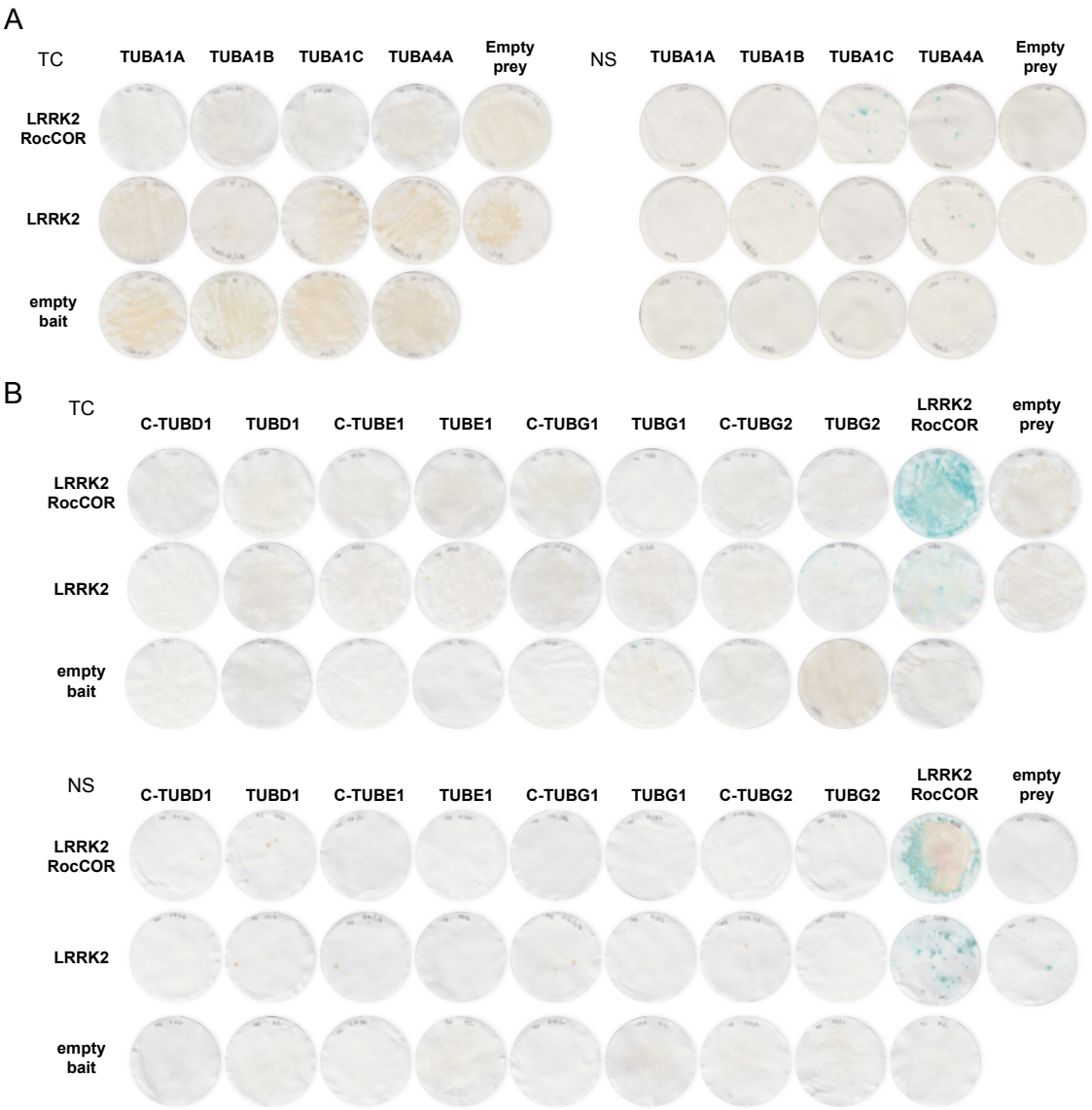

Figure 13. The LRRK2 RocCOR domain does not interact with α,δ,ε or γ tubulin isoforms. A. LRRK2 full length or the LRRK2 RocCOR domain do not interact with α-tubulin (TUBA1A, TUBA1B, TUBA1C or TUBA4A) in semi-quantitative YTH. **B.** LRRK2 full length or RocCOR domain do not interact with full-length or C-termini of TUBD1, TUBE, TUBG1, TUBG2. Both transformation control and nutritional selection plates are shown, representative of 3 separate experiments.

3.1.3 LRRK2 does not bind actin-β or actin-γ1 via the RocCOR domain

LRRK2 has been linked to the actin cytoskeleton via ARHGEF7, moesin and morphological changes caused by pathogenic mutants. ARHGEF7 regulates actin polymerisation, moesin is involved in anchoring the actin cytoskeleton to the plasma membrane and cells expressing the G2019S LRRK2 mutant contain smaller neurites (Jaleel et al., 2007; Haebig et al., 2010; Winner

et al., 2011). Additionally Meixner and colleagues detected a direct interaction between LRRK2 and F-actin (Meixner et al., 2011).

For this reason we tested for a direct interaction between LRRK2 and neuronally expressed β-actin (ACTB) and γ1-actin (ACTG1). Neither was found to bind the LRRK2 RocCOR domain or full-length LRRK2 (figure 14).

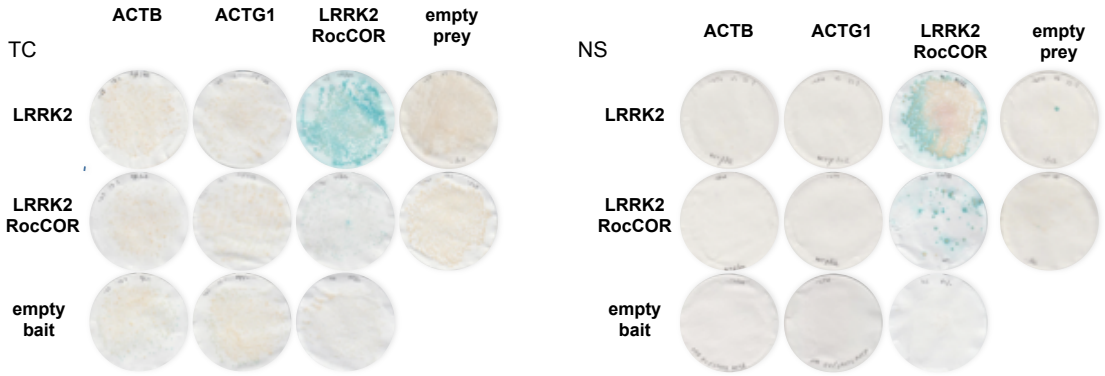

Figure 14. No interaction occurs between actins and LRRK2. Full length ACTB and ACTG1 do not interact with full length LRRK2, RocCOR domains in semi-quantitative yeast two-hybrid assays. Both transformation control and nutritional selection plates are shown, representative of 3 separate experiments.

3.1.4 TUBB6 also binds LRRK2

Alignment of the β-tubulin isoforms demonstrates high sequence homology, with virtually identical amino acid sequences until the C-terminal tail (figure 15A). Therefore interaction between all eight human β-tubulin isoforms and LRRK2 were tested. Besides TUBB and TUBB4 as reported previously, TUBB6 was also found to interact with the LRRK2 RocCOR domain (figure 15B). Furthermore, the interactions were seen with the full length LRRK2 protein on the transformational control (TC) plates. The lack of interaction on the nutritional selection plates may be attributed to the combination of an additional selection pressure and the large size of the LRRK2 protein being toxic to the yeast cells.

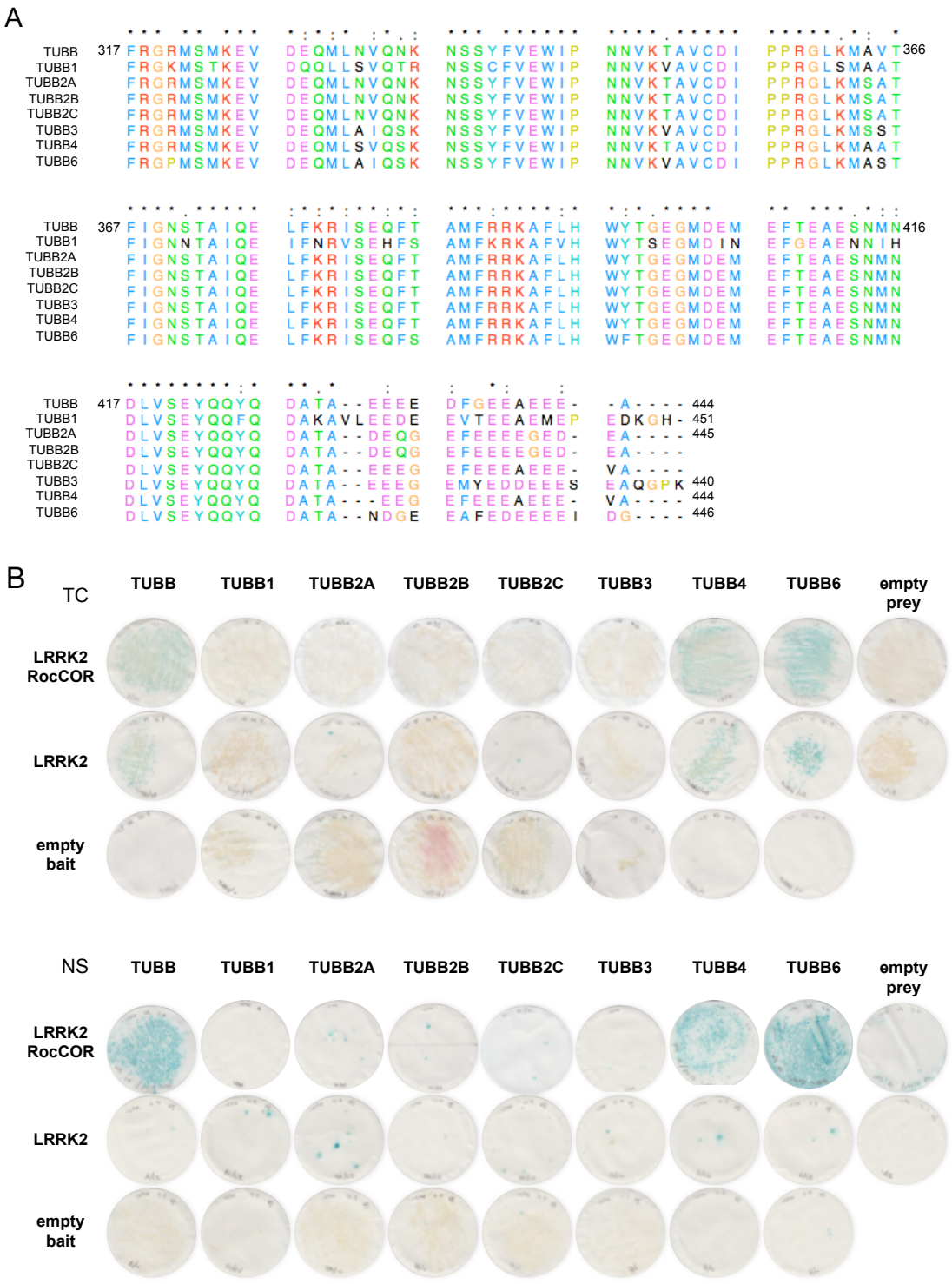

Figure 15. The RocCOR tandem domain and full length LRRK2 interact with TUBB, TUBB4 and TUBB6 C-termini. A. Multiple sequence alignment of the highly conserved β-tubulin C-termini demonstrates few differences in amino acid sequence between the isoforms, except at the extreme C-terminal tail**. B.** Full-length LRRK2 and the RocCOR domain interact with TUBB, TUBB4 and TUBB6. There is no interaction between LRRK2 and TUBB1, TUBB2 or TUBB3. Both transformation control and nutritional selection plates are shown, representative of 3 separate experiments.

3.1.5 The divergent C-terminus is not necessary to the interaction

The final 20 amino acids are the most variable region between β-tubulin isoforms (figure 16A), projecting from the surface of the MTs and acting as a site to which MAPs and motor proteins are able to bind (figure 16B) (Serrano et al., 1984; Hammond et al., 2008; Skiniotis et al., 2004; Lefevre et al., 2011). It is a region with a strong negative charge due to the high proportion of aspartic and glutamic acid residues (figure 16A). Hypothesising that this site was likely to be involved in the interaction between β-tubulin and LRRK2, C-terminal deletion constructs were tested for an interaction with the LRRK2 RocCOR domain. These constructs ended at the highly conserved alanine residue preceding the variable tail (Phe317 – Ala430). The deletions did not abolish or appear to affect the strength of the association (figure 16C), suggesting that the LRRK2 interaction site in tubulin is not the C-terminal projection from the MT surface.

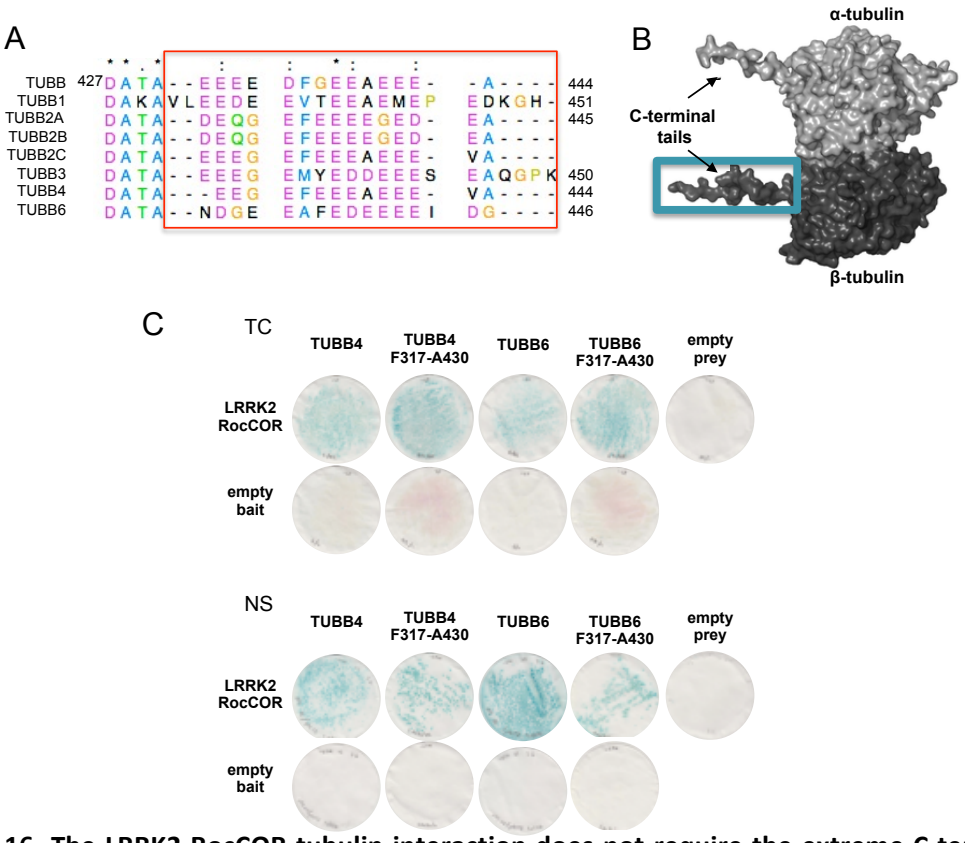

Figure 16. The LRRK2 RocCOR-tubulin interaction does not require the extreme C-termini of tubulin isoforms. A. A multiple sequence alignment highlights the highly variable, negatively charged final 14-21 amino acid tail of β-tubulin. **B**. Tubulin dimer with projecting C-termini. Blue box indicates truncated β-tubulin region. Image taken from introduction figure 5. **C.** Truncation of TUBB4 and TUBB6 at Ala430 removing the C-terminal region indicated in A and B does not affect the interaction with the LRRK2 RocCOR domain. Both transformation control and nutritional selection plates are shown, representative of 3 separate experiments.

3.1.6 Identification of specific residues required for LRRK2-tubulin binding

It had been shown by a fellow PhD student in the laboratory that the presence of an alanine at position 364 was required for the interaction of TUBB and TUBB4 with LRRK2. Interestingly, introduction of Ala364 (S364A) to the TUBB2 and TUBB3 isoforms which do not interact with LRRK2 enabled an interaction (figure 17), whereas the reciprocal A364S substitutions in TUBB and TUBB4 prevented the interaction with LRRK2 (Law et al., 2014). However, the TUBB6–LRRK2 interaction is maintained in the presence of the TUBB6 A364S mutation. This is discussed in section 3.1.9.

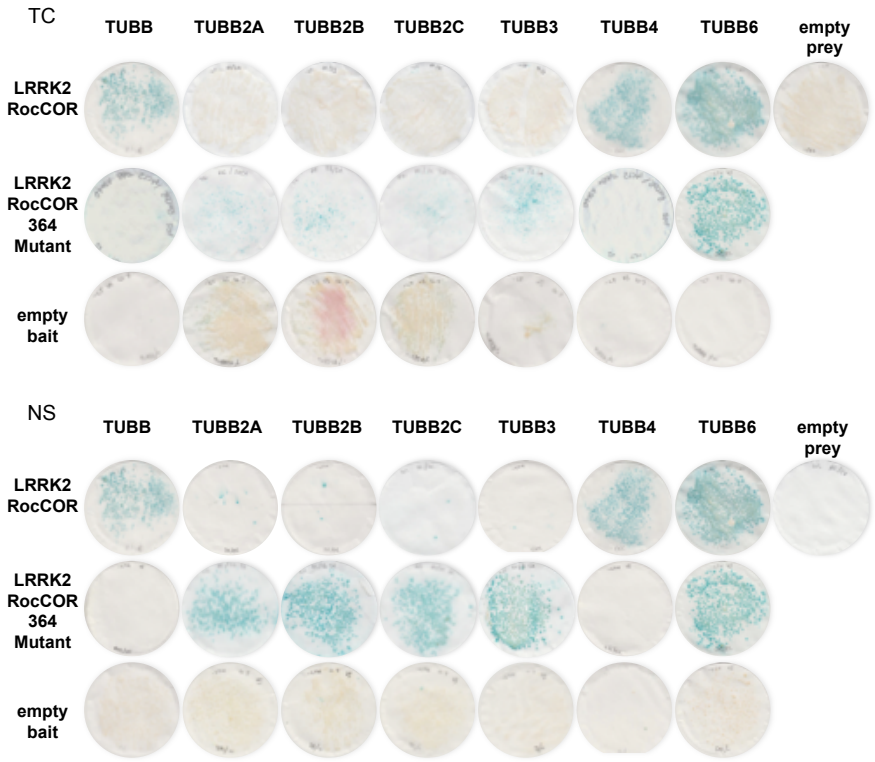

Figure 17. The tubulin Ala364 residue is required for the LRRK2-tubulin interaction. A. The A364S mutation in TUBB and TUBB4 abolishes the interaction with LRRK2 RocCOR, whereas the reciprocal S364A mutation in TUBB2 and TUBB3 enables the LRRK2-tubulin interaction to occur. The interaction with TUBB6 is maintained. Both transformation control and nutritional selection plates are shown, representative of 3 separate experiments.

Sequence alignment of the β-tubulin isoforms indicates the Ala364 residue is also present in the TUBB1 isoform (figure 18), which doesn't interact with LRRK2 (figure 15).

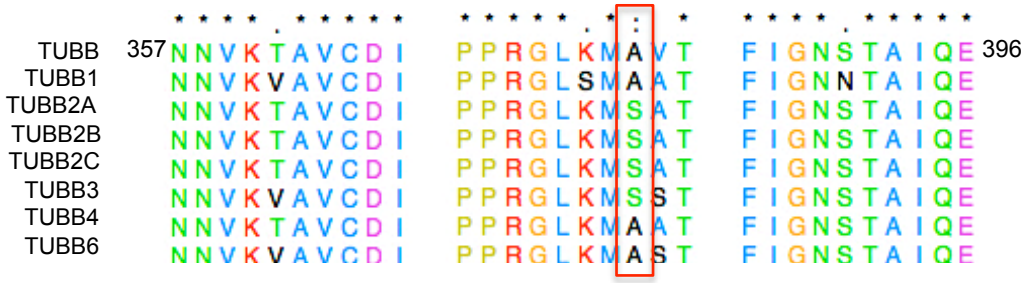

Figure 18. β-tubulin sequence alignment of the 364 residue conferring the LRRK2 interaction. Multiple sequence alignment of β-tubulin isofoms indicated a serine at position 364 in non-LRRK2 interactors TUBB2 and TUBB3 with an alanine in interactors TUBB, TUBB4 and TUBB6. TUBB1 also has an alanine at position 364 but does not interact with LRRK2. The 364 residues are highlighted.

That an alanine at position 364 could confer interaction in all tubulin isoforms except TUBB1 suggested that an additional amino acid might be inhibiting the interaction in this isoform. Two nearby residues were identified as differing only in TUBB1, Ser362 and Asp371 (figure 19B). All other β-tubulin isoforms have a Lys362 and an Ser371 respectively. Demonstrating the requirement for a lysine at position 362, a S362K amino acid substitution in TUBB1 allowed LRRK2 to bind, whereas the N371S mutation was not able to confer an interaction (figure 19A). Thus the binding of LRRK2 to β-tubulin requires two near adjacent residues, Lys362 and Ala364. Interestingly, the alanine at position 364 is conserved in α-tubulin (figure 12B), although they do not have the accompanying lysine, instead there is an uncharged glutamine. The tubulin isoforms that are not part of MTs all have a serine at this location (Figure 12B).

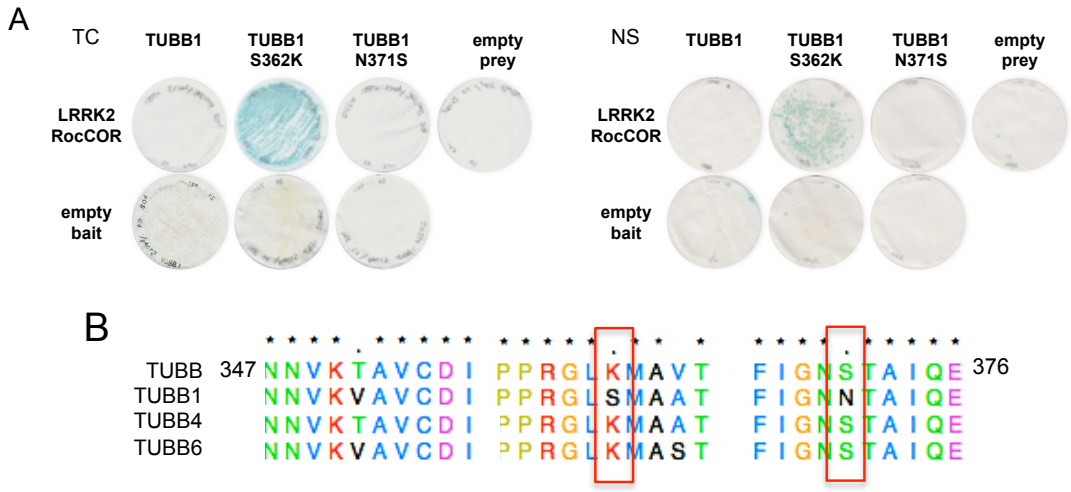

Figure 19. Lys362 is required for the RocCOR-tubulin interaction. A. Substituting a lysine for the serine in the TUBB1 sequence at position 362 confers interaction with the LRRK2 RocCOR domain. Substituting serine for asparagine at 371 did not facilitate an interaction with LRRK2. Both transformation control and nutritional selection plates are shown, representative of 3 separate experiments. **B.** Multiple sequence alignment of the tubulin isoforms showing Ser362 and Asn371 two residues differing only in TUBB1, adjacent to the Ala364 putative interaction site.

Confirming that Lys362 is involved in the tubulin-LRRK2 interaction, reciprocal K362S mutations in both TUBB and TUBB4 reduced the strength of the interaction, most significantly in TUBB where it was almost abolished, but also in TUBB4 where it was reduced by approximately half (figure 20).

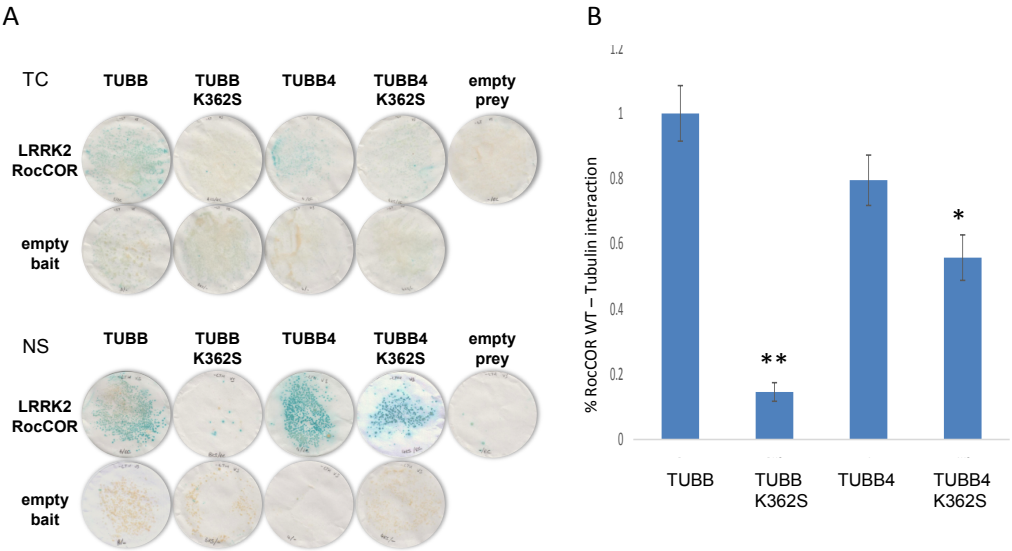

Figure 20. The positive charge at Lys362 is important for the interaction between LRRK2 and both TUBB and TUBB4. **A.** Replacing Lys362 with Ser362 prevents the LRRK2 interaction with TUBB but not TUBB4. Both transformation control and nutritional selection plates are shown, representative of 3 separate experiments **B.** Quantitative yeast two-hybrid demonstrates the strength of the interaction between tubulin and the LRRK2 RocCOR domain is reduced by approximately half in TUBB4 K362S mutants and almost completely blocked in TUBB K362S mutants, relative to the wildtype proteins. Statistical significance was determined using a paired two-tailed students' t-test, n=3 per experiments, 3 experiments, * P<0.05, **P<0.01, error = SEM.

3.1.7 Conservation of the interaction site throughout evolution

Tubulin proteins are highly conserved throughout evolution (figure 21). Across 14 different species, including plants, mammals and fish, the TUBB4 Lys–Met–Ala LRRK2 interaction site and surrounding sequence is almost identical. In addition, a LRRK2 protein is expressed in each of these species (NCBI gene database, search 'LRRK2', April 2014), with the exception of the plant Arabidopsis thaliana, which expresses a LRRK protein paralogue, LPK (Schlögl et al., 2012).

Figure 21. Multiple sequence alignment showing conservation of TUBB4 amino acid sequences. The highly conserved region containing the LRRK2 interaction residues Lys362 and Ala364 is outlined. Representatives shown from Eukaryota are: Hs, *Homo sapiens; Mm, Mus muscularis; At, Arabidopsis thaliana; Xt, Xenopus (silurana) tropicalis; Hg, Heterocephalus glaber; Ml, Myotis lucifugus; Oo, Orcinus orca; Ee, Elephantulus edwardii; Xl, Xenopus laevis; Sh, Sarcophilus harrisii; Ord, Odobenus rosmarus divergens; Dn, Dasypus novemcictus; Et, Echinops telfairi; Dr, Danio rerio.*

3.1.8 Post-translational modifications may modulate the LRRK2- tubulin association

Phosphosite is a database listing amino acids post-translationally modified according to mass-spectrometry or site-specific methods (such as modification specific antibodies) (Hornbeck et al., 2012). The database lists β-tubulin Lys362 and Ser364 as residues undergoing modification. Lys362 is ubiquitinated in all of the β-tubulin isoforms. Ser364 is phosphorylated in human TUBB3. To determine whether either of these modifications might influence the association with LRRK2, we introduced mutations mimicking the different states. Phosphomimetic mutations were introduced into TUBB and TUBB4 (A364D, A364E). These acidic amino acids mimic the larger sidechain and negative charge of a phosphorylated serine residue. Both mutations abolished the interaction with LRRK2 in a similar manner to the A364S mutation (Figure 17), suggesting phosphorylation of Ser364 may be involved in preventing LRRK2 binding to MTs. TUBB6 continued to interact with LRRK2, whether Ala364 was mutated to a serine or one of the phosphomimetic residues (Figure 22). The interaction between TUBB6 and the LRRK2 RocCOR domain is discussed in section 3.1.9.

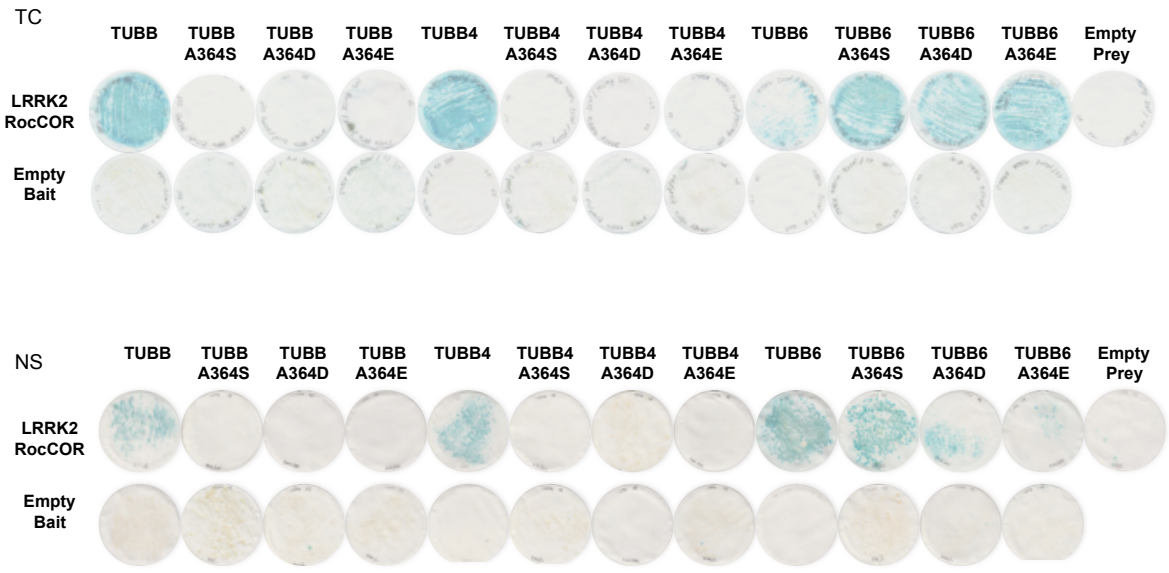

Figure 22. Mutations mimicking post-translational phosphorylation at A364 blocked the interaction with TUBB and TUBB4. Phosphomimetic aspartic acid and glutamic acid residues at 364 block the interaction between tubulin and the LRRK2 RocCOR domain, similarly to the A364S mutant. The mutations have no effect on the interaction between LRRK2 and TUBB6. Both transformation control and nutritional selection plates are shown, representative of 3 separate experiments.

Replacing Lys362 with an arginine residue maintained the large, positively charged side-chain while preventing the site being a target for post-translational ubiquitination. This mutation maintained the interaction in TUBB K362R, TUBB4 K362R and TUBB1 S362R (figure 23A) without seeming to affect binding strength, implying that it is the charge and prominent location of the 362 residue that confers binding with LRRK2. However this is a non-physiological result and is only suggestive.

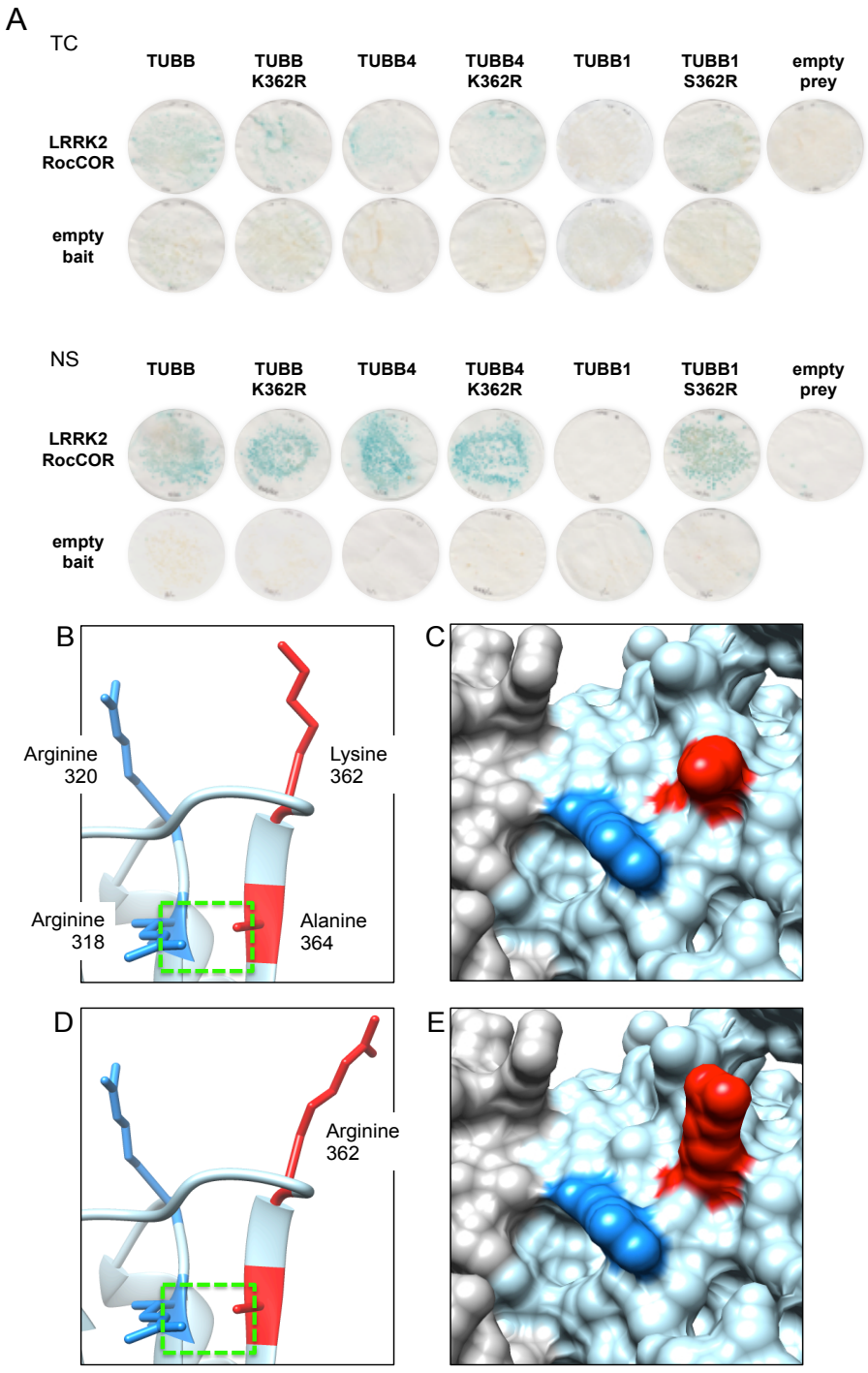

Figure 23. Blocking post-translatinal modification at Lys362 does not affect the tubulin-LRRK2 interaction. A. Introducing the similarly charged and sized arginine at 362 maintains the interaction between LRRK2 and TUBB, TUBB4 and TUBB1. Both transformation control and nutritional selection plates are shown, representative of 3 separate experiments. **B-E**. Modelling of the mutation on the tubulin structure and surface**. B,C.** Lys362 projects from the surface of the molecule. **B.** Side view of the surface projection, with the four residues involved in the interaction highlighted**. C.** Tubulin surface with the Lys362 side-chain (red) adjacent to the Arg320 (blue) indicating the LRRK2 binding site. **D,E.** Arg362 projects in a similar manner from the surface of the molecule. **D.** Side view of the Arg362 projection, with the four residues involved in the interaction highlighted**. E.** Tubulin surface with the Arg362 side-chain (red) adjacent to the Arg320 (blue) indicating similar accessibility to LRRK2.

The crystal structure of α/β-tubulin heterodimers has been resolved to a high resolution. We were able to use molecular modelling derived from this crystal structure to further characterise the proposed LRRK2 interaction site on β-tubulin as inside the MT lumen. Unsurprisingly, the large, positively charged side chain of K362 is exposed at the protein surface, projecting away from the protein core. This is consistent with both the proposed role as part of a docking site for LRRK2 and the lack of an interaction between LRRK2 and TUBB1, which contains a serine at position 362 (Figure 24,C-E). It is important to note that Lys362 is located near to the MT paclitaxel binding site (Figure 21, A and B). Paclitaxel acts to stabilise MTs and is used as a chemotherapy treatment in cancer. This binding site is also located on the luminal surface of MTs.

Surprisingly, the key tubulin Ala364 residue is not exposed at the surface, instead located beneath Lys362 as part of an internal β-sheet. To determine whether the presence of an alanine or (slightly larger) serine altered the surface topology and thus inhibited binding with LRRK2, prediction of the internal hydrogen bonds was performed. This predicted that the hydroxyl group of Ser364 would form a hydrogen bond with the backbone of Arg318 in the neighbouring β-sheet strand (Figure 24C), whereas Ala364 would not form a hydrogen bond (Figure 24D). It seems reasonable to propose that the presence of this hydrogen bond would stabilise the β-sheet, resulting in a loss of flexibility at the protein surface. This spatial constraint could reduce or alter the accessibility of the surface Lys362 in tubulin isoforms that do not bind LRRK2. Therefore, the necessary surface topology, including the position of Lys362, depends on whether the amino acid at position 364 is a serine or an alanine.

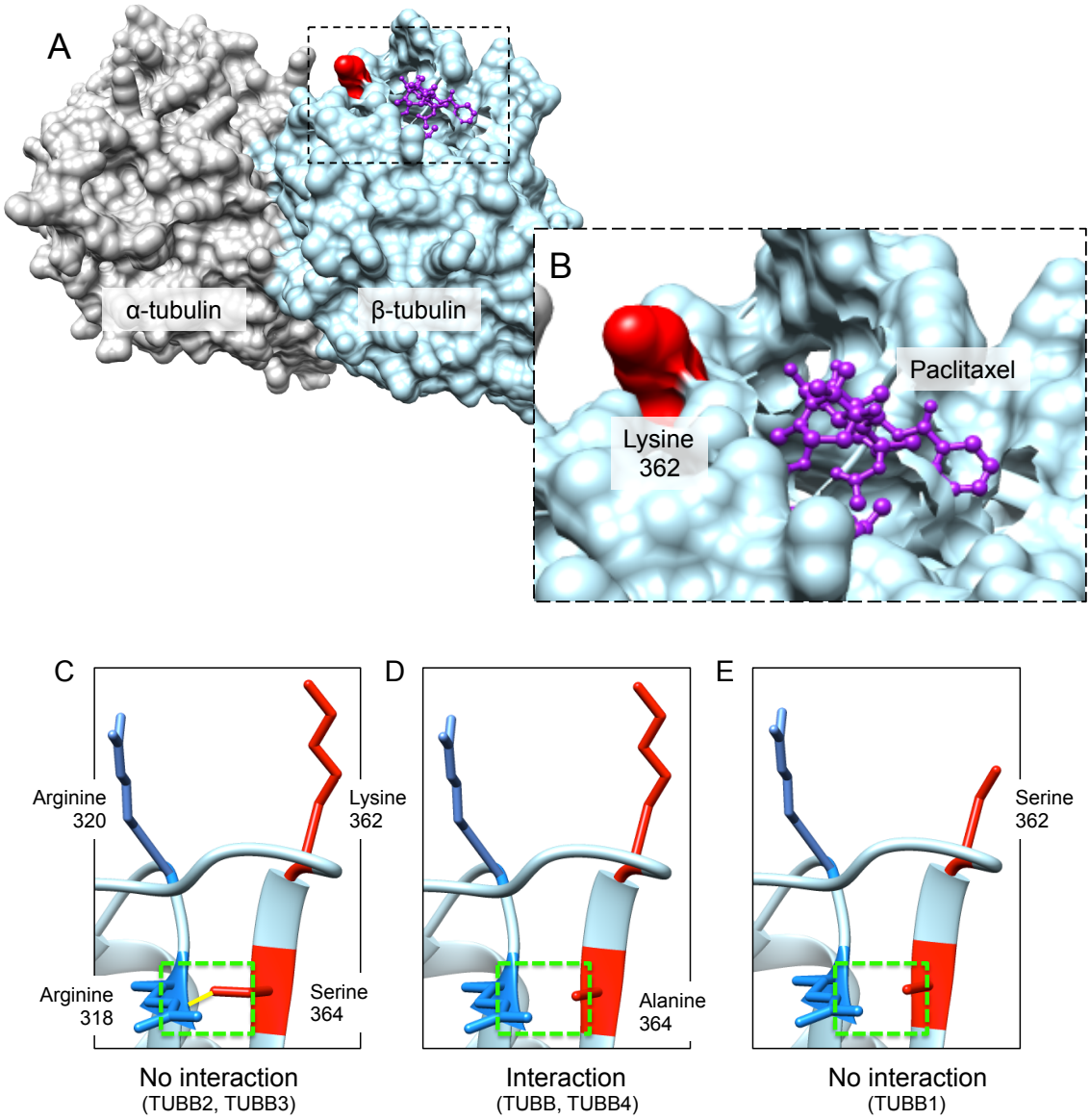

Figure 24. The β-tubulin 362 and 364 residues control the conformation of the LRRK2 binding site. **A.** Modelling shows Lys362 (red) extending from the surface of the tubulin dimer, on the luminal MT surface. The adjacent paclitaxel binding region is indicated, with paclitaxel in purple. **B.** Magnification of the area marked in A. **C-E**. Modelling of the different tubulin structures of LRRK2 binders and non-binders. **C.** Ser364 is predicted to form an internal hydrogen bond with the backbone of the neighbouring Arg318 residue in TUBB2 and TUBB3 isoforms**. D.** Ala364 is not predicted to form a hydrogen bond with neighbouring residues, allowing for increased surface flexibility in TUBB and TUBB4 isoforms. **E.** The shorter, unchanged surface Ser362 side chain does not facilitate LRRK2 docking to TUBB1, despite the flexibility of the site conferred by the internal Ala364. A and B use the PDB1JFF molecule derived from the crystal structure of bovine α/β dimers bound to paclitaxel. C-E used the PDB1TUB tubulin model derived from the crystal structure of α/β dimers not bound to paclitaxel (Nogales et al., 1998).

3.1.9 TUBB6 Pro320 strongly facilitates the LRRK2-tubulin interaction

The TUBB6 A364S or phosphomimetic A364D and A364E mutants did not abolish the LRRK2-tubulin interaction (figure 22), whereas TUBB/TUBB4 A364S, A364D and A364E did abolish the interaction with LRRK2. A sequence comparison revealed that TUBB6 is almost identical to TUBB3 (which doesn't interact with LRRK2) with the exception of four amino acids and the extreme C-terminal tail (figure 25A). Truncation of the C-terminal tail did not abolish the interaction between LRRK2 and tubulin (figure 16). Mutation of the remaining sites that differ between TUBB3 and TUBB6 (P320R, S386T and F398Y) also did not prevent binding to LRRK2 (figure 25B).

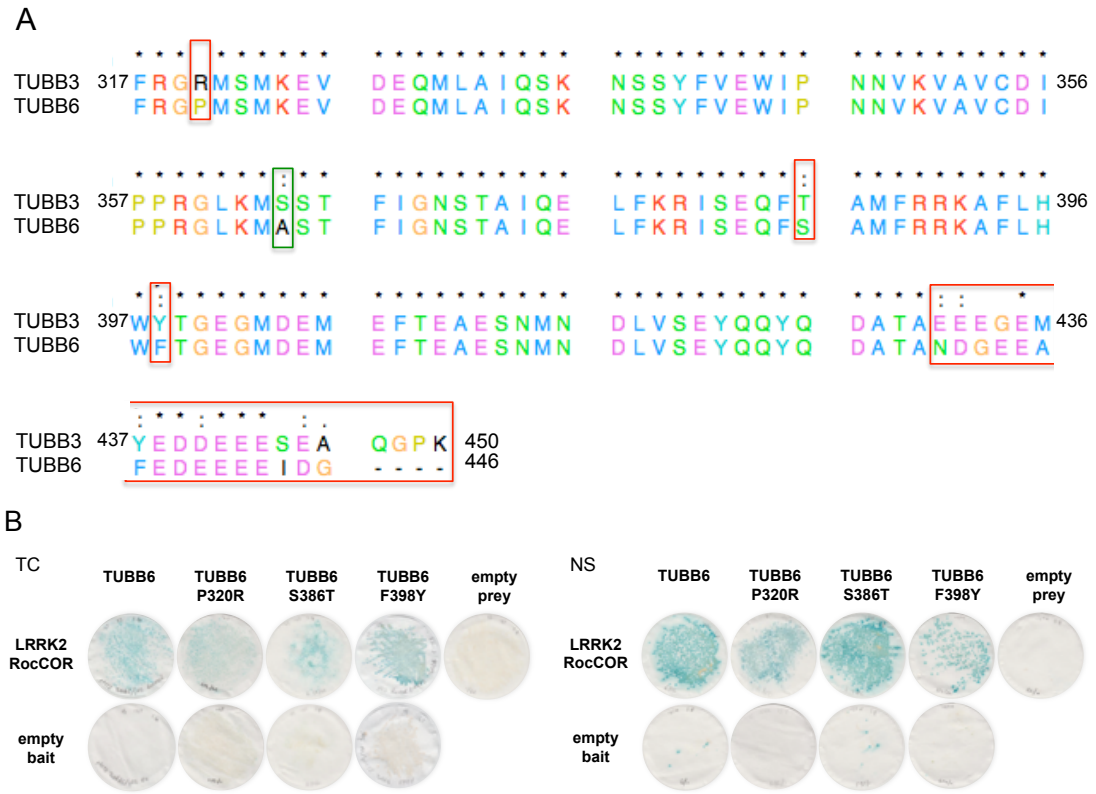

Figure 25. The RocCOR-TUBB6 interaction is strongly facilitated by one of three residues. **A.** Sequence alignment of TUBB6 and TUBB3 revealed four differences in the amino acid sequence, at least one of which confers the TUBB6-LRRK2 association: Pro320, Ser386, Phe398 and the C-terminal tail. **B.** Mutagenesis of each of the sites did not alter the interaction. Both transformation control and nutritional selection plates are shown, representative of 3 separate experiments.

Examination of these sites in a molecular model of tubulin surface topology indicated that the amino acid side-chain at position 320 also extends from the surface of the tubulin molecule, being located after Arg318 on the β-sheet strand neighbouring the 364 residue. Arg318 was previously identified as forming a hydrogen bond with Ser364 in the tubulin isoforms which do not interact with LRRK2. In all tubulin isoforms excepting TUBB6, the amino acid at position 320 is an arginine or a lysine (figure 15A). These amino acids project large, positively charged side-chains into the MT lumen. By contrast, TUBB6 has a small, uncharged proline at this location (figure 26, B and D). Hypothesising that the proline side-chain might facilitate the interaction, double mutants of P320R and K362S, and P320R and A364S were made, mimicking the TUBB2/TUBB3 and TUBB1 sequences respectively. These double mutants prevented the association with the LRRK2 RocCOR domain (figure 26A).

Therefore the reason the internal hydrogen bond does not hinder the LRRK2-TUBB6 A364S interaction (figure 22), is likely due to the altered charge or side-chain size of Pro320 (TUBB6) compared to Arg320 (TUBB and TUBB4) (figure 26 B and D). The increased accessibility to LRRK2 of Lys362, in the presence of Pro320, is particularly apparent when comparing protein surfaces of TUBB/TUBB4 and TUBB6 models (figure 26, C and E). In TUBB and TUBB4, the larger Arg320 side-chain hampers access to Lys362, hence the requirement for surface flexibility provided by Ala364.

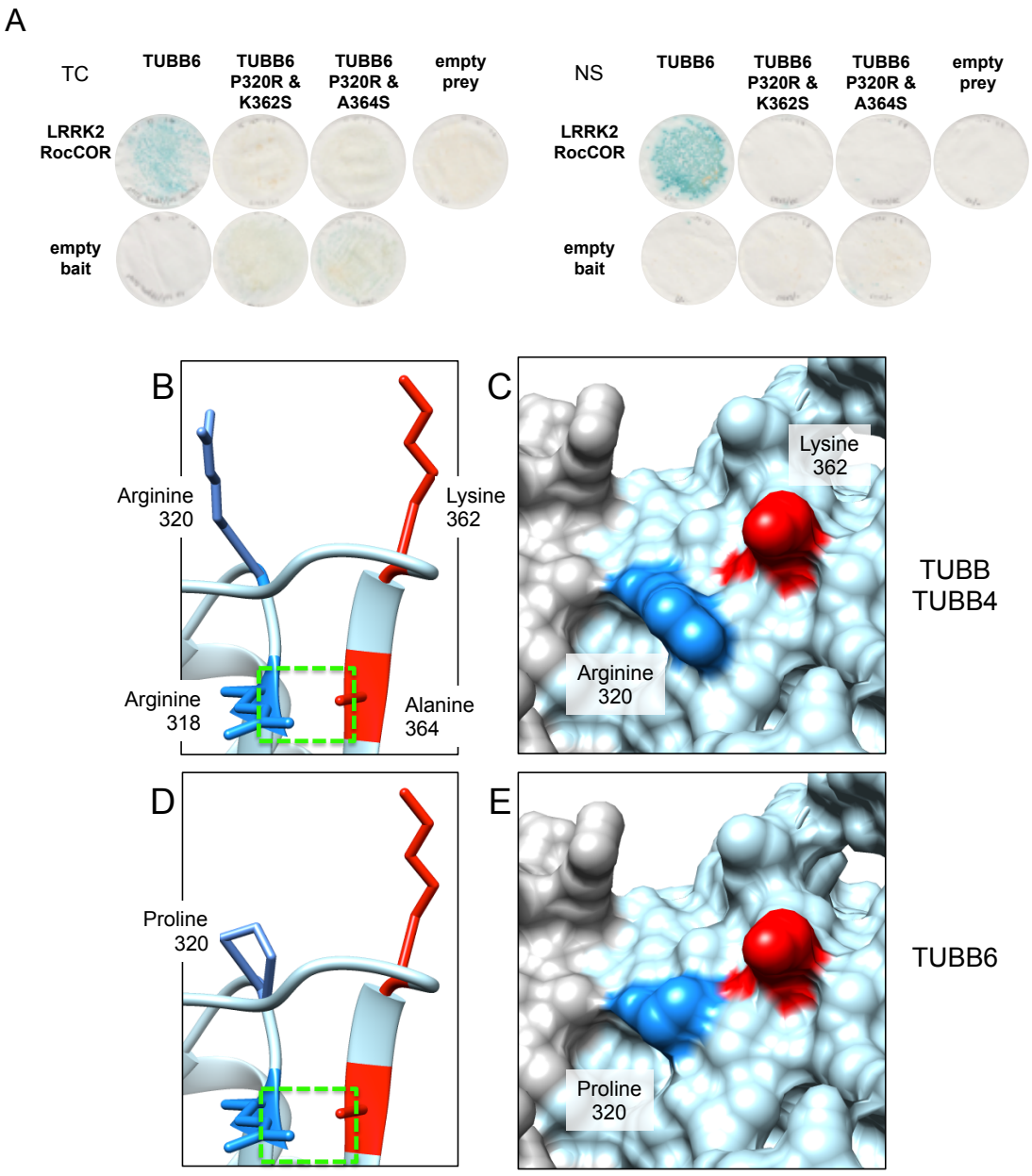

Figure 26. Pro320 strongly facilitates the TUBB6-LRRK2 RocCOR domain interacton. A. Introducing double mutations of P320R and A364S or P320R and K362S blocked the TUBB6-LRRK2 RocCOR domain interaction. Both transformation control and nutritional selection plates are shown, representative of 3 separate experiments. **E.** Structure models of the TUBB, TUBB4 and TUBB6 isoforms. **B,D.** Tubulin models with the four residues involved in binding to the LRRK2 RocCOR domain highlighted. The green box emphasises that there is no inhibitory internal hydrogen bond in these residues. **C,E.** The protein surface, with the tubulin Arg320 and Lys362 residues identified. **B.** In TUBB and TUBB4, Arg320 protrudes parallel to the Lys362 site of the tubulin-LRRK2 interaction. **C.** A surface view of figure B. **D.** The TUBB6 Pro320 residue facilitates increased accessibility of the Lys362 tubulin-LRRK2 interaction site. **E.** A surface view of figure D emphasises the increased access to the Lys362 residue. Modelling used the PDB1TUB molecule.

The residues involved in the interaction are recapped in table 24:

	Binds LRRK2	318	320	362	364
TUBB	Yes	R	R	K	A
TUBB1	No	R	K*	S	A
TUBB2A	No	R	R	K	S
TUBB2B	No	R	R	K	S
TUBB2C	No	R	R	K	S
TUBB3	No	R	R	K	S
TUBB4	Yes	R	R	K	A
TUBB6	Yes	R	P	K	A

Table 24. The residues involved in the LRRK2-tubulin interaction. Ser362 and Ser364 are inhibitory to the interaction with LRRK2. Pro320 is permissive whereas Arg320 is slightly inhibitory. *Lys320 is also likely to weakly inhibit the interaction due to similarities with the arginine residue. The Arg318 backbone is the site of an internal hydrogen bond with Ser364 but does not directly influence the interaction.

In summary: on the surface of the β-tubulin protein, the presence of Lys362 is an absolute requirement to binding LRRK2, Pro320 is permissive to LRRK2 binding, whereas Arg320 is slightly inhibitory. Internally, the Ala364 residue is permissive of the association, allowing flexibility in the surface loops containing the Lys362 and Arg320 residues but the Ser364 is inhibitory, spatially constraining the surface Lys362 and Arg320 residues via an internal hydrogen bond to the neighbouring Arg318 residue, blocking the association with LRRK2.

3.1.10 Tubulin complexes preclude specific co-IPs

As discussed previously, LRRK2 RocCOR immunoprecipitates with both α- and β-tubulins. Figure 27 shows co-IP of myc-LRRK2 with a variety of flag-tagged tubulin isoforms, including those identified as interactors (TUBB4, TUBB6) and those shown not to interact (TUBB1, TUBB3).

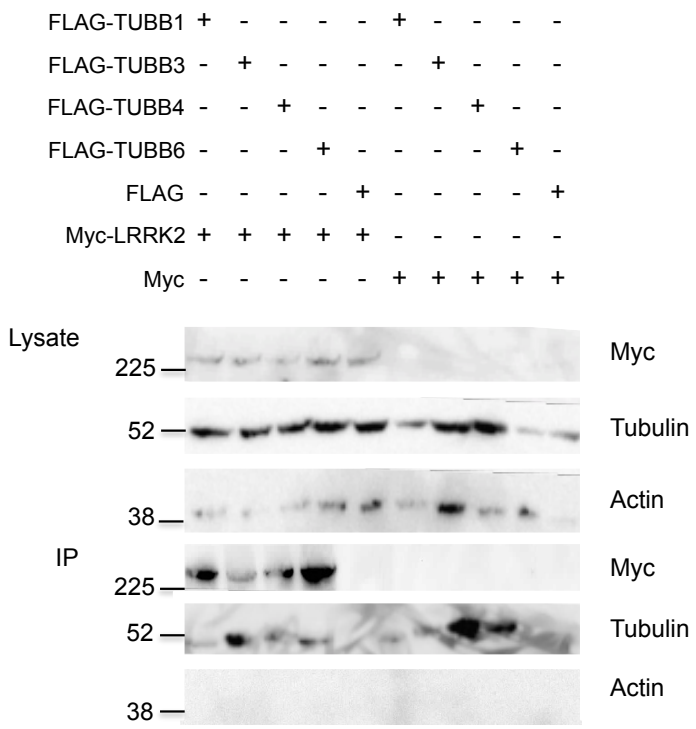

Figure 27. LRRK2 immunoprecipitate with all tubulin isoforms in HEK cells. IP of LRRK2 with flag-tagged TUBB1, TUBB3, TUBB4 and TUBB6. These have been shown in yeast to be a mix of LRRK2 interactors and non-interactors yet LRRK2 immunoprecipitates with every isoform.

Following the suggestion that tubulins immunoprecipitate in protein complexes, HEK cells were transfected with flag-tagged TUBB1 (full-length and C-terminus) and probed with antibodies specific to other tubulins (figure 28).

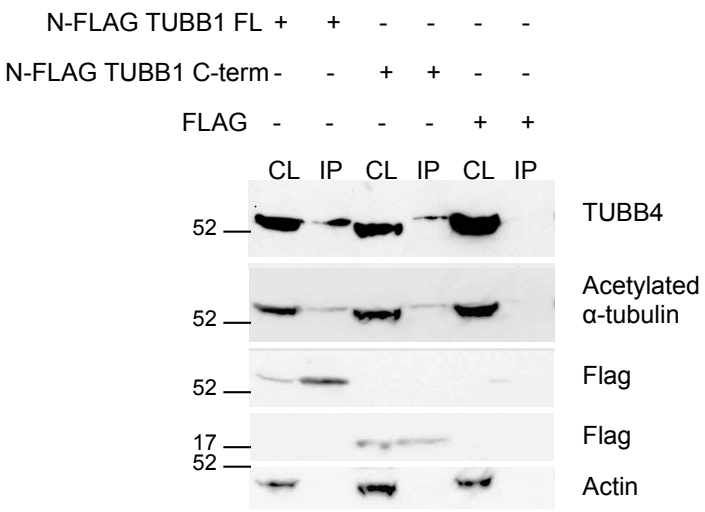

Figure 28. Tubulin isoforms immunoprecipitate in complexes. HEK cells transfected with full length and C-terminal flag-TUBB1 immunoprecipitated with endogenous TUBB4 and acetylated α-tubulin. CL – cell lysate, IP – immunoprecipitation, C-term – C-terminal, FL – full length.

The immunoprecipitate contained endogenous TUBB4 and acetylated α-tubulin in addition to the transfected Flag-TUBB1. Thus it seems likely that the co-IP of LRRK2 with tubulin isoforms which we have shown are not direct LRRK2 interactors in yeast is due to multiple tubulin isoforms immunoprecipitating in a protein complex with LRRK2. Therefore it was not possible to validate the specific residues conferring the association in yeast with *in-vitro* cell studies.

3.1.11 Discussion

3.1.11.1 Specificity of the LRRK2-tubulin interaction

The data described in this thesis confirm the reported association between the LRRK2 Roc domain and tubulin. Previous studies identified co-IP of tubulin with the LRRK2 Roc domain in primary hippocampal neurons (Gloekner et al., 2006), that tubulin and LRRK2 colocalise in HEK293 cells (Gandhi et al., 2008) and LRRK2 preferentially phosphorylates β-tubulin in mouse brain (Gillardon, 2009).

This thesis describes novel evidence that the LRRK2-tubulin interaction is direct and specific to three neuronally expressed β-tubulin isoforms. The LRRK2 Roc domain binds only β-tubulin isoforms TUBB, TUBB4 and TUBB6, there is no interaction with the additional common β-tubulin isoforms TUBB1, TUBB2A, TUBB2B, TUBB2C and TUBB3. Neither was an interaction detected between the LRRK2 Roc domain and human α–tubulin isoforms (TUBA1A, TUBA1B, TUBA1C, TUBA4A), MT-organising tubulin isoforms (TUBG1 and TUBG2), centrosomal tubulins (TUBD1 and TUBE1) or neuronally expressed actin isoforms (ACTB and ACTG1). This demonstrates the specificity of the interaction. However Meixner and colleagues detected F-actin in LRRK2 immunoprecipitate (Meixner et al., 2011). Multiple proteins containing WD40 domains are known to interact directly with actin including AIP1, CORO1A and CORO3 (Iida and Yahara, 1999; de Hostos, 1999; Rosentreter et al., 2007). Therefore an interaction between LRRK2 and F-actin might be mediated by the WD40 domain.

Reports that LRRK2 binds both α- and β-tubulins (Gandi et al., 2008; Kett et al., 2011) can be explained by the IP of tubulin in complexes, either by direct association or via MAPs, causing the detection of indirect associations. Following transfection of flag-TUBB1 into HEK cells, specific antibodies detected TUBA1A and TUBB4 in the immunoprecipitate. This explains the immunoprecipitation of LRRK2 with β-tubulin isoforms not found to interact in yeast, such as the LRRK2 Roc-TUBB2C association described by Gillardon (2009). IPs indicate which proteins function together but not whether or not the interaction is direct, whereas yeast two-hybrid is a more reliable system for providing evidence that an interaction is direct. The interaction occurs in the cell nucleus, which is not usually the endogenous interaction site, meaning accessory and intermediary proteins are not present, thus for transcription of reporter genes to occur, the interaction must be direct. Yeast two-hybrid also enables the

comparison of interaction strength between proteins in which a single residue has been mutated. This is unlike a cell system where the associations occur in their endogenous compartment alongside their intermediary proteins, meaning proteins are often extracted in a complex. The yeast reporter system also detects transient interactions which cannot always be captured in mammalian cell systems, such as those mediating post-translational modifications. Therefore IPs and yeast assays are often used in conjunction.

As described in the introduction, both *LRRK2* and tubulin expression levels vary in different cell types and tissues. *LRRK2* expression levels change little during development and aging (Biskup et al., 2007; Westerlund et al., 2008), whereas tubulin levels and isoform expression change substantially (Lee et al., 2005; Jiang et al., 1992; Hoffman et al., 1988; Lewis et al., 1985; Bond et al., 1984). Unfortunately the results obtained by different investigators are not consistent, likely due to the use of different cell types and unclear tubulin nomenclature. However, within our lab, a qPCR using foetal and adult brain revealed TUBB and TUBB3 as the dominant isoforms in foetal brains, whereas TUBB4 was the most abundant isoform in the adult brain (Bernard Law-unpublished data). Therefore the distribution of LRRK2 at MTs could be determined by the β-tubulin composition within the MTs, known to alter throughout development but with isoforms which interact with LRRK2 consistently expressed. This could explain differences between LRRK2-cytoskeletal associations within different regions and cells.

3.1.11.2 Interaction requirements

The β-tubulin isoforms share 92%-97% identity with the C-terminus of TUBB4, except the megakaryocyte and platelet specific TUBB1 which shares 77% identity. This conservation enabled the identification of individual sites involved in the interaction.

Excepting the less conserved TUBB1, β-tubulin isoforms which do not interact with LRRK2 have a serine at position 364, while those which do interact have an alanine. An A364S mutation blocked the interaction in TUBB and TUBB4 and a S364A mutation facilitated an interaction with the TUBB2 and TUBB3 isoforms. Serine and alanine are both small amino acids, however the serine has an additional hydroxyl group, conferring the ability to form hydrogen bonds. Serines are also a common site of phosphorylation, often used to regulate protein-protein interactions and as a switch in signalling cascades. Following phosphorylation, the addition of a phosphoryl group increases the size of the residue and

confers a negative charge. Initially postulating that phosphorylation-dependent inhibition could mediate the interaction, it was demonstrated that the phosphomimetic A364D/A364E mutations inhibit LRRK2 binding in both TUBB and TUBB4, but not TUBB6. This was supported by functional evidence from the online protein phosphorylation database Phosphosite, which identified TUBB3 Ser364 as a phosphorylation site in two cancer cell lines. However this theory was subsequently altered following protein modelling.

Examination of tubulin residue 364 in the freely available porcine tubulin structure PDB1TUB identified the site surrounding residue 364 as being in the MT lumen and the amino acid at 364, as part of an internal β-sheet. As the residue is internal, it is unlikely to be phosphorylated. It is therefore probable that the increased size and charge introduced by the phosphomimetic mutations disrupted the internal protein structure preventing the interaction occurring. The molecular model predicted the formation of a hydrogen bond between the Ser364 hydroxyl group and neighbouring Arg318 backbone, which was not present between Ala364 and Arg318. As these residues are in close proximity to the surface of the protein in adjacent β-sheet strands, it seems likely that the formation of a hydrogen bond spatially constrains the structure, maintaining a proximity between the surface residues which prevents LRRK2 binding. In the presence of Ala364, there is flexibility within the loops containing the Lys362 and Arg320 residues, enabling the interaction between tubulin and LRRK2.

TUBB1 has an alanine at position 364 but does not bind LRRK2. The mutation of nearby residues differing only in TUBB1 revealed the near-adjacent 362 residue was also important to the interaction. This is a conserved lysine in all isoforms except TUBB1, where it is a serine. A S362K mutation facilitated the association between TUBB1 and the LRRK2 RocCOR domain. Conversely a K362S mutation blocked the LRRK2 interaction with TUBB and halved the interaction strength between LRRK2 and TUBB4. Thus residues Lys362 and Ala364 are required for the LRRK2 RocCOR-tubulin interaction.

To determine if the interaction required the positive charge of the lysine residue or whether the interaction might be ubiquitination-dependant, an arginine mutation was introduced at position 362. Arginine has a similarly large side-chain and negative charge to lysine, but does not undergo post-translational ubiquitination. K362R maintained the TUBB- and TUBB4-LRRK2 interaction and TUBB1 S362R-LRRK2 also facilitated an association. This suggests that

the interaction in this region is charge dependant. However, the Phosphosite database contains over 120 mass spectrometry studies which have detected ubiquitination of Lys362 across every β-tubulin isoform in human, mouse and rat, therefore ubiquitination of Lys362 residues may be a mechanism by which additional, dynamic regulation of the LRRK2-tubulin interaction could occur. This would allow rapid blocking or enabling of the association in response to triggers within the cell, not just by tubulin isoform expression.

Contrastingly, where A364S and K362S blocked the interaction between LRRK2-TUBB and LRRK2-TUBB4, the LRRK2-TUBB6 interaction was maintained. Further structure analysis and double-mutation testing revealed that the interaction was strongly facilitated by a Pro320 residue. Neither of the TUBB6 P320R/K362S and P320R/A364S mutants interacted with LRRK2 RocCOR. The small proline sidechain enables increased access to the Lys362 residue for LRRK2 compared with the Arg320 of the other tubulin isoforms. Therefore the surface spatial flexibility modulated by the internal hydrogen bond between Ala364 and Arg318 is not significant in the LRRK2-TUBB6 interaction, explaining why the interaction is maintained with TUBB6 A364S. Additionally, the presence of Arg320, a second negatively charged side-chain close to the Lys362, may introduce a slight repulsion of LRRK2 by TUBB and TUBB4. This does not occur with the uncharged Pro320 residue of TUBB6, further facilitating the interaction with LRRK2.

It is noteworthy that the γ-tubulins have an R-V-S motif, in the same region as the β-tubulin K-M-S/K-M-A motifs which control the interaction with LRRK2. These amino acids are very similar-it would be interesting to see if mutagenesis of the R-V-A motif introduced an interaction with RocCOR. Though this is not functionally relevant, if an interaction with LRRK2 was introduced then further sequence comparison between the β– and γ–tubulins might reveal additional residues involved in this LRRK2-tubulin association.

Having characterised the interaction site in tubulin, the next chapter addresses the site of the interaction in LRRK2.

3. Results

3.2 Characterisation of LRRK2-tubulin binding: LRRK2

In order to further characterise the LRRK2-tubulin interaction, the binding site within LRRK2 was investigated next. This was done using multiple simultaneous approaches: division of the LRRK2 RocCOR domain into three truncated constructs, an alanine block scan and the parallel investigation of the interaction with the homologous LRRK1 RocCOR tandem domain.

3.2.1 The tubulin-LRRK2 interaction is mediated by the N-terminus of the Roc domain

The LRRK2 Roc domain was divided into three overlapping fragments at sites located between structurally important regions in the *C. tepidum* Roco molecular model (figure 29).

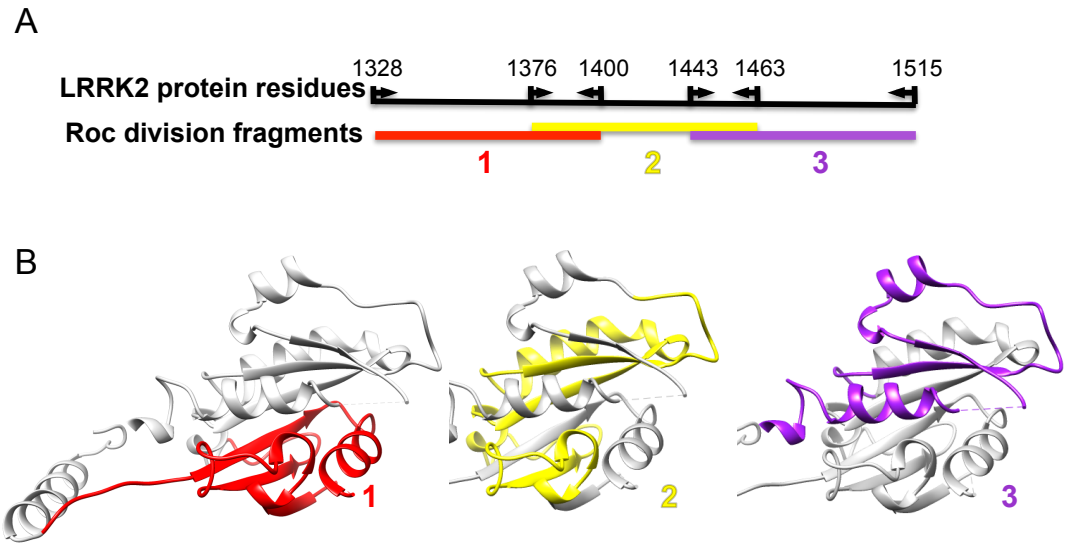

Figure 29. Roc domain division fragments narrow-down the tubulin-interaction region of the Roc domain. A. Schematic of the 3 overlapping Roc fragments used to identify the tubulin-Roc interaction region. **B**. Modelling of the Roc truncation regions, demonstrating three distinct regions of the Roc domain in PDB3DPT, *C. tepidum* Roco LRRK2 homolog. The colours used accord to the regions marked in A.

Each of the three β-tubulin isoforms previously identified as interacting with LRRK2 continued to interact with the first third of the protein (figure 30), revealing the interaction site is between amino acids 1328 and 1400. They did not interact with either of the other regions. The interaction with RocCOR was maintained with regions 1328-1400 and 1443-1515, though weakened in the latter, suggesting structural integrity was maintained. In region 1376-1463, the association no longer occurred. These truncation may have lost structural integrity or be uninvolved in dimerisation. However as the truncation(s) failed to

interact convincingly with the full-length RocCOR domain, it is also possible that the truncated proteins were not expressed.

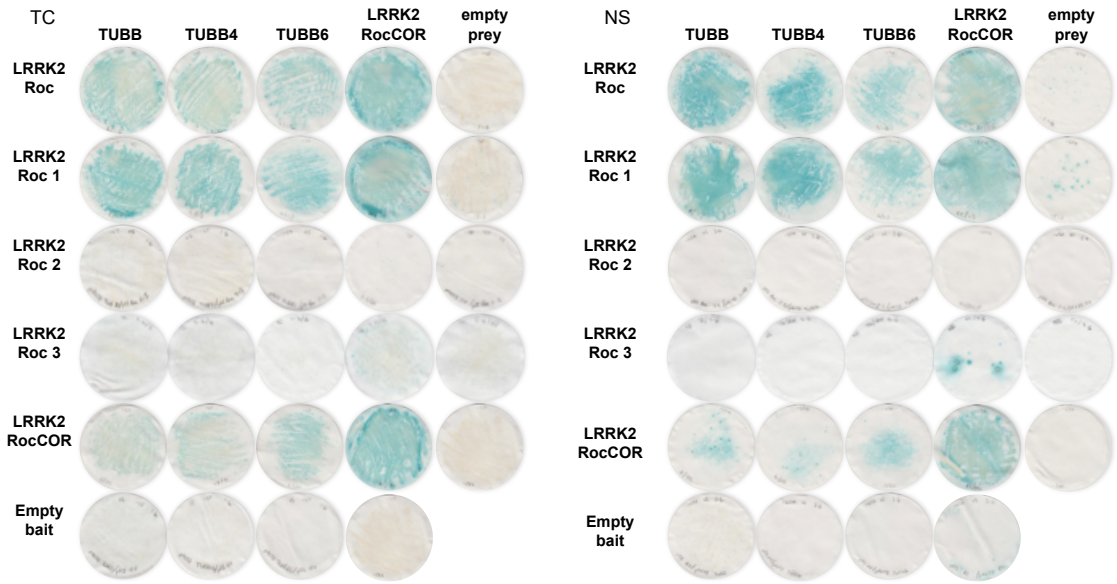

Figure 30. The β-tubulin-LRRK2 interaction is mediated by the first third of the Roc domain. TUBB, TUBB4 and TUBB6 continue to interact with Roc fragment 1 (LRRK2 residues 1328-1400) but not 2 (LRRK2 residues 1376-1463) or 3 (LRRK2 residues 1443-1515). Roc truncations 1 and 3 continue to interact with intact RocCOR. Both transformation control and nutritional selection plates are shown, representative of 3 separate experiments.

3.2.2 The tubulin-LRRK1 interaction shows similarities to the tubulin-LRRK2 interaction

TUBB, TUBB4 and TUBB6 also interact with the LRRK1 RocCOR domain, whereas TUBB1, TUBB2 and TUBB3 do not (figure 31A). As with LRRK2, the association is conferred by the Lys362 and Ala364 residues.

The LRRK1 RocCOR and LRRK2 Roc truncation results suggested that the interaction occurs at a site (or sites) conserved in the LRRK1 and LRRK2 Roc domains, between LRRK2 amino acids 1328 and 1400 (figure 31B), of which there are 23 identical residues and 13 highly conserved residues. An alanine block scan within this region was used to identify a specific interaction site.

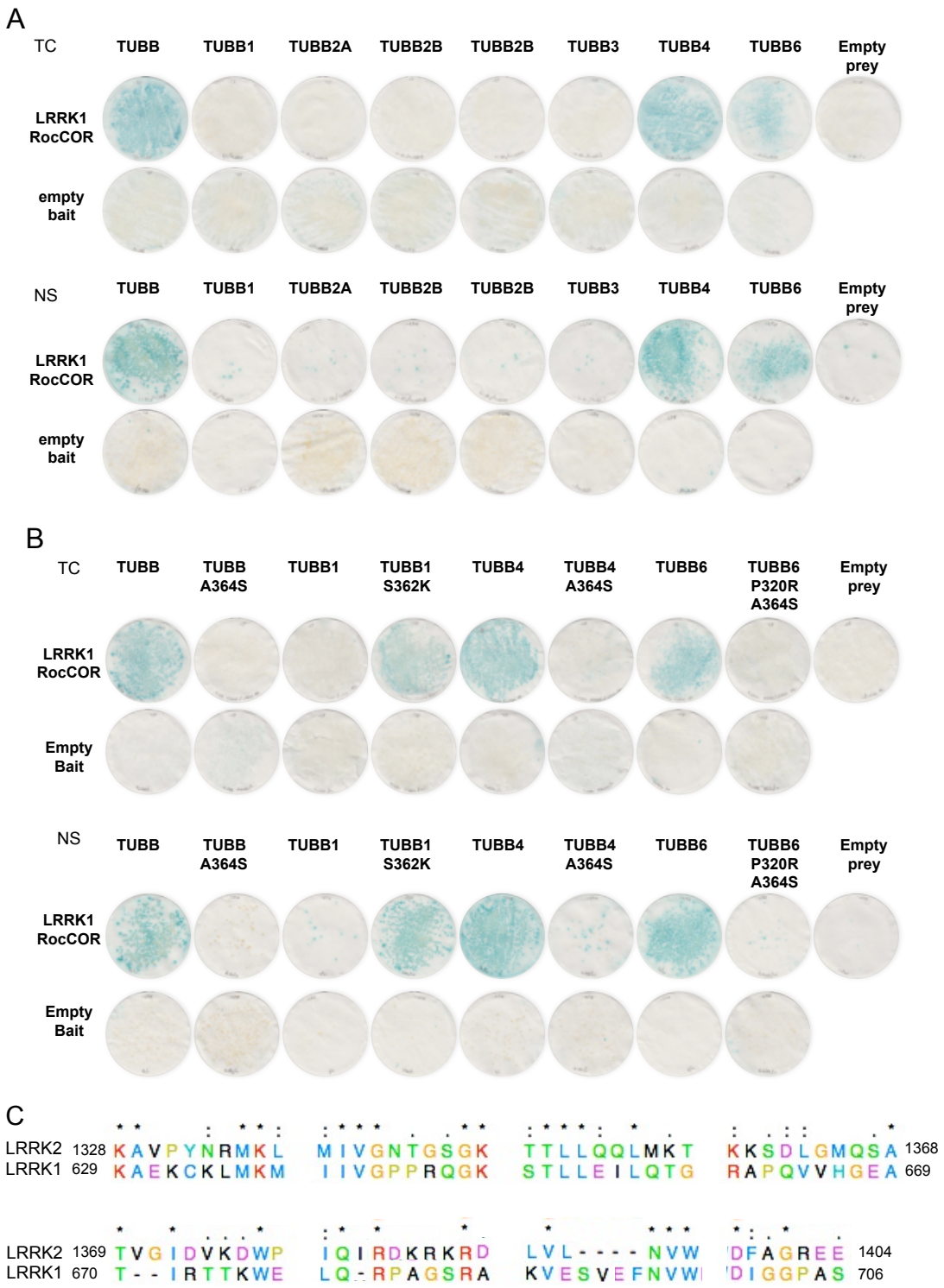

Figure 31. The LRRK1 interaction with TUBB, TUBB4 and TUBB6 is conferred by the same residues as the LRRK2-β-tubulin interaction. A. TUBB, TUBB4 and TUBB6 interact with the LRRK1 RocCOR domain. **B**. The interaction is mediated by the residues at β-tubulin position 362 and 364, as identified previously. Both transformation control and nutritional selection plates are shown, representative of 3 separate experiments. **C.** Alignment of the region in which the interaction occurs (figure 30) in both LRRK1 and LRRK2 shows 26 conserved residues between the two proteins.

3.2.3 Alanine block scan to determine the Roc domain amino acid residues required for the interaction with tubulin

Sequential blocks of five amino acids throughout the region previously identified as the tubulin-LRRK2 interaction site were replaced with alanine residues, thus inhibiting or impeding interactions occurring involving these residues. The scan included LRRK2 residues 1328 to 1402, incorporating the residues present in the Roc truncation 1 which maintained an interaction with β-tubulin isoforms. However the mutations were introduced within the full LRRK2 RocCOR domain to minimise disruption to the rest of the structure. The residues replaced in each alanine block are indicated in figure 32A, alongside their aligned LRRK1 counterparts. The results of the alanine block scan are shown in figure 32B.

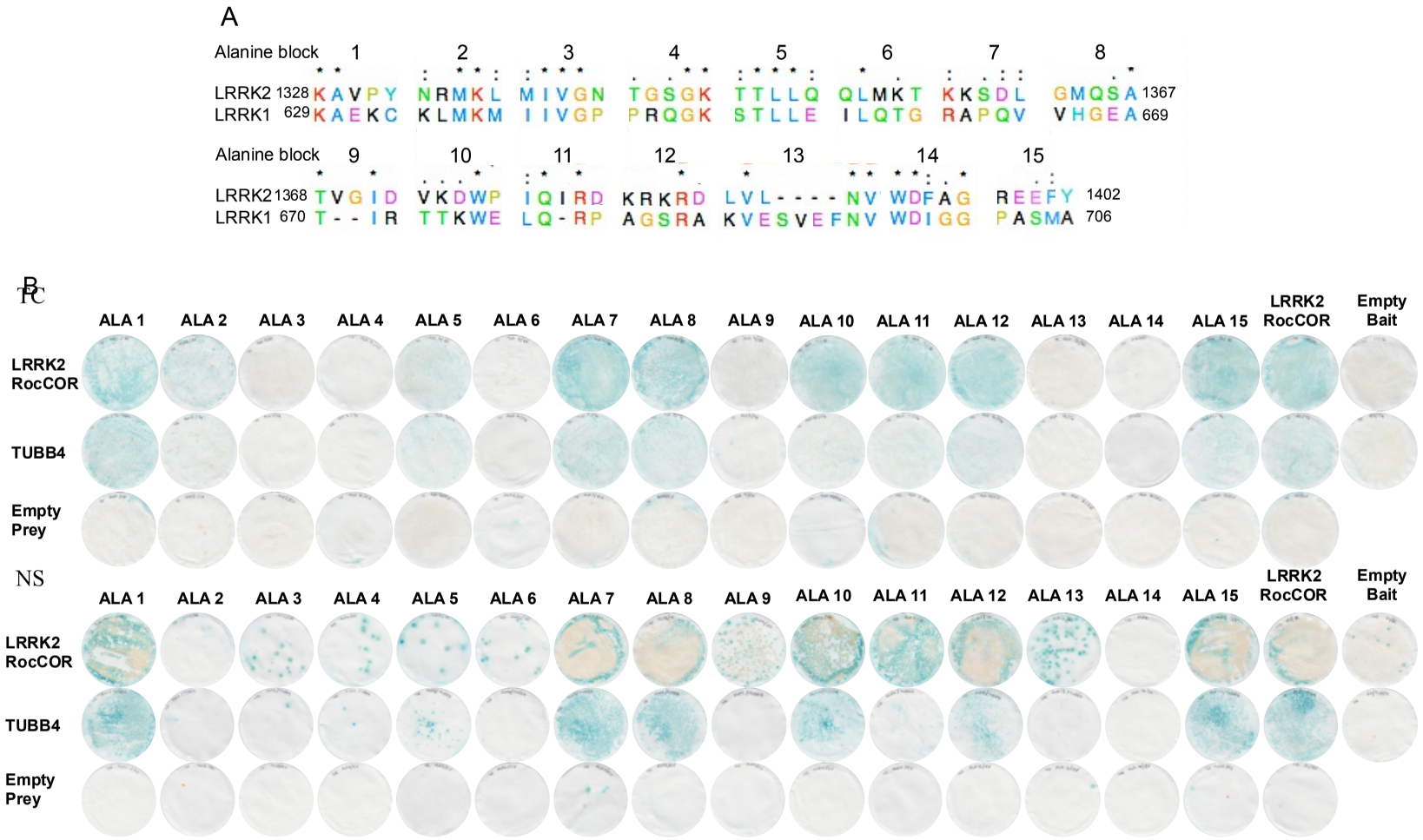

Figure 32. Alanine block scan of the LRRK2 Roc-tubulin interaction site. A. Schematic indicating the LRRK2 RocCOR alanine blocks. Successive blocks of 5 amino acids throughout LRRK2 RocCOR region 1 (LRRK2 residues 1328-1400) were replaced by alanines in the groupings indicated. The LRRK2 sequence is aligned with the identical LRRK1 region. **B.** Yeast two-hybrid results of a sequential alanine block scan to identify the region of interaction between LRRK2 RocCOR and tubulin suggests a weakened LRRK2-tubulin interaction across blocks 10-12, residues 1374-1389, with maintained RocCOR dimerisation. Both transformation control and nutritional selection plates are shown, representative of 3 separate experiments.

In the alanine scan, the presence or absence of a β-tubulin-LRRK2 interaction was consistent with the RocCOR dimerisation in the majority of cases. The loss of interaction might correlate with regions of structural significance to the protein tertiary structure or might be required for dimerisation, in turn required for the interaction between LRRK2 and tubulin.

In order to determine which sites were likely to be structurally relevant, the internal or external location of RocCOR truncation 1 residues were examined in the C*. tepidum* Roco structure (figure 33). The *C. tepidum* Roco sequence and the human LRRK2 sequence are aligned beneath. These indicate a high degree of conservation, particularly in internal residues and those involved in α-helices such as Leu1350 and Leu1351 (Alanine block 5).

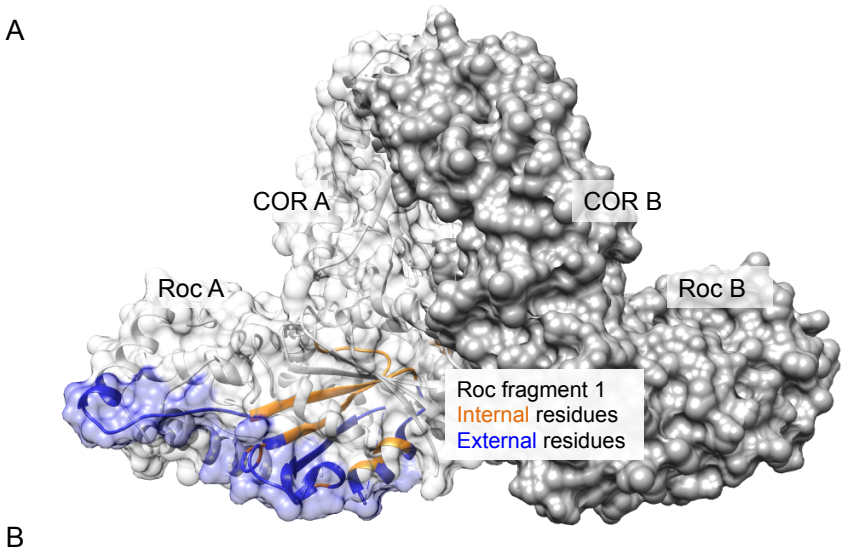

Figure 33. The equivalent location of the LRRK2 RocCOR alanine blocks in the Roco homology model with internal and external residues indicated. A. The *C. tepidum* Roco dimer with internal and external residues indicated in the equivalent region to the LRRK2 Roc fragment 1 (residues 1328-1400, figure 29). Internal amino acids are marked in orange, those at the surface are marked in blue. RocCOR A - internal ribbon structure shown with surface overlay at 30% transparency. RocCOR B surface indicated only. Modelled using *C. tepidum* Roco PDB3DPT**. B.** The residues replaced by alanine blocks in LRRK2 RocCOR, with *C. tepidum* Roco alignment. Internal residues in the Roco protein and their aligned equivalents with LRRK2 are marked in orange, external residues marked in blue.

Alanine blocks replacing predominantly internal or involving architecturally important internal residues disrupt the structure preventing the association of LRRK2 with tubulin, as well as LRRK2 dimerisation (figure 34). This can be seen with the LRRK2 RocCOR proteins containing alanine blocks 3 (LRRK2 residues 1338-1342) and 13-14 (LRRK2 residues 1388-1397), in which the amino acids were all internal. There was also no interaction between tubulin and LRRK2 RocCOR proteins containing alanine blocks 5 and 6 (residues 1348-1357). These proteins contain leucine residues, structurally involved in α-helices. However the interaction was maintained between tubulin and LRRK2 RocCOR alanine block 15, in which the amino acids are all predicted to be located internally (residues 1498-1402).

LRRK2 RocCOR proteins containing alanine blocks 1, 7 and 8 (LRRK2 residues 1328-1332 and 1358-1367) are predicted to replace only external residues. Both the interaction with tubulin and RocCOR are maintained, thus these locations are unlikely to be the site by which LRRK2 RocCOR binds tubulin.

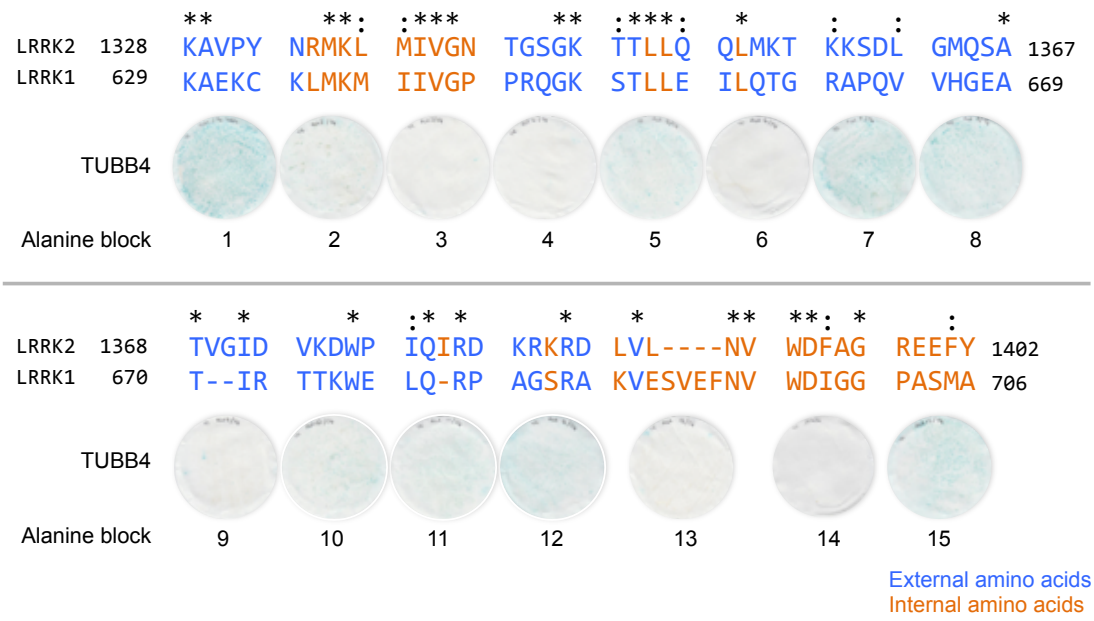

Figure 34. Alignment of the TUBB4-RocCOR alanine yeast two-hybrid interaction results with the LRRK1 and LRRK2 sequences. The TUBB4-RocCOR alanine yeast two-hybrid results shown in figure 33 aligned with the respective LRRK2 RocCOR sequences. The equivalent LRRK1 sequence is also aligned to LRRK2, with the internal and external residues as predicted by the *C. tepidum* Roco sequence model also indicated; internal residues are marked in orange, external residues marked in blue.

One region seemed to differ between the two sets of results. Proteins with the alanine blocks 10, 11, and 12 (LRRK2 residues 1372-1388) show equivalent dimerisation strength to the wild-type RocCOR protein, however the interaction with tubulin appears weaker (figure 32), particularly the association with block 11. These are the only residues presenting a clear difference in the LRRK2 RocCOR-tubulin interaction strength with maintained LRRK2 dimerisation. Therefore it is likely that this is the location of the interaction site. This region is indicated in figure 35. It is a prominent projection from the surface of the Roc domain.

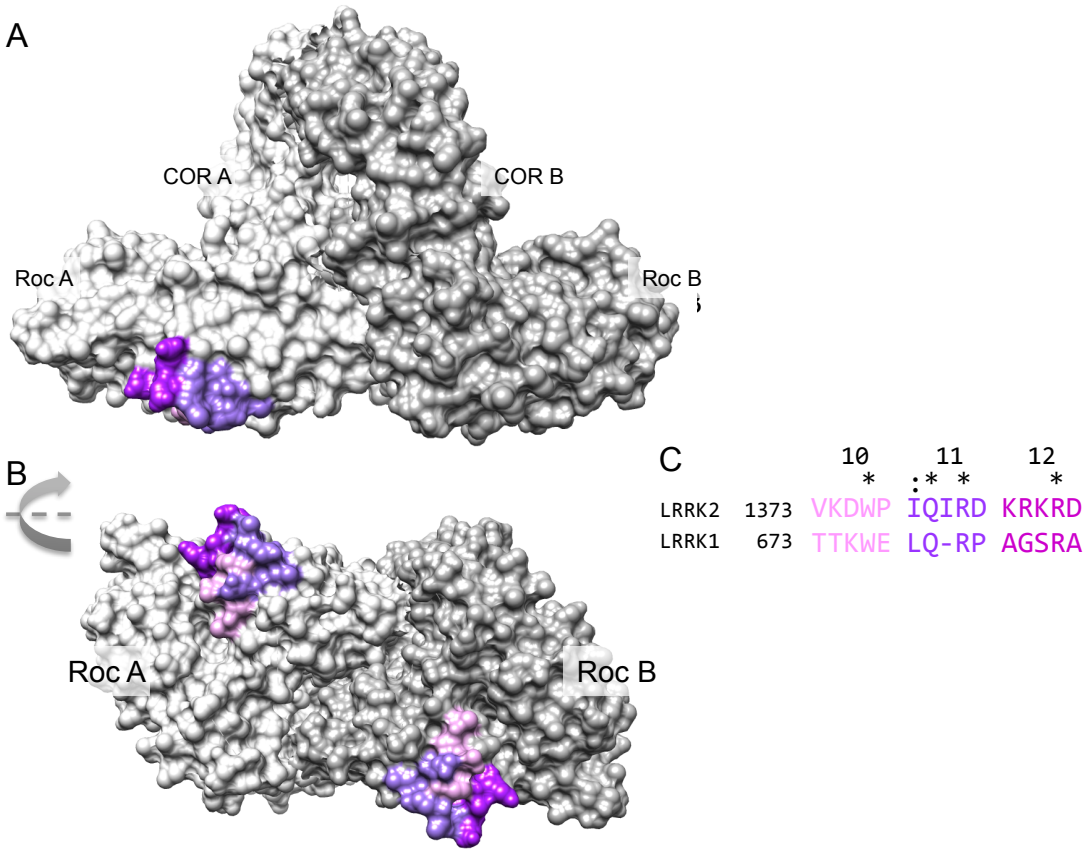

Figure 35. The proposed site of the LRRK2 RocCOR-β-tubulin interaction. A. The LRRK2 RocCOR domain dimer with the site of alanine blocks 10-12 indicated (residues 1373-1387). Block 10 is light purple, block 11 medium purple and block 12 is magenta, as shown in C. **B.** A 90° pivot of the figure reveals the full extent of the site, along with the comparable location on the second RocCOR domain within the dimer. **C.** Alignment of the LRRK1 and LRRK2 sequences within these alanine blocks, with the conserved residues highlighted.

There are four conserved residues between LRRK1 and LRRK2 in this 15 amino acid span. The first is internal (Trp1376) and it seems likely that the reason for a reduced interaction strength between tubulin and alanine block 10 (residues 1373-1377) is because the altered structure displaced the prominent residues of blocks 11 and 12 (residues 1378-1387). As the

interaction was not blocked, but simply weakened, it is expected that the interaction site spans more than one region.

There are three amino acids conserved between LRRK1 and LRRK2 in this region: Glu1379, Arg1381 and Arg1386. Thus it is proposed that these residues confer the interaction with TUBB4. The sites are indicated in figure 36.

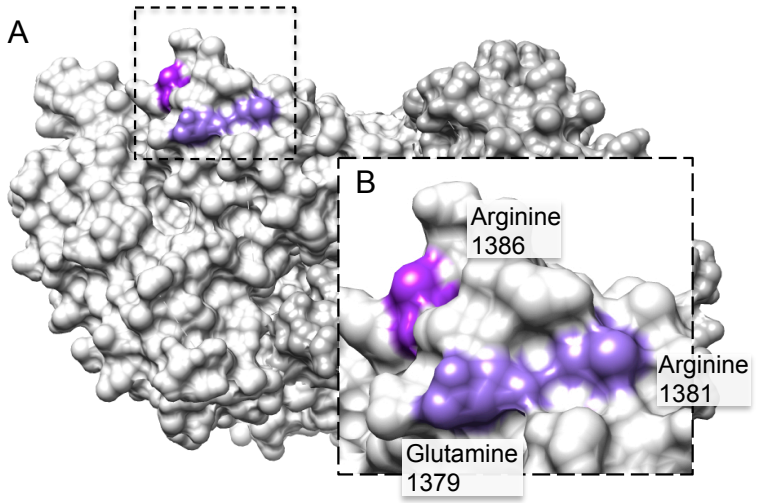

Figure 36. The proposed LRRK2 RocCOR residues involved in the β-tubulin interaction. A. The residues anticipated to be involved in the association between LRRK2 RocCOR and β-tubulin are indicated in shades of purple. The residues from block 11 are medium purple and the residue from block 12 is magenta, as used previously in figure 35C. **B.** A close-up view of the region highlighted in A, with the residues conserved between LRRK1 and LRRK2 marked.

The residues identified here as important for the LRRK2-β-tubulin interaction are predominantly positively charged (Lys362 in tubulin, Arg1386 and Arg1381 in LRRK2 RocCOR), suggesting the interaction may be mediated or stabilised by charge. Therefore the location of corresponding basic residues was investigated. Interestingly there are two basic residues in close proximity to Lys362 within the tubulin C-terminal construct, Glu325 and Asp357 (figure 37). These amino acids in tubulin are situated in a similar orientation to the arginine residues identified in LRRK2 and LRRK1, as modelled on the *C. tepidum* Roco protein. Thus it is possible that these negatively charged tubulin residues associate with the positively charged RocCOR residues to orient the interaction between tubulin and LRRK2.

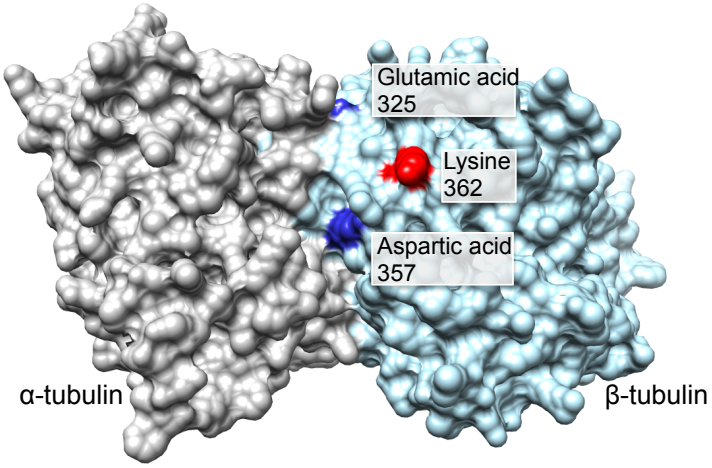

Figure 37. Negatively charged residues of the tubulin construct show comparable positions to the Roc arginines. The basic residues near Lys362 of the β-tubulin construct are indicated in blue. This may be relevant to the association with the LRRK2 RocCOR arginines suggested to facilitate the LRRK2- β –tubulin association.

3.2.4 Discussion

The site of the interaction between the LRRK2 RocCOR domain and β-tubulin has been identified in both β-tubulin and LRRK2.

The division of the Roc domain into overlapping thirds revealed that the association with tubulin occurred between amino acid residues 1328 and 1400, with an interaction strength indistinguishable to the full Roc domain. Importantly, dimerisation with full-length RocCOR was retained with this truncated construct, suggesting that structural integrity was maintained. This was also true of the Roc truncation protein 3 (1443-1515), though the interaction strength was reduced. However the central truncation protein 2 (1376-1465) did not interact with the RocCOR domain. This may be due to the absence of regions necessary to the interaction or because the tertiary structure was not retained. Modelling of the three fragments demonstrates that this second truncation is the least compact of the three, supporting the theory of a loss of structural integrity.

The Roc domain construct 1 (LRRK2 residues 1328-1400) includes multiple residues conserved between LRRK2 and the homologue LRRK1. According to the NCBI basic local alignment tool (Altschul et al., 1990), LRRK1-LRRK2 conservation is 35% in this region. LRRK1

is shorter than LRRK2, with a similar domain structure in enzymatic domains and leucine-rich and ankyrin repeats, but lacking armadillo repeats and a WD40 domain.

Due to the conservation between LRRK1 and LRRK2, a tubulin-LRRK1 RocCOR domain association was tested. Reyniers and colleagues previously reported that both LRRK1 and LRRK2 proteins interact with tubulin following mass-spectrometry of SHSY-5Y cells (Reyniers et al., 2014). Interestingly, the association with LRRK1 was limited to the TUBB, TUBB4 and TUBB6 tubulin isoforms and required tubulin Ala364 and Lys362 residues, as described previously in regard to the tubulin-LRRK2 interaction. This implicated the 23 fully conserved residues and 14 semi-conserved residues between LRRK1 and LRRK2 in the Roc truncation proteins as possibly contributing to protein-protein interaction.

LRRK1 and *LRRK2* show differential expression both throughout development and spatially (Westerlund et al., (2008); Zechel et al., 2010). *LRRK1* was found to be evenly distributed at low levels throughout the brain (Westerlund et al., 2008; but LRRK2 shows regional disparity (Galter et al., 2006; Melrose et al., 2006; Simon-Sanchez et al., 2006; Biskup et al., 2007; Higashi et al., 2007; Westerlund et al., 2008; Zechel et al., 2010). It is possible to speculate that although both LRRK1 and LRRK2 bind tubulin, their role as scaffolding structures facilitates the association of distinct proteins with the cytoskeleton at different time points and in different cell populations due to the spatial and temporal variances in expression.

The tubulin interaction site in residues 1328-1400 was then defined further with an alanine block scan. Sequences of 5 amino acids were replaced by alanines, an unreactive amino acid with a small side chain, meaning inhibition of associations with an interaction site within these 5 amino acids. This consistently revealed that the protein containing the alanine residue mutations would either associate with both RocCOR and tubulin, or neither. This suggests that either RocCOR dimerisation is required in order for the LRRK2-tubulin interaction to occur, or the residues replaced by alanine are important for both RocCOR dimerisation and the LRRK2-tubulin interaction, but the two interactions are independent of each other. It is likely that LRRK2 dimerisation is necessary for the LRRK2-tubulin interaction

as there is no instance of an interaction with tubulin in the absence of dimerisation. This may be mediated by structural alterations between the monomeric and dimeric forms of the LRRK2 RocCOR domain.

There was a partial correlation between whether the alanine block was internal or external to the protein structure (according to the *C. tepidum* LRRK2 homolog) and whether the association of the mutated RocCOR with the RocCOR domain and tubulin were maintained.

Amino acids located within the protein are likely to have a structural role, maintaining the surface morphology required to facilitate dimerisation and protein-protein interactions. Four proteins containing alanine blocks that replaced internal residues no longer interacted with LRRK2 RocCOR or tubulin (alanine blocks 2-3, residues 1333-1342 and 13-14, residues 1388-1397). The structural importance of these regions is shown by the conservation of 12 residues across LRRK2, LRRK1 and *C. tepidum* RocCOR here (1335-1337, 1339-41, 1389, 1391, 1393-1395, 1397). Therefore it is predicted that proteins containing these alanine blocks were unable to dimerise correctly, inhibiting the association with tubulin and LRRK2.

Alternately, mutation of the internal alanine block 15 (residues 1398-1404) did not prevent the association of the mutated RocCOR protein with RocCOR or tubulin. None of the residues in this region are conserved across LRRK1, LRRK2 or *C. tepidum* Roco and only the first residue is part of the original Roc truncation. Therefore the site of these mutations is likely to be away from the core interaction region and any structural changes resulting from the alanines may not have impacted the associations under investigation.

The mutation of residues located on the protein surface is less likely to cause wide-spread changes, unless the residues are located within the interaction site of interest. The interaction was maintained with proteins containing alanine blocks 7-8 (residues 1358-1367) (predicted to be on the RocCOR surface by the C. tepidum homolog model) and both RocCOR and tubulin. However, the association with both LRRK2 and tubulin was lost in RocCOR proteins containing alanine blocks 4-6 (residues 1343-1357), despite the predominantly external location of these residues. The *LRRK2* K1347A mutation in alanine

block 4 has been shown previously to obstruct the interaction with tubulin (Taymans et al., 2011; Law et al., 2014), either by blocking GTPase activity or by structural alteration leading to a loss of dimerisation. Meanwhile the leucine residues in blocks 5 and 6 are essential residues within alpha-helices (Leu1350, Leu 1351 and Leu 1354). Although the majority of residues in these blocks are external, incorrectly formed alpha helices are also likely to obstruct dimerisation and the association with tubulin.

The RocCOR protein containing external alanine block 9 (residues 1368-1372) does not interact with LRRK2 RocCOR or tubulin. This region contains two residues, Thr1368 and Iso1371, which are conserved in LRRK1, LRRK2 and *C. tepidum* Roco. Therefore this site is also likely to be structurally important, perhaps to dimerisation or the protein tertiary structure as the RocCOR domain changes orientation between GTP-bound and GDP-bound.

Finally, there is one region in which proteins containing the alanine mutations had an altered association between RocCOR and tubulin, suggesting that this region is the site of the tubulin-LRRK2 RocCOR domain interaction. In proteins containing alanine blocks 10, 11 and 12 (residues 1373-1387), the interaction with tubulin was weakened while RocCOR dimerisation strength maintained. Modelling located this putative interaction region away from the dimerisation site, on a slight protrusion of the Roc domain. Alanine block 10 appeared not to be as prominently exposed as the other two and it is possible that structural changes in this region weakened the interaction due to the close proximity to the interaction site.

Within this identified interaction sequence (1373-1388), there are three conserved residues between LRRK1 and LRRK2: Glu1379, Arg1381 and Arg1386. As the interaction was not fully blocked by any of the alanine block mutants, it is likely that the interaction site overlaps the boundaries of the alanine blocks. A follow-up experiment would be to test double and triple mutants of Glu1379, Arg1381 and Arg1386 to determine the importance of these residues further.

The LRRK2-tubulin interaction requires a positively charged lysine residue in tubulin and two of the three sites identified in the RocCOR domains are also positively charged arginines. Thus it is likely that these residues associate with corresponding negatively charged residues in the corresponding protein, in the proximity of the tubulin Lys362 binding site. The model of the interaction region in tubulin revealed two basic residues near tubulin Lys362: Glu325 and Asp357. They are oriented in a similar manner to the LRRK2 RocCOR Arg1381 and Arg1386 residues, supporting the evidence that these residues are involved in the LRRK2 RocCOR-tubulin association. The final LRRK2 residue proposed to be involved in the LRRK2 RocCOR-tubulin association is Glu1379. Glutamine residues are often involved in protein binding; they interact with other amino acids with polar side-chains.

Much of the work included here relies on the accuracy of the *C. tepidum* Roco LRRK2 homolog model. The correlation between the predicted Roco structure and the LRRK2 experimental results suggests that the organisation of this model is correct. There is an alternative model, in which the Roc and COR domains interlink with one another (Deng et al., 2008) and a re-analysed version in which extended flanking boundaries introduced a hydrophobic patch, orienting the domain in a similar way to the *C. tepidum* Roco model (Liao et al, 2014). This structure is missing several regions, including the putative tubulin binding site (1379-1386), suggesting they are regions of high flexibility. As the region of interest to the interaction could not be visualised with this structure, analyses using this model were not pursued.

This is the first work to identify a specific protein interaction region within the Roc domain, as well as regions important for LRRK2 dimerisation. It is not known if this site is specific to tubulins or a common interaction location between LRRK2 and associated proteins. The presence of an interaction site on each Roc domain within the LRRK2 dimer may be part of the process by which LRRK2 modulates the stability of microtubules, as discussed in chapter 3.3.

3. Results

3.3 LRRK2 and MT stability

As mentioned previously, the proximity of the RocCOR-tubulin interaction and the paclitaxel-tubulin binding site suggested a role for LRRK2 in MT stability (figure 38).

Paclitaxel is a cancer chemotherapy treatment, derived from the bark of the Western Yew tree. It binds tubulins in a stoichiometric ratio inside the MT lumen, promoting polymerisation into stable MTs and blocking disassembly (Parness and Horowitz, 1981; Kingston, 1994).

Also supporting the hypothesis of a role for LRRK2 in MT stability is the presence of the α-tubulin Lys40 acetylation site close to the LRRK2 binding site on β-tubulin. Acetylation occurs at α-tubulin Lys40 in stable MTs and strengthens interprotofibril interactions. Unacetylated MTs are therefore more flexible and dynamic (Piperno et al., 1987, Janke and Bulinski, 2011; Cueva et al., 2012).

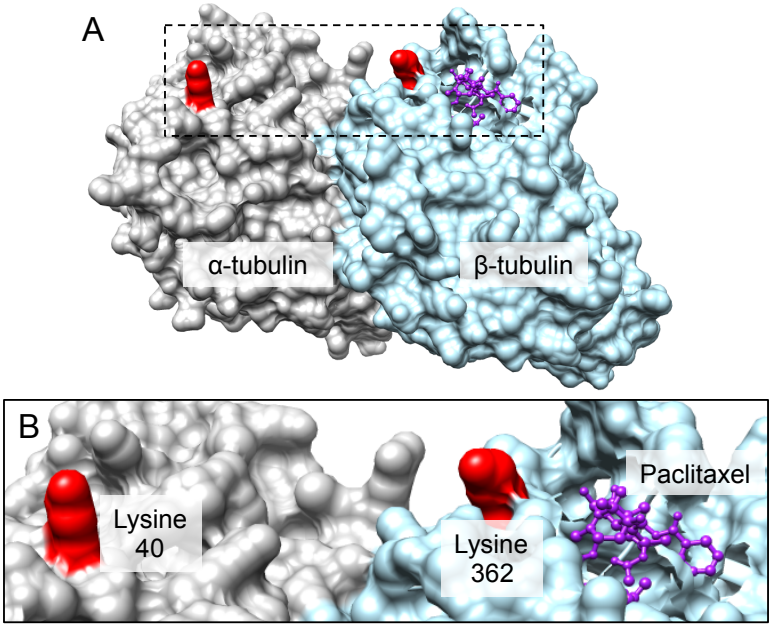

Figure 38. The β-tubulin Lys362 LRRK2 binding site is near two sites important for MT stabilisation. A. β-tubulin Lys362 is on a similar plane to both the stabilising paclitaxel binding site and α-tubulin Lys40 acetylation site, a marker for stable MTs. They are all located inside the MT lumen. **B.** A close-up view of the region indicated in A.

3.3.1 LRRK2 localises to dynamic growth cone MTs

The predicted luminal binding site of LRRK2 is likely to be poorly accessible to the 280 KDa LRRK2. Thus the expectation that LRRK2 is interacting with dynamic MTs or protofibrils was

explored. Dynamic MTs have increased flexibility in the inter-protofibril connections, therefore improved luminal accessibility to large proteins such as LRRK2.

Using a fixation technique specific to cytoskeletal structures, we were able to detect LRRK2 in SH-SY5Y neurite growth cones. Levels declined along the axon toward the cell body (figure 39) in both wild-type cells expressing endogenous *LRRK2* levels and in cells stably overexpressing LRRK2.

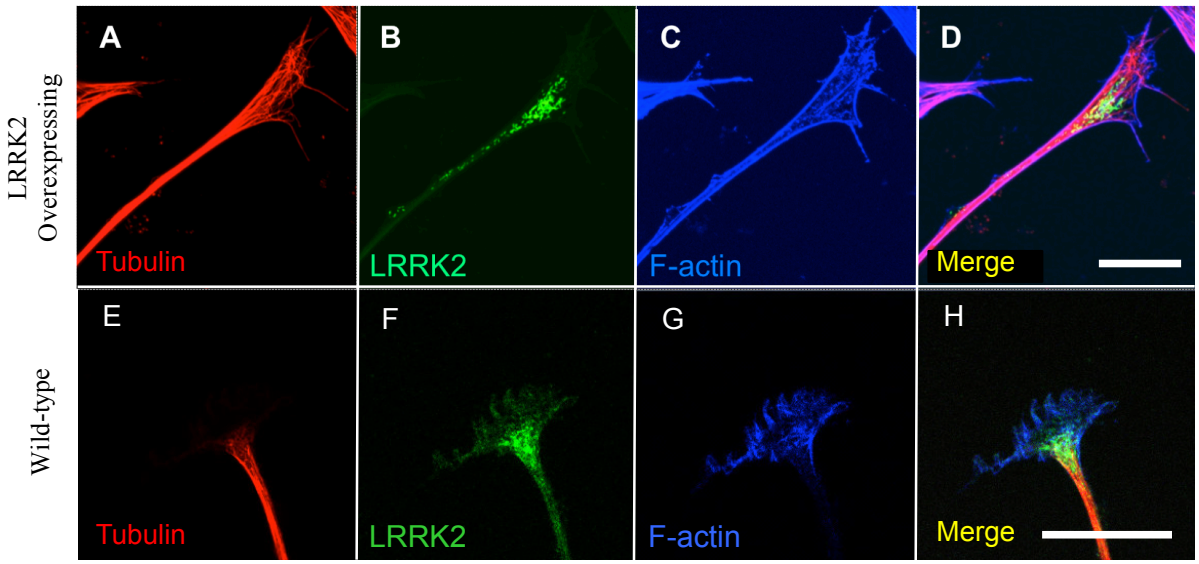

Figure 39. LRRK2 localises preferentially to growth cones. LRRK2 localises preferentially to growth cones in both stably overexpressing (**A-D**) and wild-type (**F-H**) SH-SY5Y neurites. A cytoskeletal specific fixation method revealed stably overexpressed LRRK2 and endogenous LRRK2 localised to growth cones in SH-SY5Y neurites with association declining along the axon (**B** and **F**). LRRK2 imaged using Epitomics LRRK2 antibody (details in Materials and Methods). Scale bars 20 µm, A-D imaged by Veronica Leinster.

Stable MTs are found predominantly in the 'C' (central) zone of the growth cone, the site of the transition between stable and dynamic MTs, whereas the 'P' (peripheral) zone is composed of actin filaments and more dynamic (tyrosinated) MTs. The detection of over-expressed LRRK2 in the 'C-zone', (Law et al., 2013), supports the notion that LRRK2 associates with dynamic MTs, in a region where the MT lumen is more accessible.

3.3.2 LRRK2 reduces α-tubulin acetylation

As mentioned previously, MTs undergo acetylation and deacetylation at residue Lys40, located in the MT lumen. Due to the close proximity of this location in α-tubulin and the LRRK2-β-tubulin binding site, combined with the LRRK2 association with the dynamic growth cone, a functional connection between LRRK2 and acetylation was next investigated.

An antibody specific for acetylated α-tubulin Lys40 revealed a dramatic difference in acetylation between *Lrrk2* knock-out MEFs and their wild-type counterparts. *Lrrk2* knock-outs displayed a striking increase in tubulin acetylation (figure 40).

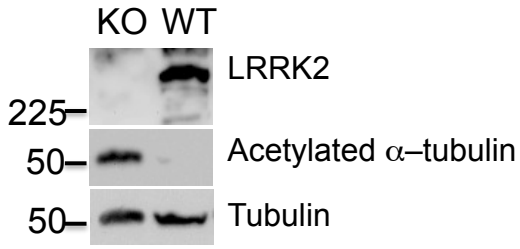

Figure 40. *Lrrk2* expression correlates inversely with tubulin acetylation. Western blotting demonstrates acetylation of α-tubulin Lys40 is strongly increased in *Lrrk2* knock-out (KO) MEF cells, compared with wild-type (WT) cells (from Daniel Berwick).

This inverse correlation between LRRK2 and acetylation of α-tubulin Lys40 was confirmed in immunofluorescence studies comparing wild-type and *Lrrk2* knock-out MEF cells. A clear increase in acetylated tubulin was shown in the knock-out MEF cell line (figure 41). Not only was a dramatic increase in acetylation seen in the *Lrrk2* knock-out cells, but morphological changes were also visible: changes in the MT and actin cytoskeleton structure included a reduction in F-actin stress fibres, an increase in filopodia and increased cell adhesion. In addition, there was a reduction in nuclear density, an apparent loss of polarity and an increase in cell and nucleus size.

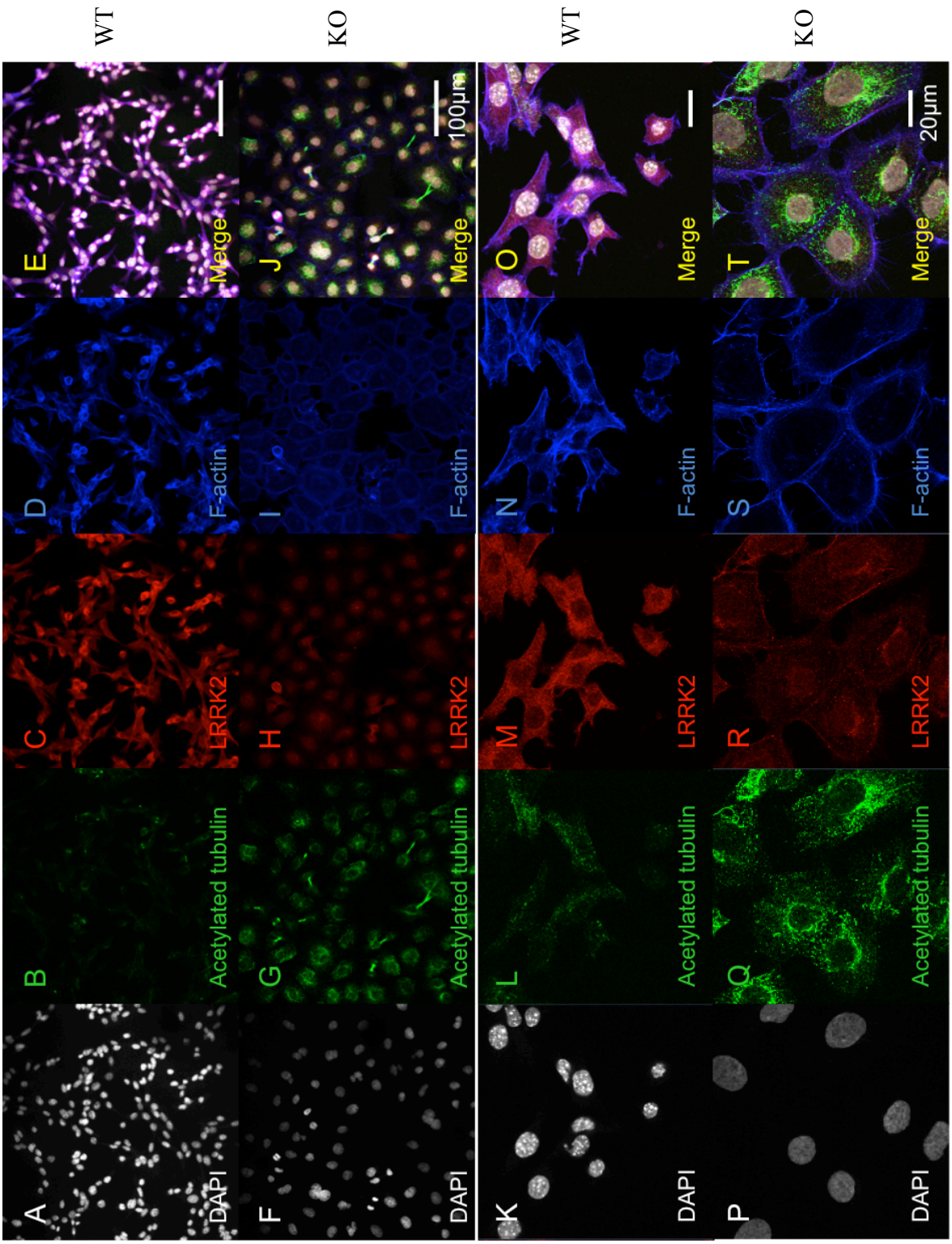

Figure 41. *Lrrk2* knock-out MEF cells reveal dramatic morphological changes. 20x magnified (**A-J**) and 63x magnified (**K-T**) wild-type (WT) (**A-E, K-O**) and *Lrrk2* knock-out (KO) (**F-J, P-T**). *Lrrk2* knock-out MEF cells showing increased acetylated tubulin in the knock-out cells as well as morphological changes including changes in the size and density of nuclei, a loss of polarity and altered stress fibre, filopodia and cell adhesion. The scale bars are 100 µm (20x zoom) and 20 M (63x zoom).

3.3.3 Tubulin isoform overexpression differently alters the proportion of acetylated tubulin

After detecting isoform-specific differences in the LRRK2-tubulin interaction in yeast, acetylation levels were compared in the presence of overexpressed tubulin isoforms. Cells overexpressing tubulin isoforms that do not interact directly with LRRK2 (TUBB1 and TUBB3), exhibit an increased proportion of acetylated tubulin compared with endogenous levels (figure 42). Conversely, overexpression of tubulin isoforms that do interact with LRRK2 (TUBB4 and TUBB6) do not alter the proportion of acetylation.

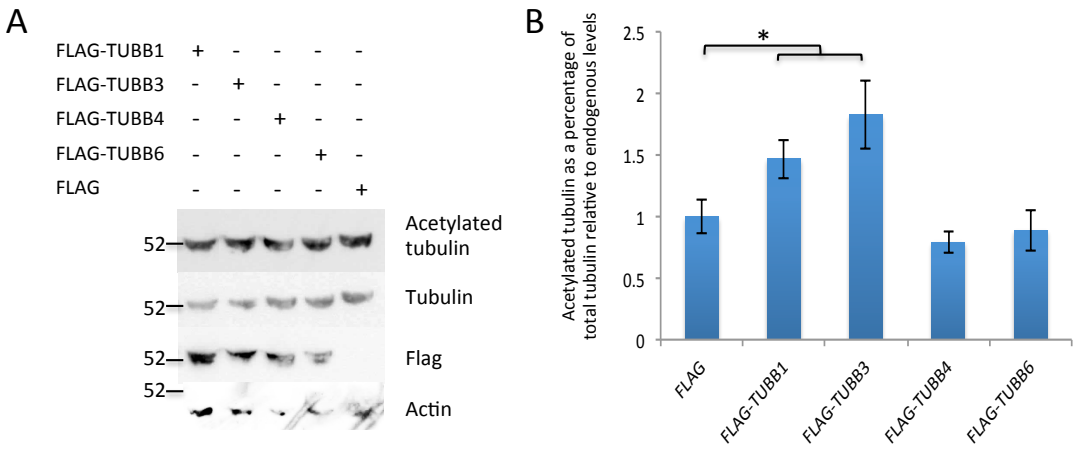

Figure 42. The proportion of acetylated tubulin varies with the tubulin isoform overexpressed. A. Western blot showing increased acetylated tubulin as a proportion of total tubulin in HEK cells overexpressing TUBB1 and TUBB3. **B.** The proportion of acetylated tubulin is increased by 50-80% in cells overexpressing TUBB1 and TUBB3 (no LRRK2 interaction) compared with TUBB4 and TUBB6 (LRRK2 interaction). Statistical significance was determined using a two sample equal variance T-test, n=3, * $p<0.05$, Error bars = SD.

3.3.4 The LRRK2 N-terminus effects the changes in acetylation

Western blots to determine if altered acetylation could be attributed to a single LRRK2 region surprisingly suggest that it is the region prior to RocCOR effecting the changes (figure 43). This includes the N-terminal LRR, armadillo repeat and ankyrin domains.

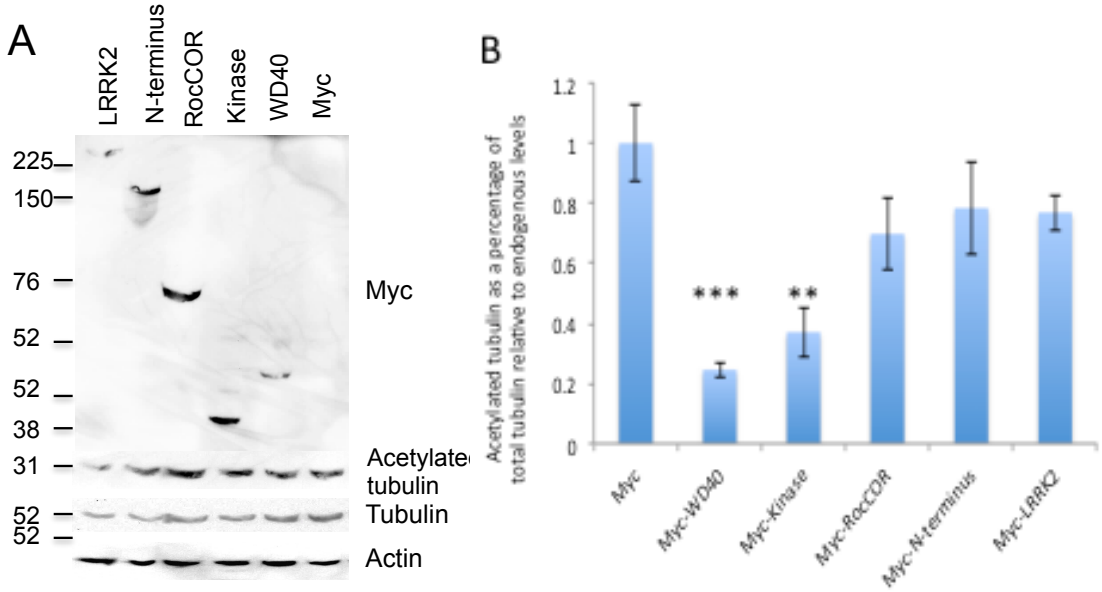

Figure 43. The LRRK2 N-terminus mediates reduced α-tubulin acetylation in HEK cells. A. Western blot demonstrating the reduction in acetylation relates to the region of LRRK2 prior to RocCOR, incorporating the N-terminus, leucine rich repeat, ankyrin and armadillo repeat domains**. B.** The LRRK2 reduction in acetylation is facilitated by the N-terminus (incorporating the entire region prior to RocCOR), which reduces the proportion of acetylated tubulin to a similar level as full-length LRRK2. Statistical significance was determined using a paired T-test, n=6, ** p<0.01, *** p<0.001, error =SD.

3.3.5 Blocking the paclitaxel binding site prevents LRRK2 binding tubulin

Alignment of α- and β-tubulin amino acid sequences revealed an eight amino acid insertion in the α-tubulin S9-S10 loop (figure 44A). This loop spans the equivalent region of the β-tubulin-paclitaxel binding site (figure 44B). It also revealed that α-tubulin has an alanine residue at 374, equivalent to the Ala364 residue in β-tubulin isoforms that bind LRRK2.

A

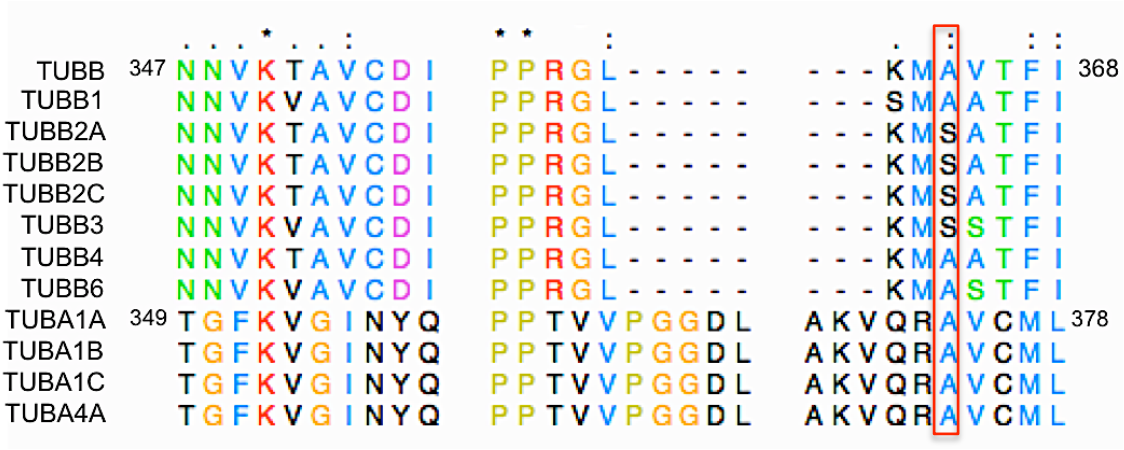

B

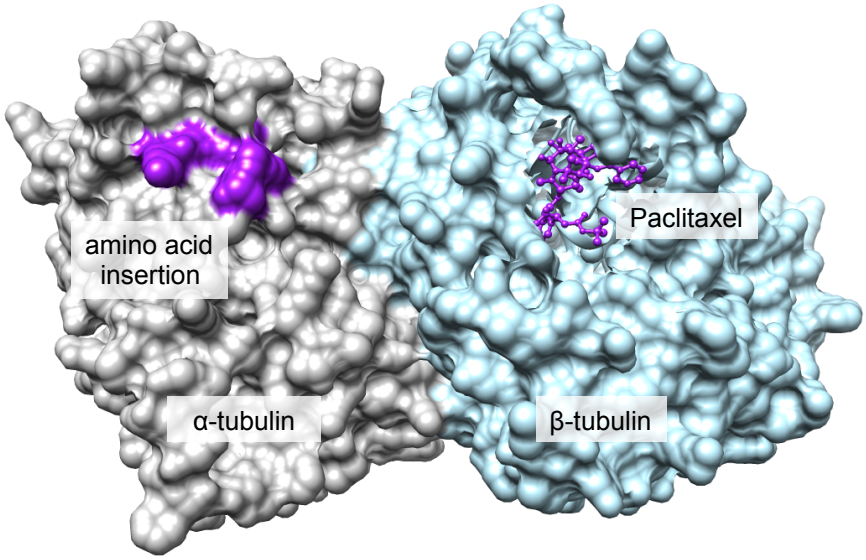

Figure 44. Differences between α- and β-tubulin in the paclitaxel/LRRK2 binding site. A. Alignment of the α- and β-tubulins demonstrates an insert in α-tubulin equivalent to the β-tubulin-paclitaxel binding site, immediately prior to residues involved in the β-tubulin-LRRK2 association and reveals an Ala374, equivalent to the β-tubulin Ala364 required for the interaction with LRRK2. **B.** The paclitaxel binding site in β-tubulin. α-tubulin has an 8 amino acid insertion in the equivalent location, indicated in purple.

Hypothesising that the 40% similarity between α- and β-tubulins may mean that a) without the B9-B10 loop, α-tubulin could interact with LRRK2 RocCOR and that b) LRRK2 may compete with paclitaxel or require access to the paclitaxel-binding site in interacting with β-tubulin, reciprocal mutations were made; the loop extension was added to β-tubulin and removed from α-tubulin.

Deletion of the extension in TUBA1A did not facilitate an association (figure 45). The deletion of the insertion is not sufficient to facilitate a LRRK2-α-tubulin interaction, demonstrating that additional residues are important for the β-tubulin-RocCOR domain interaction. However, inserting it into TUBB4 and TUBB6 prevented their interaction with

the RocCOR domain, showing the presence of the B9-B10 loop extension is inhibitory to the interaction with LRRK2. This may indicate that the tubulin-LRRK2 interaction blocks this region and is inhibitory to paclitaxel binding and vice-versa.

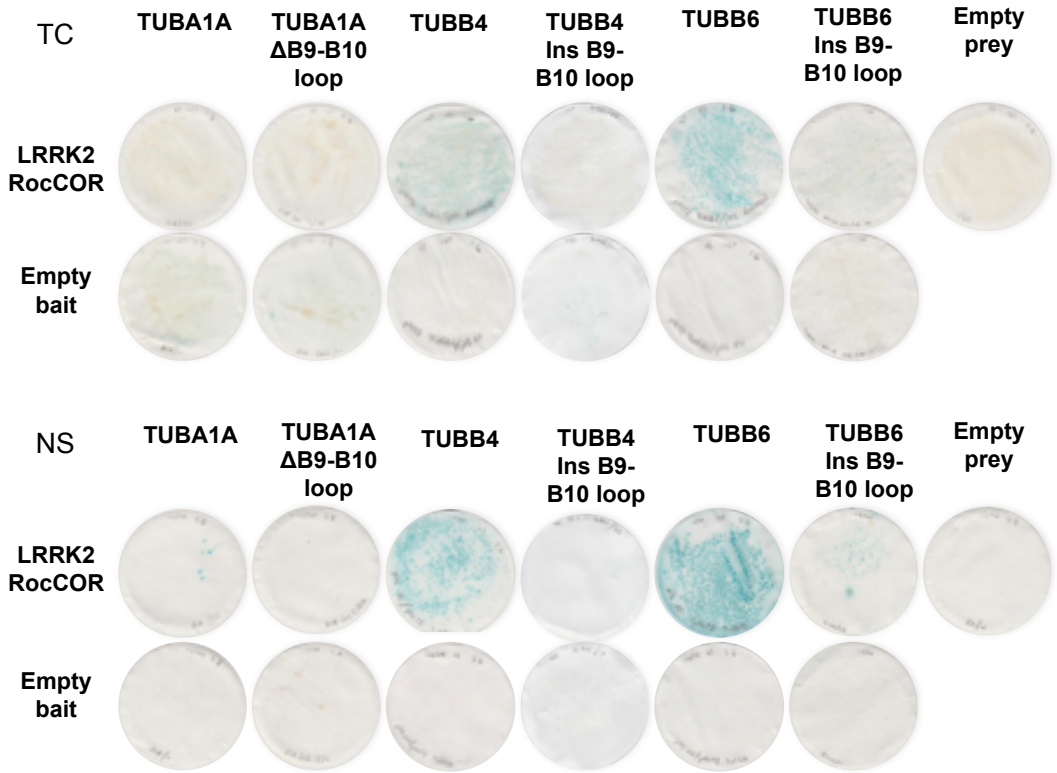

Figure 45. Tubulin-LRRK2 binding requires access to the paclitaxel binding site. Deletion of the B9-10 loop in α-tubulin (ΔB9-B10 loop) does not facilitate an interaction with the LRRK2 RocCOR domain. Insertion of the loop into β-tubulin (Ins B9-B10 loop) prevents the interaction between tubulin and the LRRK2 RocCOR domain. T Both transformation control and nutritional selection plates are shown, images representative of 3 separate experiments.

Paclitaxel-bound tubulin alters the tubulin crystal structure (figure 46) in the LRRK2 binding region, with the parallel Arg320 and Lys362 projections no longer extending in a parallel, aligned manner. Instead, they project away from each other in different planes. Therefore it is possible that LRRK2 doesn't bind across the paclitaxel binding site, but that the structure of paclitaxel bound MTs is changed in a manner inhibitory to the LRRK2-tubulin interaction.

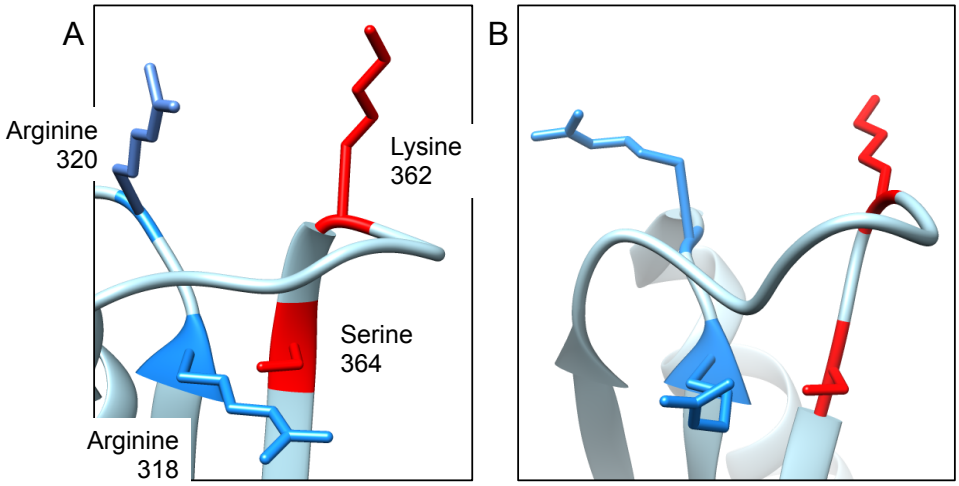

Figure 46. Models derived from paclitaxel-bound and unbound tubulin crystal structures alter the tubulin configuration at the LRRK2 binding site. A. Residues relevant to the LRRK2-tubulin interaction using PDB model 1TUB derived from the crystal structure of porcine α/β dimers unbound to paclitaxel (Model used in previous figures). **B.** The same residues in PDB model 1JFF derived from the crystal structure of bovine α/β tubulin dimers bound to paclitaxel.

3.3.6 LRRK2 reduces MT acetylation in paclitaxel treated cell lines

To see if the suggestion that LRRK2 is unable to bind tubulin if the paclitaxel binding site is blocked could be validated, paclitaxel-treated HEK cells were transfected with LRRK2.

A preliminary blot showed growth of cells in media containing 10 nM paclitaxel induced a strong increase in acetylated α-tubulin (figure 47).

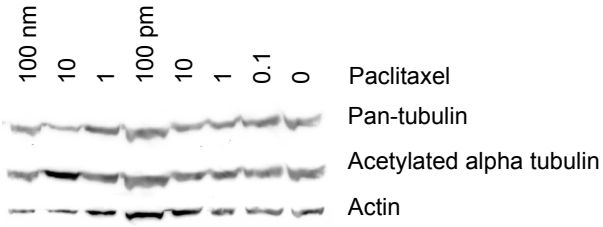

Figure 47. A preliminary concentration gradient indicates strong acetylation in the presence of 10nM paclitaxel. A Western blot of HEK cells incubated in media containing paclitaxel for 24 hours demonstrate a clear increase in acetylated tubulin following a 10 nM paclitaxel incubation.

HEK cells grown in 0 or 10 nM paclitaxel revealed a clear increase in the proportion of acetylated tubulin in the presence of paclitaxel, which was reduced by overexpression of LRRK2.

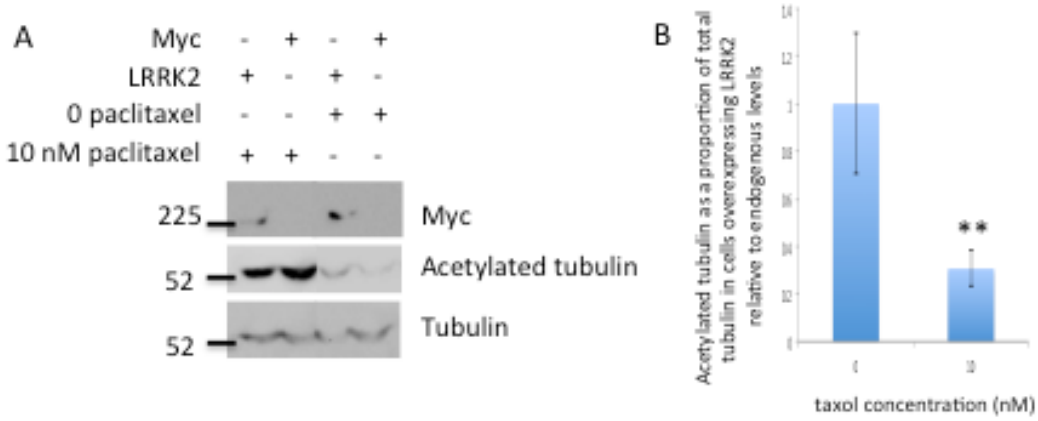

Figure 48. LRRK2 reduces paclitaxel-induced acetylation in HEK cells. **A.** Western blotting reveals increased acetylation in the presence of 10nM paclitaxel is reduced by LRRK2 overexpression. **B.** In cells grown in the presence and absence of 10nM paclitaxel, the proportion of acetylated tubulin declined in the presence of overexpressed LRRK2. Statistical significance was determined using a paired t-test, n=3, , ** p<0.01, error bars = SEM.

3.3.7 Discussion

3.3.7.1 The site of the LRRK2-tubulin interaction within cell growth cones

This thesis identified the location of the interaction site between LRRK2 and MTs on the MT luminal surface, a region likely to be poorly accessible to the large LRRK2 protein. This suggested that the association was likely to occur either with tubulin dimers/protofilaments, prior to incorporation into stable microtubules, or at the microtubule +end, within the growth cone. Garvalov and colleagues (2006) described the presence of 7 nM particles within MTs, including some with dual associations. They predict that a protein of this size is likely to be at least 200 KDa, which could include the 280 KDa LRRK2. There is some disparity however, with a different study identifying the average internal MT diameter as approximately equivalent to three tubulin monomers (Cueva et al., 2012). Although the crystal structure of LRRK2 has not been resolved, at 280 KDa, the protein is far larger than the compact 50 KDa of tubulin and is thus unlikely to fit within MTs, not withstanding that it is expected to dimerise. The particles within the MTs were not identified at the MT growth cones, but within the axonal lumen (Garvalov et al., 2006). It has previously been reported that tau may associate with-and stabilise-MTs internally, as well as externally and is thus a likely candidate for the particles identified (Makrides et al., 2004).

MTs in the central growth cone region do not follow the strict bundle formation of MTs in axons, the structure is elastic due to the requirement for dynamic instability. They are defasciculated into single tubules which follow no strict pattern. They may be straight, crooked, form loops or bends, remain in the C domain or extend out into the P domain (Tankak and Kirschner, 1991). Indeed, using a cytoskeletal-specific fixation technique, this thesis reveals that the LRRK2 association with MTs is predominantly located at the growth cone, with some association along the stable axons. Thus the lack of regulated structure and weaker interprotofibril interactions in this region are likely to facilitate a less structured luminal region, allowing LRRK2 to bind. Alternately, it is possible that LRRK2 plays a

structural role in maintaining this increased luminal space, by spanning the MT lumen. Each RocCOR domain within the LRRK2 dimer could then associate with a tubulin monomer on different MT filaments.

3.3.7.2 A role for LRRK2 in MT stability

As mentioned previously, the site of the LRRK2-tubulin interaction is in the vicinity of two sites important for MT stability: the paclitaxel binding site and the α-tubulin Lys40 MT acetylation site. This proximity suggested the possibility that the role of LRRK2 at MTs could be to modulate stability.

Comparing levels of acetylated tubulin in wild-type and knock-out MEF cells revealed a dramatic reduction in acetylated tubulin in the wild-type cells compared to the *Lrrk2* knock-outs, both in Western blotting and in immunohistochemical studies. Additionally, morphological changes were seen, with cytoskeletal alterations, a loss of polarity and increased cell adhesion. It would be interesting to examine additional markers of cytoskeletal stability between *Lrrk2* wild-type and knock-out MEF cells. These would include tyrosinated tubulin, glycosylated tubulin, MAPs (including tau and MAP1B, identified as LRRK2 interactors (Kawakami et al., 2012; Chan et al., 2014)), G-actin and F-actin, in order to determine how other cytoskeletal features are affected in the absence of LRRK2.

The phenotypic change identified between *Lrrk2* knock-out and wild-type MEF cells is similar to well-known effects of the small GTPases Rho, Rac and cdc42 on Swiss-3T3 fibroblasts, particularly the changes in filopodia and adhesion complexes (Hall, 1998), suggesting the RocCOR GTPase domain mediates the effects of LRRK2 on the cytoskeleton. As discussed in section 1.3.3, LRRK2 has been linked with multiple signalling pathways, including MAPK, TNF-α, JNK and Wnt. The small GTPases (Rho, Rac and cdc42) have also been linked to these cascades (Chen et al., 2012a; Hall, 1998, Wojciak-Stothard et al., 1998; Habas and He 2006) which have many roles, including actin cytoskeleton remodelling, cell polarity regulation, cell

adhesion and regulation of MT dynamics (Wojack-Stothard et al., 1998; Mezzacappa et al., 2012; Habas et al., 2006; Akiyama and Kawasaki, 2006; Ciani et al., 2004).

Interestingly, it has been reported that over-expression of the small GTPase Rac1 rescues LRRK2 G2019S mutant-induced reduced neurite length, where cdc42 and RhoA had no effect (Chan et al., 2011) suggesting that Rac1 is a downstream target of LRRK2, or that they work in tandem, antagonistically regulating cytoskeletal dynamics.

The overexpression of different β-tubulin isoforms revealed an effect on the proportion of acetylated tubulin within cells, consistent with both the β-tubulin-LRRK2 interaction and alterations in MT stability previously observed. Cells overexpressing the β-tubulin isoforms which do not interact with LRRK2 (TUBB1, TUBB3) demonstrated an increased proportion of acetylated tubulin, unlike cells overexpressing tubulin isoforms which do interact with LRRK2 (TUBB4, TUBB6). Only tubulin was overexpressed in these cells, indicating that these effects are mediated by endogenous LRRK2 and supporting the theory that particular tubulin isoforms are expressed to control the LRRK2-MT interaction and thus MT stability. Although we were unable to co-IP LRRK2 with specific tubulin isoforms to support the findings identified in yeast two-hybrid experiments (chapter 3.1, figure 27), this result suggests that the yeast LRRK2-tubulin interaction results are transferrable to mammalian cells. As an extension to this experiment, it would be useful to transfect the tubulin isoforms into both wild-type and knock-out MEF cells to confirm the effect is mediated by LRRK2.

In further support of a role for the LRRK2-tubulin association in MT stability, TUBB6 content has previously been associated with reduced stability in MTs. Individuals naturally expressing higher levels of *TUBB6* have reduced MT stability and reduced inflammatory cell death (Salinas et al., 2014) while RNAi-induced inhibition of *TUBB6* expression resulted in highly acetylated, hyperstable MTs which inhibited cell proliferation. This indicates that the ubiquitous low *TUBB6* expression throughout the body is vital to MT function, preventing

the cells becoming overly stable (Bhattacharya et al., 2008). The data presented here suggests this may be related to an interaction with LRRK2.

Whether the reduced MT acetylation in the presence of LRRK2 is caused by decreased acetylation, increased de-acetylation or a combination of the two, has not been defined. The enzymes involved in these processes are α-tubulin Lys40 acetyltransferase (MEC-17), which catalyses acetylation and the tubulin deacetylating enzymes sirtuin2 (SIRT2) and histone deacetylase 6 (HDAC6) (Castro-Castro et al., 2012; North et al., 2003). It is possible that LRRK2 alters the activity of these enzymes. Alternately the large size of LRRK2 may simply block access to the Lys40 site. Although it is not clear how LRRK2 alters acetylation at MTs, it is clear that the LRRK2-tubulin interaction affects MT acetylation, promoting reduced MT stabilisation.

Meanwhile, it was surprising to detect that the LRRK2 region mediating the changes in acetylation is not the β-tubulin-interacting RocCOR domain. Instead, it is mediated by the N-terminal regions situated prior to the RocCOR domain. There is less data available on these domains, however they have been linked with LRRK2 function and structure. Gotthardt and colleagues (2008) postulate that LRRK2 dimerisation is triggered by a domain other than the RocCOR domain, such as the LRR domain. The LRR domain was also found to interact directly with the Roc domain in a yeast two-hybrid screen (Greggio et al., 2008). Thus, it is possible that the overexpressed LRRK2 N-terminus could dimerise with endogenous LRRK2 to mediate the changes in acetylation. The LRRK2 N-terminal domains may physically block acetylation within the cells as the RocCOR domain alone is not large enough.

Additionally, truncated LRRK2 which lacks an N-terminus has increased autophosphorylation activity (Greggio et al., 2008), demonstrating an intervention between this region and the catalytic LRRK2 domains. Altered LRRK2 autophosphorylation could control the association with MTs or alternately, the N-terminus may mediate reduced acetylation via enzyme activity as mentioned previously, without a direct MT association.

It would be interesting to identify if LRRK1 is also involved in acetylation. The results described above suggest the N-terminal domains are involved in the ability of LRRK2 to reduce acetylation. The LRRK1 N-terminus is particularly divergent from the LRRK2 N-terminus, being much shorter, with reduced numbers of LRRs, additional ankyrin-rich repeats and no armadillo repeats (Taylor et al., 2007; Gilsbach and Kortholt, 2014). As described in results section 3.2, expression of *Lrrk1* and *Lrrk2* differs throughout rat brain development and into adulthood. As LRRK1 is not linked with PD and neither are pathogenic *LRRK2* mutations introduced into *LRRK1* pathogenic (Greggio et al., 2007), the ability to inhibit tubulin acetylation and alter MT stability could be a clear point of divergence between the two proteins.

At the MT luminal surface, where the RocCOR-β-tubulin interaction occurs, α-tubulin isoforms contain a comparable β-tubulin paclitaxel-binding site blocked by an eight amino acid insertion, referred to as the B9-B10 loop (Löwe et al., 2001) and an alanine at the site equivalent to β-tubulin Ala364. Removal of the loop did not enable an interaction between TUBA1A and LRRK2. In the analogous location of the important β-tubulin Lys362 residue, α-tubulin has a glutamine residue. This has a similarly large side-chain but is uncharged and may thus be inhibitory to the association, or additional structural differences between α- and β-tubulins could prevent binding with LRRK2. However, the introduction of the B9-B10 loop into TUBB4 and TUBB6 did prevent the association with LRRK2, suggesting that LRRK2 requires access to the paclitaxel binding site in order to associate with MTs.

It is anticipated that the lumen of growth cones is not the only location where LRRK2 associates with the cytoskeleton; additional cytoskeletal LRRK2 binding partners including tau and MAP1B (Kawakamie et al., 2012; Chan et al., 2014) and a LRRK2 WD40-actin association might confer additional functions of LRRK2 at the cytoskeleton. Many protocols routinely stabilise microtubules using paclitaxel before looking at cytoskeletal associations. Concentrations of up to 100nM, a similar magnitude to the 10nM used here were also Included for testing the MT association with LRRK2 (Yvon et al., 1999; Arnal et al., 1995;

Brabander et al., 1981a, 1981b; Gillardon, 2009; Kett et al., 2012). As paclitaxel has been found to bind tubulin with a 1:1 stoichiometry, it is possible that the paclitaxel-stabilised MTs are not able to bind LRRK2 in the same manner as untreated MTs. In these studies, the alternative means of association between LRRK2 and the cytoskeletal network may show increased prominence. This, or the specific cytoskeletal fixation method, may explain why the significant presence of LRRK2 at the growth cone detected here in SH-SY5Y cells has not been previously described.

In order to test whether LRRK2 continues to associate with MTs in the presence of paclitaxel, cells were seeded in media containing 10nM paclitaxel. 24 hours later these cells were transfected with LRRK2. In this case, the MT-paclitaxel association would already have formed, yet LRRK2 was still able to induce a reduction in the proportion of acetylated tubulin within the cells. This may be due to LRRK2 reducing acetylation not simply by binding the MTs, instead being involved in enzyme activation or recruitment as mentioned previously, or LRRK2 outcompeting paclitaxel as the cells continued to grow and divide. Alternately the dynamic MT structure at growth cones may result in slightly distorted tubulin conformations; inhibitory to the paclitaxel association (which occurs within a pocket) but not to LRRK2 docking at the exposed Lys362 residue, meaning that LRRK2 continues to be able to bind in the dynamic growth cone in the absence of paclitaxel. It is of interest that, in HEK cells, LRRK2 does not have the dramatic effect on acetylation in the absence of paclitaxel. This may relate to a reduced innate MT stability within HEK cells compared to MEF cells but the levels of tubulin acetylation in HEK and MEF cells should be directly compared.

In support of an increased acetylation and MT stability in the absence of LRRK2, neuronal cultures grown from *Lrrk2* knock-out mice develop significantly longer neurites, with increased branching, than cultures grown from their wild-type littermates (MacLeod et al., 2006; Parisiadou et al., 2009; Dächsel et al., 2010).

Acetylation occurs on long-lived, depolymerisation resistant, MTs with slow dynamics (Piperno et al., 1987, Schulze et al., 1987 and Webster and Borisy, 1989), with the enzyme

MEC-17 diffusing along the MT from each end. (Szyk et al., 2014). However this does not happen to all MTs, there is a process by which specific MTs become stabilised in this manner. It is possible that the presence of a lumenal LRRK2-MT association inhibits diffusion of MEC-17, preventing acetylation of α-tubulin K40 in that MT.

Additionally, both overexpression of rodent Lrrk2 and expression of *Lrrk2* containing pathogenic mutations cause an accumulation of phosphorylated tau (Macleod et al., 2006; Li et al., 2009; Lin et al., 2010, Melrose et al., 2010), while *Lrrk2* knock-out mice have reduced tau phosphorylation (Gillardon, 2009). Phosphorylated tau detaches from MTs, destabilising them and increasing their dynamic flexibility. The reduced phosphorylation of tau in *Lrrk2* knock-out mice would also contribute to MT stabilisation. Therefore the role for LRRK2 in MT stability described here is widely supported by current literature and introduces a novel function for LRRK2. However it is noted that as not all PD sufferers develop tangles, this does not fully explain onset of the disease. It has been suggested that LRRK2 is able to direct toxicity through both tau and alpha-synuclein, and seemingly without deposition of either protein, though the mechanisms are not fully understood (Taymans and Cookson, 2010).

As mentioned in section 1.3.4.2, the depolymerising agent rotenone is significantly more toxic to SN neurons than in other brain regions (Ren et al., 2005). The LRRK2 R1441C, R1441G and R1441H mutations have all been found to disrupt the association between LRRK2 and tubulin, with the R1441C mutation enhancing the association strength and the others reducing it (Law et al., 2014). Therefore it is particularly important to the vulnerable cells in the SN that MT function and homeostasis is maintained. This indicates that alterations in MT stability caused by changes in LRRK2 could contribute to the pathogenesis of PD.

It is important for future studies to identify the exact mechanisms by which LRRK2 mediates alterations in MT stability. This may eventually be the basis of a novel therapeutic approach for PD sufferers.

3. Results

3.4 The identification of novel PD-associated variants in familial, late-onset PD

In a collaboration between the University of Tübingen and the Centre de Recherché de l'Institut du Cerveau et de la Moelle Epiniere, 26 late-onset, familial PD patients and their families were included in a linkage analysis to detect novel genes involved in the disease. The 13 German index cases were then exome sequenced. Following error removal, inheritance analysis and frequency detection, the remaining variants were screened for causative mutations. Those deemed plausibly linked to PD were confirmed by chain-termination sequencing and the family screened for segregation with the disease.

3.4.1 Linkage analysis revealed novel suggestive PD loci

A total of 71 PD sufferers from the 26 families were analysed by Affymetrix 250K DNA microarray. The microarray detected 262263 SNPs, which was reduced to 18422 SNPs by the removal of variants in linkage with each other. These remaining markers were used in the linkage analysis by Claudia Schulte of the University of Tübingen.

The linkage was analysed using both a classic dominant and non-parametric model, as the mode of inheritance was unlikely to be simple autosomal dominant in all families. The classic dominant model revealed a maximum heterogeneity logarithm of the odds (HLOD) score of 3.2 at 3p21-p23. A suggestive score of 2.2 was also obtained in region 17p13 (figure 49A). The non-parametric analysis identified an allele of interest in region 1p31-p22 with a score of 2.7 (figure 49B). A score of 3 or above is considered evidence for linkage.

Three novel sites of PD variance were identified, none of which overlaps with known PD genes or loci, though the Chromosome 1 site is close to *PARK10* at p32 (figure 49C). Following exome sequencing, this data was used in the detection of potentially pathogenic SNPs.

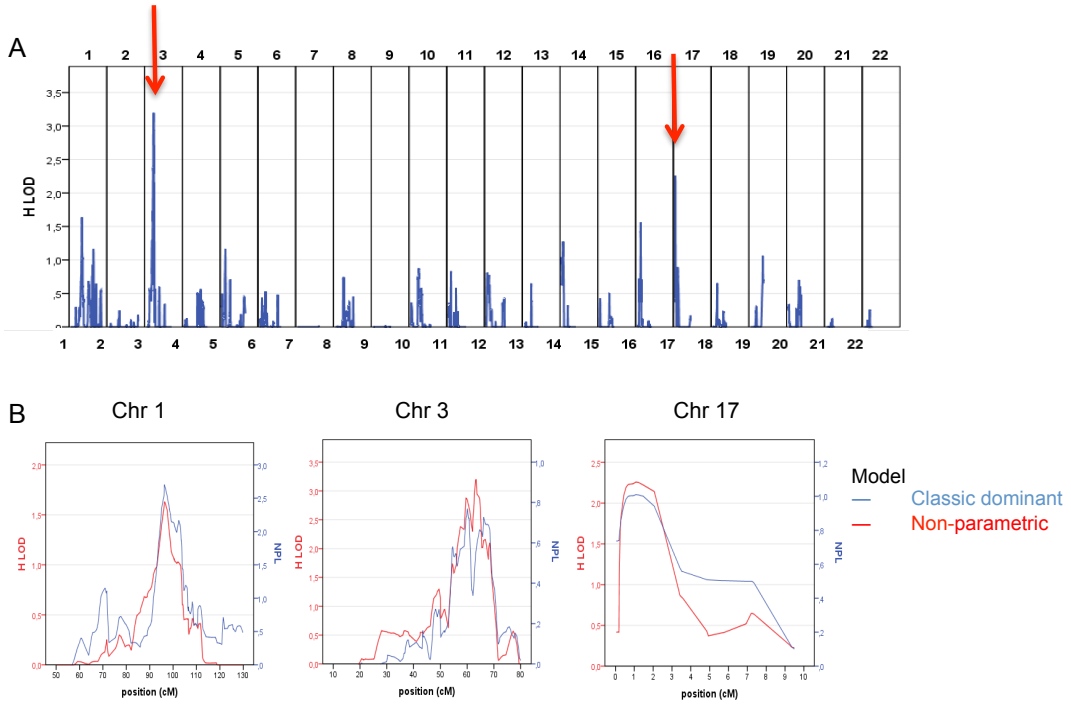

C

Chromosome	1	3	17
Location	p22-p31	p21-23	p13
Position (cM)	90-110	55-70	0-10
Position (Mb)	64-86	30-47	0-3
LOD score	1.6	3.2	2.2
% families linked	36	39	26
NPL score	2.7	0.8	1.0

Figure 49. Linkage analysis results. A. In a dominant linkage analysis model the HLOD value for each marker shows a linkage peak in chromosome 3 and a suggestive peak in chromosome 17. A score of 3 and above is evidence for linkage. **B.** The classic dominant and non-parametric LOD scores (NPL). Chromosome 1 shows a NPL score of 2.7, a third suggestive linkage peak. **C.** The specific locations, HLOD and NPL score for each locus, along with the percentage of families linked to each linkage peak. Chromosomes 1, 3 and 17 contain a marker with a linkage score over 2 in at least one of the models and between 26% and 39% of the 26 families contain a marker linked to this location. Analysis performed by Claudia Schulte

3.4.2 Variant selection and segregation analysis

The targeted exome capture generated approximately 120 million 72 base pair reads per genome. However these were not the complete exomes. The exome coverage for each index sequence is shown in table 25. In three cases there was almost a third of the exome missing and in all cases over 10% was absent.

Index Patient	≤0 reads (%)	≤5 reads (%)
1	14.3	23.5
2	14.8	25.0
3	23.3	29.1
4	25.9	31.3
5	25.6	31.4
6	27.3	32.8
7	32.7	38.8
8	35.0	40.5
9	30.0	35.3
10	24.7	30.2
11	17.4	31.8
12	17.7	33.0
13	17.7	32.7
Average	23.6	32.0

Table 25. The percentage of index patient exomes with low sequence coverage. An average next generation sequence is missing coverage on 23% of the exome.

There is no coverage in areas without variation between isoforms. This can be seen in *TUBB2A* (figure 50), where exon 1 and regions of exon 2 and 4 are entirely missing (highlighted in red).

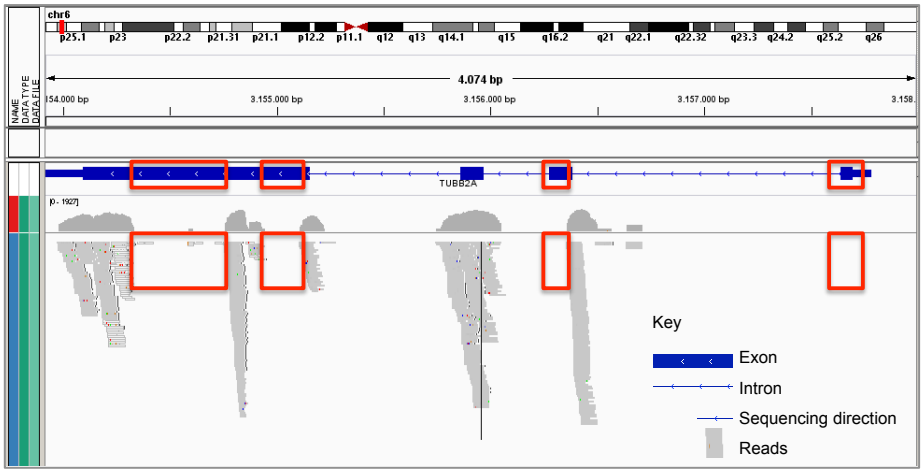

Figure 50. An example of regions of the exome without coverage. An overview of *TUBB2A* in IGV following SOLiD sequencing. There are multiple exon regions with no associated reads.

Despite these missing regions, the software called approximately 30,000 SNPs per genome. These were combined and filtered; reducing 389,521 raw SNPs to only 12,977 SNPs before a final selection based on various PD-related categories. The sorting process and categories are explained further in section 2.5.4.1, but briefly, raw SNPs were excluded based on population frequency, incorrect inheritance pattern and predicted neutrality across multiple software programs. Variants were then selected by specific criteria: cytoskeleton-linked proteins, linkage analysis peaks, known and suspected PD genes, clinical data, pathways or

gene expression linked to PD and genes with mutations in multiple patients. These were researched and those deemed most interesting were re-sequenced as a final validity check. See appendix 2 for a list of the genes included.

From these approaches, 79 genes were identified and confirmed by chain-termination sequencing, then analysed for segregation with the disease. A variant was considered to segregate if it was present in family members with PD and absent in members without PD. If a family member had PD but not the variant, the SNP did not segregate. Where the SNP was present without the disease, this was still considered to segregate, due to the possibility of incomplete penetrance or that disease onset had not yet occurred.

The full list of variants sequenced is shown in appendix 3. Of these, 35 were confirmed by chain-termination sequencing and seven segregated with the disease. The genes with PD-segregating mutations were: *CADPS2, ERCC6, FUCA1, FZD4, SEZ6L,* and *STK4. SEZ6L* mutations segregated with PD in more than one family. A tabular summary of the results, including a segregation overview and bioinformatic analyses (table 26) is given overleaf, followed by review of each of the putative pathogenic variants:

							Segregation analysis				Predicted pathogenicity					
	Family	Gene-symbol	Gene - name	Mutation	Reference SNP number	MAF EA%	No. family members	Y PD Y SNP	N PD N SNP	N PD Y SNP	MTa	PP-div	PP-var	Provean	SIFT	MutPred
1	3	*CADPS2*	Calcium-dependent secretion activator 2	p.S326L	rs372372999	0.02	2	1	1	0	DC 1	Prob Dam 0.991	Poss Dam 0.778	Deleterious -4.771	Tolerated 0.1	0.20
2	2	*ERCC6*	Excision repair cross-complementing rodent repair deficiency, complementation group 6	p.R744W	rs139913322	0.01	8	4	2	2	DC 1	Prob Dam 1	Prob Dam 1	Deleterious -7.62	Damaging 0	0.90 Gain catalytic residue, loss of disorder, loss o sheet
3	5	*FUCA1*	Fucosidase, alpha-L- 1, tissue	p.L134F	rs143691289	0.4	6	2	2	2	DC 1	Benign 0.112	Benign 0.181	Deleterious -3.26	Tolerated 0.12	0.75
4	4	*FZD4*	Frizzled family receptor 4	p.R127C	-	0.01	2	2	0	0	DC 1	Prob Dam 1	Poss Dam 0.849	Deleterious -3.322	Damaging 0	0.74
5	3	*SEZ6L*	Seizure related 6 homolog (mouse)-like	p.I916M	-	-	2	1	0	1	DC 1	Prob Dam 1	Prob Dam 0.999	Neutral -1.543-1.996	Damaging 0.02	0.55
6	2	*SEZ6L*	Seizure related 6 homolog (mouse)-like	p.G1015R	-	-	8	4	1	3	DC 1	Prob Dam 1	Prob Dam 0.992	Deleterious -3.385-6.237	Damaging 0	0.73 Loss of sheet
7	9	*STK4*	Serine/threonine kinase 4	p.T353A	rs140089638	0.1	2	1	1	0	DC 1	Prob Dam 0.999	Prob Dam 0.94	Deleterious -2.87	Tolerated 0.08	0.16

Table 26. The putative pathogenic variants with segregation analysis and predicted pathogenicity results. The reference number allocated to each SNP by dbSNP is indicated, along with the minor allele frequency determined by the exome variant server. The segregation pattern and number of family members is indicated; with family members with the disease and SNP, without either and with the SNP but without PD denoted. The pathogenicity prediction software results include a verbal indication of the expected effect of the SNP, accompanied by numerical ranges indicating damaging/benign variants: MutPred, Mutation Taster, PolyPhen = 0-1 (benign - damaging). SIFT = 0-1 where damaging = < 0.05, tolerated = >0.05. Provean: < -2.5 = damaging, >-2.5 = neutral. Where there is a range of results, the mutation is predicted differs between transcripts. Colours indicate whether the SNP is considered damaging (red) or benign (green). Abbreviations: rs-reference SNP number (dbSNP database), MAF-minor allele frequency (exome variant server), EA – European ancestry, Y/N PD – yes/no PD sufferer, Y/N SNP – yes/no polymorphism present, MTa – Mutation taster, PP – PolyPhen, div/var – different PolyPhen diagnostic model systems, DC – disease causing, Prob Dam – probably damaging, Poss Dam – possibly damaging.

3.4.2.1 *CADPS2*

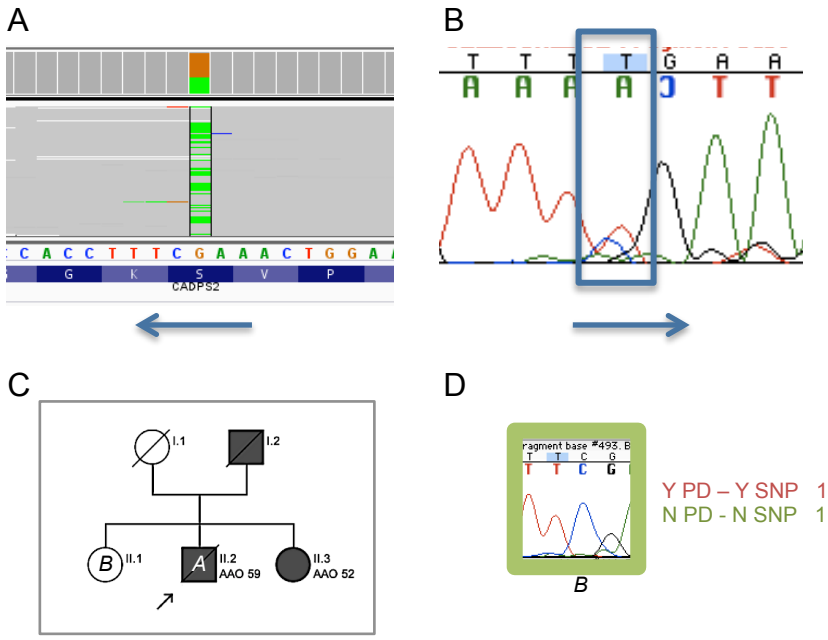

Gene	Location	Nucleotide change	Amino acid change	Reason selected	Programs predicting pathogenicity
CADPS2	Chr7:122261662	c.1098C>T	p.S326L	SN expression (PDBase)	3/6

Figure 51. The *CADPS2* S326 mutation. A. The SOLiD sequence alignment. **B.** Chain-termination sequencing confirmation of the mutation in the index patient. The arrows indicate the read orientation. **C.** The family pedigree with the member involved in the segregation analysis marked. The index patient is '*A*'. **D.** Segregation analysis. Family members with PD and the mutation are framed in red, without PD or the mutation in green. The letter identifier matches the family member marked in the pedigree (C). **E.** SNP summary, including location and reason for SNP inclusion in the selection process.

CADPS2 encodes the protein 'calcium-dependent secretion activator 2', which regulates neurotrophin release, including BDNF (bone–derived neurotrophic factor) and NT-3 (neurotrophin 3) (Sadakata et al., 2007). It is highly expressed in the dopaminergic neurons of the SN where it interacts with the dopamine receptor 2, regulating vesicle release (Sadakata and Furuchi, 2006; Brunk et al., 2009; Binda et al., 2005).

CADPS2 transcription was found to be upregulated in both PD patient SN (PDBase-Yang et al., 2009) and *LRRK2* G2019S mice, accompanied by altered ERK phosphorylation. These changes were rescued by inhibition of LRRK2 kinase activity (Reinhardt et al., 2013). Dysregulation of *CADPS2* may therefore contribute to PD pathogenesis downstream of LRRK2 which could also be caused by mutations in *CADPS2* directly, leading to altered dopaminergic and neurotrophin transmission.

Netphos predicts that Ser326 is a phosphorylation site, unlike Leu326 (Blom et al., 1999). It is considered a damaging SNP in 3/6 prediction programs and segregates fully using the DNA available from members of family 3. However, as there are only two DNA samples, it is impossible to be confident in the segregation results. The analysis results are summarised in figure 51.

3.4.2.2 *ERCC6*

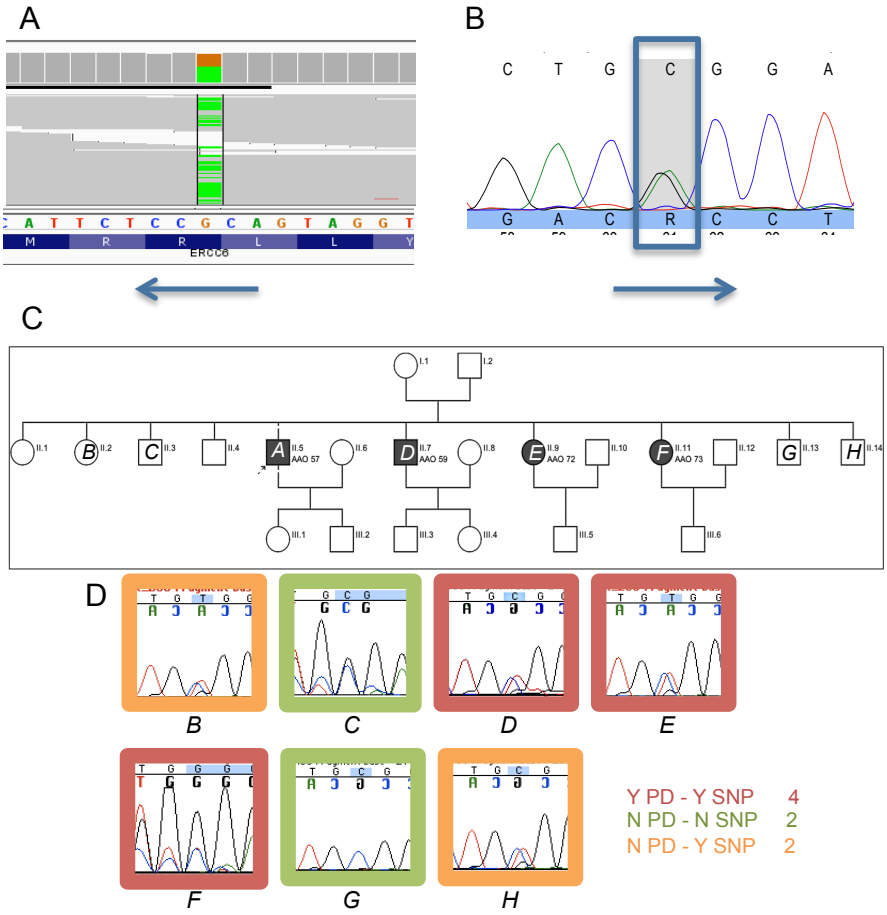

E

Gene	Location	Nucleotide change	Amino acid change	Reason selected	Programs predicting pathogenicity
ERCC6	Chr10:50732239	c.1316C>T	p.R744W	Literature review	6/6

Figure 52. The *ERCC6* R744W mutation. A. The SOLiD sequence alignment. **B.** Chain-termination sequencing confirmation. The arrows indicate the read orientation. **C.** The family pedigree with members involved in the segregation analysis marked. The index patient is '*A*'. **D.** Segregation analysis. Family members with PD and the mutation are framed in red, without PD or the mutation in green and without PD but with the mutation in orange. The letter

identifiers match the family members marked in the pedigree (C). **E.** SNP summary, including location and reason for SNP inclusion in the selection process.

ERCC6 (also known as *CSB*) encodes the excision repair cross-complementing group 6 protein. It is involved in nucleotide excision repair in active genes and is thus important for the eradication of DNA lesions.

Damaged nuclear and mitochondrial DNA have been detected in PD brain post-mortems (Zhang et al., 1999; Ciccone et al., 2013), and several repair proteins and pathways are implicated in PD pathogenesis (Jeppesen et al., 2011; Hegde et al., 2012; Bohgaki et al., 2010; Gencer et al., 2012; Canugovi et al., 2013). A DNA repair network with reduced function, combined with the increased ROS-induced damage in dopaminergic neurons, could result in an accumulation of damaged DNA over time, eventually leading to degeneration.

The *ERCC6* R744W SNP is considered damaging in every prediction program used. Tryptophan is hydrophobic and therefore usually at an internal location within a protein, whereas arginine residues are often on the protein surface, where they impart a charge and can be post-translationally modified. It is not clear if this residue is located internally or on the protein surface, but this variant introduces an amino acid with very different properties to the wild-type residue. The analysis results are summarised in figure 52. There were a lot of background guanine nucleotides in figure 52D, sequence F, suggesting sample contamination. However as the residues involved were cytosine and thymine, these peaks were ignored.

3.4.2.3 *FUCA1*

E

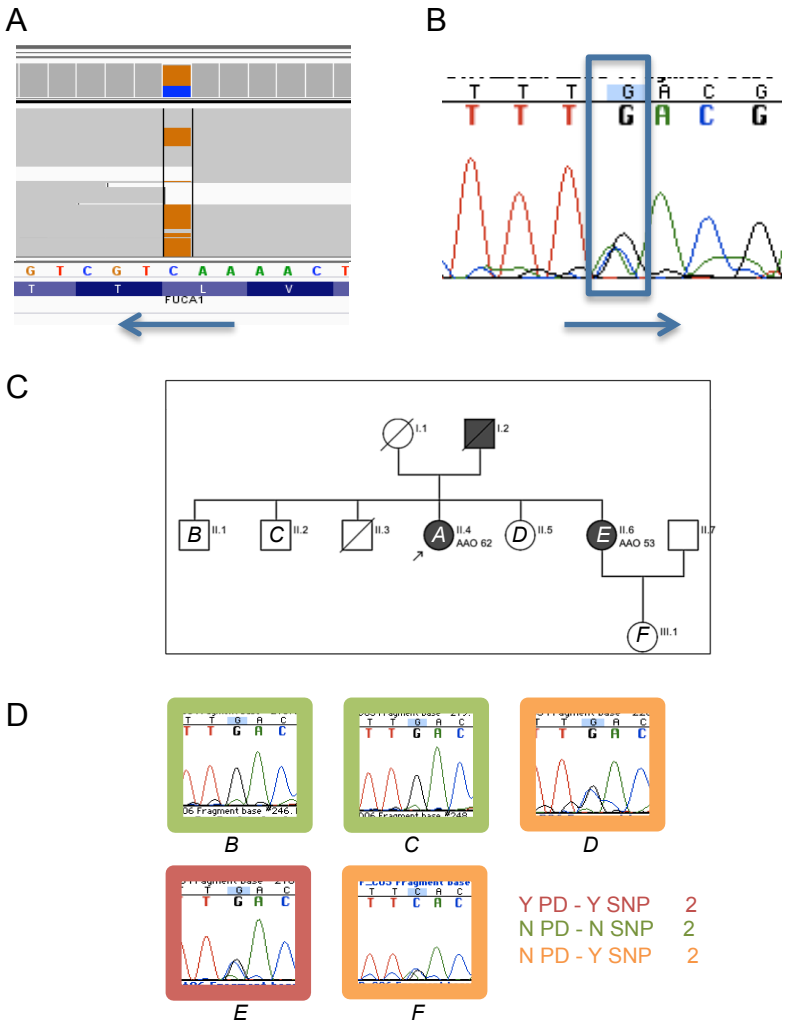

Gene	Location	Nucleotide change	Amino acid change	Reason selected	Programs predicting pathogenicity
FUCA1	Chr1:24192103	c.410G>C	p.L134F	Linkage analysis Neurodegeneration Cytoskeleton	3/6

Figure 53. The *FUCA1* L134F mutation. A. The SOLiD sequence alignment. **B.** Chain-termination sequencing confirmation. The arrows indicate the read orientation. **C.** The family pedigree with members involved in the segregation analysis marked. The index patient is '*A*'. **D.** Family members with PD and the mutation are framed in red, without PD or the mutation in green and without PD but with the mutation in orange. The letter identifiers match the family members marked in the pedigree (C). **E.** SNP summary, including location and reason for SNP inclusion in the selection process.

FUCA1 encodes the fucosidase, alpha-L- 1, tissue enzyme, which hydrolyses the sugar fucose. Deletions and premature STOP codons in *FUCA1* lead to fucosidosis, an autosomal recessive lysosomal storage disease similar to the PD-associated Gaucher disease, caused by mutations in glucocerebrosidase (Nichols et al., 2009b; Schachar et al., 2011). However fucosidosis is very

rare, with an estimated incidence of 0.6 per 100,000 people (Tiberio et al., 1995; Menendez-Sainz et al., 2012).

FUCA1 was identified as a protein of interest via multiple selection processes. It is located in chromosome 1, it may interact with the cytoskeletal protein MT-affininity regulating kinase 2 (STRING 9.0, Szklarczyk et al., 2011) and is included in the CeGaT neurodegeneration panel.
The *FUCA1* L134F mutation is considered damaging by half the prediction software programs. However, both amino acids are non-polar, neutral amino acids and the allele frequency is 0.4%, high to be an unidentified causative PD variant.The analysis results are summarised in figure 53.

3.4.2.4 *FZD4*

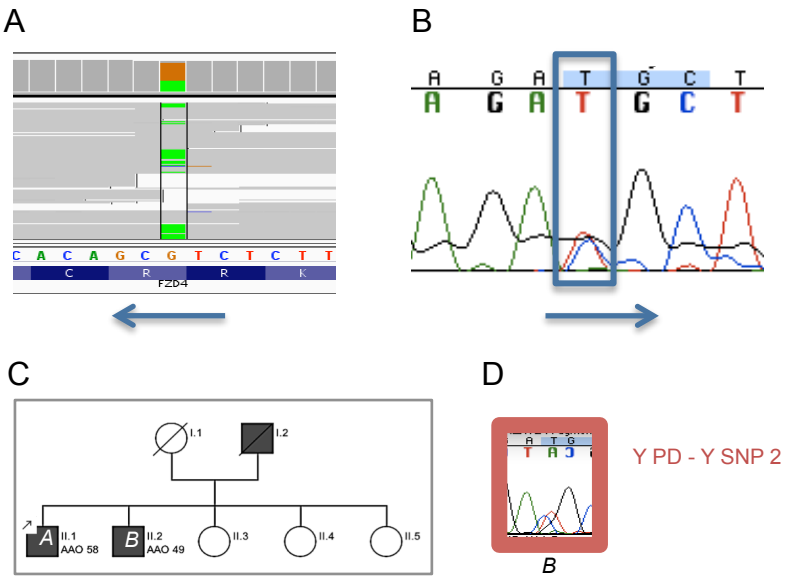

E

Gene	Location	Nucleotide change	Amino acid change	Reason selected	Programs predicting pathogenicity
FZD4	Chr11:86663419	c.685C>T	p.R127C	Literature review	5/6

Figure 54. The *FZD4* R127C mutation. A. The SOLiD sequence alignment. **B.** Chain-termination sequencing confirmation. The arrows indicate the read orientation. **C.** The family pedigree with members involved in the segregation analysis marked. The index patient is '*A*'. **D.** Family members with PD and the mutation are framed in red, without PD or the mutation in green. The letter identifier matches the family member marked in the pedigree (C). **E.** SNP summary, including location and reason for SNP inclusion in the selection process.

FZD4 encodes the frizzled family receptor 4 protein. This is a receptor for wnt proteins, which bind and initiate wnt signalling cascades. Wnt signalling is implicated in LRRK2-mediated PD, with LRRK2 mutants reducing activation of the wnt pathway compared with wild-type LRRK2

(Sancho et al., 2009; Berwick and Harvey, 2012; Rehn et al., 1998). The analysis results are summarised in figure 54.

The *FZD4* R127C mutation introduces a cysteine residue immediately prior to a highly conserved cysteine in the C8 cysteine-rich N-terminal domain. This domain is important for wnt signalling and the residue at 127 is typically a positively charged arginine or lysine throughout evolution, although it is not fully conserved (Toomes et al., 2004; PolyPhen-Adzhubei et al., 2010). The residue projects externally and Cys127 is predicted to introduce an additional, second, hydrogen bond with the neighbouring Arg123 residue in the alpha helix (see figure 55), compared to the single bond formed by Arg127.

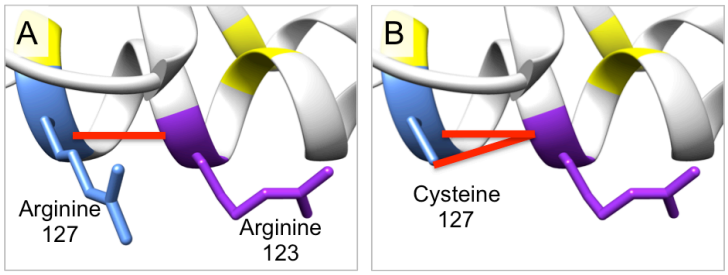

Figure 55. Homology model of the FZD4 wild-type and variant within the C8 cysteine-rich N-terminal domain. The conserved cysteine residues are indicated in yellow. **A.** Arg127 is predicted to form a single hydrogen bond (red) with the neighbouring Arg123 residue (purple). **B.** Cys127 forms an additional hydrogen bond with Arg123. PDB model 1IJY using *m. musculus* FZD8 C8 cysteine-rich N-terminal domain (Dann et al., 2001), which has 40% identity conservation with FZD4, including all the highly conserved cysteine residues (BLAST).

Although this mutation is not in a region predicted to influence wnt binding (Dann et al., 2001), the introduction of a hydrogen bond and loss of a charged residue may result in structural changes and altered interaction sites, causing downstream signalling changes. Altered wnt signalling could affect spine morphogenesis, synaptic plasticity and cell survival, all of which have been implicated in PD.

3.4.2.5 *SEZ6L*

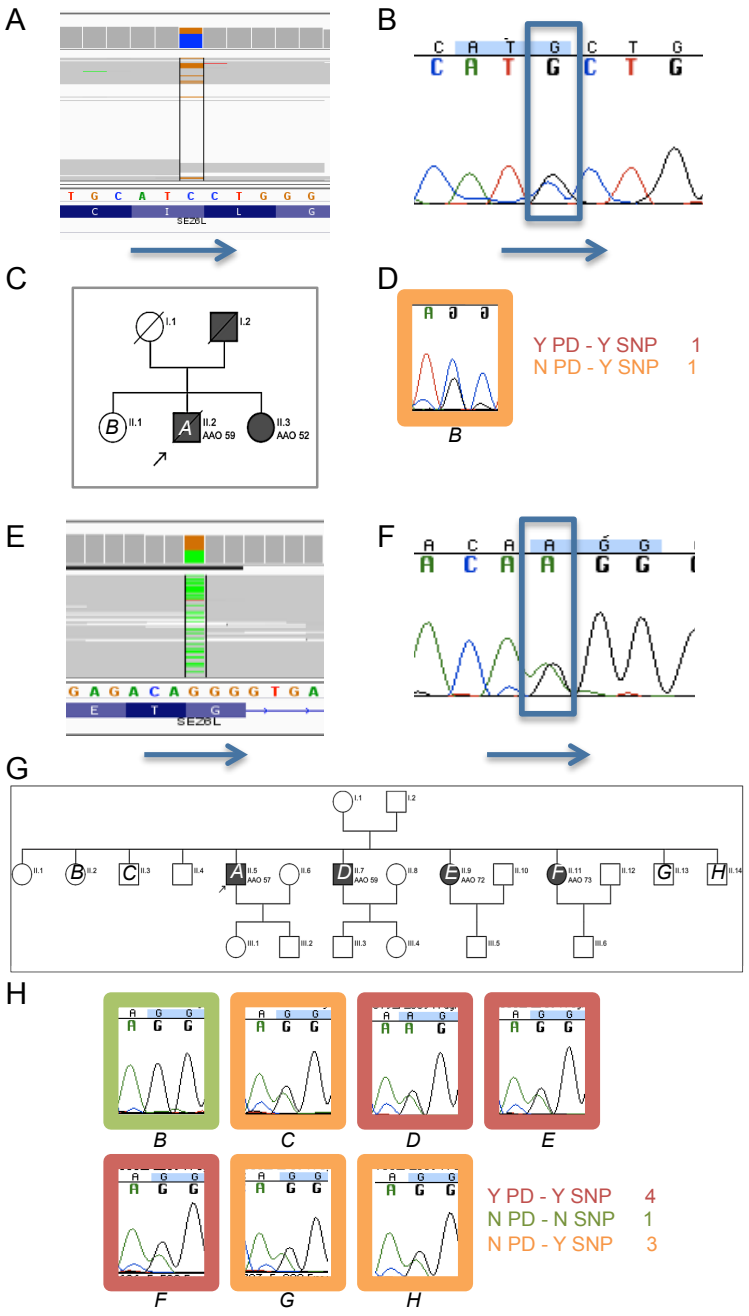

I

Gene	Location	Nucleotide change	Amino acid change	Reason selected	Programs predicting pathogenicity
SEZ6L	Chr22:26761486 Chr22:26773739	c.2843C>G c.3138G>A	p.I916M p.G1015R	Clinical data Multiple families	4/6 6/6

Figure 56. The *SEZ6L* I916M (A-D) and G1015R mutations (E-H). A. The SOLiD sequence alignment indicating the *SEZ6L* I916M SNP. **B.** Chain-termination sequencing confirmation. The arrows indicate the read orientation. **C.** The family pedigree with members involved in the segregation analysis marked. The index patient is '*A*'. **D.** Family members with PD and the mutation are framed in red, without PD or the mutation in green and without PD but with the

mutation in orange. The letter identifiers match the family members marked in the pedigree (C). **E.** The SOLiD sequence alignment indicating the *SEZ6L* G1015R SNP. **F.** Chain-termination sequencing confirmation. The arrows indicate the read orientation. **G.** The family pedigree with members involved in the segregation analysis marked. The index patient is '*A*'. **H.** Family members with PD and the mutation are framed in red, without PD or the mutation in green and without PD but with the mutation in orange. The letter identifiers match the family members marked in the pedigree (C). **I.** SNP summary, including location and reason for SNP inclusion in the selection process.

SEZ6L encodes the seizure-related 6 homolog (mouse)-like gene and was selected by a gene distiller scan of proteins implicated in diabetes or psoriasis (Smink et al., 2005), both of which accompanied PD in family 2 and are increasingly accepted to be linked to PD (Sandyk, 1993; Hu et al., 2007; Sheu et al., 2013). Elevated interleukin-6 (IL-6) levels were found to be associated with an intronic *SEZ6L* variant by GWAS (Shah et al., 2013). Increased circulating IL-6 is also a feature of PD, diabetes and psoriasis (Scalzo et al., 2010; Hofmann et al., 2009; Grossman et al., 1989; Schultz et al., 2010). Two mutations were identified in *SEZ6L*, in separate families, each of which were previously unreported. I916M is predicted to be a damaging variant in the majority of programs. This mutation replaces an aliphatic, hydrophobic, non-reactive isoleucine with a similarly hydrophobic, unreactive methionine. However the methionine has an additional sulphur atom, potentially increasing the number of interaction partners, or altering interaction strength. Meanwhile the G1015R mutation is considered damaging by every prediction program, with a small glycine residue being replaced by a large, positively charged, polar, arginine residue. The analysis results are summarised in figure 56.

3.4.2.6 *STK4*

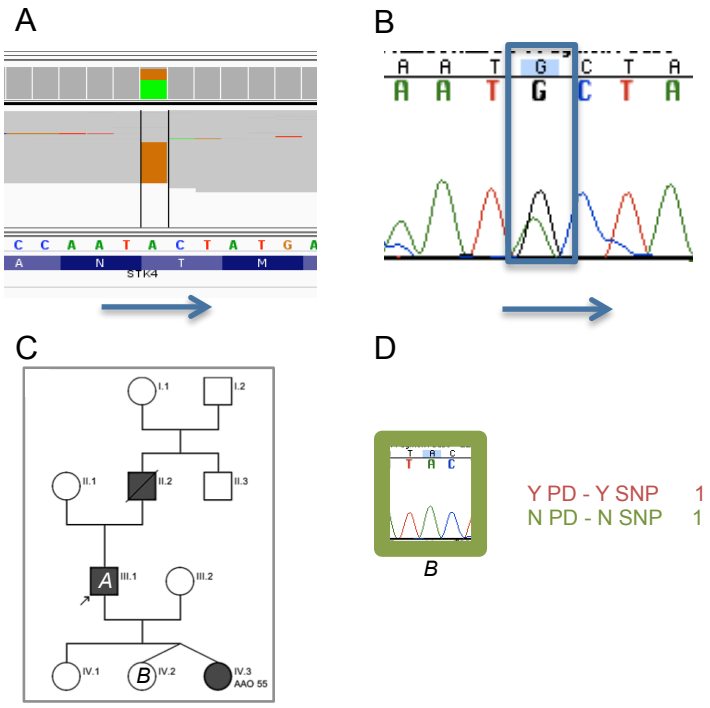

E

Gene	Location	Nucleotide change	Amino acid change	Reason selected	Programs predicting pathogenicity
STK4	Chr20:43629904	c.1152A>G	p.T353A	SN expression (PDBase)	4/6

Figure 57. The *STK4* T353A mutation. A. The SOLiD sequence alignment. **B.** Chain-termination sequencing confirmation. The arrows indicate the read orientation. **C.** The family pedigree with members involved in the segregation analysis marked. The index patient is '*A*'. **D.** Family members with PD and the mutation are framed in red, without PD or the mutation in green. The letter identifier matches the family member marked in the pedigree (C). **E.** SNP summary, including location and reason for SNP inclusion in the selection process.

STK4 encodes serine/threonine kinase 4. This protein phosphorylates forkhead box, subgroup O (FOXO) transcription factors in response to ROS, at a conserved site across the FOXO protein family (Lehtinen et al., 2006). FOXO proteins protect against cell death in conditions of oxidative stress (Mei et al., 2009). Both FOXO1 and FOXO3 have been implicated in PD, with *FOXO1* expression upregulated in PD brain (Dumitriu et al., 2012) and implicated in cell survival downstream of LRRK2 (Chuang et al., 2014). FOXO3 regulates PINK1 transcription in lymphocytes and HEK293 cells (Mei et al., 2009) and has been found to localise ectopically to Lewy bodies in PD brain tissue (Su et al., 2009). *STK4* expression is reduced in PD SN, possibly resulting in reduced ability of cells to react appropriately to oxidative stress; either by altering gene expression or entering apoptotic pathways (PDBase-Yang et al., 2009).

The *STK4* T353A variant is considered damaging in 5/6 prediction programs. Both threonine and alanine are small, hydrophobic amino acids. However the loss of a threonine could remove a vital phosphorylation site, important for kinase activation and deactivation. The *STK4* T353A variant fully segregates in family 9, however with only two family members involved in the segregation analysis, this segregation is inconclusive. The analysis results are summarised in figure 58.

3.4.3 Discussion

3.4.3.1 Exome and next generation sequencing

Whole exome sequencing is a practical and cheap alternative to traditional chain-termination sequencing, providing researchers with vast amounts of information covering large sections of the genome in a relatively short space of time. It has revolutionised genetic approaches to disease. However there are still mechanical, informatic and predictional limitations to the approach, as discussed below:

3.4.3.1.1 Mechanical limitations

Within the 1% of the genome analysed in exome sequencing, there are often gaps in the sequence due to lower sequencing efficiency in GC or AT-rich regions and in regions with high homology. Problems with GC rich/low regions are partially due to reduced amplification during the PCR steps and also due to a reduced hybridisation efficiency, which can reduce target enrichment.

3.4.3.1.2 Informatic limitations

In regions where there is high homology between sequences, such as β-tubulins (80-98% shared identity), alignment programs are unable to definitively locate identical sequences that are repeated throughout the genome. This can result in one of several options: the reads are excluded so they are not incorrectly located, they are randomly allocated between the regions or included in all the sites. Additionally, duplication, insertion and inversion of long stretches of DNA are not detected as these reads are mapped to the original source in the wild-type sequence. Alterations such as these can be detected by other methods such as fluorescence in-situ hybridisation assays, however increased read lengths in future models will also resolve these issues - third generation sequencers are able to read up to 1300bp (Liu et al., 2012). Fourth generation sequencing technologies directly sequence a complete strand of DNA,

including epigenetic modifications (Schneider and Dekker 2012) but these are not yet widely available.

As well as coverage and mapping restrictions, there are further bioinformatic limitations. Reference sequences can differ between databases (especially in genes which are not well studied) and different analysis systems call different variants, especially within nucleotide repeats. Using multiple methods of analysis would increase security that the variant has been detected but also dramatically increase the number of variants to be analysed.

The sheer volume of data produced makes determination of phenotypically relevant variants a challenge, especially if only single family members are sequenced, as was the case here. Additionally, a lot of the filter steps use databases such as dbsnp and the EVS. Accurate analysis therefore relies on these being correct and up-to-date. Furthermore, in the index cases investigated here, an average of 32% of genes had a coverage of 5 reads or less, meaning that even following extensive analysis, it was impossible to be certain the pathogenic variants were even in the data.

Finally NGS has a significant rate of false positives - the vast amounts of data generated by NGS means the SOLiD platform accuracy level of 99.4% (Applied Biosystems SOLiD factsheet) would be expected to produce 1,800 false calls on an exome with 30,000 SNPs. This means confirmation using chain-termination sequencing is required for each SNP, and time and effort is wasted on these incorrect variant calls.

3.4.3.1.3 Predictional limitations

Although exome sequencing is cheaper and more cost effective than whole genome sequencing, the exome covers only 1-2% of the genome. Monogenetic diseases usually result from variation in the coding portion of the genome but this is not always so, for example an intronic mutation in presenilin 1 intron 4 was found to cause an early-onset autosomal dominant form of Alzheimer's disease (Janssen et al., 2000) and an intronic C9orf72 repeat has been associated with amyloid lateral sclerosis, fronto-temporal dementia and possibly PD (Renton et al., 2011; Lesage et al., 2013).

Even after extensive filtering, it is very difficult to predict the effect of SNPs. Prediction tools are available which analyse evolutionary conservation and likely structural effects but over-reliance on these has associated dangers. A study of multiple prediction programs, including

MutPred, PolyPhen and SIFT, put their various accuracies, precision and specificities at 50% - 92% (Thusberg et al., 2011) but no single method was found to be the best over multiple parameters. Combining analysis programs reduced the proportion of false positives but there was still error (Saunders and Baker, 2002). Following sequencing and the initial variant filtering, many SNPs were removed based on prediction software results. The removal of mutations predicted to be polymorphisms across five prediction programs may have excluded causative variants. However the volume of data necessitated prioritising the likely pathogenic cases. Where no plausible variants were found, it would be possible to return to the earlier stages and reanalyse these data for putative pathogenic variants.

As the cost of sequencing continues to fall while technology and analysis improve, it is likely that many of these limitations will be addressed. With low costs, whole genome sequencing will become standard practice. Sequencing of multiple family members with the disease immediately removes many non-contributory and de novo variants, which we were unable to do in this case. As more exomes are sequenced, allele frequencies will increase in accuracy, reducing time spent on common variants.

Despite these issues, the benefits of NGS should not be underestimated. Identification of novel pathogenic mutations can be life saving, such as the case of a 15 month old with a novel early-onset Crohn's disease-like illness, which could not be definitively diagnosed. Exome sequencing revealed a mutation in *XIAP* (*X-linked inhibitor of apoptosis*), revealing a bone-marrow transplant was required to prevent the development of life-threatening complications (Worthey et al., 2011). As well as saving lives, the use of patient-specific treatment will reduce the unnecessary side-effects of superfluous drugs. Additionally, the more genomes that are sequenced, the better allele penetrance can be understood, revealing how the pathogenic effects of mutations can be ameliorated.

3.4.3.2 Comparison of approaches

Although small cohorts such as this can reveal genes of interest to disease, they require an accurate and detailed initial diagnosis and a large family for further analysis. Where either of these is missing, the likelihood of finding and proving pathogenicity of mutations quickly deteriorates. It is also unlikely that rare genes can be validated by identification in multiple families within the cohort.

In large cohorts, the volume of participants means none of these are confounding factors. It is also possible to identify risk variants which are at a higher proportion in the disease cohort to the general population and the involvement of environmental factors can be incorporated, such as extracting and collating the data of participants who smoke.

However, assembling data on thousands of patients has high costs, requires large-scale participation between research centres, significant organisation and therefore take a long time. Small cohorts are a cost-effective alternative where there is a clear familial component to the disease and DNA and clinical data from several family members is available.

3.4.3.3 Selection bias

Following the large-scale filtering steps, the subsequent gene selections were biased; firstly by the categories chosen to identify genes of interest and secondly by which of the SNPs resulting from these categories were resequenced.

It is clear that PD may develop due to a wide-range of cellular defects. The involvement of many pathways and proteins in disease progression made it unlikely that all the areas could be covered by the categories selected. The inclusion of a broad 'proteins with changed expression in the PD SN' category was intended to incorporate these additional pathways not included by the narrower categories. However it is acknowledged that in cells undergoing apoptotic and necrotic cell death, as in the PD SN, changed expression of many genes is to be expected. Thus most of these gene expression changes are likely to be downstream effects of the pathogenic change.

Finally, there was a personal bias in selecting from the variants identified by the filtering process. It was not feasible to resequence all of the SNPs identified, therefore only those deemed most plausible based on the prediction software and research of available literature were analysed further.

3.4.3.4 Putative pathogenic variants

Seven SNPs of interest to PD were identified, each causing non-synonymous amino-acid changes in proteins not previously described in familial PD cases.

With a disease incidence of 0.6% at 60, increasing to 2% by the age of 80, the frequency of these SNPs is less common than PD (Alcalay et al., 2014). However, it is likely they are very rare mutations as, despite intensive study into the disease, the disease-causing variants in these

cases (and many others) remain unknown. It is therefore encouraging that the *SEZ6L* variants were previously unreported.

In several of these cases, the SNP is present not only in sufferers but also in healthy family members. The effects of penetrance and epigenetics mean that a SNP found in healthy family members is not necessarily benign, making determining a disease-causing allele even more of a challenge. Unfortunately, this, and the low 'n' numbers involved in several of the segregation analyses, mean none of these SNPs can be clearly classed as pathogenic mutations. Further work is required; firstly the identification of these genes in large populations of PD patients, but also functional studies establishing whether the mutations affect protein interactions and cell viability. These would confirm which of the variants are simply polymorphisms and which (if any) are causative mutations.

Of the putatively pathogenic SNPs identified in this cohort, the novel *SEZ6L* variants would be of most interest for follow-up studies. The *SEZ6L* variants segregated in two families and the link between SEZ6L and IL-6 connects the diabetes, psoriasis and PD suffered by family two.

4. Final Discussion

LRRK2 has been an important research focus since pathogenic *LRRK2* mutations were identified as a cause of PD in 2004. This is not only due to the fact that pathogenic *LRRK2* mutations lead to a disease phenotype very similar to that of the idiopathic phenotype, but also due to the lack of clarity regarding the role of LRRK2 in the cell. Despite the presence of two enzymatic domains, the only convincing LRRK2 substrate identified to date is itself. Thus, understanding LRRK2 function by the identification and characterisation of interaction partners was pursued.

A yeast two-hybrid screen previously identified multiple interactors of LRRK2, including TUBB4. Within this thesis, understanding of the LRRK2-tubulin association was refined and a new role for LRRK2 as a mediator of MT stability was identified. This provides new insight into LRRK2 function, supports evidence that MT stability plays an important role in the pathogenesis of PD and may lead to new therapeutic strategies for the treatment of PD.

4.1 The LRRK2-tubulin interaction sites

The isoforms and specific sites involved in the interaction between LRRK2 and tubulin were identified using yeast two-hybrid experiments. Following on from previous reports of a LRRK2-tubulin interaction (Gloekner et al., 2006; Gandhi et al., 2008; Gillardon et al., 2009), an association between LRRK2 and neuronally expressed α-, β-, δ-, ε- and γ-tubulins was investigated. The interaction with LRRK2 was specific to three β-tubulin isoforms: TUBB, TUBB4 and TUBB6.

Tubulin sequence comparison, mutagenesis and molecular modelling further refined the site of the interaction with LRRK2 to β-tubulin Lys362, a charged residue protruding from the lumenal surface of the MT. The β-tubulin-LRRK2 association also requires an internal alanine at β-tubulin residue 364. This unreactive amino acid, situated immediately under the protein surface, makes no associations with neighbouring β-sheet residues and thus permits surface flexibility, enabling LRRK2 to dock. β-tubulin isoforms with a Ser364 do not associate with LRRK2 due to a hydrogen bond with the nearby Arg320 residue, situated in a neighbouring β-sheet strand, spatially constraining the surface residues and inhibiting the interaction. However this does not occur in the LRRK2-TUBB6 association. Instead of a surface Arg320 residue near-adjacent to the Lys362 docking site, TUBB6 has a Pro320 residue, with an associated small, uncharged side-chain. This facilitates the interaction with LRRK2, irrespective

of the internal hydrogen bond due to increased space in the vicinity of Lys362 on the tubulin surface.

As previously reported, the LRRK2 Roc domain was sufficient to confer an association with tubulin/MTs (Gandhi et al., 2008; Gloekner et al., 2006). The site of the tubulin association with LRRK2 was located to LRRK2 residues 1328-1400 using truncated Roc domain proteins. An alanine block scan, replacing blocks of five consecutive residues with unreactive alanines, demonstrated a weakening of the association between the mutated LRRK2 RocCOR domain and tubulin when residues 1373-1382 were replaced by alanines. However, LRRK2 dimerisation strength appeared unchanged in semi-quantitative yeast two-hybrid assays.

An association between LRRK1 and tubulin was previously detected by mass-spectrometry, but not investigated (Reyniers et al., 2014). This thesis demonstrates the same tubulin residues confer the interaction between β-tubulin and LRRK1 as confer the interaction with LRRK2. Therefore residues conserved between LRRK1 and LRRK2 within the ten amino acids important for the protein-protein interaction were considered further. These amino acids were LRRK2 Glu1379, Arg1381 and Arg1386 (LRRK1 Glu680, Arg 681 and Arg686), including two positively charged arginine residues. Interestingly, two negatively charged residues were identified within the tubulin structure (Glu325 and Asp357), in the vicinity of the Lys362 residue, essential for the interaction. These negatively charged tubulin residues are situated in a similar orientation to the positively charged LRRK2 Arg1381 and Arg1386 residues.

My data also suggests that LRRK2 dimerisation is necessary for the tubulin-LRRK2 interaction, as the association between LRRK2 RocCOR proteins containing alanine blocks and tubulin was only observed when RocCOR dimerisation was maintained.

The location of the LRRK2 interaction site inside MT on the tubulin lumenal surface posed multiple questions as to how the large LRRK2 protein was able to interact within MTs. This was revealed by imaging SHSY-5Y cells fixed using a cytoskeletal-specific fixation technique. This demonstrated preferred MT-LRRK2 association in growth-cones, where MTs are less regular in their structure, tubulin protofilaments are less tightly associated and oriented in multiple directions (Tankak and Kirschner, 1991). Therefore LRRK2 may play a role in control of growth cone dynamics. This location of LRRK2 at the growth cone is in accordance with previous work which found that LRRK2 regulates neurite outgrowth, though via actin polymerization (Häbig et al., 2013), possibly by an additional interaction between the LRRK2 WD40 domain and actin.

4.2 LRRK2 reduces MT acetylation

Yeast-two hybrid revealed that the LRRK2-tubulin association occurs in close proximity to two sites important for MT stability. These are the paclitaxel binding site and the α-tubulin Lys40 acetylation site, considered to be a marker for MT stabilisation. Further work comparing wild-type and *Lrrk2* knock-out MEF cells revealed that there is a reduction in tubulin acetylation in the presence of Lrrk2 and this was maintained in HEK cells in the presence of the MT-stabilising agent paclitaxel.

Lrrk2 knock-out MEF cells revealed a dramatic phenotypic change compared to wild-type cells, involving not just MT acetylation but also cell morphology. Additional alterations were an increase in filopodia and cell-cell adhesion, a loss of cell polarity, reduced F-actin stress fibres, accompanied by reduced nuclear density and increased cell and nucleus size. The phenotypic change is similar to that seen when the small GTPases Rho, Rac and cdc42 are activated (Hall, 1998), including a loss of polarity, reduced F-actin stress fibres and nuclear density. This is accompanied by an increase in filopodia, cell adhesion, cell and nucleus size. Both the small GTPases are LRRK2 are known to regulate cell pathways which mediate cytoskeletal dynamics, such as wnt signalling, actin cytoskeleton remodelling and cell adhesion (Hall, 1998, Wojciak-Stothard et al., 1998; Habas and He, 2006; Berwick and Harvey, 2011; Ferrer et al., 2001; Chen et al., 2012a; Ho et al., 2009; Sancho et al, 2009; Min et al., 2011). Therefore overexpression of the small GTPases and knock-out of *Lrrk2* have similar effects on the cell. As overexpression of Rac1 can rescue neurite length in *LRRK2* G2019S cells, the small GTPases may act downstream of LRRK2, or they may work in tandem with LRRK2 to regulate the processes.

Acetylation of α-tubulin leads to stable, structurally uniform MTs by promoting the formation of salt bridges between protofilaments (Cueva et al., 2012). We have described an increase in acetylation in *Lrrk2* knock-out compared with wild-type MEF cells. In support of this finding, neurons from *Lrrk2* knock-out mice develop longer neurites (MacLeod et al., 2006; Parisiadou et al., 2009). These longer neurites could result from an increased MT stability in the absence of LRRK2, possibly by enabling MEC-17 diffusion and therefore α-tubulin K40 acetylation (Szyk et al., 2014). This increased stability would reduce dynamic instability and treadmilling behaviours within the MT, resulting in longer MTs and therefore neurites.

Surprisingly this change in MT acetylation is mediated by the LRRK2 N-terminal region, prior to the tubulin-interacting RocCOR domain. There are several mechanisms by which this could occur. It has previously been suggested that the LRR region associates with the RocCOR

domain and may promote LRRK2 dimerisation (Gotthardt et al., 2008; Greggio et al., 2008). This region may be binding endogenous LRRK2, physically blocking α-tubulin Lys40, or instead altering enzyme activity; promoting deacetylation or inhibiting acetylation of α-tubulin.

Over-expression of β-tubulin isoforms which do not interact with LRRK2 in yeast revealed an increase in the proportion of tubulin acetylation, but no difference was observed following overexpression of isoforms which do interact with LRRK2. It had not been possible to confirm the isoform specific association between LRRK2 and β-tubulin detected in yeast two-hybrid by co-IP, as multiple tubulin isoforms associated as part of a protein complex. However this altered acetylation in HEK cells following tubulin isoform overexpression does support the idea that LRRK2 affects tubulin acetylation by associating with specific tubulin isoforms in mammalian systems.

Meanwhile, Bhattacharya and colleagues (2008) previously described a link between *TUBB6* expression and MT stability. MTs of Individuals with higher *TUBB6* expression levels are less stable and knock-down of *TUBB6* expression lead to an inhibition of cell proliferation due to hyperstable MTs. This is likely to relate to the LRRK2-MT association, providing further support to the 'tubulin code' hypothesis and the role of LRRK2 in mediating MT stability.

4.3 Identification of novel putative PD-causing variants

Finally, in a cohort of 13 families, I identified seven SNPs segregating with PD. None of the SNPs fully segregated, indicating possible incomplete penetrance. Of particular interest for follow-up studies are the two novel *SEZ6L* variants, I916M and G1015R, found in separate families. SEZ6L expression has been linked to increased circulating IL-6 levels, also found in PD patients (Scalzo et al., 2010).

4.4 Future work

There are several possibilities by which continuation of the work begun in this thesis could occur, in order to further the understanding of the role LRRK2 plays in MT stability.

4.4.1 Additional LRRK2 cytoskeletal substrates

It is likely that LRRK2 interacts with the cytoskeleton by more than one mechanism. Associations between LRRK2 and MAP1B and tau have been previously described (Chan et al., 2014; Kawakami et al., 2012). Further examination of the association with additional MT-

associated proteins such as MAPT, MAP2, MAP4, MT-associated kinases and a possible LRRK2 WD40-F-actin interaction could be tested for, via yeast two-hybrid and co-immunoprecipitation, as described in this thesis. Co-IP of tubulin and probing for the cytoskeletal proteins of interest in LRRK2 wild-type and knock-out MEF cells would reveal associations which occurred via LRRK2 directly or were facilitated/inhibited in the presence of LRRK2.

4.4.2 The role of LRRK1 and the N-terminus

This thesis provides evidence that the LRRK2-mediated reduction in acetylation is facilitated by the N-terminus of the protein. As this is the region that differs most between LRRK1 and LRRK2, a logical continuation of the project is to investigate whether LRRK1, which also binds β-tubulin, is similarly involved in MT stability. This would be done in the same way as LRRK2, by creating a *Lrrk1* knock-out MEF cell line and determining the morphology versus wild-type controls, using immunocytochemistry and western blotting to determine the proportion of acetylation in the cell lysate. If the changes in acetylation are proven to be mediated by the N-terminus, truncated LRRK2 and LRRK1 proteins, as well as LRRK1 and LRRK2 fragments missing specific regions would be transfected into the knock-out MEF cells to determine the specific regions associated with the morphological changes.

4.4.3 Rescuing the *Lrrk2* knock-out and G2019S MEF cells

The novel and dramatic change in *Lrrk2* knock-out MEF cells reveals that there are many phenotypic changes, beyond MT acetylation, when LRRK2 is absent from a cell. The pathways and processes by which LRRK2 modulates α-tubulin acetylation and additional cytoskeletal changes would be determined by rescuing the phenotype in both *Lrrk2* knock-out and G2019S MEF cells (as the G2019S mutation is known to cause cytoskeletal alterations). This could be investigated by overexpressing kinase-dead or GTPase deficient LRRK2, the use of functional inhibitors and overexpression of truncated LRRK2 proteins in the knock-out cells and studying the changed cell phenotypes.

4.4.4 Functional characterisation of novel PD variants

Finally, it would be interesting to characterise the PD variants detected in the PD cohort, to determine if any of them are disease causing. This could be done by knocking down the genes *in vitro* and *in vivo* and seeing if they lead to PD-like symptoms. Additionally, performing functional experiments which fit the roles of these genes as described individually, such as whether the *CADPS2* S362L variant directly alters ERK phosphorylation or whether the *FZD4*

R127C mutation alters wnt signalling activity, would provide evidence for pathogenicity of each variant. It would then be possible to search for additional mutations in these genes in larger cohorts of sporadic PD patients.

4.5 Conclusions

Determining the processes by which LRRK2 mutations lead to PD pathology will inform our understanding of the processes behind familial and idiopathic PD. This thesis contributes to current knowledge by isolating how and where the LRRK2-tubulin interaction occurs and demonstrating a previously unreported role for LRRK2 in mediation of MT acetylation.

The data in this thesis demonstrate that the association with LRRK2 is specific to TUBB, TUBB4 and TUBB6 isoforms, the interaction site in β-tubulin is luminal and binding LRRK2 conferred by the presence of tubulin residues Lys362 and Ala364 or Pro320. The β-tubulin binding site in the LRRK2 Roc domain involves residues Glu1379, Arg1381 and Arg1386, situated in a protruding, accessible site.

Also described is a robust LRRK2 association preference with dynamic MTs in the growth-cone and an inverse correlation between α-tubulin Lys40 acetylation and LRRK2 expression, conferred by the N-terminus of LRRK2. In HEK cells overexpressing specific β-tubulin isoforms, there was an increased proportion of acetylated tubulin in cells overexpressing tubulin isoforms that did not associate with LRRK2 in yeast two-hybrid assays, attributable to endogenous LRRK2.

I have also identified several novel variants in late-onset PD sufferers, which may be pathogenic. The variants were in *CADPS2, ERCC6, FUCA1, FZD4, SEZ6l* and *STK4*. Of particular interest are the two previously unreported *SEZ6L* SNPs in different families.

In summary, I have characterised the β-tubulin-LRRK2 Roc domain association and identified a novel role for LRRK2 mediating MT acetylation. This thesis describes a newly identified LRRK2 function and provides further evidence towards understanding how LRRK2 dysfunction leads to neurodegeneration and PD pathology.

Future work to test the effects of pathogenic *LRRK2* mutations on MT function will reveal further insight into the contribution of LRRK2-mediated MT stability in PD pathogenesis.

5. References

Aasly, J. O., Vilariño-Güell, C., Dachsel, J. C., Webber, P. J., West, A. B., Haugarvoll, K., Johansen, K. K., Toft, M., Nutt, J. G., Payami, H., Kachergus, J. M., Lincoln, S. J., Felic, A., Wider, C., Soto-Ortolaza, A. I., Cobb, S. A., White, L. R., Ross, O. A., and Farrer, M. J. (2010) Novel pathogenic LRRK2 p.Asn1437His substitution in familial Parkinson's disease. *Mov Disord* **25**, 2156-2163

Abecasis, G. R., Cherny, S. S., Cookson, W. O., and Cardon, L. R. (2002) Merlin--rapid analysis of dense genetic maps using sparse gene flow trees. *Nat Genet* **30**, 97-101

Adzhubei, I. A., Schmidt, S., Peshkin, L., Ramensky, V. E., Gerasimova, A., Bork, P., Kondrashov, A. S., and Sunyaev, S. R. (2010) A method and server for predicting damaging missense mutations. *Nat Methods* **7**, 248-249

Ahn, T. B., Kim, S. Y., Kim, J. Y., Park, S. S., Lee, D. S., Min, H. J., Kim, Y. K., Kim, S. E., Kim, J. M., Kim, H. J., Cho, J., and Jeon, B. S. (2008) alpha-Synuclein gene duplication is present in sporadic Parkinson disease. *Neurology* **70**, 43-49

Akiyama, T., and Kawasaki, Y. (2006) Wnt signalling and the actin cytoskeleton. *Oncogene* **25**, 7538-7544

Alcalay, R. N., Dinur, T., Quinn, T., Sakanaka, K., Levy, O., Waters, C., Fahn, S., Dorovski, T., Chung, W. K., Pauciulo, M., Nichols, W., Rana, H. Q., Balwani, M., Bier, L., Elstein, D., and Zimran, A. (2014) Comparison of Parkinson Risk in Ashkenazi Jewish Patients With Gaucher Disease and GBA Heterozygotes. *JAMA Neurol* **71**, 752-757

Alim, M. A., Hossain, M. S., Arima, K., Takeda, K., Izumiyama, Y., Nakamura, M., Kaji, H., Shinoda, T., Hisanaga, S., and Ueda, K. (2002) Tubulin seeds alpha-synuclein fibril formation. *J Biol Chem* **277**, 2112-2117

Alonso, A. C., Grundke-Iqbal, I., and Iqbal, K. (1996) Alzheimer's disease hyperphosphorylated tau sequesters normal tau into tangles of filaments and disassembles microtubules. *Nat Med* **2**, 783-787

Altschul, S. F., Gish, W., Miller, W., Myers, E. W., and Lipman, D. J. (1990) Basic local alignment search tool. *J Mol Biol* **215**, 403-410

Anand, V. S., Reichling, L. J., Lipinski, K., Stochaj, W., Duan, W., Kelleher, K., Pungaliya, P., Brown, E. L., Reinhart, P. H., Somberg, R., Hirst, W. D., Riddle, S. M., and Braithwaite, S. P. (2009) Investigation of leucine-rich repeat kinase 2 : enzymological properties and novel assays. *FEBS J* **276**, 466-478

Ariga, H., Takahashi-Niki, K., Kato, I., Maita, H., Niki, T., and Iguchi-Ariga, S. M. (2013) Neuroprotective function of DJ-1 in Parkinson's disease. *Oxid Med Cell Longev* **2013**, 683920, http://dx.doi.org/10.1155/2013/683920

Arnal, I., and Wade, R. H. (1995) How does taxol stabilize microtubules? *Curr Biol* **5**, 900-908

Audebert, S., Desbruyères, E., Gruszczynski, C., Koulakoff, A., Gros, F., Denoulet, P., and Eddé, B. (1993) Reversible polyglutamylation of alpha- and beta-tubulin and microtubule dynamics in mouse brain neurons. *Mol Biol Cell* **4**, 615-626

Avila, M. E., Sepúlveda, F. J., Burgos, C. F., Moraga-Cid, G., Parodi, J., Moon, R. T., Aguayo, L. G., Opazo, C., and De Ferrari, G. V. (2010) Canonical Wnt3a modulates intracellular calcium and enhances excitatory neurotransmission in hippocampal neurons. *J Biol Chem* **285**, 18939-18947

Baba, M., Nakajo, S., Tu, P. H., Tomita, T., Nakaya, K., Lee, V. M., Trojanowski, J. Q., and Iwatsubo, T. (1998) Aggregation of alpha-synuclein in Lewy bodies of sporadic Parkinson's disease and dementia with Lewy bodies. *Am J Pathol* **152**, 879-884

Badiola, N., de Oliveira, R. M., Herrera, F., Guardia-Laguarta, C., Gonçalves, S. A., Pera, M., Suárez-Calvet, M., Clarimon, J., Outeiro, T. F., and Lleó, A. (2011) Tau enhances α-synuclein aggregation and toxicity in cellular models of synucleinopathy. *PLoS One* **6**, e26609, doi: 10.1371/journal.pone.0026609.

Banerjee, A., and Kasmala, L. T. (1998) Differential assembly kinetics of alpha-tubulin isoforms in the presence of paclitaxel. *Biochem Biophys Res Commun* **245**, 349-351

Barrett, J. C., Hansoul, S., Nicolae, D. L., Cho, J. H., Duerr, R. H., Rioux, J. D., Brant, S. R., Silverberg, M. S., Taylor, K. D., Barmada, M. M., Bitton, A., Dassopoulos, T., Datta, L. W., Green, T., Griffiths, A. M., Kistner, E. O., Murtha, M. T., Regueiro, M. D., Rotter, J. I., Schumm, L. P., Steinhart, A. H., Targan, S. R., Xavier, R. J., Libioulle, C., Sandor, C., Lathrop, M., Belaiche, J., Dewit, O., Gut, I., Heath, S., Laukens, D., Mni, M., Rutgeerts, P., Van Gossum, A., Zelenika, D., Franchimont, D., Hugot, J. P., de Vos, M., Vermeire, S., Louis, E., Cardon, L. R., Anderson, C. A., Drummond, H., Nimmo, E., Ahmad, T., Prescott, N. J., Onnie, C. M., Fisher, S. A., Marchini, J., Ghori, J., Bumpstead, S., Gwilliam, R., Tremelling, M., Deloukas, P., Mansfield, J., Jewell, D., Satsangi, J., Mathew, C. G., Parkes, M., Georges, M., Daly, M. J., Consortium, N. I. G., Consortium, B.-F. I., and Consortium, W. T. C. C. (2008) Genome-wide association defines more than 30 distinct susceptibility loci for Crohn's disease. *Nat Genet* **40**, 955-962

Behl, C., Moosmann, B., Manthey, D., and Heck, S. (2000) The female sex hormone oestrogen as neuroprotectant: activities at various levels. *Novartis Found Symp* **230**, 221-234; discussion 234-228

Bekris, L. M., Mata, I. F., and Zabetian, C. P. (2010) The genetics of Parkinson disease. *J Geriatr Psychiatry Neurol* **23**, 228-242

Belenkaya, T. Y., Wu, Y., Tang, X., Zhou, B., Cheng, L., Sharma, Y. V., Yan, D., Selva, E. M., and Lin, X. (2008) The retromer complex influences Wnt secretion by recycling wntless from endosomes to the trans-Golgi network. *Dev Cell* **14**, 120-131

Berg, D., Niwar, M., Maass, S., Zimprich, A., Möller, J. C., Wuellner, U., Schmitz-Hübsch, T., Klein, C., Tan, E. K., Schöls, L., Marsh, L., Dawson, T. M., Janetzky, B., Müller, T., Woitalla, D., Kostic, V., Pramstaller, P. P., Oertel, W. H., Bauer, P., Krueger, R., Gasser, T., and Riess, O. (2005) Alpha-synuclein and Parkinson's disease: implications from the screening of more than 1,900 patients. *Mov Disord* **20**, 1191-1194

Berger, Z., Smith, K. A., and Lavoie, M. J. (2010) Membrane localization of LRRK2 is associated with increased formation of the highly active LRRK2 dimer and changes in its phosphorylation. *Biochemistry* **49**, 5511-5523

Bernheimer, H., Birkmayer, W., Hornykiewicz, O., Jellinger, K., and Seitelberger, F. (1973) Brain dopamine and the syndromes of Parkinson and Huntington. Clinical, morphological and neurochemical correlations. *J Neurol Sci* **20**, 415-455

Berwick, D. C., and Harvey, K. (2011) LRRK2 signaling pathways: the key to unlocking neurodegeneration? *Trends Cell Biol* **21**, 257-265

Berwick, D. C., and Harvey, K. (2012a) LRRK2 functions as a Wnt signaling scaffold, bridging cytosolic proteins and membrane-localized LRP6. *Hum Mol Genet* **21**, 4966-4979

Berwick, D. C., and Harvey, K. (2012b) The importance of Wnt signalling for neurodegeneration in Parkinson's disease. *Biochem Soc Trans* **40**, 1123-1128

Betarbet, R., Sherer, T. B., MacKenzie, G., Garcia-Osuna, M., Panov, A. V., and Greenamyre, J. T. (2000) Chronic systemic pesticide exposure reproduces features of Parkinson's disease. *Nat Neurosci* **3**, 1301-1306

Bhattacharya, R., and Cabral, F. (2004) A ubiquitous beta-tubulin disrupts microtubule assembly and inhibits cell proliferation. *Mol Biol Cell* **15**, 3123-3131

Bhattacharya, R., and Cabral, F. (2009) Molecular basis for class V beta-tubulin effects on microtubule assembly and paclitaxel resistance. *J Biol Chem* **284**, 13023-13032

Bhattacharya, R., Frankfurter, A., and Cabral, F. (2008) A minor beta-tubulin essential for mammalian cell proliferation. *Cell Motil Cytoskeleton* **65**, 708-720

Binda, A. V., Kabbani, N., and Levenson, R. (2005) Regulation of dense core vesicle release from PC12 cells by interaction between the D2 dopamine receptor and calcium-dependent activator protein for secretion (CAPS). *Biochem Pharmacol* **69**, 1451-1461

Biosa, A., Trancikova, A., Civiero, L., Glauser, L., Bubacco, L., Greggio, E., and Moore, D. J. (2013) GTPase activity regulates kinase activity and cellular phenotypes of Parkinson's disease-associated LRRK2. *Hum Mol Genet* **22**, 1140-1156

Biskup, S., Moore, D. J., Rea, A., Lorenz-Deperieux, B., Coombes, C. E., Dawson, V. L., Dawson, T. M., and West, A. B. (2007) Dynamic and redundant regulation of LRRK2 and LRRK1 expression. *BMC Neurosci* **8**, 102

Blom, N., Gammeltoft, S., and Brunak, S. (1999) Sequence and structure-based prediction of eukaryotic protein phosphorylation sites. *J Mol Biol* **294**, 1351-1362. Netphos: http://www.cbs.dtu.dk/services/NetPhos/, accessed April 2013

Bohgaki, T., Bohgaki, M., and Hakem, R. (2010) DNA double-strand break signaling and human disorders. *Genome Integr* **1**, 15

Bond, J. F., Robinson, G. S., and Farmer, S. R. (1984) Differential expression of two neural cell-specific beta-tubulin mRNAs during rat brain development. *Mol Cell Biol* **4**, 1313-1319

Bonnet, C., Boucher, D., Lazereg, S., Pedrotti, B., Islam, K., Denoulet, P., and Larcher, J. C. (2001) Differential binding regulation of microtubule-associated proteins MAP1A, MAP1B, and MAP2 by tubulin polyglutamylation. *J Biol Chem* **276**, 12839-12848

Bosgraaf, L., and Van Haastert, P. J. (2003) Roc, a Ras/GTPase domain in complex proteins. *Biochim Biophys Acta* **1643**, 5-10

Boucher, D., Larcher, J. C., Gros, F., and Denoulet, P. (1994) Polyglutamylation of tubulin as a progressive regulator of in vitro interactions between the microtubule-associated protein Tau and tubulin. *Biochemistry* **33**, 12471-12477

Braak, H., and Braak, E. (1990) Cognitive impairment in Parkinson's disease: amyloid plaques, neurofibrillary tangles, and neuropil threads in the cerebral cortex. *J Neural Transm Park Dis Dement Sect* **2**, 45-57

Braak, H., Braak, E., Yilmazer, D., de Vos, R. A., Jansen, E. N., Bohl, J., and Jellinger, K. (1994) Amygdala pathology in Parkinson's disease. *Acta Neuropathol* **88**, 493-500

Braak, H., Braak, E., Yilmazer, D., Schultz, C., de Vos, R. A., and Jansen, E. N. (1995) Nigral and extranigral pathology in

Parkinson's disease. *J Neural Transm Suppl* **46**, 15-31

Braak, H., Del Tredici, K., Rüb, U., de Vos, R. A., Jansen Steur, E. N., and Braak, E. (2003) Staging of brain pathology related to sporadic Parkinson's disease. *Neurobiol Aging* **24**, 197-211

Bradford, M. M. (1976) A rapid and sensitive method for the quantitation of microgram quantities of protein utilizing the principle of protein-dye binding. *Anal Biochem* **72**, 248-254

Braga, M., Pederzoli, M., Antonini, A., Beretta, F., and Crespi, V. (2014) Reasons for hospitalization in Parkinson's disease: A case-control study. *Parkinsonism Relat Disord* **20**, 488-492

Bras, J., Simón-Sánchez, J., Federoff, M., Morgadinho, A., Januario, C., Ribeiro, M., Cunha, L., Oliveira, C., and Singleton, A. B. (2009) Lack of replication of association between GIGYF2 variants and Parkinson disease. *Hum Mol Genet* **18**, 341-346

Breuss, M., Heng, J. I., Poirier, K., Tian, G., Jaglin, X. H., Qu, Z., Braun, A., Gstrein, T., Ngo, L., Haas, M., Bahi-Buisson, N., Moutard, M. L., Passemard, S., Verloes, A., Gressens, P., Xie, Y., Robson, K. J., Rani, D. S., Thangaraj, K., Clausen, T., Chelly, J., Cowan, N. J., and Keays, D. A. (2012) Mutations in the β-tubulin gene TUBB5 cause microcephaly with structural brain abnormalities. *Cell Rep* **2**, 1554-1562

Brockmann, K., Hilker, R., Pilatus, U., Baudrexel, S., Srulijes, K., Magerkurth, J., Hauser, A. K., Schulte, C., Csoti, I., Merten, C. D., Gasser, T., Berg, D., and Hattingen, E. (2012) GBA-associated PD. Neurodegeneration, altered membrane metabolism, and lack of energy failure. *Neurology* **79**, 213-220

Brunk, I., Blex, C., Speidel, D., Brose, N., and Ahnert-Hilger, G. (2009) Ca2+-dependent activator proteins of secretion promote vesicular monoamine uptake. *J Biol Chem* **284**, 1050-1056

Bryan, J., and Wilson, L. (1971) Are cytoplasmic microtubules heteropolymers? *Proc Natl Acad Sci U S A* **68**, 1762-1766

Burchell, V. S., Nelson, D. E., Sanchez-Martinez, A., Delgado-Camprubi, M., Ivatt, R. M., Pogson, J. H., Randle, S. J., Wray, S., Lewis, P. A., Houlden, H., Abramov, A. Y., Hardy, J., Wood, N. W., Whitworth, A. J., Laman, H., and Plun-Favreau, H. (2013) The Parkinson's disease-linked proteins Fbxo7 and Parkin interact to mediate mitophagy. *Nat Neurosci* **16**, 1257-1265

Burgoyne, R. D., Cambray-Deakin, M. A., Lewis, S. A., Sarkar, S., and Cowan, N. J. (1988) Differential distribution of beta-tubulin isotypes in cerebellum. *EMBO J* **7**, 2311-2319

Caesar, M., Zach, S., Carlson, C. B., Brockmann, K., Gasser, T., and Gillardon, F. (2013) Leucine-rich repeat kinase 2 functionally interacts with microtubules and kinase-dependently modulates cell migration. *Neurobiol Dis* **54**, 280-288

Cantuti-Castelvetri, I., Keller-McGandy, C., Bouzou, B., Asteris, G., Clark, T. W., Frosch, M. P., and Standaert, D. G. (2007) Effects of gender on nigral gene expression and parkinson disease. *Neurobiol Dis* **26**, 606-614

Canugovi, C., Misiak, M., Ferrarelli, L. K., Croteau, D. L., and Bohr, V. A. (2013) The role of DNA repair in brain related disease pathology. *DNA Repair (Amst)* **12**, 578-587

Carmine Belin, A., Westerlund, M., Bergman, O., Nissbrandt, H., Lind, C., Sydow, O., and Galter, D. (2007) S18Y in ubiquitin carboxy-terminal hydrolase L1 (UCH-L1) associated with decreased risk of Parkinson's disease in Sweden. *Parkinsonism Relat Disord* **13**, 295-298

Castro-Castro, A., Janke, C., Montagnac, G., Paul-Gilloteaux, P., and Chavrier, P. (2012) ATAT1/MEC-17 acetyltransferase and HDAC6 deacetylase control a balance of acetylation of alpha-tubulin and cortactin and regulate MT1-MMP trafficking and breast tumor cell invasion. *Eur J Cell Biol* **91**, 950-960

Chan, D., Citro, A., Cordy, J. M., Shen, G. C., and Wolozin, B. (2011) Rac1 protein rescues neurite retraction caused by G2019S leucine-rich repeat kinase 2 (LRRK2). *J Biol Chem* **286**, 16140-16149

Chan, S. L., Chua, L. L., Angeles, D. C., and Tan, E. K. (2014) MAP1B rescues LRRK2 mutant-mediated cytotoxicity. *Mol Brain* **7**, 29

Chang, P., and Stearns, T. (2000) Delta-tubulin and epsilon-tubulin: two new human centrosomal tubulins reveal new aspects of centrosome structure and function. *Nat Cell Biol* **2**, 30-35

Chang, W., Webster, D. R., Salam, A. A., Gruber, D., Prasad, A., Eiserich, J. P., and Bulinski, J. C. (2002) Alteration of the C-terminal amino acid of tubulin specifically inhibits myogenic differentiation. *J Biol Chem* **277**, 30690-30698

Chartier-Harlin, M. C., Dachsel, J. C., Vilariño-Güell, C., Lincoln, S. J., Leprêtre, F., Hulihan, M. M., Kachergus, J., Milnerwood, A. J., Tapia, L., Song, M. S., Le Rhun, E., Mutez, E., Larvor, L., Duflot, A., Vanbesien-Mailliot, C., Kreisler, A., Ross, O. A., Nishioka, K., Soto-Ortolaza, A. I., Cobb, S. A., Melrose, H. L., Behrouz, B., Keeling, B. H., Bacon, J. A., Hentati, E., Williams, L., Yanagiya, A., Sonenberg, N., Lockhart, P. J., Zubair, A. C., Uitti, R. J., Aasly, J. O., Krygowska-Wajs, A., Opala, G., Wszolek, Z. K., Frigerio, R., Maraganore, D. M., Gosal, D., Lynch, T., Hutchinson, M., Bentivoglio, A. R., Valente, E. M., Nichols, W. C., Pankratz, N., Foroud, T., Gibson, R. A., Hentati, F., Dickson, D. W., Destée, A., and Farrer, M. J. (2011) Translation initiator

EIF4G1 mutations in familial Parkinson disease. *Am J Hum Genet* **89**, 398-406

Chen, C. Y., Weng, Y. H., Chien, K. Y., Lin, K. J., Yeh, T. H., Cheng, Y. P., Lu, C. S., and Wang, H. L. (2012a) (G2019S) LRRK2 activates MKK4-JNK pathway and causes degeneration of SN dopaminergic neurons in a transgenic mouse model of PD. *Cell Death Differ* **19**, 1623-1633

Chen, H., Chan, B. K., Drummond, J., Estrada, A. A., Gunzner-Toste, J., Liu, X., Liu, Y., Moffat, J., Shore, D., Sweeney, Z. K., Tran, T., Wang, S., Zhao, G., Zhu, H., and Burdick, D. J. (2012b) Discovery of selective LRRK2 inhibitors guided by computational analysis and molecular modeling. *J Med Chem* **55**, 5536-5545

Chen, J., Kanai, Y., Cowan, N. J., and Hirokawa, N. (1992) Projection domains of MAP2 and tau determine spacings between microtubules in dendrites and axons. *Nature* **360**, 674-677

Chen, L., Zhang, S., Liu, Y., Hong, H., Wang, H., Zheng, Y., Zhou, H., Chen, J., Xian, W., He, Y., Li, J., Liu, Z., Pei, Z., and Zeng, J. (2011) LRRK2 R1398H polymorphism is associated with decreased risk of Parkinson's disease in a Han Chinese population. *Parkinsonism Relat Disord* **17**, 291-292

Cheng, H. C., Ulane, C. M., and Burke, R. E. (2010) Clinical progression in Parkinson disease and the neurobiology of axons. *Ann Neurol* **67**, 715-725

Choi, H. G., Zhang, J., Deng, X., Hatcher, J. M., Patricelli, M. P., Zhao, Z., Alessi, D. R., and Gray, N. S. (2012a) Brain Penetrant LRRK2 Inhibitor. *ACS Med Chem Lett* **3**, 658-662

Choi, Y., Sims, G. E., Murphy, S., Miller, J. R., and Chan, A. P. (2012b) Predicting the functional effect of amino acid substitutions and indels. *PLoS One* **7**, e46688, doi: 10.1371/journal.pone.0046688

Chuang, C. L., Lu, Y. N., Wang, H. C., and Chang, H. Y. (2014) Genetic dissection reveals that Akt is the critical kinase downstream of LRRK2 to phosphorylate and inhibit FOXO1, and promotes neuron survival. *Hum Mol Genet,* 1;23(21):5649-58

Ciani, L., Krylova, O., Smalley, M. J., Dale, T. C., and Salinas, P. C. (2004) A divergent canonical WNT-signaling pathway regulates microtubule dynamics: dishevelled signals locally to stabilize microtubules. *J Cell Biol* **164**, 243-253

Ciani, L., and Salinas, P. C. (2007) c-Jun N-terminal kinase (JNK) cooperates with Gsk3beta to regulate Dishevelled-mediated microtubule stability. *BMC Cell Biol* **8**, 27

Ciccone, S., Maiani, E., Bellusci, G., Diederich, M., and Gonfloni, S. (2013) Parkinson's disease: a complex interplay of mitochondrial DNA alterations and oxidative stress. *Int J Mol Sci* **14**, 2388-2409

Ciucci, M. R., Schaser, A. J., and Russell, J. A. (2013) Exercise-induced rescue of tongue function without striatal dopamine sparing in a rat neurotoxin model of Parkinson disease. *Behav Brain Res* **252**, 239-245

Cleveland, D. W. (1987) The multitubulin hypothesis revisited: what have we learned? *J Cell Biol* **104**, 381-383

Cookson, M. R., Xiromerisiou, G., and Singleton, A. (2005) How genetics research in Parkinson's disease is enhancing understanding of the common idiopathic forms of the disease. *Curr Opin Neurol* **18**, 706-711

Costello, S., Cockburn, M., Bronstein, J., Zhang, X., and Ritz, B. (2009) Parkinson's disease and residential exposure to maneb and paraquat from agricultural applications in the central valley of California. *Am J Epidemiol* **169**, 919-926

Craddock, T. J., St George, M., Freedman, H., Barakat, K. H., Damaraju, S., Hameroff, S., and Tuszynski, J. A. (2012a) Computational predictions of volatile anesthetic interactions with the microtubule cytoskeleton: implications for side effects of general anesthesia. *PLoS One* **7**, e37251, doi: 10.1371/journal.pone.0037251

Craddock, T. J., Tuszynski, J. A., and Hameroff, S. (2012b) Cytoskeletal signaling: is memory encoded in microtubule lattices by CaMKII phosphorylation? *PLoS Comput Biol* **8**, e1002421, doi: 10.1371/journal.pcbi.1002421

Cueva, J. G., Hsin, J., Huang, K. C., and Goodman, M. B. (2012) Posttranslational acetylation of α-tubulin constrains protofilament number in native microtubules. *Curr Biol* **22**, 1066-1074

Cushion, T. D., Paciorkowski, A. R., Pilz, D. T., Mullins, J. G., Seltzer, L. E., Marion, R. W., Tuttle, E., Ghoneim, D., Christian, S. L., Chung, S. K., Rees, M. I., and Dobyns, W. B. (2014) De novo mutations in the beta-tubulin gene TUBB2A cause simplified gyral patterning and infantile-onset epilepsy. *Am J Hum Genet* **94**, 634-641

Da Cunha, C., Angelucci, M. E., Canteras, N. S., Wonnacott, S., and Takahashi, R. N. (2002) The lesion of the rat substantia nigra pars compacta dopaminergic neurons as a model for Parkinson's disease memory disabilities. *Cell Mol Neurobiol* **22**, 227-237

Dächsel, J. C., and Farrer, M. J. (2010) LRRK2 and Parkinson disease. *Arch Neurol* **67**, 542-547

Dächsel, J. C., Behrouz, B., Yue, M., Beevers, J. E., Melrose, H. L., and Farrer, M. J. (2010) A comparative study of Lrrk2 function in primary neuronal cultures. *Parkinsonism Relat Disord* **16**, 650-655

Daniëls, V., Vancraenenbroeck, R., Law, B. M., Greggio, E., Lobbestael, E., Gao, F., De Maeyer, M., Cookson, M. R., Harvey, K., Baekelandt, V., and Taymans, J. M. (2011) Insight into the mode of action of the LRRK2 Y1699C pathogenic mutant. *J Neurochem* **116**, 304-315

Dann, C. E., Hsieh, J. C., Rattner, A., Sharma, D., Nathans, J., and Leahy, D. J. (2001) Insights into Wnt binding and signalling from the structures of two Frizzled cysteine-rich domains. *Nature* **412**, 86-90

De Brabander, M., Geuens, G., Nuydens, R., Willebrords, R., and De Mey, J. (1981) Microtubule assembly in living cells after release from nocodazole block: the effects of metabolic inhibitors, taxol and PH. *Cell Biol Int Rep* **5**, 913-920

De Brabander, M., Geuens, G., Nuydens, R., Willebrords, R., and De Mey, J. (1981) Taxol induces the assembly of free microtubules in living cells and blocks the organizing capacity of the centrosomes and kinetochores. *Proc Natl Acad Sci U S A* **78**, 5608-5612

de Hostos, E. L. (1999) The coronin family of actin-associated proteins. *Trends Cell Biol* **9**, 345-350

de Rijk, M. C., Launer, L. J., Berger, K., Breteler, M. M., Dartigues, J. F., Baldereschi, M., Fratiglioni, L., Lobo, A., Martinez-Lage, J., Trenkwalder, C., and Hofman, A. (2000) Prevalence of Parkinson's disease in Europe: A collaborative study of population-based cohorts. Neurologic Diseases in the Elderly Research Group. *Neurology* **54**, S21-23

Dehay, B., Martinez-Vicente, M., Caldwell, G. A., Caldwell, K. A., Yue, Z., Cookson, M. R., Klein, C., Vila, M., and Bezard, E. (2013) Lysosomal impairment in Parkinson's disease. *Mov Disord* **28**, 725-732

Dehmelt, L., and Halpain, S. (2005) The MAP2/Tau family of microtubule-associated proteins. *Genome Biol* **6**, 204

DeLong, M. R. (1990) Primate models of movement disorders of basal ganglia origin. *Trends Neurosci* **13**, 281-285

Deng, H., Gao, K., and Jankovic, J. (2013) The VPS35 gene and Parkinson's disease. *Mov Disord* **28**, 569-575

Deng, J., Lewis, P. A., Greggio, E., Sluch, E., Beilina, A., and Cookson, M. R. (2008) Structure of the ROC domain from the Parkinson's disease-associated leucine-rich repeat kinase 2 reveals a dimeric GTPase. *Proc Natl Acad Sci U S A* **105**, 1499-1504

Dereeper, A., Guignon, V., Blanc, G., Audic, S., Buffet, S., Chevenet, F., Dufayard, J. F., Guindon, S., Lefort, V., Lescot, M., Claverie, J. M., and Gascuel, O. (2008) Phylogeny.fr: robust phylogenetic analysis for the non-specialist. *Nucleic Acids Res* **36**, W465-469

Derry, W. B., Wilson, L., Khan, I. A., Luduena, R. F., and Jordan, M. A. (1997) Taxol differentially modulates the dynamics of microtubules assembled from unfractionated and purified beta-tubulin isotypes. *Biochemistry* **36**, 3554-3562

Detwiler, M. M., Hamp, T. J., and Kazim, A. L. (2004) DNA sequencing using the liquid polymer POP-7 on an ABI PRISM 3100 Genetic Analyzer. *Biotechniques* **36**, 932-933

Drewes, G. (2004) MARKing tau for tangles and toxicity. *Trends Biochem Sci* **29**, 548-555

Drewes, G., Ebneth, A., Preuss, U., Mandelkow, E. M., and Mandelkow, E. (1997) MARK, a novel family of protein kinases that phosphorylate microtubule-associated proteins and trigger microtubule disruption. *Cell* **89**, 297-308

Dugger, B. N., Adler, C. H., Shill, H. A., Caviness, J., Jacobson, S., Driver-Dunckley, E., Beach, T. G., and Consortium, A. P. s. D. (2014) Concomitant pathologies among a spectrum of parkinsonian disorders. *Parkinsonism Relat Disord* **20**, 525-529

Duka, T., Rusnak, M., Drolet, R. E., Duka, V., Wersinger, C., Goudreau, J. L., and Sidhu, A. (2006) Alpha-synuclein induces hyperphosphorylation of Tau in the MPTP model of parkinsonism. *FASEB J* **20**, 2302-2312

Dumitriu, A., Latourelle, J. C., Hadzi, T. C., Pankratz, N., Garza, D., Miller, J. P., Vance, J. M., Foroud, T., Beach, T. G., and Myers, R. H. (2012) Gene expression profiles in Parkinson disease prefrontal cortex implicate FOXO1 and genes under its transcriptional regulation. *PLoS Genet* **8**, e1002794, doi: 10.1371/journal.pgen.1002794

Dunbrack, R. L. (2002) Rotamer libraries in the 21st century. *Curr Opin Struct Biol* **12**, 431-440

Dutcher, S. K. (2001) The tubulin fraternity: alpha to eta. *Curr Opin Cell Biol* **13**, 49-54

Dzamko, N., Deak, M., Hentati, F., Reith, A. D., Prescott, A. R., Alessi, D. R., and Nichols, R. J. (2010) Inhibition of LRRK2 kinase activity leads to dephosphorylation of Ser(910)/Ser(935), disruption of 14-3-3 binding and altered cytoplasmic localization. *Biochem J* **430**, 405-413

Estrada, A. A., Liu, X., Baker-Glenn, C., Beresford, A., Burdick, D. J., Chambers, M., Chan, B. K., Chen, H., Ding, X., DiPasquale, A. G., Dominguez, S. L., Dotson, J., Drummond, J., Flagella, M., Flynn, S., Fuji, R., Gill, A., Gunzner-Toste, J., Harris, S. F., Heffron, T. P., Kleinheinz, T., Lee, D. W., Le Pichon, C. E., Lyssikatos, J. P., Medhurst, A. D., Moffat, J. G., Mukund, S., Nash, K., Scearce-Levie, K., Sheng, Z., Shore, D. G., Tran, T., Trivedi, N., Wang, S., Zhang, S., Zhang, X., Zhao, G., Zhu, H., and Sweeney, Z. K. (2012) Discovery of highly potent, selective, and brain-penetrable leucine-rich repeat kinase 2 (LRRK2) small molecule inhibitors. *J Med Chem* **55**, 9416-9433

Farrer, M., Gwinn-Hardy, K., Muenter, M., DeVrieze, F. W., Crook, R., Perez-Tur, J., Lincoln, S., Maraganore, D., Adler, C., Newman, S., MacElwee, K., McCarthy, P., Miller, C., Waters, C., and Hardy, J. (1999) A chromosome 4p haplotype segregating with Parkinson's disease and postural tremor. *Hum Mol Genet* **8**, 81-85

Feany, M. B., and Pallanck, L. J. (2003) Parkin: a multipurpose neuroprotective agent? *Neuron* **38**, 13-16

Fearnley, J. M., and Lees, A. J. (1991) Ageing and Parkinson's disease: substantia nigra regional selectivity. *Brain* **114 (Pt 5)**, 2283-2301

Ferrer, I., Blanco, R., Carmona, M., Puig, B., Barrachina, M., Gómez, C., and Ambrosio, S. (2001) Active, phosphorylation-dependent mitogen-activated protein kinase (MAPK/ERK), stress-activated protein kinase/c-Jun N-terminal kinase (SAPK/JNK), and p38 kinase expression in Parkinson's disease and Dementia with Lewy bodies. *J Neural Transm* **108**, 1383-1396

Fields, S., and Song, O. (1989) A novel genetic system to detect protein-protein interactions. *Nature* **340**, 245-246

Fisher, B. E., Li, Q., Nacca, A., Salem, G. J., Song, J., Yip, J., Hui, J. S., Jakowec, M. W., and Petzinger, G. M. (2013) Treadmill exercise elevates striatal dopamine D2 receptor binding potential in patients with early Parkinson's disease. *Neuroreport* **24**, 509-514

Flicek, P., Ahmed, I., Amode, M. R., Barrell, D., Beal, K., Brent, S., Carvalho-Silva, D., Clapham, P., Coates, G., Fairley, S., Fitzgerald,S., Gil, L., Garcia-Girón, C., Gordon, L., Hourlier, T., Hunt, S., Juettemann, T., Kähäri, A., Keenan, S., Komorowska, M., Kulesha, E., Longden, I., Maurel, T., McLaren, W., Muffato, M., Nag, R., Overduin, B., Pignatelli, M., Pritchard, B., Pritchard, E., Singh Riat, H., Ritchie, G. R. S., Ruffier, M., Schuster, M., Sheppard, D., Sobral, D., Taylor, K., Thormann, A., Trevanion, S., White, S., Wilder, S. P., Aken, B. L., Birney, E., Cunningham, F., Dunham, I., Harrow, J., Herrero, J., Hubbard, T. J. P., Johnson, N., Kinsella,R., Parker, A., Spudich, G., Yates, A., Zadissa, A., Searle, S. M. J. (2013) Ensembl 2013 *Nuc Acids Res* **41**, D48-D55

Follett, J., Norwood, S. J., Hamilton, N. A., Mohan, M., Kovtun, O., Tay, S., Zhe, Y., Wood, S. A., Mellick, G. D., Silburn, P. A., Collins, B. M., Bugarcic, A., and Teasdale, R. D. (2014) The Vps35 D620N mutation linked to Parkinson's disease disrupts the cargo sorting function of retromer. *Traffic* **15**, 230-244

Freedman, H., Luchko, T., Luduena, R. F., and Tuszynski, J. A. (2011) Molecular dynamics modeling of tubulin C-terminal tail interactions with the microtubule surface. *Proteins* **79**, 2968-2982

Fu, X., Zheng, Y., Hong, H., He, Y., Zhou, S., Guo, C., Liu, Y., Xian, W., Zeng, J., Li, J., Liu, Z., Chen, L., and Pei, Z. (2013) LRRK2 G2385R and LRRK2 R1628P increase risk of Parkinson's disease in a Han Chinese population from Southern Mainland China. *Parkinsonism Relat Disord* **19**, 397-398

Funayama, M., Hasegawa, K., Kowa, H., Saito, M., Tsuji, S., and Obata, F. (2002) A new locus for Parkinson's disease (PARK8) maps to chromosome 12p11.2-q13.1. *Ann Neurol* **51**, 296-301

Gallo, K. A., and Johnson, G. L. (2002) Mixed-lineage kinase control of JNK and p38 MAPK pathways. *Nat Rev Mol Cell Biol* **3**, 663-672

Galter, D., Westerlund, M., Carmine, A., Lindqvist, E., Sydow, O., and Olson, L. (2006) LRRK2 expression linked to dopamine-innervated areas. *Ann Neurol* **59**, 714-719

Gandhi, P. N., Wang, X., Zhu, X., Chen, S. G., and Wilson-Delfosse, A. L. (2008) The Roc domain of leucine-rich repeat kinase 2 is sufficient for interaction with microtubules. *J Neurosci Res* **86**, 1711-1720

Gao, X., Chen, H., Fung, T. T., Logroscino, G., Schwarzschild, M. A., Hu, F. B., and Ascherio, A. (2007) Prospective study of dietary pattern and risk of Parkinson disease. *Am J Clin Nutr* **86**, 1486-1494

Garvalov, B. K., Zuber, B., Bouchet-Marquis, C., Kudryashev, M., Gruska, M., Beck, M., Leis, A., Frischknecht, F., Bradke, F., Baumeister, W., Dubochet, J., and Cyrklaff, M. (2006) Luminal particles within cellular microtubules. *J Cell Biol* **174**, 759-765

Gasper, R., Meyer, S., Gotthardt, K., Sirajuddin, M., and Wittinghofer, A. (2009) It takes two to tango: regulation of G proteins by dimerization. *Nat Rev Mol Cell Biol* **10**, 423-429

Gasser, T., Müller-Myhsok, B., Wszolek, Z. K., Oehlmann, R., Calne, D. B., Bonifati, V., Bereznai, B., Fabrizio, E., Vieregge, P., and Horstmann, R. D. (1998) A susceptibility locus for Parkinson's disease maps to chromosome 2p13. *Nat Genet* **18**, 262-265

Gegg, M. E., Cooper, J. M., Chau, K. Y., Rojo, M., Schapira, A. H., and Taanman, J. W. (2010) Mitofusin 1 and mitofusin 2 are

ubiquitinated in a PINK1/parkin-dependent manner upon induction of mitophagy. *Hum Mol Genet* **19**, 4861-4870

Gencer, M., Dasdemir, S., Cakmakoglu, B., Cetinkaya, Y., Varlibas, F., Tireli, H., Kucukali, C. I., Ozkok, E., and Aydin, M. (2012) DNA repair genes in Parkinson's disease. *Genet Test Mol Biomarkers* **16**, 504-507

Giesert, F., Hofmann, A., Bürger, A., Zerle, J., Kloos, K., Hafen, U., Ernst, L., Zhang, J., Vogt-Weisenhorn, D. M., and Wurst, W. (2013) Expression analysis of Lrrk1, Lrrk2 and Lrrk2 splice variants in mice. *PLoS One* **8**, e63778, doi: 10.1371/journal.pone.0063778

Gietz, R. D., Schiestl, R. H., Willems, A. R., and Woods, R. A. (1995) Studies on the transformation of intact yeast cells by the LiAc/SS-DNA/PEG procedure. *Yeast* **11**, 355-360

Gillardon, F. (2009) Leucine-rich repeat kinase 2 phosphorylates brain tubulin-beta isoforms and modulates microtubule stability--a point of convergence in parkinsonian neurodegeneration? *J Neurochem* **110**, 1514-1522

Gilsbach, B. K., Ho, F. Y., Vetter, I. R., van Haastert, P. J., Wittinghofer, A., and Kortholt, A. (2012) Roco kinase structures give insights into the mechanism of Parkinson disease-related leucine-rich-repeat kinase 2 mutations. *Proc Natl Acad Sci U S A* **109**, 10322-10327

Gilsbach, B. K., and Kortholt, A. (2014) Structural biology of the LRRK2 GTPase and kinase domains: implications for regulation. *Front Mol Neurosci* **7**, 32

Glauser, L., Sonnay, S., Stafa, K., and Moore, D. J. (2011) Parkin promotes the ubiquitination and degradation of the mitochondrial fusion factor mitofusin 1. *J Neurochem* **118**, 636-645

Gloeckner, C. J., Kinkl, N., Schumacher, A., Braun, R. J., O'Neill, E., Meitinger, T., Kolch, W., Prokisch, H., and Ueffing, M. (2006) The Parkinson disease causing LRRK2 mutation I2020T is associated with increased kinase activity. *Hum Mol Genet* **15**, 223-232

Goker-Alpan, O., Schiffmann, R., LaMarca, M. E., Nussbaum, R. L., McInerney-Leo, A., and Sidransky, E. (2004) Parkinsonism among Gaucher disease carriers. *J Med Genet* **41**, 937-940

Goldman, S. M., Tanner, C. M., Oakes, D., Bhudhikanok, G. S., Gupta, A., and Langston, J. W. (2006) Head injury and Parkinson's disease risk in twins. *Ann Neurol* **60**, 65-72

Gómez-Suaga, P., and Hilfiker, S. (2012) LRRK2 as a modulator of lysosomal calcium homeostasis with downstream effects on autophagy. *Autophagy* **8**, 692-693

Gorell, J. M., Johnson, C. C., Rybicki, B. A., Peterson, E. L., Kortsha, G. X., Brown, G. G., and Richardson, R. J. (1997) Occupational exposures to metals as risk factors for Parkinson's disease. *Neurology* **48**, 650-658

Gotthardt, K., Weyand, M., Kortholt, A., Van Haastert, P. J., and Wittinghofer, A. (2008) Structure of the Roc-COR domain tandem of C. tepidum, a prokaryotic homologue of the human LRRK2 Parkinson kinase. *EMBO J* **27**, 2239-2249

Grandinetti, A., Morens, D. M., Reed, D., and MacEachern, D. (1994) Prospective study of cigarette smoking and the risk of developing idiopathic Parkinson's disease. *Am J Epidemiol* **139**, 1129-1138

Grant, S. F., Thorleifsson, G., Reynisdottir, I., Benediktsson, R., Manolescu, A., Sainz, J., Helgason, A., Stefansson, H., Emilsson, V., Helgadottir, A., Styrkarsdottir, U., Magnusson, K. P., Walters, G. B., Palsdottir, E., Jonsdottir, T., Gudmundsdottir, T., Gylfason, A., Saemundsdottir, J., Wilensky, R. L., Reilly, M. P., Rader, D. J., Bagger, Y., Christiansen, C., Gudnason, V., Sigurdsson, G., Thorsteinsdottir, U., Gulcher, J. R., Kong, A., and Stefansson, K. (2006) Variant of transcription factor 7-like 2 (TCF7L2) gene confers risk of type 2 diabetes. *Nat Genet* **38**, 320-323

Greggio, E., Civiero, L., Bisaglia, M., and Bubacco, L. (2012) Parkinson's disease and immune system: is the culprit LRRKing in the periphery? *J Neuroinflammation* **9**, 94

Greggio, E., and Cookson, M. R. (2009) Leucine-rich repeat kinase 2 mutations and Parkinson's disease: three questions. *ASN Neuro* 1 e00002doi: 10.1042/AN20090007

Greggio, E., Jain, S., Kingsbury, A., Bandopadhyay, R., Lewis, P., Kaganovich, A., van der Brug, M. P., Beilina, A., Blackinton, J., Thomas, K. J., Ahmad, R., Miller, D. W., Kesavapany, S., Singleton, A., Lees, A., Harvey, R. J., Harvey, K., and Cookson, M. R. (2006) Kinase activity is required for the toxic effects of mutant LRRK2/dardarin. *Neurobiol Dis* **23**, 329-341

Greggio, E., Lewis, P. A., van der Brug, M. P., Ahmad, R., Kaganovich, A., Ding, J., Beilina, A., Baker, A. K., and Cookson, M. R. (2007a) Mutations in LRRK2/dardarin associated with Parkinson disease are more toxic than equivalent mutations in the homologous kinase LRRK1. *J Neurochem* **102**, 93-102

Greggio, E., and Singleton, A. (2007b) Kinase signaling pathways as potential targets in the treatment of Parkinson's disease. *Expert Rev Proteomics* **4**, 783-792

Greggio, E., Taymans, J. M., Zhen, E. Y., Ryder, J., Vancraenenbroeck, R., Beilina, A., Sun, P., Deng, J., Jaffe, H., Baekelandt, V., Merchant, K., and Cookson, M. R. (2009) The Parkinson's disease kinase LRRK2 autophosphorylates its GTPase domain at multiple sites. *Biochem Biophys Res Commun* **389**, 449-454

Greggio, E., Zambrano, I., Kaganovich, A., Beilina, A., Taymans, J. M., Daniëls, V., Lewis, P., Jain, S., Ding, J., Syed, A., Thomas, K. J., Baekelandt, V., and Cookson, M. R. (2008) The Parkinson disease-associated leucine-rich repeat kinase 2 (LRRK2) is a dimer that undergoes intramolecular autophosphorylation. *J Biol Chem* **283**, 16906-16914

Gregory, A., Polster, B. J., and Hayflick, S. J. (2009) Clinical and genetic delineation of neurodegeneration with brain iron accumulation. *J Med Genet* **46**, 73-80

Grossman, R. M., Krueger, J., Yourish, D., Granelli-Piperno, A., Murphy, D. P., May, L. T., Kupper, T. S., Sehgal, P. B., and Gottlieb, A. B. (1989) Interleukin 6 is expressed in high levels in psoriatic skin and stimulates proliferation of cultured human keratinocytes. *Proc Natl Acad Sci U S A* **86**, 6367-6371

Grünblatt, E., Mandel, S., Jacob-Hirsch, J., Zeligson, S., Amariglo, N., Rechavi, G., Li, J., Ravid, R., Roggendorf, W., Riederer, P., and Youdim, M. B. (2004) Gene expression profiling of parkinsonian substantia nigra pars compacta; alterations in ubiquitin-proteasome, heat shock protein, iron and oxidative stress regulated proteins, cell adhesion/cellular matrix and vesicle trafficking genes. *J Neural Transm* **111**, 1543-1573

Guichet, A., Wucherpfennig, T., Dudu, V., Etter, S., Wilsch-Bräuniger, M., Hellwig, A., González-Gaitán, M., Huttner, W. B., and Schmidt, A. A. (2002) Essential role of endophilin A in synaptic vesicle budding at the Drosophila neuromuscular junction. *EMBO J* **21**, 1661-1672

Guo, J. L., Covell, D. J., Daniels, J. P., Iba, M., Stieber, A., Zhang, B., Riddle, D. M., Kwong, L. K., Xu, Y., Trojanowski, J. Q., and Lee, V. M. (2013) Distinct α-synuclein strains differentially promote tau inclusions in neurons. *Cell* **154**, 103-117

Guo, L., Gandhi, P. N., Wang, W., Petersen, R. B., Wilson-Delfosse, A. L., and Chen, S. G. (2007) The Parkinson's disease-associated protein, leucine-rich repeat kinase 2 (LRRK2), is an authentic GTPase that stimulates kinase activity. *Exp Cell Res* **313**, 3658-3670

Guridi, J., González-Redondo, R., and Obeso, J. A. (2012) Clinical features, pathophysiology, and treatment of levodopa-induced dyskinesias in Parkinson's disease. *Parkinsons Dis* **2012**, 943159, doi: 10.1155/2012/943159

Haaxma, C. A., Bloem, B. R., Borm, G. F., Oyen, W. J., Leenders, K. L., Eshuis, S., Booij, J., Dluzen, D. E., and Horstink, M. W. (2007) Gender differences in Parkinson's disease. *J Neurol Neurosurg Psychiatry* **78**, 819-824

Habas, R., and He, X. (2006) Activation of Rho and Rac by Wnt/frizzled signaling. *Methods Enzymol* **406**, 500-511

Häbig, K., Gellhaar, S., Heim, B., Djuric, V., Giesert, F., Wurst, W., Walter, C., Hentrich, T., Riess, O., and Bonin, M. (2013) LRRK2 guides the actin cytoskeleton at growth cones together with ARHGEF7 and Tropomyosin 4. *Biochim Biophys Acta* **1832**, 2352-2367

Haebig, K., Gloeckner, C. J., Miralles, M. G., Gillardon, F., Schulte, C., Riess, O., Ueffing, M., Biskup, S., and Bonin, M. (2010) ARHGEF7 (Beta-PIX) acts as guanine nucleotide exchange factor for leucine-rich repeat kinase 2. *PLoS One* **5**, e13762, doi: 10.1371/journal.pone.001376

Haggerty, T., Credle, J., Rodriguez, O., Wills, J., Oaks, A. W., Masliah, E., and Sidhu, A. (2011) Hyperphosphorylated Tau in an α-synuclein-overexpressing transgenic model of Parkinson's disease. *Eur J Neurosci* **33**, 1598-1610

Hall, A. (1998) Rho GTPases and the actin cytoskeleton. *Science* **279**, 509-514

Hammond, J. W., Cai, D., and Verhey, K. J. (2008) Tubulin modifications and their cellular functions. *Curr Opin Cell Biol* **20**, 71-76

Hammond, J. W., Huang, C. F., Kaech, S., Jacobson, C., Banker, G., and Verhey, K. J. (2010) Posttranslational modifications of tubulin and the polarized transport of kinesin-1 in neurons. *Mol Biol Cell* **21**, 572-583

Hampshire, D. J., Roberts, E., Crow, Y., Bond, J., Mubaidin, A., Wriekat, A. L., Al-Din, A., and Woods, C. G. (2001) Kufor-Rakeb syndrome, pallido-pyramidal degeneration with supranuclear upgaze paresis and dementia, maps to 1p36. *J Med Genet* **38**, 680-682

Haugarvoll, K., Toft, M., Ross, O. A., White, L. R., Aasly, J. O., and Farrer, M. J. (2007) Variants in the LRRK1 gene and susceptibility to Parkinson's disease in Norway. *Neurosci Lett* **416**, 299-301

Hayashi, T., Ishimori, C., Takahashi-Niki, K., Taira, T., Kim, Y. C., Maita, H., Maita, C., Ariga, H., and Iguchi-Ariga, S. M. (2009) DJ-1 binds to mitochondrial complex I and maintains its activity. *Biochem Biophys Res Commun* **390**, 667-672

Healy, D. G., Abou-Sleiman, P. M., Lees, A. J., Casas, J. P., Quinn, N., Bhatia, K., Hingorani, A. D., and Wood, N. W. (2004) Tau gene and Parkinson's disease: a case-control study and meta-analysis. *J Neurol Neurosurg Psychiatry* **75**, 962-965

Healy, D. G., Falchi, M., O'Sullivan, S. S., Bonifati, V., Durr, A., Bressman, S., Brice, A., Aasly, J., Zabetian, C. P., Goldwurm, S., Ferreira, J. J., Tolosa, E., Kay, D. M., Klein, C., Williams, D. R., Marras, C., Lang, A. E., Wszolek, Z. K., Berciano, J., Schapira, A. H., Lynch, T., Bhatia, K. P., Gasser, T., Lees, A. J., Wood, N. W., and Consortium, I. L. (2008) Phenotype, genotype, and worldwide genetic penetrance of LRRK2-associated Parkinson's disease: a case-control study. *Lancet Neurol* **7**, 583-590

Hegde, M. L., Mantha, A. K., Hazra, T. K., Bhakat, K. K., Mitra, S., and Szczesny, B. (2012) Oxidative genome damage and its repair: implications in aging and neurodegenerative diseases. *Mech Ageing Dev* **133**, 157-168

Hellenbrand, W., Seidler, A., Boeing, H., Robra, B. P., Vieregge, P., Nischan, P., Joerg, J., Oertel, W. H., Schneider, E., and Ulm, G. (1996) Diet and Parkinson's disease. I: A possible role for the past intake of specific foods and food groups. Results from a self-administered food-frequency questionnaire in a case-control study. *Neurology* **47**, 636-643

Hersheson, J., Haworth, A., and Houlden, H. (2012) The inherited ataxias: genetic heterogeneity, mutation databases, and future directions in research and clinical diagnostics. *Hum Mutat* **33**, 1324-1332

Hicks, A. A., Pétursson, H., Jónsson, T., Stefánsson, H., Jóhannsdóttir, H. S., Sainz, J., Frigge, M. L., Kong, A., Gulcher, J. R., Stefánsson, K., and Sveinbjörnsdóttir, S. (2002) A susceptibility gene for late-onset idiopathic Parkinson's disease. *Ann Neurol* **52**, 549-555

Higashi, S., Biskup, S., West, A. B., Trinkaus, D., Dawson, V. L., Faull, R. L., Waldvogel, H. J., Arai, H., Dawson, T. M., Moore, D. J., and Emson, P. C. (2007) Localization of Parkinson's disease-associated LRRK2 in normal and pathological human brain. *Brain Res* **1155**, 208-219

Hikita, N., Hattori, H., Kato, M., Sakuma, S., Morotomi, Y., Ishida, H., Seto, T., Tanaka, K., Shimono, T., Shintaku, H., and Tokuhara, D. (2014) A case of TUBA1A mutation presenting with lissencephaly and Hirschsprung disease. *Brain Dev* **36**, 159-162

Hill-Burns, E. M., Singh, N., Ganguly, P., Hamza, T. H., Montimurro, J., Kay, D. M., Yearout, D., Sheehan, P., Frodey, K., McLear, J. A., Feany, M. B., Hanes, S. D., Wolfgang, W. J., Zabetian, C. P., Factor, S. A., and Payami, H. (2013) A genetic basis for the variable effect of smoking/nicotine on Parkinson's disease. *Pharmacogenomics J* **13**, 530-537

Ho, C. C., Rideout, H. J., Ribe, E., Troy, C. M., and Dauer, W. T. (2009) The Parkinson disease protein leucine-rich repeat kinase 2 transduces death signals via Fas-associated protein with death domain and caspase-8 in a cellular model of neurodegeneration. *J Neurosci* **29**, 1011-1016

Hoffman, P. N. (1988) Distinct roles of neurofilament and tubulin gene expression in axonal growth. *Ciba Found Symp* **138**, 192-204

Hofmann, K. W., Schuh, A. F., Saute, J., Townsend, R., Fricke, D., Leke, R., Souza, D. O., Portela, L. V., Chaves, M. L., and Rieder, C. R. (2009) Interleukin-6 serum levels in patients with Parkinson's disease. *Neurochem Res* **34**, 1401-1404

Hornbeck, P. V., Kornhauser, J. M., Tkachev, S., Zhang, B., Skrzypek, E., Murray, B., Latham, V., Sullivan, M. (2012) PhosphoSitePlus: a comprehensive resource for investigating the structure and function of experimentally determined post-translational modifications in man and mouse *Nucleic Acids Res* **40**, D261-D270

Hu, G., Jousilahti, P., Bidel, S., Antikainen, R., and Tuomilehto, J. (2007) Type 2 diabetes and the risk of Parkinson's disease. *Diabetes Care* **30**, 842-847

Iaccarino, C., Crosio, C., Vitale, C., Sanna, G., Carrì, M. T., and Barone, P. (2007) Apoptotic mechanisms in mutant LRRK2-mediated cell death. *Hum Mol Genet* **16**, 1319-1326

Iida, K., and Yahara, I. (1999) Cooperation of two actin-binding proteins, cofilin and Aip1, in Saccharomyces cerevisiae. *Genes Cells* **4**, 21-32

Inclán, Y. F., and Nogales, E. (2001) Structural models for the self-assembly and microtubule interactions of gamma-, delta- and epsilon-tubulin. *J Cell Sci* **114**, 413-422

International Parkinson's Disease Genomics Consortium (IPDGC), Wellcome Trust Case Control Consortium 2 (WTCCC2) (2011) A Two-Stage Meta-Analysis Identifies Several New Loci for Parkinson's Disease. PLoS Genet 7(**6**): e1002142. doi:10.1371/journal.pgen.1002142, doi: 10.1038/mp.2014.107.

Irrcher, I., Aleyasin, H., Seifert, E. L., Hewitt, S. J., Chhabra, S., Phillips, M., Lutz, A. K., Rousseaux, M. W., Bevilacqua, L., Jahani-Asl, A., Callaghan, S., MacLaurin, J. G., Winklhofer, K. F., Rizzu, P., Rippstein, P., Kim, R. H., Chen, C. X., Fon, E. A., Slack, R. S., Harper, M. E., McBride, H. M., Mak, T. W., and Park, D. S. (2010) Loss of the Parkinson's disease-linked gene DJ-1 perturbs mitochondrial dynamics. *Hum Mol Genet* **19**, 3734-3746

Ishikawa, S., Taira, T., Niki, T., Takahashi-Niki, K., Maita, C., Maita, H., Ariga, H., and Iguchi-Ariga, S. M. (2009) Oxidative status of DJ-1-dependent activation of dopamine synthesis through interaction of tyrosine hydroxylase and 4-dihydroxy-L-phenylalanine (L-DOPA) decarboxylase with DJ-1. *J Biol Chem* **284**, 28832-28844

Ishikawa, S., Tanaka, Y., Takahashi-Niki, K., Niki, T., Ariga, H., and Iguchi-Ariga, S. M. (2012) Stimulation of vesicular

monoamine transporter 2 activity by DJ-1 in SH-SY5Y cells. *Biochem Biophys Res Commun* **421**, 813-818

Ito, G., Okai, T., Fujino, G., Takeda, K., Ichijo, H., Katada, T., and Iwatsubo, T. (2007) GTP binding is essential to the protein kinase activity of LRRK2, a causative gene product for familial Parkinson's disease. *Biochemistry* **46**, 1380-1388

Jaglin, X. H., Poirier, K., Saillour, Y., Buhler, E., Tian, G., Bahi-Buisson, N., Fallet-Bianco, C., Phan-Dinh-Tuy, F., Kong, X. P., Bomont, P., Castelnau-Ptakhine, L., Odent, S., Loget, P., Kossorotoff, M., Snoeck, I., Plessis, G., Parent, P., Beldjord, C., Cardoso, C., Represa, A., Flint, J., Keays, D. A., Cowan, N. J., and Chelly, J. (2009) Mutations in the beta-tubulin gene TUBB2B result in asymmetrical polymicrogyria. *Nat Genet* **41**, 746-752

Jaleel, M., Nichols, R. J., Deak, M., Campbell, D. G., Gillardon, F., Knebel, A., and Alessi, D. R. (2007) LRRK2 phosphorylates moesin at threonine-558: characterization of how Parkinson's disease mutants affect kinase activity. *Biochem J* **405**, 307-317

Janke, C., and Bulinski, J. C. (2011) Post-translational regulation of the microtubule cytoskeleton: mechanisms and functions. *Nat Rev Mol Cell Biol* **12**, 773-786

Janke, C., and Kneussel, M. (2010) Tubulin post-translational modifications: encoding functions on the neuronal microtubule cytoskeleton. *Trends Neurosci* **33**, 362-372

Janssen, J. C., Hall, M., Fox, N. C., Harvey, R. J., Beck, J., Dickinson, A., Campbell, T., Collinge, J., Lantos, P. L., Cipolotti, L., Stevens, J. M., and Rossor, M. N. (2000) Alzheimer's disease due to an intronic presenilin-1 (PSEN1 intron 4) mutation: A clinicopathological study. *Brain* **123 (Pt 5)**, 894-907

Jendrach, M., Gispert, S., Ricciardi, F., Klinkenberg, M., Schemm, R., and Auburger, G. (2009) The mitochondrial kinase PINK1, stress response and Parkinson's disease. *J Bioenerg Biomembr* **41**, 481-486

Jeppesen, D. K., Bohr, V. A., and Stevnsner, T. (2011) DNA repair deficiency in neurodegeneration. *Prog Neurobiol* **94**, 166-200

Jiang, Y. Q., and Oblinger, M. M. (1992) Differential regulation of beta III and other tubulin genes during peripheral and central neuron development. *J Cell Sci* **103 (Pt 3)**, 643-651

Jiménez-Jiménez, F. J., Mateo, D., and Giménez-Roldan, S. (1992) Premorbid smoking, alcohol consumption, and coffee drinking habits in Parkinson's disease: a case-control study. *Mov Disord* **7**, 339-344

Jorgensen, N. D., Peng, Y., Ho, C. C., Rideout, H. J., Petrey, D., Liu, P., and Dauer, W. T. (2009) The WD40 domain is required for LRRK2 neurotoxicity. *PLoS One* **4**, e8463, doi: 10.1371/journal.pone.0008463

Katsuki, M., Drummond, D. R., and Cross, R. A. (2014) Ectopic A-lattice seams destabilize microtubules. *Nat Commun* **5**, 3094

Kavanagh, M. E., Doddareddy, M. R., and Kassiou, M. (2013) The development of CNS-active LRRK2 inhibitors using property-directed optimisation. *Bioorg Med Chem Lett* **23**, 3690-3696

Kawakami, F., Yabata, T., Ohta, E., Maekawa, T., Shimada, N., Suzuki, M., Maruyama, H., Ichikawa, T., and Obata, F. (2012) LRRK2 phosphorylates tubulin-associated tau but not the free molecule: LRRK2-mediated regulation of the tau-tubulin association and neurite outgrowth. *PLoS One* **7**, e30834, doi: 10.1371/journal.pone.0030834

Keays, D. A., Tian, G., Poirier, K., Huang, G. J., Siebold, C., Cleak, J., Oliver, P. L., Fray, M., Harvey, R. J., Molnár, Z., Piñon, M. C., Dear, N., Valdar, W., Brown, S. D., Davies, K. E., Rawlins, J. N., Cowan, N. J., Nolan, P., Chelly, J., and Flint, J. (2007) Mutations in alpha-tubulin cause abnormal neuronal migration in mice and lissencephaly in humans. *Cell* **128**, 45-57

Kent, W. J. (2002) BLAT – the BLAST-like alignment tool. *Genome Res* **12(4)**, 656-664

Kett, L. R., Boassa, D., Ho, C. C., Rideout, H. J., Hu, J., Terada, M., Ellisman, M., and Dauer, W. T. (2012) LRRK2 Parkinson disease mutations enhance its microtubule association. *Hum Mol Genet* **21**, 890-899

Khateeb, S., Flusser, H., Ofir, R., Shelef, I., Narkis, G., Vardi, G., Shorer, Z., Levy, R., Galil, A., Elbedour, K., and Birk, O. S. (2006) PLA2G6 mutation underlies infantile neuroaxonal dystrophy. *Am J Hum Genet* **79**, 942-948

Kim, J. M., Lee, K. H., Jeon, Y. J., Oh, J. H., Jeong, S. Y., Song, I. S., Lee, D. S., and Kim, N. S. (2006) Identification of genes related to Parkinson's disease using expressed sequence tags. *DNA Res* **13**, 275-286

Kingston, D. G. (1994) Taxol: the chemistry and structure-activity relationships of a novel anticancer agent. *Trends Biotechnol* **12**, 222-227

Klein, C., and Westenberger, A. (2012) Genetics of Parkinson's disease. *Cold Spring Harb Perspect Med* **2**, a008888,doi: 10.1101/cshperspect.a008888

Kleiner-Fisman, G., Herzog, J., Fisman, D. N., Tamma, F., Lyons, K. E., Pahwa, R., Lang, A. E., and Deuschl, G. (2006) Subthalamic nucleus deep brain stimulation: summary and meta-analysis of outcomes. *Mov Disord* **21 Suppl 14**, S290-304

Kobe, B., and Kajava, A. V. (2001) The leucine-rich repeat as a protein recognition motif. *Curr Opin Struct Biol* **11**, 725-732

Kondapalli, C., Kazlauskaite, A., Zhang, N., Woodroof, H. I., Campbell, D. G., Gourlay, R., Burchell, L., Walden, H., Macartney, T. J., Deak, M., Knebel, A., Alessi, D. R., and Muqit, M. M. (2012) PINK1 is activated by mitochondrial membrane potential depolarization and stimulates Parkin E3 ligase activity by phosphorylating Serine 65. *Open Biol* **2**, 120080

Korczyn, A. D., and Gurevich, T. (2010) Parkinson's disease: before the motor symptoms and beyond. *J Neurol Sci* **289**, 2-6

Kosik, K. S., and Finch, E. A. (1987) MAP2 and tau segregate into dendritic and axonal domains after the elaboration of morphologically distinct neurites: an immunocytochemical study of cultured rat cerebrum. *J Neurosci* **7**, 3142-3153

Kumar, P., Henikoff, S., and Ng, P. C. (2009) Predicting the effects of coding non-synonymous variants on protein function using the SIFT algorithm. *Nat Protoc* **4**, 1073-1081

Kumar, R. A., Pilz, D. T., Babatz, T. D., Cushion, T. D., Harvey, K., Topf, M., Yates, L., Robb, S., Uyanik, G., Mancini, G. M., Rees, M. I., Harvey, R. J., and Dobyns, W. B. (2010) TUBA1A mutations cause wide spectrum lissencephaly (smooth brain) and suggest that multiple neuronal migration pathways converge on alpha tubulins. *Hum Mol Genet* **19**, 2817-2827

Kyratzi, E., Pavlaki, M., and Stefanis, L. (2008) The S18Y polymorphic variant of UCH-L1 confers an antioxidant function to neuronal cells. *Hum Mol Genet* **17**, 2160-2171

L'Hernault, S. W., and Rosenbaum, J. L. (1985) Chlamydomonas alpha-tubulin is posttranslationally modified by acetylation on the epsilon-amino group of a lysine. *Biochemistry* **24**, 473-478

Larcher, J. C., Boucher, D., Lazereg, S., Gros, F., and Denoulet, P. (1996) Interaction of kinesin motor domains with alpha- and beta-tubulin subunits at a tau-independent binding site. Regulation by polyglutamylation. *J Biol Chem* **271**, 22117-22124

Latourelle, J. C., Sun, M., Lew, M. F., Suchowersky, O., Klein, C., Golbe, L. I., Mark, M. H., Growdon, J. H., Wooten, G. F., Watts, R. L., Guttman, M., Racette, B. A., Perlmutter, J. S., Ahmed, A., Shill, H. A., Singer, C., Goldwurm, S., Pezzoli, G., Zini, M., Saint-Hilaire, M. H., Hendricks, A. E., Williamson, S., Nagle, M. W., Wilk, J. B., Massood, T., Huskey, K. W., Laramie, J. M., DeStefano, A. L., Baker, K. B., Itin, I., Litvan, I., Nicholson, G., Corbett, A., Nance, M., Drasby, E., Isaacson, S., Burn, D. J., Chinnery, P. F., Pramstaller, P. P., Al-hinti, J., Moller, A. T., Ostergaard, K., Sherman, S. J., Roxburgh, R., Snow, B., Slevin, J. T., Cambi, F., Gusella, J. F., and Myers, R. H. (2008) The Gly2019Ser mutation in LRRK2 is not fully penetrant in familial Parkinson's disease: the GenePD study. *BMC Med* **6**, 32

Lautier, C., Goldwurm, S., Dürr, A., Giovannone, B., Tsiaras, W. G., Pezzoli, G., Brice, A., and Smith, R. J. (2008) Mutations in the GIGYF2 (TNRC15) gene at the PARK11 locus in familial Parkinson disease. *Am J Hum Genet* **82**, 822-833

Law, B. M., Spain, V. A., Leinster, V. H., Chia, R., Beilina, A., Cho, H. J., Taymans, J. M., Urban, M. K., Sancho, R. M., Ramírez, M. B., Biskup, S., Baekelandt, V., Cai, H., Cookson, M. R., Berwick, D. C., and Harvey, K. (2014) A direct interaction between leucine-rich repeat kinase 2 and specific β-tubulin isoforms regulates tubulin acetylation. *J Biol Chem* **289**, 895-908

Lazzarini, A. M., Myers, R. H., Zimmerman, T. R., Mark, M. H., Golbe, L. I., Sage, J. I., Johnson, W. G., and Duvoisin, R. C. (1994) A clinical genetic study of Parkinson's disease: evidence for dominant transmission. *Neurology* **44**, 499-506

Leandro-García, L. J., Leskelä, S., Landa, I., Montero-Conde, C., López-Jiménez, E., Letón, R., Cascón, A., Robledo, M., and Rodríguez-Antona, C. (2010) Tumoral and tissue-specific expression of the major human beta-tubulin isotypes. *Cytoskeleton (Hoboken)* **67**, 214-223

Lee, V. M., Goedert, M., and Trojanowski, J. Q. (2001) Neurodegenerative tauopathies. *Annu Rev Neurosci* **24**, 1121-1159

Lee, W. H., Kim, J. Y., Kim, Y. S., Song, H. J., Song, K. J., Song, J. W., Baek, L. J., Seo, E. Y., Kim, C. D., Lee, J. H., and Kee, S. H. (2005) Upregulation of class II beta-tubulin expression in differentiating keratinocytes. *J Invest Dermatol* **124**, 291-297

Lefèvre, J., Chernov, K. G., Joshi, V., Delga, S., Toma, F., Pastré, D., Curmi, P. A., and Savarin, P. (2011) The C terminus of tubulin, a versatile partner for cationic molecules: binding of Tau, polyamines, and calcium. *J Biol Chem* **286**, 3065-3078

Lehtinen, M. K., Yuan, Z., Boag, P. R., Yang, Y., Villén, J., Becker, E. B., DiBacco, S., de la Iglesia, N., Gygi, S., Blackwell, T. K., and Bonni, A. (2006) A conserved MST-FOXO signaling pathway mediates oxidative-stress responses and extends life span. *Cell* **125**, 987-1001

Leroy, E., Anastasopoulos, D., Konitsiotis, S., Lavedan, C., and Polymeropoulos, M. H. (1998) Deletions in the Parkin gene and genetic heterogeneity in a Greek family with early onset Parkinson's disease. *Hum Genet* **103**, 424-427

Lesage, S., and Brice, A. (2009) Parkinson's disease: from monogenic forms to genetic susceptibility factors. *Hum Mol Genet* **18**, R48-59

Lesage, S., and Brice, A. (2012) Role of mendelian genes in "sporadic" Parkinson's disease. *Parkinsonism Relat Disord* **18 Suppl 1**, S66-70

Lesage, S., Le Ber, I., Condroyer, C., Broussolle, E., Gabelle, A., Thobois, S., Pasquier, F., Mondon, K., Dion, P. A., Rochefort, D., Rouleau, G. A., Dürr, A., Brice, A., and Group, F. P. s. D. G. S. (2013) C9orf72 repeat expansions are a rare genetic cause of parkinsonism. *Brain* **136**, 385-391

Lesage, S., Condroyer, C., Lohman, E., Troiano, A., Tison, F., Viallet, F., Damier, P., Tranchant, C., Vidhaillet, M., Ouvrard-Hernandez, A. M., Dürr, A., Brice, A., and (FPDGSG), F. P. s. D. G. S. G. (2010) Follow-up study of the GIGYF2 gene in French families with Parkinson's disease. *Neurobiol Aging* **31**, 1069-1071; discussion 1072-1064

Lewis, P. A. (2009) The function of ROCO proteins in health and disease. *Biol Cell* **101**, 183-191

Lewis, S. A., Lee, M. G., and Cowan, N. J. (1985) Five mouse tubulin isotypes and their regulated expression during development. *J Cell Biol* **101**, 852-861

Li, B., Krishnan, V. G., Mort, M. E., Xin, F., Kamati, K. K., Cooper, D. N., Mooney, S. D., and Radivojac, P. (2009) Automated inference of molecular mechanisms of disease from amino acid substitutions. *Bioinformatics* **25**, 2744-2750

Li, T., Yang, D., Sushchky, S., Liu, Z., and Smith, W. W. (2011) Models for LRRK2-Linked Parkinsonism. *Parkinsons Dis* **2011**, 942412

Li, X., Tan, Y. C., Poulose, S., Olanow, C. W., Huang, X. Y., and Yue, Z. (2007) Leucine-rich repeat kinase 2 (LRRK2)/PARK8 possesses GTPase activity that is altered in familial Parkinson's disease R1441C/G mutants. *J Neurochem* **103**, 238-247

Liao, J., Wu, C., Burulak, C., Zhang, S., Sahm, H., Wang, M., Zhang, Z., Vogel, K. W., Federici, M., Riddle, S. M., Nichols, J., Liu, D., Cookson, M. R., Stone, T. A., Hoang, Q. Q. (2014) Parkinson disease-associated mutation R1441H in LRRK2 prolongs the “active state” of its GTPase domain. *Proc Natl Acad Sci U S A* **111** (11) 4055-4060

Lill, C. M., Roehr, J. T., McQueen, M. B., Kavvoura, F. K., Bagade, S., Schjeide, B. M., Schjeide, L. M., Meissner, E., Zauft, U., Allen, N. C., Liu, T., Schilling, M., Anderson, K. J., Beecham, G., Berg, D., Biernacka, J. M., Brice, A., DeStefano, A. L., Do, C. B., Eriksson, N., Factor, S. A., Farrer, M. J., Foroud, T., Gasser, T., Hamza, T., Hardy, J. A., Heutink, P., Hill-Burns, E. M., Klein, C., Latourelle, J. C., Maraganore, D. M., Martin, E. R., Martinez, M., Myers, R. H., Nalls, M. A., Pankratz, N., Payami, H., Satake, W., Scott, W. K., Sharma, M., Singleton, A. B., Stefansson, K., Toda, T., Tung, J. Y., Vance, J., Wood, N. W., Zabetian, C. P., Young, P., Tanzi, R. E., Khoury, M. J., Zipp, F., Lehrach, H., Ioannidis, J. P., Bertram, L., Consortium, a. G. E. o. P. s. D., Consortium, I. P. s. D. G., Consortium, P. s. D. G., and 2), W. T. C. C. C. (2012) Comprehensive research synopsis and systematic meta-analyses in Parkinson's disease genetics: The PDGene database. *PLoS Genet* **8**, e1002548, doi: 10.1371/journal.pgen.1002548

Lin, C. H., Tsai, P. I., Wu, R. M., and Chien, C. T. (2010) LRRK2 G2019S mutation induces dendrite degeneration through mislocalization and phosphorylation of tau by recruiting autoactivated GSK3ß. *J Neurosci* **30**, 13138-13149

Lin, C. H., Wu, R. M., Tai, C. H., Chen, M. L., and Hu, F. C. (2011) Lrrk2 S1647T and BDNF V66M interact with environmental factors to increase risk of Parkinson's disease. *Parkinsonism Relat Disord* **17**, 84-88

Lin, W., and Kang, U. J. (2008) Characterization of PINK1 processing, stability, and subcellular localization. *J Neurochem* **106**, 464-474

Lin, X., Parisiadou, L., Gu, X. L., Wang, L., Shim, H., Sun, L., Xie, C., Long, C. X., Yang, W. J., Ding, J., Chen, Z. Z., Gallant, P. E., Tao-Cheng, J. H., Rudow, G., Troncoso, J. C., Liu, Z., Li, Z., and Cai, H. (2009) Leucine-rich repeat kinase 2 regulates the progression of neuropathology induced by Parkinson's-disease-related mutant alpha-synuclein. *Neuron* **64**, 807-827

Lindwall, G., and Cole, R. D. (1984) Phosphorylation affects the ability of tau protein to promote microtubule assembly. *J Biol Chem* **259**, 5301-5305

Liu, B., and Dluzen, D. E. (2007) Oestrogen and nigrostriatal dopaminergic neurodegeneration: animal models and clinical reports of Parkinson's disease. *Clin Exp Pharmacol Physiol* **34**, 555-565

Liu, L., Li, Y., Li, S., Hu, N., He, Y., Pong, R., Lin, D., Lu, L., and Law, M. (2012) Comparison of next-generation sequencing systems. *J Biomed Biotechnol* **2012**, 251364

Liu, Y., Fallon, L., Lashuel, H. A., Liu, Z., and Lansbury, P. T. (2002) The UCH-L1 gene encodes two opposing enzymatic activities that affect alpha-synuclein degradation and Parkinson's disease susceptibility. *Cell* **111**, 209-218

Lopata, M. A., and Cleveland, D. W. (1987) In vivo microtubules are copolymers of available beta-tubulin isotypes: localization of each of six vertebrate beta-tubulin isotypes using polyclonal antibodies elicited by synthetic peptide antigens. *J Cell Biol* **105**, 1707-1720

Loy-English, I., and Feldman, H., (2004) The Emerging Spectrum of Parkinsonian Dementias, *Canadian Review of Alzheimer's Disease and Other Dementias*, **09-04**, 9-12

Löwe, J., Li, H., Downing, K. H., and Nogales, E. (2001) Refined structure of alpha beta-tubulin at 3.5 A resolution. *J Mol Biol* **313**, 1045-1057

Luzón-Toro, B., Rubio de la Torre, E., Delgado, A., Pérez-Tur, J., and Hilfiker, S. (2007) Mechanistic insight into the dominant mode of the Parkinson's disease-associated G2019S LRRK2 mutation. *Hum Mol Genet* **16**, 2031-2039

Lyons, K. E., Hubble, J. P., Tröster, A. I., Pahwa, R., and Koller, W. C. (1998) Gender differences in Parkinson's disease. *Clin Neuropharmacol* **21**, 118-121

MacLeod, D., Dowman, J., Hammond, R., Leete, T., Inoue, K., and Abeliovich, A. (2006) The familial Parkinsonism gene LRRK2 regulates neurite process morphology. *Neuron* **52**, 587-593

Makrides, V., Massie, M. R., Feinstein, S. C., and Lew, J. (2004) Evidence for two distinct binding sites for tau on microtubules. *Proc Natl Acad Sci U S A* **101**, 6746-6751

Mata, I. F., Samii, A., Schneer, S. H., Roberts, J. W., Griffith, A., Leis, B. C., Schellenberg, G. D., Sidransky, E., Bird, T. D., Leverenz, J. B., Tsuang, D., and Zabetian, C. P. (2008) Glucocerebrosidase gene mutations: a risk factor for Lewy body disorders. *Arch Neurol* **65**, 379-382

Mata, I. F., Wedemeyer, W. J., Farrer, M. J., Taylor, J. P., and Gallo, K. A. (2006) LRRK2 in Parkinson's disease: protein domains and functional insights. *Trends Neurosci* **29**, 286-293

Mateos, M. V., Uranga, R. M., Salvador, G. A., and Giusto, N. M. (2008) Activation of phosphatidylcholine signalling during oxidative stress in synaptic endings. *Neurochem Int* **53**, 199-206

Matsuda, N., Sato, S., Shiba, K., Okatsu, K., Saisho, K., Gautier, C. A., Sou, Y. S., Saiki, S., Kawajiri, S., Sato, F., Kimura, M., Komatsu, M., Hattori, N., and Tanaka, K. (2010a) PINK1 stabilized by mitochondrial depolarization recruits Parkin to damaged mitochondria and activates latent Parkin for mitophagy. *J Cell Biol* **189**, 211-221

Matsuda, N., and Tanaka, K. (2010b) Uncovering the roles of PINK1 and parkin in mitophagy. *Autophagy* **6**, 952-954

Matsumine, H., Saito, M., Shimoda-Matsubayashi, S., Tanaka, H., Ishikawa, A., Nakagawa-Hattori, Y., Yokochi, M., Kobayashi, T., Igarashi, S., Takano, H., Sanpei, K., Koike, R., Mori, H., Kondo, T., Mizutani, Y., Schäffer, A. A., Yamamura, Y., Nakamura, S., Kuzuhara, S., Tsuji, S., and Mizuno, Y. (1997) Localization of a gene for an autosomal recessive form of juvenile Parkinsonism to chromosome 6q25.2-27. *Am J Hum Genet* **60**, 588-596

Matta, S., Van Kolen, K., da Cunha, R., van den Bogaart, G., Mandemakers, W., Miskiewicz, K., De Bock, P. J., Morais, V. A., Vilain, S., Haddad, D., Delbroek, L., Swerts, J., Chávez-Gutiérrez, L., Esposito, G., Daneels, G., Karran, E., Holt, M., Gevaert, K., Moechars, D. W., De Strooper, B., and Verstreken, P. (2012) LRRK2 controls an EndoA phosphorylation cycle in synaptic endocytosis. *Neuron* **75**, 1008-1021

Mazzulli, J. R., Xu, Y. H., Sun, Y., Knight, A. L., McLean, P. J., Caldwell, G. A., Sidransky, E., Grabowski, G. A., and Krainc, D. (2011) Gaucher disease glucocerebrosidase and α-synuclein form a bidirectional pathogenic loop in synucleinopathies. *Cell* **146**, 37-52

McMurray, C. T. (2000) Neurodegeneration: diseases of the cytoskeleton? *Cell Death Differ* **7**, 861-865

Mei, Y., Zhang, Y., Yamamoto, K., Xie, W., Mak, T. W., and You, H. (2009) FOXO3a-dependent regulation of Pink1 (Park6) mediates survival signaling in response to cytokine deprivation. *Proc Natl Acad Sci U S A* **106**, 5153-5158

Meixner, A., Boldt, K., Van Troys, M., Askenazi, M., Gloeckner, C. J., Bauer, M., Marto, J. A., Ampe, C., Kinkl, N., and Ueffing, M. (2011) A QUICK screen for Lrrk2 interaction partners--leucine-rich repeat kinase 2 is involved in actin cytoskeleton dynamics. *Mol Cell Proteomics* **10**, M110.001172, doi: 10.1074/mcp.M110.001172

Melrose, H. L., Dächsel, J. C., Behrouz, B., Lincoln, S. J., Yue, M., Hinkle, K. M., Kent, C. B., Korvatska, E., Taylor, J. P., Witten, L., Liang, Y. Q., Beevers, J. E., Boules, M., Dugger, B. N., Serna, V. A., Gaukhman, A., Yu, X., Castanedes-Casey, M., Braithwaite, A. T., Ogholikhan, S., Yu, N., Bass, D., Tyndall, G., Schellenberg, G. D., Dickson, D. W., Janus, C., and Farrer, M. J. (2010) Impaired dopaminergic neurotransmission and microtubule-associated protein tau alterations in human LRRK2 transgenic mice. *Neurobiol Dis* **40**, 503-517

Melrose, H., Lincoln, S., Tyndall, G., Dickson, D., and Farrer, M. (2006) Anatomical localization of leucine-rich repeat kinase 2 in mouse brain. *Neuroscience* **139**, 791-794

Menéndez-Sainz, C., González-Quevedo, A., González-García, S., Peña-Sánchez, M., and Giugliani, R. (2012) High proportion of mannosidosis and fucosidosis among lysosomal storage diseases in Cuba. *Genet Mol Res* **11**, 2352-2359

Mezzacappa, C., Komiya, Y., and Habas, R. (2012) Activation and function of small GTPases Rho, Rac, and Cdc42 during gastrulation. *Methods Mol Biol* **839**, 119-131

Miklossy, J., Arai, T., Guo, J. P., Klegeris, A., Yu, S., McGeer, E. G., and McGeer, P. L. (2006) LRRK2 expression in normal and pathologic human brain and in human cell lines. *J Neuropathol Exp Neurol* **65**, 953-963

Mills, R. D., Mulhern, T. D., Cheng, H. C., and Culvenor, J. G. (2012) Analysis of LRRK2 accessory repeat domains: prediction of

repeat length, number and sites of Parkinson's disease mutations. *Biochem Soc Trans* **40**, 1086-1089

Min, C., Cho, D. I., Kwon, K. J., Kim, K. S., Shin, C. Y., and Kim, K. M. (2011) Novel regulatory mechanism of canonical Wnt signaling by dopamine D2 receptor through direct interaction with beta-catenin. *Mol Pharmacol* **80**, 68-78

Moehle, M. S., Webber, P. J., Tse, T., Sukar, N., Standaert, D. G., DeSilva, T. M., Cowell, R. M., and West, A. B. (2012) LRRK2 inhibition attenuates microglial inflammatory responses. *J Neurosci* **32**, 1602-1611

Moisoi, N., Klupsch, K., Fedele, V., East, P., Sharma, S., Renton, A., Plun-Favreau, H., Edwards, R. E., Teismann, P., Esposti, M. D., Morrison, A. D., Wood, N. W., Downward, J., and Martins, L. M. (2009) Mitochondrial dysfunction triggered by loss of HtrA2 results in the activation of a brain-specific transcriptional stress response. *Cell Death Differ* **16**, 449-464

Morfini, G. A., Burns, M., Binder, L. I., Kanaan, N. M., LaPointe, N., Bosco, D. A., Brown, R. H., Brown, H., Tiwari, A., Hayward, L., Edgar, J., Nave, K. A., Garberrn, J., Atagi, Y., Song, Y., Pigino, G., and Brady, S. T. (2009) Axonal transport defects in neurodegenerative diseases. *J Neurosci* **29**, 12776-12786

Morgan, N. V., Westaway, S. K., Morton, J. E., Gregory, A., Gissen, P., Sonek, S., Cangul, H., Coryell, J., Canham, N., Nardocci, N., Zorzi, G., Pasha, S., Rodriguez, D., Desguerre, I., Mubaidin, A., Bertini, E., Trembath, R. C., Simonati, A., Schanen, C., Johnson, C. A., Levinson, B., Woods, C. G., Wilmot, B., Kramer, P., Gitschier, J., Maher, E. R., and Hayflick, S. J. (2006) PLA2G6, encoding a phospholipase A2, is mutated in neurodegenerative disorders with high brain iron. *Nat Genet* **38**, 752-754

Mosavi, L. K., Cammett, T. J., Desrosiers, D. C., and Peng, Z. Y. (2004) The ankyrin repeat as molecular architecture for protein recognition. *Protein Sci* **13**, 1435-1448

Mullett, S. J., and Hinkle, D. A. (2011) DJ-1 deficiency in astrocytes selectively enhances mitochondrial Complex I inhibitor-induced neurotoxicity. *J Neurochem* **117**, 375-387

Nefzger, M. D., Quadfasel, F. A., and Karl, V. C. (1968) A retrospective study of smoking in Parkinson's disease. *Am J Epidemiol* **88**, 149-158

Nichols, R. J., Dzamko, N., Hutti, J. E., Cantley, L. C., Deak, M., Moran, J., Bamborough, P., Reith, A. D., and Alessi, D. R. (2009a) Substrate specificity and inhibitors of LRRK2, a protein kinase mutated in Parkinson's disease. *Biochem J* **424**, 47-60

Nichols, R. J., Dzamko, N., Morrice, N. A., Campbell, D. G., Deak, M., Ordureau, A., Macartney, T., Tong, Y., Shen, J., Prescott, A. R., and Alessi, D. R. (2010) 14-3-3 binding to LRRK2 is disrupted by multiple Parkinson's disease-associated mutations and regulates cytoplasmic localization. *Biochem J* **430**, 393-404

Nichols, W. C., Pankratz, N., Marek, D. K., Pauciulo, M. W., Elsaesser, V. E., Halter, C. A., Rudolph, A., Wojcieszek, J., Pfeiffer, R. F., Foroud, T., and Investigators, P. S. G.-P. (2009b) Mutations in GBA are associated with familial Parkinson disease susceptibility and age at onset. *Neurology* **72**, 310-316

Nogales, E., Wolf, S. G., and Downing, K. H. (1998) Structure of the alpha beta tubulin dimer by electron crystallography. *Nature* **391**, 199-203

North, B. J., Marshall, B. L., Borra, M. T., Denu, J. M., and Verdin, E. (2003) The human Sir2 ortholog, SIRT2, is an NAD+-dependent tubulin deacetylase. *Mol Cell* **11**, 437-444

Noureddine, M. A., Li, Y. J., van der Walt, J. M., Walters, R., Jewett, R. M., Xu, H., Wang, T., Walter, J. W., Scott, B. L., Hulette, C., Schmechel, D., Stenger, J. E., Dietrich, F., Vance, J. M., and Hauser, M. A. (2005) Genomic convergence to identify candidate genes for Parkinson disease: SAGE analysis of the substantia nigra. *Mov Disord* **20**, 1299-1309

Oakley, B. R. (2000) An abundance of tubulins. *Trends Cell Biol* **10**, 537-542

Olmsted, J. B. (1986) Microtubule-associated proteins. *Annu Rev Cell Biol* **2**, 421-457

Ozelius, L. J., Senthil, G., Saunders-Pullman, R., Ohmann, E., Deligtisch, A., Tagliati, M., Hunt, A. L., Klein, C., Henick, B., Hailpern, S. M., Lipton, R. B., Soto-Valencia, J., Risch, N., and Bressman, S. B. (2006) LRRK2 G2019S as a cause of Parkinson's disease in Ashkenazi Jews. *N Engl J Med* **354**, 424-425

Paisan-Ruiz, C., Bhatia, K. P., Li, A., Hernandez, D., Davis, M., Wood, N. W., Hardy, J., Houlden, H., Singleton, A., and Schneider, S. A. (2009) Characterization of PLA2G6 as a locus for dystonia-parkinsonism. *Ann Neurol* **65**, 19-23

Palfi, S., Gurruchaga, J. M., Ralph, G. S., Lepetit, H., Lavisse, S., Buttery, P. C., Watts, C., Miskin, J., Kelleher, M., Deeley, S., Iwamuro, H., Lefaucheur, J. P., Thiriez, C., Fenelon, G., Lucas, C., Brugières, P., Gabriel, I., Abhay, K., Drouot, X., Tani, N., Kas, A., Ghaleb, B., Le Corvoisier, P., Dolphin, P., Breen, D. P., Mason, S., Guzman, N. V., Mazarakis, N. D., Radcliffe, P. A., Harrop, R., Kingsman, S. M., Rascol, O., Naylor, S., Barker, R. A., Hantraye, P., Remy, P., Cesaro, P., and Mitrophanous, K. A. (2014) Long-term safety and tolerability of ProSavin, a lentiviral vector-based gene therapy for Parkinson's disease: a dose escalation, open-label, phase 1/2 trial. *Lancet* **383**, 1138-1146

Pankratz, N., Nichols, W. C., Uniacke, S. K., Halter, C., Murrell, J., Rudolph, A., Shults, C. W., Conneally, P. M., Foroud, T., and

Group, P. S. (2003a) Genome-wide linkage analysis and evidence of gene-by-gene interactions in a sample of 362 multiplex Parkinson disease families. *Hum Mol Genet* **12**, 2599-2608

Pankratz, N., Nichols, W. C., Uniacke, S. K., Halter, C., Rudolph, A., Shults, C., Conneally, P. M., Foroud, T., and Group, P. S. (2003b) Significant linkage of Parkinson disease to chromosome 2q36-37. *Am J Hum Genet* **72**, 1053-1057

Parisiadou, L., and Cai, H. (2010) LRRK2 function on actin and microtubule dynamics in Parkinson disease. *Commun Integr Biol* **3**, 396-400

Parisiadou, L., Xie, C., Cho, H. J., Lin, X., Gu, X. L., Long, C. X., Lobbestael, E., Baekelandt, V., Taymans, J. M., Sun, L., and Cai, H. (2009) Phosphorylation of ezrin/radixin/moesin proteins by LRRK2 promotes the rearrangement of actin cytoskeleton in neuronal morphogenesis. *J Neurosci* **29**, 13971-13980

Parkinson J. (1817) An essay on the shaking palsy. London: Sherwood, Neely and Jones; Reprinted in: Neuropsychiatric classics. *J Neuropsychiatry Clin Neuro-sci* 2002;**14**:223–236

Parness, J., and Horwitz, S. B. (1981) Taxol binds to polymerized tubulin in vitro. *J Cell Biol* **91**, 479-487

Pastor, P., Pastor, E., Carnero, C., Vela, R., García, T., Amer, G., Tolosa, E., and Oliva, R. (2001) Familial atypical progressive supranuclear palsy associated with homozigosity for the delN296 mutation in the tau gene. *Ann Neurol* **49**, 263-267

Payami, H., Larsen, K., Bernard, S., and Nutt, J. (1994) Increased risk of Parkinson's disease in parents and siblings of patients. *Ann Neurol* **36**, 659-661

Pettersen, E. F., Goddard, T. D., Huang, C. C., Couch, G. S., Greenblatt, D. M., Meng, E. C., and Ferrin, T. E. (2004) UCSF Chimera--a visualization system for exploratory research and analysis. *J Comput Chem* **25**, 1605-1612

Pihlstrøm, L., and Toft, M. (2011) Genetic variability in SNCA and Parkinson's disease. *Neurogenetics* **12**, 283-293

Piperno, G., LeDizet, M., and Chang, X. J. (1987) Microtubules containing acetylated alpha-tubulin in mammalian cells in culture. *J Cell Biol* **104**, 289-302

Poirier, K., Lebrun, N., Broix, L., Tian, G., Saillour, Y., Boscheron, C., Parrini, E., Valence, S., Pierre, B. S., Oger, M., Lacombe, D., Geneviève, D., Fontana, E., Darra, F., Cances, C., Barth, M., Bonneau, D., Bernadina, B. D., N'guyen, S., Gitiaux, C., Parent, P., des Portes, V., Pedespan, J. M., Legrez, V., Castelnau-Ptakine, L., Nitschke, P., Hieu, T., Masson, C., Zelenika, D., Andrieux, A., Francis, F., Guerrini, R., Cowan, N. J., Bahi-Buisson, N., and Chelly, J. (2013) Mutations in TUBG1, DYNC1H1, KIF5C and KIF2A cause malformations of cortical development and microcephaly. *Nat Genet* **45**, 639-647

Poirier, K., Saillour, Y., Bahi-Buisson, N., Jaglin, X. H., Fallet-Bianco, C., Nabbout, R., Castelnau-Ptakhine, L., Roubertie, A., Attie-Bitach, T., Desguerre, I., Genevieve, D., Barnerias, C., Keren, B., Lebrun, N., Boddaert, N., Encha-Razavi, F., and Chelly, J. (2010) Mutations in the neuronal ß-tubulin subunit TUBB3 result in malformation of cortical development and neuronal migration defects. *Hum Mol Genet* **19**, 4462-4473

Polymeropoulos, M. H., Higgins, J. J., Golbe, L. I., Johnson, W. G., Ide, S. E., Di Iorio, G., Sanges, G., Stenroos, E. S., Pho, L. T., Schaffer, A. A., Lazzarini, A. M., Nussbaum, R. L., and Duvoisin, R. C. (1996) Mapping of a gene for Parkinson's disease to chromosome 4q21-q23. *Science* **274**, 1197-1199

Polymeropoulos, M. H., Lavedan, C., Leroy, E., Ide, S. E., Dehejia, A., Dutra, A., Pike, B., Root, H., Rubenstein, J., Boyer, R., Stenroos, E. S., Chandrasekharappa, S., Athanassiadou, A., Papapetropoulos, T., Johnson, W. G., Lazzarini, A. M., Duvoisin, R. C., Di Iorio, G., Golbe, L. I., and Nussbaum, R. L. (1997) Mutation in the alpha-synuclein gene identified in families with Parkinson's disease. *Science* **276**, 2045-2047

Popoff, V., Mardones, G. A., Tenza, D., Rojas, R., Lamaze, C., Bonifacino, J. S., Raposo, G., and Johannes, L. (2007) The retromer complex and clathrin define an early endosomal retrograde exit site. *J Cell Sci* **120**, 2022-2031

Priyadarshi, A., Khuder, S. A., Schaub, E. A., and Priyadarshi, S. S. (2001) Environmental risk factors and Parkinson's disease: a metaanalysis. *Environ Res* **86**, 122-127

Priyadarshi, A., Khuder, S. A., Schaub, E. A., and Shrivastava, S. (2000) A meta-analysis of Parkinson's disease and exposure to pesticides. *Neurotoxicology* **21**, 435-440

Puschmann, A., Ross, O. A., Vilariño-Güell, C., Lincoln, S. J., Kachergus, J. M., Cobb, S. A., Lindquist, S. G., Nielsen, J. E., Wszolek, Z. K., Farrer, M., Widner, H., van Westen, D., Hägerström, D., Markopoulou, K., Chase, B. A., Nilsson, K., Reimer, J., and Nilsson, C. (2009) A Swedish family with de novo alpha-synuclein A53T mutation: evidence for early cortical dysfunction. *Parkinsonism Relat Disord* **15**, 627-632

Raff, E. C., Fackenthal, J. D., Hutchens, J. A., Hoyle, H. D., and Turner, F. R. (1997) Microtubule architecture specified by a beta-tubulin isoform. *Science* **275**, 70-73

Ragonese, P., D'Amelio, M., and Savettieri, G. (2006) Implications for estrogens in Parkinson's disease: an epidemiological

approach. *Ann N Y Acad Sci* **1089**, 373-382

Ramamoorthy, K., Wang, F., Chen, I. C., Norris, J. D., McDonnell, D. P., Leonard, L. S., Gaido, K. W., Bocchinfuso, W. P., Korach, K. S., and Safe, S. (1997) Estrogenic activity of a dieldrin/toxaphene mixture in the mouse uterus, MCF-7 human breast cancer cells, and yeast-based estrogen receptor assays: no apparent synergism. *Endocrinology* **138**, 1520-1527

Ramirez, A., Heimbach, A., Gründemann, J., Stiller, B., Hampshire, D., Cid, L. P., Goebel, I., Mubaidin, A. F., Wriekat, A. L., Roeper, J., Al-Din, A., Hillmer, A. M., Karsak, M., Liss, B., Woods, C. G., Behrens, M. I., and Kubisch, C. (2006) Hereditary parkinsonism with dementia is caused by mutations in ATP13A2, encoding a lysosomal type 5 P-type ATPase. *Nat Genet* **38**, 1184-1191

Ramonet, D., Daher, J. P., Lin, B. M., Stafa, K., Kim, J., Banerjee, R., Westerlund, M., Pletnikova, O., Glauser, L., Yang, L., Liu, Y., Swing, D. A., Beal, M. F., Troncoso, J. C., McCaffery, J. M., Jenkins, N. A., Copeland, N. G., Galter, D., Thomas, B., Lee, M. K., Dawson, T. M., Dawson, V. L., and Moore, D. J. (2011) Dopaminergic neuronal loss, reduced neurite complexity and autophagic abnormalities in transgenic mice expressing G2019S mutant LRRK2. *PLoS One* **6**, e18568, doi: 10.1186/1750-1326-7-15

Ramonet, D., Podhajska, A., Stafa, K., Sonnay, S., Trancikova, A., Tsika, E., Pletnikova, O., Troncoso, J. C., Glauser, L., and Moore, D. J. (2012) PARK9-associated ATP13A2 localizes to intracellular acidic vesicles and regulates cation homeostasis and neuronal integrity. *Hum Mol Genet* **21**, 1725-1743

Ray, S., Bender, S., Kang, S., Lin, R., Glicksman, M. A., and Liu, M. (2014) The Parkinson Disease-linked LRRK2 Protein Mutation I2020T Stabilizes an Active State Conformation Leading to Increased Kinase Activity. *J Biol Chem* **289**, 13042-13053

Reeve, A., Simcox, E., and Turnbull, D. (2014) Ageing and Parkinson's disease: why is advancing age the biggest risk factor? *Ageing Res Rev* **14**, 19-30

Rehn, M., Pihlajaniemi, T., Hofmann, K., and Bucher, P. (1998) The frizzled motif: in how many different protein families does it occur? *Trends Biochem Sci* **23**, 415-417

Reichling, L. J., and Riddle, S. M. (2009) Leucine-rich repeat kinase 2 mutants I2020T and G2019S exhibit altered kinase inhibitor sensitivity. *Biochem Biophys Res Commun* **384**, 255-258

Reinhardt, P., Schmid, B., Burbulla, L. F., Schöndorf, D. C., Wagner, L., Glatza, M., Höing, S., Hargus, G., Heck, S. A., Dhingra, A., Wu, G., Müller, S., Brockmann, K., Kluba, T., Maisel, M., Krüger, R., Berg, D., Tsytsyura, Y., Thiel, C. S., Psathaki, O. E., Klingauf, J., Kuhlmann, T., Klewin, M., Müller, H., Gasser, T., Schöler, H. R., and Sterneckert, J. (2013) Genetic correction of a LRRK2 mutation in human iPSCs links parkinsonian neurodegeneration to ERK-dependent changes in gene expression. *Cell Stem Cell* **12**, 354-367

Ren, Y., Liu, W., Jiang, H., Jiang, Q., and Feng, J. (2005) Selective vulnerability of dopaminergic neurons to microtubule depolymerization. *J Biol Chem* **280**, 34105-34112

Renton, A. E., Majounie, E., Waite, A., Simón-Sánchez, J., Rollinson, S., Gibbs, J. R., Schymick, J. C., Laaksovirta, H., van Swieten, J. C., Myllykangas, L., Kalimo, H., Paetau, A., Abramzon, Y., Remes, A. M., Kaganovich, A., Scholz, S. W., Duckworth, J., Ding, J., Harmer, D. W., Hernandez, D. G., Johnson, J. O., Mok, K., Ryten, M., Trabzuni, D., Guerreiro, R. J., Orrell, R. W., Neal, J., Murray, A., Pearson, J., Jansen, I. E., Sondervan, D., Seelaar, H., Blake, D., Young, K., Halliwell, N., Callister, J. B., Toulson, G., Richardson, A., Gerhard, A., Snowden, J., Mann, D., Neary, D., Nalls, M. A., Peuralinna, T., Jansson, L., Isoviita, V. M., Kaivorinne, A. L., Hölttä-Vuori, M., Ikonen, E., Sulkava, R., Benatar, M., Wuu, J., Chiò, A., Restagno, G., Borghero, G., Sabatelli, M., Heckerman, D., Rogaeva, E., Zinman, L., Rothstein, J. D., Sendtner, M., Drepper, C., Eichler, E. E., Alkan, C., Abdullaev, Z., Pack, S. D., Dutra, A., Pak, E., Hardy, J., Singleton, A., Williams, N. M., Heutink, P., Pickering-Brown, S., Morris, H. R., Tienari, P. J., Traynor, B. J., and Consortium, I. (2011) A hexanucleotide repeat expansion in C9ORF72 is the cause of chromosome 9p21-linked ALS-FTD. *Neuron* **72**, 257-268

Reyniers, L., Del Giudice, M. G., Civiero, L., Belluzzi, E., Lobbestael, E., Beilina, A., Arrigoni, G., Derua, R., Waelkens, E., Li, Y., Crosio, C., Iaccarino, C., Cookson, M. R., Baekelandt, V., Greggio, E., and Taymans, J. M. (2014) Differential protein-protein interactions of LRRK1 and LRRK2 indicate roles in distinct cellular signaling pathways. *J Neurochem*, doi: 10.1111/jnc.12798.

Robinson, J. T., Thorvaldsdóttir, H., Winckler, W., Guttman, M., Lander, E. S., Getz, G., and Mesirov, J. P. (2011) Integrative genomics viewer. *Nat Biotechnol* **29**, 24-26

Rosenbaum, J. (2000) Cytoskeleton: functions for tubulin modifications at last. *Curr Biol* **10**, R801-803

Rosentreter, A., Hofmann, A., Xavier, C. P., Stumpf, M., Noegel, A. A., and Clemen, C. S. (2007) Coronin 3 involvement in F-actin-dependent processes at the cell cortex. *Exp Cell Res* **313**, 878-895

Ross, I., Clarissa, C., Giddings, T. H., and Winey, M. (2013) ε-tubulin is essential in Tetrahymena thermophila for the assembly and stability of basal bodies. *J Cell Sci* **126**, 3441-3451

Rudenko, I. N., Kaganovich, A., Hauser, D. N., Beylina, A., Chia, R., Ding, J., Maric, D., Jaffe, H., Cookson, M. R. (2012) The G2385R variant of leucine-rich repeat kinase 2 associated with Parkinson's disease is a partial loss-of-funciton mutation. *Biochem. J.* **446**, 99-111

Sadakata, T., and Furuichi, T. (2006) Identification and mRNA expression of Ogdh, QP-C, and two predicted genes in the postnatal mouse brain. *Neurosci Lett* **405**, 217-222

Sadakata, T., Kakegawa, W., Mizoguchi, A., Washida, M., Katoh-Semba, R., Shutoh, F., Okamoto, T., Nakashima, H., Kimura, K., Tanaka, M., Sekine, Y., Itohara, S., Yuzaki, M., Nagao, S., and Furuichi, T. (2007a) Impaired cerebellar development and function in mice lacking CAPS2, a protein involved in neurotrophin release. *J Neurosci* **27**, 2472-2482

Sakaguchi-Nakashima, A., Meir, J. Y., Jin, Y., Matsumoto, K., and Hisamoto, N. (2007) LRK-1, a C. elegans PARK8-related kinase, regulates axonal-dendritic polarity of SV proteins. *Curr Biol* **17**, 592-598

Salinas, R. E., Ogohara, C., Thomas, M. I., Shukla, K. P., Miller, S. I., and Ko, D. C. (2014) A cellular genome-wide association study reveals human variation in microtubule stability and a role in inflammatory cell death. *Mol Biol Cell* **25**, 76-86

Sánchez, C., Díaz-Nido, J., and Avila, J. (2000) Phosphorylation of microtubule-associated protein 2 (MAP2) and its relevance for the regulation of the neuronal cytoskeleton function. *Prog Neurobiol* **61**, 133-168

Sancho, R. M., Law, B. M., and Harvey, K. (2009) Mutations in the LRRK2 Roc-COR tandem domain link Parkinson's disease to Wnt signalling pathways. *Hum Mol Genet* **18**, 3955-3968

Sandyk, R. (1993) The relationship between diabetes mellitus and Parkinson's disease. *Int J Neurosci* **69**, 125-130

Sanger, F., Nicklen, S., and Coulson, A. R. (1977) DNA sequencing with chain-terminating inhibitors. *Proc Natl Acad Sci U S A* **74**, 5463-5467

Satake, W., Nakabayashi, Y., Mizuta, I., Hirota, Y., Ito, C., Kubo, M., Kawaguchi, T., Tsunoda, T., Watanabe, M., Takeda, A., Tomiyama, H., Nakashima, K., Hasegawa, K., Obata, F., Yoshikawa, T., Kawakami, H., Sakoda, S., Yamamoto, M., Hattori, N., Murata, M., Nakamura, Y., and Toda, T. (2009) Genome-wide association study identifies common variants at four loci as genetic risk factors for Parkinson's disease. *Nat Genet* **41**, 1303-1307

Saunders, C. T., and Baker, D. (2002) Evaluation of structural and evolutionary contributions to deleterious mutation prediction. *J Mol Biol* **322**, 891-901

Scalzo, P., Kümmer, A., Cardoso, F., and Teixeira, A. L. (2010) Serum levels of interleukin-6 are elevated in patients with Parkinson's disease and correlate with physical performance. *Neurosci Lett* **468**, 56-58

Schlögl, P. S., Nogueira, F. T., Drummond, R., Felix, J. M., De Rosa, V. E., Vicentini, R., Leite, A., Ulian, E. C., and Menossi, M. (2008) Identification of new ABA- and MEJA-activated sugarcane bZIP genes by data mining in the SUCEST database. *Plant Cell Rep* **27**, 335-345

Schmidt, K., Wolfe, D. M., Stiller, B., and Pearce, D. A. (2009) Cd2+, Mn2+, Ni2+ and Se2+ toxicity to Saccharomyces cerevisiae lacking YPK9p the orthologue of human ATP13A2. *Biochem Biophys Res Commun* **383**, 198-202

Schneider, G. F., and Dekker, C. (2012) DNA sequencing with nanopores. *Nat Biotechnol* **30**, 326-328

Schulte, C., and Gasser, T. (2011) Genetic basis of Parkinson's disease: inheritance, penetrance, and expression. *Appl Clin Genet* **4**, 67-80

Schultz, O., Oberhauser, F., Saech, J., Rubbert-Roth, A., Hahn, M., Krone, W., and Laudes, M. (2010) Effects of inhibition of interleukin-6 signalling on insulin sensitivity and lipoprotein (a) levels in human subjects with rheumatoid diseases. *PLoS One* **5**, e14328, DOI: 10.1371/journal.pone.0014328

Schulze, E., Asai, D. J., Bulinski, J. C., and Kirschner, M. (1987) Posttranslational modification and microtubule stability. *J Cell Biol* **105**, 2167-2177

Schwarz, J. M., Rödelsperger, C., Schuelke, M., and Seelow, D. (2010) MutationTaster evaluates disease-causing potential of sequence alterations. *Nat Methods* **7**, 575-576

Schwarz, J. M., Cooper, D. N., Schuelke, M., Seelow, D. (2014) MutationTaster2:mutation prediction for the deep-sequencing age. *Nat Methods* **11**, 361-362

Seelow, D., Schwarz, J. M., and Schuelke, M. (2008) GeneDistiller--distilling candidate genes from linkage intervals. *PLoS One* **3**, e3874, doi: 10.1371/journal.pone.0003874

Sen, S., Webber, P. J., and West, A. B. (2009) Dependence of leucine-rich repeat kinase 2 (LRRK2) kinase activity on dimerization. *J Biol Chem* **284**, 36346-36356

Sepulveda, B., Mesias, R., Li, X., Yue, Z., and Benson, D. L. (2013) Short- and long-term effects of LRRK2 on axon and dendrite growth. *PLoS One* **8**, e61986, doi: 10.1371/journal.pone.0061986

Serrano, L., de la Torre, J., Maccioni, R. B., and Avila, J. (1984) Involvement of the carboxyl-terminal domain of tubulin in the

regulation of its assembly. *Proc Natl Acad Sci U S A* **81**, 5989-5993

Shachar, T., Lo Bianco, C., Recchia, A., Wiessner, C., Raas-Rothschild, A., and Futerman, A. H. (2011) Lysosomal storage disorders and Parkinson's disease: Gaucher disease and beyond. *Mov Disord* **26**, 1593-1604

Shah, T., Zabaneh, D., Gaunt, T., Swerdlow, D. I., Shah, S., Talmud, P. J., Day, I. N., Whittaker, J., Holmes, M. V., Sofat, R., Humphries, S. E., Kivimaki, M., Kumari, M., Hingorani, A. D., and Casas, J. P. (2013) Gene-centric analysis identifies variants associated with interleukin-6 levels and shared pathways with other inflammation markers. *Circ Cardiovasc Genet* **6**, 163-170

Shen, L., and Ji, H. F. (2013) Low uric acid levels in patients with Parkinson's disease: evidence from meta-analysis. *BMJ Open* **3**, e003620, doi: 10.1136/bmjopen-2013-003620

Sherry, S. T., Ward, M. H., Kholodov, M., Baker, J., Phan, L., Smigielski, E. M., and Sirotkin, K. (2001) dbSNP: the NCBI database of genetic variation. *Nucleic Acids Res* **29**, 308-311

Sheu, J. J., Wang, K. H., Lin, H. C., and Huang, C. C. (2013) Psoriasis is associated with an increased risk of parkinsonism: a population-based 5-year follow-up study. *J Am Acad Dermatol* **68**, 992-999

Shojaee, S., Sina, F., Banihosseini, S. S., Kazemi, M. H., Kalhor, R., Shahidi, G. A., Fakhrai-Rad, H., Ronaghi, M., and Elahi, E. (2008) Genome-wide linkage analysis of a Parkinsonian-pyramidal syndrome pedigree by 500 K SNP arrays. *Am J Hum Genet* **82**, 1375-1384

Silva, B. A., Breydo, L., Fink, A. L., and Uversky, V. N. (2013) Agrochemicals, α-synuclein, and Parkinson's disease. *Mol Neurobiol* **47**, 598-612

Simón-Sánchez, J., Herranz-Pérez, V., Olucha-Bordonau, F., and Pérez-Tur, J. (2006) LRRK2 is expressed in areas affected by Parkinson's disease in the adult mouse brain. *Eur J Neurosci* **23**, 659-666

Simons, C., Wolf, N. I., McNeil, N., Caldovic, L., Devaney, J. M., Takanohashi, A., Crawford, J., Ru, K., Grimmond, S. M., Miller, D., Tonduti, D., Schmidt, J. L., Chudnow, R. S., van Coster, R., Lagae, L., Kisler, J., Sperner, J., van der Knaap, M. S., Schiffmann, R., Taft, R. J., and Vanderver, A. (2013) A de novo mutation in the β-tubulin gene TUBB4A results in the leukoencephalopathy hypomyelination with atrophy of the basal ganglia and cerebellum. *Am J Hum Genet* **92**, 767-773

Singleton, A. B., Farrer, M., Johnson, J., Singleton, A., Hague, S., Kachergus, J., Hulihan, M., Peuralinna, T., Dutra, A., Nussbaum, R., Lincoln, S., Crawley, A., Hanson, M., Maraganore, D., Adler, C., Cookson, M. R., Muenter, M., Baptista, M., Miller, D., Blancato, J., Hardy, J., and Gwinn-Hardy, K. (2003) alpha-Synuclein locus triplication causes Parkinson's disease. *Science* **302**, 841

Sirajuddin, M., Rice, L. M., and Vale, R. D. (2014) Regulation of microtubule motors by tubulin isotypes and post-translational modifications. *Nat Cell Biol* **16**, 335-344

Skiniotis, G., Cochran, J. C., Müller, J., Mandelkow, E., Gilbert, S. P., and Hoenger, A. (2004) Modulation of kinesin binding by the C-termini of tubulin. *EMBO J* **23**, 989-999

Smink, L. J., Helton, E. M., Healy, B. C., Cavnor, C. C., Lam, A. C., Flamez, D., Burren, O. S., Wang, Y., Dolman, G. E., Burdick, D. B., Everett, V. H., Glusman, G., Laneri, D., Rowen, L., Schuilenburg, H., Walker, N. M., Mychaleckyj, J., Wicker, L. S., Eizirik, D. L., Todd, J. A., and Goodman, N. (2005) T1DBase, a community web-based resource for type 1 diabetes research. *Nucleic Acids Res* **33**, D544-549

Smith, W. W., Pei, Z., Jiang, H., Dawson, V. L., Dawson, T. M., and Ross, C. A. (2006) Kinase activity of mutant LRRK2 mediates neuronal toxicity. *Nat Neurosci* **9**, 1231-1233

Smrzka, O. W., Delgehyr, N., and Bornens, M. (2000) Tissue-specific expression and subcellular localisation of mammalian delta-tubulin. *Curr Biol* **10**, 413-416

Spillantini, M. G., Schmidt, M. L., Lee, V. M., Trojanowski, J. Q., Jakes, R., and Goedert, M. (1997) Alpha-synuclein in Lewy bodies. *Nature* **388**, 839-840

Spina, M. B., and Cohen, G. (1989) Dopamine turnover and glutathione oxidation: implications for Parkinson disease. *Proc Natl Acad Sci U S A* **86**, 1398-1400

Stafa, K., Trancikova, A., Webber, P. J., Glauser, L., West, A. B., and Moore, D. J. (2012) GTPase activity and neuronal toxicity of Parkinson's disease-associated LRRK2 is regulated by ArfGAP1. *PLoS Genet* **8**, e1002526, doi: 10.1371/journal.pgen.1002526

Stenson, P. D., Ball, E. V., Mort, M., Phillips, A. D., Shiel, J. A., Thomas, N. S., Abeysinghe, S., Krawczak, M., and Cooper, D. N. (2003) Human Gene Mutation Database (HGMD): 2003 update. *Hum Mutat* **21**, 577-581

Strauss, K. M., Martins, L. M., Plun-Favreau, H., Marx, F. P., Kautzmann, S., Berg, D., Gasser, T., Wszolek, Z., Müller, T., Bornemann, A., Wolburg, H., Downward, J., Riess, O., Schulz, J. B., and Krüger, R. (2005) Loss of function mutations in the

gene encoding Omi/HtrA2 in Parkinson's disease. *Hum Mol Genet* **14**, 2099-2111

Su, B., Liu, H., Wang, X., Chen, S. G., Siedlak, S. L., Kondo, E., Choi, R., Takeda, A., Castellani, R. J., Perry, G., Smith, M. A., Zhu, X., and Lee, H. G. (2009) Ectopic localization of FOXO3a protein in Lewy bodies in Lewy body dementia and Parkinson's disease. *Mol Neurodegener* **4**, 32

Sullivan, K. F., Havercroft, J. C., Machlin, P. S., and Cleveland, D. W. (1986) Sequence and expression of the chicken beta 5- and beta 4-tubulin genes define a pair of divergent beta-tubulins with complementary patterns of expression. *Mol Cell Biol* **6**, 4409-4418

Szyk, A., Deaconescu, A. M., Spector, J., Goodman, B., Valenstein, M. L., Ziolkowska, N. E., Kormendi, V., Grigorieff, N., and Roll-Mecak, A. (2014) Molecular basis for age-dependent microtubule acetylation by tubulin acetyltransferase. *Cell* **157**, 1405-1415

Szklarczyk, D., Franceschini, A., Kuhn, M., Simonovic, M., Roth, A., Minguez, P., Doerks, T., Stark, M., Muller, J., Bork, P., Jensen, L. J., and von Mering, C. (2011) The STRING database in 2011: functional interaction networks of proteins, globally integrated and scored. *Nucleic Acids Res* **39**, D561-568

Tabuchi, M., Yanatori, I., Kawai, Y., and Kishi, F. (2010) Retromer-mediated direct sorting is required for proper endosomal recycling of the mammalian iron transporter DMT1. *J Cell Sci* **123**, 756-766

Tan, E. K. (2006) Identification of a common genetic risk variant (LRRK2 Gly2385Arg) in Parkinson's disease. *Ann Acad Med Singapore* **35**, 840-842

Tanner, C. M., Kamel, F., Ross, G. W., Hoppin, J. A., Goldman, S. M., Korell, M., Marras, C., Bhudhikanok, G. S., Kasten, M., Chade, A. R., Comyns, K., Richards, M. B., Meng, C., Priestley, B., Fernandez, H. H., Cambi, F., Umbach, D. M., Blair, A., Sandler, D. P., and Langston, J. W. (2011) Rotenone, paraquat, and Parkinson's disease. *Environ Health Perspect* **119**, 866-872

Taylor, J. P., Hulihan, M. M., Kachergus, J. M., Melrose, H. L., Lincoln, S. J., Hinkle, K. M., Stone, J. T., Ross, O. A., Hauser, R., Aasly, J., Gasser, T., Payami, H., Wszolek, Z. K., and Farrer, M. J. (2007) Leucine-rich repeat kinase 1: a paralog of LRRK2 and a candidate gene for Parkinson's disease. *Neurogenetics* **8**, 95-102

Taymans, J. M. (2012) The GTPase function of LRRK2. *Biochem Soc Trans* **40**, 1063-1069

Taymans, J. M., Cookson, M. R. (2010) Mechanisms in dominant Parkinsonism: The toxic triangle of LRRK2, alpha-synuclein, and tau. *BioEssays* **32** 227-235

Taymans, J. M., Van den Haute, C., and Baekelandt, V. (2006) Distribution of PINK1 and LRRK2 in rat and mouse brain. *J Neurochem* **98**, 951-961

Taymans, J. M., Vancraenenbroeck, R., Ollikainen, P., Beilina, A., Lobbestael, E., De Maeyer, M., Baekelandt, V., and Cookson, M. R. (2011) LRRK2 kinase activity is dependent on LRRK2 GTP binding capacity but independent of LRRK2 GTP binding. *PLoS One* **6**, e23207, doi: 10.1371/journal.pone.0023207

Thacker, E. L., Chen, H., Patel, A. V., McCullough, M. L., Calle, E. E., Thun, M. J., Schwarzschild, M. A., and Ascherio, A. (2008) Recreational physical activity and risk of Parkinson's disease. *Mov Disord* **23**, 69-74

The International HapMap3 Consortium. (2010) Integrating common and rare genetic variation in diverse human populations. *Nature* **467**, 52-58

The 1000 Genomes Project Consortium. (2012) An integrated map of genetic variation from 1,092 human genomes. *Nature* **491**, 56-65

Thusberg, J., Olatubosun, A., and Vihinen, M. (2011) Performance of mutation pathogenicity prediction methods on missense variants. *Hum Mutat* **32**, 358-368

Tiberio, G., Filocamo, M., Gatti, R., and Durand, P. (1995) Mutations in fucosidosis gene: a review. *Acta Genet Med Gemellol (Roma)* **44**, 223-232

Todd, A. M., and Staveley, B. E. (2008) Pink1 suppresses alpha-synuclein-induced phenotypes in a Drosophila model of Parkinson's disease. *Genome* **51**, 1040-1046

Todorova, A., Jenner, P., and Ray Chaudhuri, K. (2014) Non-motor Parkinson's: integral to motor Parkinson's, yet often neglected. *Pract Neurol*, doi: 10.1136/practneurol-2013-000741

Tolleson, C. M., and Fang, J. Y. (2013) Advances in the mechanisms of Parkinson's disease. *Discov Med* **15**, 61-66

Toomes, C., Bottomley, H. M., Scott, S., Mackey, D. A., Craig, J. E., Appukuttan, B., Stout, J. T., Flaxel, C. J., Zhang, K., Black, G. C., Fryer, A., Downey, L. M., and Inglehearn, C. F. (2004) Spectrum and frequency of FZD4 mutations in familial exudative vitreoretinopathy. *Invest Ophthalmol Vis Sci* **45**, 2083-2090

Tsika, E., and Moore, D. J. (2012) Mechanisms of LRRK2-mediated neurodegeneration. *Curr Neurol Neurosci Rep* **12**, 251-260

Tsujimoto, Y., and Shimizu, S. (2002) The voltage-dependent anion channel: an essential player in apoptosis. *Biochimie* **84**, 187-193

Untergrasser, A., Cutcutache, I., Koressaar, T., Ye, J., Faircloth, B. C., Remm, M., Rozen, S. G. (2007) Primer3-new capabilities and interfaces. *Nuc Acids Res* **40(15),** e115, doi: 10.1093/nar/gks596

Valente, E. M., Bentivoglio, A. R., Dixon, P. H., Ferraris, A., Ialongo, T., Frontali, M., Albanese, A., and Wood, N. W. (2001) Localization of a novel locus for autosomal recessive early-onset parkinsonism, PARK6, on human chromosome 1p35-p36. *Am J Hum Genet* **68**, 895-900

Van Criekinge, W., and Beyaert, R. (1999) Yeast Two-Hybrid: State of the Art. *Biol Proced Online* **2**, 1-38

Van Den Eeden, S. K., Tanner, C. M., Bernstein, A. L., Fross, R. D., Leimpeter, A., Bloch, D. A., and Nelson, L. M. (2003) Incidence of Parkinson's disease: variation by age, gender, and race/ethnicity. *Am J Epidemiol* **157**, 1015-1022

van Duijn, C. M., Dekker, M. C., Bonifati, V., Galjaard, R. J., Houwing-Duistermaat, J. J., Snijders, P. J., Testers, L., Breedveld, G. J., Horstink, M., Sandkuijl, L. A., van Swieten, J. C., Oostra, B. A., and Heutink, P. (2001) Park7, a novel locus for autosomal recessive early-onset parkinsonism, on chromosome 1p36. *Am J Hum Genet* **69**, 629-634

Vancraenenbroeck, R., Lobbestael, E., Weeks, S. D., Strelkov, S. V., Baekelandt, V., Taymans, J. M., and De Maeyer, M. (2012) Expression, purification and preliminary biochemical and structural characterization of the leucine rich repeat namesake domain of leucine rich repeat kinase 2. *Biochim Biophys Acta* **1824**, 450-460

Verdier-Pinard, P., Shahabi, S., Wang, F., Burd, B., Xiao, H., Goldberg, G. L., Orr, G. A., and Horwitz, S. B. (2005) Detection of human betaV-tubulin expression in epithelial cancer cell lines by tubulin proteomics. *Biochemistry* **44**, 15858-15870

Verhey, K. J., and Gaertig, J. (2007) The tubulin code. *Cell Cycle* **6**, 2152-2160

Vilariño-Güell, C., Wider, C., Ross, O. A., Dachsel, J. C., Kachergus, J. M., Lincoln, S. J., Soto-Ortolaza, A. I., Cobb, S. A., Wilhoite, G. J., Bacon, J. A., Behrouz, B., Melrose, H. L., Hentati, E., Puschmann, A., Evans, D. M., Conibear, E., Wasserman, W. W., Aasly, J. O., Burkhard, P. R., Djaldetti, R., Ghika, J., Hentati, F., Krygowska-Wajs, A., Lynch, T., Melamed, E., Rajput, A., Rajput, A. H., Solida, A., Wu, R. M., Uitti, R. J., Wszolek, Z. K., Vingerhoets, F., and Farrer, M. J. (2011) VPS35 mutations in Parkinson disease. *Am J Hum Genet* **89**, 162-167

Waak, J., Weber, S. S., Waldenmaier, A., Görner, K., Alunni-Fabbroni, M., Schell, H., Vogt-Weisenhorn, D., Pham, T. T., Reumers, V., Baekelandt, V., Wurst, W., and Kahle, P. J. (2009) Regulation of astrocyte inflammatory responses by the Parkinson's disease-associated gene DJ-1. *FASEB J* **23**, 2478-2489

Wang, D., Villasante, A., Lewis, S. A., and Cowan, N. J. (1986) The mammalian beta-tubulin repertoire: hematopoietic expression of a novel, heterologous beta-tubulin isotype. *J Cell Biol* **103**, 1903-1910

Webber, P. J., Smith, A. D., Sen, S., Renfrow, M. B., Mobley, J. A., and West, A. B. (2011) Autophosphorylation in the leucine-rich repeat kinase 2 (LRRK2) GTPase domain modifies kinase and GTP-binding activities. *J Mol Biol* **412**, 94-110

Webster, D. R., and Borisy, G. G. (1989) Microtubules are acetylated in domains that turn over slowly. *J Cell Sci* **92 (Pt 1)**, 57-65

Webster, D. R., Gundersen, G. G., Bulinski, J. C., and Borisy, G. G. (1987a) Assembly and turnover of detyrosinated tubulin in vivo. *J Cell Biol* **105**, 265-276

Webster, D. R., Gundersen, G. G., Bulinski, J. C., and Borisy, G. G. (1987b) Differential turnover of tyrosinated and detyrosinated microtubules. *Proc Natl Acad Sci U S A* **84**, 9040-9044

Webster, D. R., Wehland, J., Weber, K., and Borisy, G. G. (1990) Detyrosination of alpha tubulin does not stabilize microtubules in vivo. *J Cell Biol* **111**, 113-122

Wehland, J., Henkart, M., Klausner, R., and Sandoval, I. V. (1983) Role of microtubules in the distribution of the Golgi apparatus: effect of taxol and microinjected anti-alpha-tubulin antibodies. *Proc Natl Acad Sci U S A* **80**, 4286-4290

West, A. B., Moore, D. J., Biskup, S., Bugayenko, A., Smith, W. W., Ross, C. A., Dawson, V. L., and Dawson, T. M. (2005) Parkinson's disease-associated mutations in leucine-rich repeat kinase 2 augment kinase activity. *Proc Natl Acad Sci U S A* **102**, 16842-16847

West, A. B., Moore, D. J., Choi, C., Andrabi, S. A., Li, X., Dikeman, D., Biskup, S., Zhang, Z., Lim, K. L., Dawson, V. L., and Dawson, T. M. (2007) Parkinson's disease-associated mutations in LRRK2 link enhanced GTP-binding and kinase activities to neuronal toxicity. *Hum Mol Genet* **16**, 223-232

Westerlund, M., Belin, A. C., Anvret, A., Bickford, P., Olson, L., and Galter, D. (2008) Developmental regulation of leucine-rich

repeat kinase 1 and 2 expression in the brain and other rodent and human organs: Implications for Parkinson's disease. *Neuroscience* **152**, 429-436

Winner, B., Melrose, H. L., Zhao, C., Hinkle, K. M., Yue, M., Kent, C., Braithwaite, A. T., Ogholikhan, S., Aigner, R., Winkler, J., Farrer, M. J., and Gage, F. H. (2011) Adult neurogenesis and neurite outgrowth are impaired in LRRK2 G2019S mice. *Neurobiol Dis* **41**, 706-716

Wittinghofer, A., and Vetter, I. R. (2011) Structure-function relationships of the G domain, a canonical switch motif. *Annu Rev Biochem* **80**, 943-971

Wójciak-Stothard, B., Entwistle, A., Garg, R., and Ridley, A. J. (1998) Regulation of TNF-alpha-induced reorganization of the actin cytoskeleton and cell-cell junctions by Rho, Rac, and Cdc42 in human endothelial cells. *J Cell Physiol* **176**, 150-165

Wooten, G. F., Currie, L. J., Bovbjerg, V. E., Lee, J. K., and Patrie, J. (2004) Are men at greater risk for Parkinson's disease than women? *J Neurol Neurosurg Psychiatry* **75**, 637-639

Worthey, E. A., Mayer, A. N., Syverson, G. D., Helbling, D., Bonacci, B. B., Decker, B., Serpe, J. M., Dasu, T., Tschannen, M. R., Veith, R. L., Basehore, M. J., Broeckel, U., Tomita-Mitchell, A., Arca, M. J., Casper, J. T., Margolis, D. A., Bick, D. P., Hessner, M. J., Routes, J. M., Verbsky, J. W., Jacob, H. J., and Dimmock, D. P. (2011) Making a definitive diagnosis: successful clinical application of whole exome sequencing in a child with intractable inflammatory bowel disease. *Genet Med* **13**, 255-262

Xiong, Y., Coombes, C. E., Kilaru, A., Li, X., Gitler, A. D., Bowers, W. J., Dawson, V. L., Dawson, T. M., and Moore, D. J. (2010) GTPase activity plays a key role in the pathobiology of LRRK2. *PLoS Genet* **6**, e1000902

Xiong, Y., Yuan, C., Chen, R., Dawson, T. M., and Dawson, V. L. (2012) ArfGAP1 is a GTPase activating protein for LRRK2: reciprocal regulation of ArfGAP1 by LRRK2. *J Neurosci* **32**, 3877-3886

Xiong Y, Coombes CE, Kilaru A, Li X, Gitler AD, et al. (2010) GTPase Activity Plays a Key Role in the Pathobiology of LRRK2. PLoS Genet 6(4): e1000902. doi:10.1371/journal.pgen.1000902

Xu, Q., Park, Y., Huang, X., Hollenbeck, A., Blair, A., Schatzkin, A., and Chen, H. (2010) Physical activities and future risk of Parkinson disease. *Neurology* **75**, 341-348

Yang, J. O., Kim, W. Y., Jeong, S. Y., Oh, J. H., Jho, S., Bhak, J., and Kim, N. S. (2009) PDbase: a database of Parkinson's disease-related genes and genetic variation using substantia nigra ESTs. *BMC Genomics* **10 Suppl 3**, S32

Yun, H. J., Park, J., Ho, D. H., Kim, H., Kim, C. H., Oh, H., Ga, I., Seo, H., Chang, S., Son, I., and Seol, W. (2013) LRRK2 phosphorylates Snapin and inhibits interaction of Snapin with SNAP-25. *Exp Mol Med* **45**, e36, doi: 10.1038/emm.2013.68.

Yvon, A. M., Wadsworth, P., and Jordan, M. A. (1999) Taxol suppresses dynamics of individual microtubules in living human tumor cells. *Mol Biol Cell* **10**, 947-959

Zechel, S., Meinhardt, A., Unsicker, K., and von Bohlen Und Halbach, O. (2010) Expression of leucine-rich-repeat-kinase 2 (LRRK2) during embryonic development. *Int J Dev Neurosci* **28**, 391-399

Zhang, D., Grode, K. D., Stweman, S., Diaz, D., Liebling, E., Rath, U., Riera, T., Currie, J., Buster, D. W., Asenjo, A. B., Sosa, H. J., Ross, J., Ma, A., Rogers S. L., and Sharp, D. J. (2011) Drosophila Katanin is a microtubule depolymerase that regulates cortical-microtubule plus-end interactions and cell migration. *Nat Cell Biol* **13**, 361-370

Zhang, F. R., Huang, W., Chen, S. M., Sun, L. D., Liu, H., Li, Y., Cui, Y., Yan, X. X., Yang, H. T., Yang, R. D., Chu, T. S., Zhang, C., Zhang, L., Han, J. W., Yu, G. Q., Quan, C., Yu, Y. X., Zhang, Z., Shi, B. Q., Zhang, L. H., Cheng, H., Wang, C. Y., Lin, Y., Zheng, H. F., Fu, X. A., Zuo, X. B., Wang, Q., Long, H., Sun, Y. P., Cheng, Y. L., Tian, H. Q., Zhou, F. S., Liu, H. X., Lu, W. S., He, S. M., Du, W. L., Shen, M., Jin, Q. Y., Wang, Y., Low, H. Q., Erwin, T., Yang, N. H., Li, J. Y., Zhao, X., Jiao, Y. L., Mao, L. G., Yin, G., Jiang, Z. X., Wang, X. D., Yu, J. P., Hu, Z. H., Gong, C. H., Liu, Y. Q., Liu, R. Y., Wang, D. M., Wei, D., Liu, J. X., Cao, W. K., Cao, H. Z., Li, Y. P., Yan, W. G., Wei, S. Y., Wang, K. J., Hibberd, M. L., Yang, S., Zhang, X. J., and Liu, J. J. (2009) Genomewide association study of leprosy. *N Engl J Med* **361**, 2609-2618

Zhang, J., Perry, G., Smith, M. A., Robertson, D., Olson, S. J., Graham, D. G., and Montine, T. J. (1999) Parkinson's disease is associated with oxidative damage to cytoplasmic DNA and RNA in substantia nigra neurons. *Am J Pathol* **154**, 1423-1429

Zimprich, A., Benet-Pagès, A., Struhal, W., Graf, E., Eck, S. H., Offman, M. N., Haubenberger, D., Spielberger, S., Schulte, E. C., Lichtner, P., Rossle, S. C., Klopp, N., Wolf, E., Seppi, K., Pirker, W., Presslauer, S., Mollenhauer, B., Katzenschlager, R., Foki, T., Hotzy, C., Reinthaler, E., Harutyunyan, A., Kralovics, R., Peters, A., Zimprich, F., Brücke, T., Poewe, W., Auff, E., Trenkwalder, C., Rost, B., Ransmayr, G., Winkelmann, J., Meitinger, T., and Strom, T. M. (2011) A mutation in VPS35, encoding a subunit of the retromer complex, causes late-onset Parkinson disease. *Am J Hum Genet* **89**, 168-175

Zimprich, A., Biskup, S., Leitner, P., Lichtner, P., Farrer, M., Lincoln, S., Kachergus, J., Hulihan, M., Uitti, R. J., Calne, D. B., Stoessl, A. J., Pfeiffer, R. F., Patenge, N., Carbajal, I. C., Vieregge, P., Asmus, F., Müller-Myhsok, B., Dickson, D. W., Meitinger, T., Strom, T. M., Wszolek, Z. K., and Gasser, T. (2004) Mutations in LRRK2 cause autosomal-dominant parkinsonism with pleomorphic pathology. *Neuron* **44**, 601-607

Ziviani, E., Tao, R. N., and Whitworth, A. J. (2010) Drosophila parkin requires PINK1 for mitochondrial translocation and ubiquitinates mitofusin. *Proc Natl Acad Sci U S A* **107**, 5018-5023

Ziviani, E., and Whitworth, A. J. (2010) How could Parkin-mediated ubiquitination of mitofusin promote mitophagy? *Autophagy* **6**, 660-662

5.1 Web resources

Applied Biosystems SOLiD factsheet, accessed June 2014
https://www3.appliedbiosystems.com/cms/groups/mcb_marketing/documents/generaldocuments/cms_057511.pdf

CeGaT pedigree chart designer, accessed July 2014
http://www.cegat.de/Pedigree-chart-designer_155.html

European Brain Council 2011 Parkinson's disease fact sheet accessed January 2014
http://www.europeanbraincouncil.org/pdfs/Documents/Parkinson%27s%20fact%20sheet%20July%202011.pdf)

Exome Variant Server, accessed April 2014
NHLBI GO Exome Sequencing Project (ESP), Seattle, WA, http://evs.gs.washington.edu/EVS/).

HGNC database, accessed June 2014
HGNC Database, HUGO Gene Nomenclature Committee (HGNC), EMBL Outstation - Hinxton, European Bioinformatics Institute, Wellcome Trust Genome Campus, Hinxton, Cambridgeshire, CB10 1SD, UK www.genenames.org.
http://www.genenames.org/genefamilies/PARK
http://www.genenames.org/genefamilies/TUB

Online Mendelian Inheritance in Man, OMIM®. McKusick-Nathans Institute of Genetic Medicine, Johns Hopkins University (Baltimore, MD) (2012-2014). http://omim.org/

Parkinson's society 'Drug treatments for PD' booklet, released August 2012, accessed March 2014
http://www.parkinsons.org.uk/content/drug-treatments-parkinsons-booklet

Welcome Trust case control consortia 2 data, accessed April 2014
http://www.wtccc.org.uk/ccc2/wtccc2_studies.html

6. Appendices

6.1 Chain-termination sequencing primers

GENE	F/R	PRIMER
ACTG2	F	TCATGGAGATCAAAATGGGACAACCA
ACTG2	R	CAAAGTGGCCATGACTCCTGGTGTT
ARHGEF7	F	ATGTTTTGGTTGTGGCTCTTCC
ARHGEF7	R	GGTGAGAGATATATGAGCAACAGC
ASAH1	F	CAATTTTATCATTTGGAAAACAGA
ASAH1	R	CGGAAGACCCAGGACTAGAA
ATP13A5-1	F	AGTTGTGACGATTCCAAGTTCAC
ATP13A5-1	R	GGTCCTAAAGCCTGAAGCATAAA
ATP13A5-2	F	TCATGCAAGTGACCCAAATG
ATP13A5-2	R	TCCTGGCTCTCAGTGGAAATAC
ATP13A5-3	F	ATAATTGGCCTGGAAGAGAAAATA
ATP13A5-3	R	AGCGTACACAGGTAGTGTTTGTTG
ATP5E	F	CAATAAGGTACAACCAAACCAAAA
ATP5E	R	ACCATCCCAATAACTAACTTCCAA
ATXN10	F	GGGTAGATCCATAAGCATGAGC
ATXN10	R	ACCAAATGACAGAACCAGCA
C10ORF112-1	F	ACCTTCCGCTTCTATTACCACA
C10ORF112-1	R	CAGCGATCTTTCATATTCCTTAGAC
C10ORF112-2	R	AGGCTGGAACAAAGCTGTAACT
C10ORF112-2	F	TGTGAAAATCATGTGAAAGCAA
C10ORF112-3	F	AATGAGTACAAATGTCTTGATGCTG
C10ORF112-3	R	AAGATGAGTGGGTTTCTTGGTC
C6	F	TATTGTAATTCTGTGGTGGGAATG
C6	R	TCCTCACTGCTAAACTGATAGAGAAG
CADPS2	F	TTGGAAAGCTGTGTGTCCTG
CADPS2	R	AATAGCCTCGCTGGCATAAA
CLASP1	F	CAGCTTTCTGAGGTATTGAGCA
CLASP1	R	CCAAGAGCAAGTGGTCACAA
CLDN20	F	TTCTTTCGCTCAATCCTGGT
CLDN20	R	TGCAGACATGAAACAGACTCCT
CLIC5	F	TGGACACACTTCCTGGGTCACACC
CLIC5	R	TGGTATCCTAGGGCTCCTAAAATCACT CTGTG
DNAJC14	F	TCTCAAGTTCCCCAGTGATTTT
DNAJC14	R	GTCCACACTCCCATCCAAAC
DNMT3A-1	F	CGACTCCTTTCTCTCCACCTC
DNMT3A-1	R	TCAATCATGGGCTTGTTCTG
DNMT3A-2	R	GGGAGTTTGAAGAGAGTTATGACG
DNMT3A-2	F	TGGAGCTGACCTTGGCTATC
DNMT3A-3	F	TTCAGCAAAGTGAGGACCATTA
DNMT3A-3	R	GCTTGATAAAACCCACTGTTCC
EFCAB6-1	F	GAGGTGCTCTGGGAGTAGTGAC
EFCAB6-1	F	TTCAACATCTCAGCTTGTGCTAC
EFCAB6-2	R	GAAGTATTCATTTGACAGGATTTGC
EFCAB6-2	R	CAGAGAAAACAAGCTCCCAAAC
EFCAB6-3	F	ATGACTTCTGCTCCTTCTCCAG
EFCAB6-3	F	CAGACTCACCCGTCTTCTCAG
EFCAB6-4	R	CGCATCTTTGTGACGAGTTC
EFCAB6-4	R	AACCTTTGGGAAGGAGAACC
EPB41L3	F	CTCCTTGGTGAATGGCACTT
EPB41L3	R	TGAAATGTGAGCCCAAACAG
EPB41L5	F	TGAAATGGTGTCGTGTTTGC
EPB41L5	R	GATTTACTGTCTCCTTTTAACCTTCA
ESR2	F	GGGGAGGTAAGACCATGCTT
ESR2	R	CTCTGTGCCCATCTTTGCTT

GENE	F/R	PRIMER
ETFA	F	GGAAAAAGAGAACTGTAGGTTAAGGA
ETFA	R	CAGGACCAAAGTGAAGCAGA
ETNK2	F	GCTTTCCTCAATCCCACAGA
ETNK2	R	AGGGAACAGGGCATCAAGTA
FAM104B	F	CCAAGCCAAGTAGGAAAAATGT
FAM104B	R	GCTTCAATGCACAGGAGAAGTT
FUCA1	F	ACTGAGGGTTGGGACTTCCT
FUCA1	R	GCATCAAACACTGCCAATTC
GDNF	F	GGATTTTATTCAAGCCACCATT
GDNF	R	TTTGTCACTCACCAGCCTTCTA
GPR37	F	GGAATAAACGGCAGATTCAACT
GPR37	R	AGGGTTTGCAGAGACAGAAAAG
GRIN2B	F	GGGTTGGGCAAATAGAAATCTCTCAGC A
GRIN2B	R	CGATCAAATTTAACTTGGAAATCCATA AAGAGCA
GRN-1	F	GACGGAGTCAGGACCATTTTT
GRN-1	F	AGCCAGGATGGAGGAAACTT
GRN-2	R	CAGTGAGGGGACAGGAACAT
GRN-2	R	GGTCCAGGGAGAATTTGGTTA
HPCA	F	CAATGTGGATGAGTTCAAGAAGA
HPCA	R	CTACGAGGTCTGCTGAGAGGAT
IDH1	F	TGGAAACCTGTCTGGGACTT
IDH1	R	GAAAGAATGGAAATGGGTCTGA
IGSF10-1	F	GCTTAGTAGCACCACCAACAAACT
IGSF10-1	R	CTGGGAAGACAGGACAGACAT
IGSF10-2	F	CTATCACCAAGCCACCAATGA
IGSF10-2	R	GCTTTTTGTACTTGAGTCTTTGCTT
IGSF10-3	F	GACCAGCCCCAGGATAGAAG
IGSF10-3	R	AAGTTGACCCTTTGAGTTAAGCA
IL16	F	TTGAAACCTTTGGCTCCTCTC
IL16	R	ACTGGGCCTTGAGATTCCTC
IREB2	F	CCCTGGAGTAGTAGAATAAGACTGC
IREB2	R	GGTACTTAGAGATCACCATTTTCAC
IRF3	F	GGTCCTCTTCTCATCCCTGACTA
IRF3	R	GAGCAACCTCTTCCCTCTGTAAG
KIAA0196	F	TTCAAGGATGGCACTCCATGTCAGA
KIAA0196	R	CCCCAGTGAAAGGAGGCACTACAGG
LEPREL1	F	AGCAACCTGGAGGAACACAC
LEPREL1	R	TGATGTCTGTAATGATGAACCACA
LRP6	F	AACCAGAGAGCTGATTAGTGTTACTC
LRP6	R	AAAGAAACGTAGGGGGCAGT
LRRK2-1	F	CTCTGTTGAAAGGTTGTGCAAG
LRRK2-1	F	ATGAAAGGCAAATGACACACAG
LRRK2-2	R	TAGGCCACATGGTTGCTAGAG
LRRK2-2	R	GGTTTTCTTTACCTGCTTGGAA
MAOA	F	CCTCCTTGTCAGCATGAGTTTT
MAOA	R	CCAGTGAGCAGAGAGCATAAGA
MAOB	F	GGTTGGAGTCTGGGAATCTACA
MAOB	R	CATCAAAGGACATCACTCTGGA
MAP1A-1	F	CATGGGAGGACACATCTCCTGAGCA
MAP1A-1	R	TGCAGCCACCACACTGTCATACTCG
MAP1A-2	F	GCAGGACCCACTGTACCCCCAAG
MAP1A-2	R	TGCTGGGCTCAGAGGAGTGAGGTC
MAP1A-3	F	AAGCAACAGGGCCGACAGTGTGAT
MAP1A-3	R	TGTGCTCCCTCATCTTCCCAGTACAAA

GENE	F/R	PRIMER
MAP1B	F	GGAGGACAAAGCTGAAGATGCCAGAG
MAP1B	R	GCAGAGACTTTAATCTCATTGGGCGTCA
MAP2	F	TTCCAGAAATGGTCTGTAAAACTCAAGATGAACTAA
MAP2	R	GGGAATGGGATTGAGAATACAGATAATGTGG
MGST2	F	AATGTTCAAAGAAACCAAGTGATCT
MGST2	R	TATTGAGGTCCAGATATTCATCCA
MTHFD1	F	TCAGCTGGGTGTTTTAACAAATGCCAGTA
MTHFD1	R	CCCCCTAGGTGTTGCTTTTGCTGA
MYH1	F	GATGTTGGTGGTTTGTTGTCAC
MYH1	R	TGATGTTTGATTCCTGATCTCCTA
NDST1	F	AGACTGTGTCCTTTGGGGTTC
NDST1	R	CTCATAGGTGGAGTGATTTGACTG
NEFH	F	CATTTCAGACCTTCTCCAGTCTGAGGTCAC
NEFH	R	TGCCGCAATTTAAAAAGAATTTTGTCCCTA
NINJ2	F	ACGACCACCTCCCTTGATTT
NINJ2	R	GCTCTTGCAGATCCTCTCCTT
NPC1	F	GTGCTGGCTCCTTGTATCTGTA
NPC1	R	TAATCCTGGCACCAACTTACCT
PANK2	F	AGTTAGGGAGCCGACTGGAC
PANK2	R	AACAAGCGGGAAGTGCATAC
PDE1B	F	GAGGGGACTGATTGCTTCTCT
PDE1B	R	GTAAAGACCTGGCACACCAAC
PLXND1-1	F	CCTGGGCACTGACATAGTGAT
PLXND1-1	R	ACTGGGAGTAGGGCACATTCT
PLXND1-2	F	CTTATGTGGCAGGAGGGATG
PLXND1-2	R	CCTCAAACTCTGGGAAAATGC
QSER2-1	F	GAGTCTGCACCCCATCTTTTAC
QSER2-1	F	GACTGAGCAAGTTCCACTGAGA
QSER2-2	R	TGCCATCTATTGTTCATTCACAG
QSER2-2	R	TTGGAAAACCATCTTCTTGCTT
RDX	F	CCTGCACTCATTTCTGTGTGT
RDX	R	TCTGAAACTGCAAGGTGATAAGA
SELENBP1	F	TCTTCCAGAGGGGTCATTTG
SELENBP1	R	CCAGGTCTCCTTGTGACGAT
SEZ6L	F	TCCCCCAGATGTCGCTACTA
SEZ6L	R	TGTGAGCAATAGGAAATGAAATGT
GENE	**F/R**	**PRIMER**
SEZ6L-1	F	GTCCTCTTGGTCTGGTTTCATC
SEZ6L-1	F	TAATAAAAGCCCCTGTCGAAAA
SEZ6L-2	R	GATTCCTCAGCCAACTTCATTC
SEZ6L-2	R	TCTCGAACTCCTAGTCCAATTTTT
SH2B1	F	GTTCTCAGCTTTGCCCTTTTT
SH2B1	R	AGAGGTGGTCAGGAAGGTAGG
SLC6A3	F	GCTGAAGACCAAGAGGGAAGA
SLC6A3	R	CCACCATTTTTGTAGCACAGG
SNCAIP	F	GCTCATTTCTTCTTTCCAGTGC
SNCAIP	R	TGTTCATTTGCTCTTTGCTTGA
SNCG	F	ATATTTCATCGGCGTCAATAGG
SNCG	R	GAGTAAGGTCTGGCGAAGGTAA
SORL1	F	CGTTCATGGTCTCTGTGGATCATTGG
SORL1	R	TTCTGGCACAGGTTCCTTATCTCATCAAA
SQLE	F	TTATCTGAAGCCCACGTAACAG
SQLE	R	TTCCTTGGCATTTCTCCTCTAA
STK4	F	CGCTTTCATTTCTGGAAGGT
STK4	R	CCTCACCAAACCTCCTGTCC
STON2	F	ACCATTCCGTGAGTTCAAGC
STON2	R	TGATGTCCTGCCTCAAAACT
SYNE1	F	CCAGATGATGTGAGCAAACAAGTCAAAACA
SYNE1	R	CTTGCAGAGAAAGAGCCTCCTCAACG
TACR3	F	TTTCTTTCTGTGGCCTGCTT
TACR3	R	CTGCCTAAAAATTGCTTTCTGTTT
TEKT5	F	TCACTTCTTGCAACCGAATCTGTGGA
TEKT5	R	GGTGCCTGCCACCTTCATCTTCAG
TFR2	F	AGCATGTTGGGCTGGACGTGATG
TFR2	R	CCCGCAACCTACTCCCCTTCACC
TM7SF2	F	CCCAAGTGATGATGCTGAGA
TM7SF2	R	GTGGTCAAGGTCAAGGGTTG
TUBB3	F	GTGAAGGTGGCCGTGTGTGACATC
TUBB3	R	TCAGCCCCTCCACCTACTGGACAC
TUBB4	F	GCCAGCTGAACGCCGACCTG
TUBB4	R	GCCCGCACTTGCTGTAAGAGAGGAA
TUBG1	F	CTGCATCTGCTGGCCCTGCTTCTA
TUBG1	R	ACCCCACCAGCGTTCTCCAAAACT

Appendix 1. The primers used to confirm variants of interest and in the segregation analyses of the PD cohort, by chain-termination sequencing. F/R = forward/reverse

6.2 Genes included in the Cegat panel and PDBase

6.2.1 Cegat Neurodegeneration panel

ABCA7	CD47	DYNC1H1	KIAA0226	POLG2	STX6
ABCB1	CDC42	EFEMP1	KIFAP3	PON1	SUSD1
ABHD12	CHMP2B	EIF2AK3	LIF	PON2	SYN1
ACE	CHRNB2	EIF4G1	LOX	PON3	SYNE1
ACO1	CLDN1	EN1	LRRK2	PPHLN1	TAF1
ADAM10	CLDN10	EPHA1	MAOB	PRKRA	TARDBP
ADARB1	CLDN11	EPO	MAPT	PRNP	TBP
AKT1	CLDN12	EPOR	MECP2	PSEN1	TF
ALAD	CLDN14	EVL	MFN2	PSEN2	TFR2
ALS2	CLDN15	EXOC3L2	MOBKL2B	PVR	TFRC
ANG	CLDN16	GDNF	MOBP	RAB7L1	TGFB1
APEX1	CLDN17	GJC2	MS4A6A	RBMS1	TH
APOE	CLDN18	GLE1	MTHFD1	RET	THAP1
APP	CLDN19	GRIA2	MTHFR	RNF19A	TIMM8A
AR	CLDN2	GRIN2A	MTTP	RRM2B	TJP1
ARHGEF7	CLDN20	GRN	NAIP	SCN7A	TJP2
ARHGEF9	CLDN22	GSK3B	NCAM1	SELL	TJP3
ARSA	CLDN23	HEPH	NEFH	SEMA6A	TLR2
ATM	CLDN3	HEXA	NOTCH3	SETX	TLR4
ATN1	CLDN4	HEXB	NPC1	SGCE	TLR5
ATP13A2	CLDN5	HFE	NPC2	SLC11A2	TMEM106B
ATP1A3	CLDN6	HIPK4	NT5C1A	SLC16A2	TMEM126A
ATP7B	CLDN7	HMGCR	NUCKS1	SLC1A2	TNF
ATXN1	CLDN8	HMOX1	OCLN	SLC25A4	TOMM40
ATXN2	CLDN9	HPRT1	OGG1	SLC2A1	TOR1A
ATXN3	CLN3	HSPA1A	OPA1	SLC39A11	TP53
B4GALT6	CLU	HTRA2	OPA3	SLC6A3	TYR
BDNF	CNR1	HTT	OPTN	SMN1_dup1	UBAP1
BIN1	CNTF	ICAM5	OTC	SMN1_dup2	UBQLN1
BSCL2	CNTN4	IFNG	PANK2	SMN2_dup1	UNC13A
BST1	CP	IFNK	PARK2	SMN2_dup2	VAPB
C10orf2	CR1	IL10	PARK7	SMPD1	VCP
C19orf12	CSNK1G3	IL1A	PCDH11X	SNCA	VDR
C9orf72	CST3	IL1B	PDE8B	SNCB	VEGFA
CACNA1A	CXCL1	IL6	PDXK	SNCG	VPS13A
CCR2	CYP2D6	IL8	PGK1	SOD1	VPS13C
CCR3	DAO	IREB2	PICALM	SORL1	VPS35
CCR4	DAPK1	IRF4	PINK1	SPAST	VPS54
CCS	DCAF17	ITPR2	PITX3	SPG11	WFS1
CD200	DCTN1	JAK2	PLA2G6	SPG20	ZFP64
CD22	DISC1	JPH3	PLP1	SPG21	ZFYVE26
CD2AP	DNM1	KDR	PM20D1	SPG7	ZNF746
CD33	DPP6	KIAA0196	POLG	SRGAP3	

Appendix 2. Cegat Neurodegeneration panel, version 2.0, February 2013

6.2.2 PDBase genes with altered SN expression in PD patients

A2M	AHI1	APBB1	ATG12	BCAS1	C11orf79	C2orf25	CAMK2G	CD14	CHUK
AAK1	AHNAK	APC	ATL3	BCAS2	C12orf52	C3	CAMLG	CD177	CIAO1
AARSD1	AK2	APC2	ATP10B	BCDIN3D	C12orf60	C3orf1	CAMTA1	CD276	CIAPIN1
ABAT	AK3	APEX1	ATP13A2	BCKDHA	C14orf147	C3orf10	CANX	CD34	CIRBP
ABCB1	AKAP11	APLP1	ATP1A1	BCL2L1	C14orf166	C3orf17	CAP1	CD37	CISD2
ABCD3	AKAP8L	APOD	ATP1B1	BCL7B	C14orf2	C4A	CAP2	CD44	CIT
ABCD4	AKR1A1	APOE	ATP2A2	BCLAF1	C14orf94	C4orf10	CAPG	CD53	CKB
ABCF3	AKR1B1	APOL2	ATP2B2	BCOR	C15orf15	C4orf12	CAPN3	CD59	CKMT1B
ABCG2	AKR1C1	APOM	ATP2B4	BCR	C15orf17	C4orf18	CAPRIN1	CD68	CKMT2
ABHD12	ALDH2	APP	ATP5A1	BDH2	C15orf23	C4orf41	CAPRIN2	CD74	CLASP1
ABL1	ALDH9A1	APPBP2	ATP5B	BDNF	C15orf41	C5orf13	CAPZA2	CD79B	CLASP2
ABR	ALDOA	APTX	ATP5C1	BECN1	C16orf14	C5orf32	CARS2	CD86	CLCN4
ACAA1	ALDOC	AQP1	ATP5F1	BEX2	C16orf45	C6orf1	CASC4	CD9	CLDN11
ACACB	ALG1	AQP4	ATP5G3	BEX4	C16orf52	C6orf125	CASD1	CD99	CLDN5
ACAD11	ALG12	ARC	ATP5J	BGN	C16orf59	C6orf130	CASKIN1	CDC123	CLDND1
ACAT2	ALG9	ARCN1	ATP5S	BID	C16orf62	C6orf136	CASP4	CDC27	CLEC16A
ACD	ALKBH1	ARF1	ATP5SL	BIVM	C16orf80	C6orf203	CAT	CDC37L1	CLEC4M
ACE	ALKBH6	ARF3	ATP6AP2	BLMH	C17orf45	C6orf62	CBLB	CDC42	CLGN
ACLY	AMD1	ARFGAP1	ATP6V0A1	BLOC1S2	C17orf59	C6orf89	CBWD1	CDC5L	CLIC1
ACO2	AMN1	ARFIP1	ATP6V0D1	BLVRA	C17orf80	C7orf20	CBX3	CDCP2	CLIC4
ACOT7	AMT	ARG2	ATP6V1C1	BMPR2	C17orf85	C7orf23	CBX5	CDH20	CLIP3
ACOT8	AMY2A	ARGLU1	ATP6V1D	BNIP2	C17orf90	C7orf25	CBY1	CDH4	CLK1
ACOX3	AMZ2	ARHGAP26	ATP6V1E1	BNIP3	C18orf32	C7orf26	CC2D1A	CDH8	CLN3
ACP1	ANAPC13	ARHGAP9	ATP6V1G1	BNIP3L	C19orf2	C7orf41	CCDC104	CDK2AP2	CLN5
ACP2	ANAPC5	ARHGDIB	ATP8A1	BRD3	C19orf25	C7orf42	CCDC109B	CDK4	CLN8
ACSM5	ANAPC7	ARHGEF10	ATPAF2	BRD4	C19orf46	C8orf4	CCDC115	CDK5	CLNS1A
ACTA1	ANG	ARHGEF9	ATPIF1	BRD7	C19orf60	C8orf41	CCDC127	CDK6	CLPTM1
ACTA2	ANGPTL2	ARL1	ATR	BRD9	C19orf62	C9orf23	CCDC132	CDKAL1	CLPTM1L
ACTB	ANK1	ARL17	ATRX	BRE	C1D	C9orf25	CCDC24	CDKN1B	CLSTN1
ACTL6A	ANK2	ARL2	ATXN1	BRMS1	C1GALT1C1	C9orf3	CCDC28A	CDKN2AIPNL	CLTA
ACTN4	ANKFY1	ARL4A	ATXN10	BSCL2	C1QA	C9orf5	CCDC41	CDKN2D	CLTC
ACTR10	ANKH	ARL6IP1	ATXN2	BSG	C1orf124	C9orf61	CCDC44	CDO1	CLU
ACTR1A	ANKHD1	ARL6IP5	ATXN3	BSN	C1orf128	C9orf80	CCDC6	CDS2	CMAS
ACTR3B	ANKIB1	ARL8B	ATXN7L3	BST2	C1orf149	CA10	CCDC85B	CEACAM21	CMTM5
ACTR6	ANKRD10	ARMC9	AUH	BTBD16	C1orf156	CA14	CCDC88A	CEBPZ	CNBP
ACY1	ANKRD17	ARMCX6	AUP1	BTBD3	C1orf192	CABC1	CCK	CECR1	CNDP2
ADAR	ANKRD2	ARNT2	AUTS2	BTD	C1orf27	CABYR	CCKAR	CEND1	CNIH3
ADCY5	ANKRD22	ARPC1A	AVPI1	BTF3	C1orf57	CACNA1A	CCKBR	CENPF	CNN3
ADCYAP1R1	ANKRD35	ARPC1B	AZGP1	BTF3L4	C1orf85	CACNA1D	CCL2	CENPT	CNOT1
ADH1A	ANKS1B	ARPC2	AZIN1	BTG1	C1orf88	CACNA2D3	CCL4L1	CEP57	CNOT7
ADH1C	ANKS3	ARPC4	B2M	BTRC	C20orf103	CACNG4	CCL5	CEP68	CNP
ADH4	ANKS6	ARPC5	B3GALT6	BUB1B	C20orf27	CACYBP	CCM2	CES2	CNPY2
ADHFE1	ANKZF1	ARRB1	B3GAT3	BUB3	C20orf29	CADPS2	CCND2	CETN2	CNR1
ADI1	ANLN	ARRDC3	B3GNT1	BUD31	C20orf3	CALB1	CCNG1	CFC1B	CNTLN
ADNP	ANP32B	ASAH1	B3GNT2	BXDC5	C20orf43	CALB2	CCNH	CFDP1	CNTN1
ADO	ANXA2P2	ASB3	B9D2	C10orf58	C20orf94	CALCA	CCNI	CFL2	CNTN2
ADRA1A	ANXA5	ASCL1	BAALC	C10orf72	C20orf96	CALCB	CCNL1	CHD3	CNTN6
ADRA2A	ANXA7	ASF1A	BACE1	C10orf84	C21orf130	CALD1	CCNL2	CHD8	CNTNAP4
ADSS	AP1S2	ASGR1	BACE2	C11orf17	C21orf131	CALM1	CCPG1	CHD9	COL27A1
AGA	AP2B1	ASH2L	BAIAP2	C11orf49	C21orf56	CALM2	CCR2	CHI3L2	COMMD1
AGL	AP2M1	ASNA1	BAT1	C11orf57	C21orf59	CALML4	CCR5	CHID1	COMMD5
AGT	AP3B2	ASRGL1	BAZ2B	C11orf58	C21orf62	CALU	CCT3	CHL1	COMMD7
AHCTF1	AP3M2	ASTN2	BBOX1	C11orf59	C21orf91	CAMK1	CCT4	CHMP2A	COMMD9
AHCY	AP3S2	ATF4	BBS2	C11orf60	C22orf28	CAMK1D	CCT6A	CHN2	COMT
AHCYL1	AP4S1	ATF5	BCAP29	C11orf71	C22orf36	CAMK2B	CCT7	CHRNA4	COPE

COPG	CYB5B	DNAJC1	EIF3EIP	FAM107B	FLJ40606	GIT2	H2AFY	HPSE2	IL6
COPS2	CYB5D1	DNAJC10	EIF3F	FAM108A1	FLJ46906	GJA1	H3F3A	HSBP1	IL6ST
COPS4	CYB5R3	DNAJC12	EIF3G	FAM118B	FLT1	GJA4	H3F3B	HSD11B1L	IL8
COPS5	CYBRD1	DNAJC15	EIF3H	FAM123A	FLYWCH1	GJB6	HAAO	HSD17B11	ILF3
COPS6	CYCS	DNER	EIF3I	FAM124A	FMR1	GLA	HABP4	HSD17B14	IMP3
COPZ1	CYFIP1	DNTTIP1	EIF3J	FAM134A	FNTA	GLO1	HADHB	HSD17B2	IMP4
COQ6	CYFIP2	DOK5	EIF3K	FAM136A	FNTB	GLRB	HAGHL	HSD17B4	IMPAD1
CORO1A	CYP1A1	DPP6	EIF4A1	FAM13A1	FPGT	GLS	HAPLN2	HSD17B6	INA
CORO1B	CYP1B1	DPYSL2	EIF4A2	FAM13A1OS	FPR1	GLT8D1	HAX1	HSD17B7	ING1
CORT	CYP27A1	DPYSL3	EIF4A3	FAM35A	FRAXA	GMNN	HCCA2	HSDL2	ING3
COTL1	CYP2D6	DRD1	EIF4G1	FAM38B	FRAXE	GNAI2	HDHD1A	HSP90AA1	INPP1
COX6C	CYP2E1	DRD2	EIF4G2	FAM3A	FRG1B	GNAS	HDHD2	HSP90AB1	INPP5F
COX7A2L	CYP2R1	DRD3	EIF5A	FAM3C	FRZB	GNB2L1	HDLBP	HSP90B1	INTS10
COX7C	CYorf15B	DRD4	EIF5B	FAM40A	FSCN1	GNG10	HEBP2	HSPA1A	IPO8
CP	D4S234E	DRD5	EIF6	FAM44A	FSD1	GNG11	HEL308	HSPA1B	IPO9
CPLX3	DAP	DRG1	ELAVL3	FAM44B	FTH1	GNG2	HEPH	HSPA1L	IQCK
CPM	DAP3	DSN1	ELAVL4	FAM45A	FTL	GNG3	HEPN1	HSPA2	IRAK1BP1
CPSF2	DARS	DSP	ELFN2	FAM49B	FTSJ1	GNL1	HERC5	HSPA4	IREB2
CPSF3	DAZAP2	DST	ELL2	FAM53B	FUBP1	GNL3	HERPUD1	HSPA8	IRF2BP2
CPSF3L	DBH	DSTN	ELOVL1	FAM53C	FUNDC1	GNPTAB	HES6	HSPA9	ISCU
CRBN	DBN1	DTD1	ELP2	FAM58A	FUNDC2	GNPTG	HEXDC	HSPB1	ISOC1
CREB5	DBNDD2	DTNA	EMCN	FAM62A	FUT1	GOT1	HEY1	HSPB2	ISOC2
CREBL2	DBNL	DTNBP1	EMG1	FAM81B	FUT2	GPAM	HEYL	HSPC159	ITFG2
CRELD1	DBP	DUSP28	EMILIN2	FAM82B	FXR1	GPATCH8	HFE	HSPD1	ITGAV
CRELD2	DCHS1	DUT	ENAH	FAM84A	FYTTD1	GPBP1	HHIP	HTATIP2	ITGB2
CREM	DCLK1	DYNC1H1	ENDOD1	FAM91A1	GAB1	GPC2	HIBCH	HTR2A	ITM2A
CRH	DCN	DYNC1I2	ENO1	FAM92A1	GABARAP	GPM6A	HIF1A	HTR6	ITM2B
CRHR1	DCP2	DYNC1LI1	ENOPH1	FAM96A	GABARAPL1	GPM6B	HIGD1A	HTRA1	ITM2C
CRIP2	DCTN1	DYNC1LI2	ENPP2	FARP1	GABRA1	GPR146	HIRIP3	HTRA2	ITPKC
CRIPT	DCTN2	DYNC2H1	ENPP6	FARSB	GABRB1	GPR149	HIST1H2BD	HUWE1	IVNS1ABP
CRNKL1	DCUN1D5	DYNC2LI1	ENTPD1	FAT3	GADD45B	GPR177	HIST1H2BK	HVCN1	JAGN1
CROCCL1	DCXR	DYNLL1	EPAS1	FBL	GAL3ST1	GPRC5B	HIST3H2A	IARS	JAM2
CROT	DDA1	E2F6	EPB41L2	FBLN1	GALE	GPS2	HIVEP3	ICAM1	JARID1A
CRTAP	DDAH1	EBNA1BP2	EPB41L3	FBRS	GALNT10	GPSM2	HLA-A	ICAM2	JTB
CRY2	DDAH2	ECE1	EPB41L5	FBXL12	GALNT6	GPSN2	HLA-B	ICAM3	JUND
CRYAB	DDB1	ECH1	EPHX1	FBXO11	GALNTL2	GPX4	HLA-DMA	ICMT	KALRN
CRYL1	DDR2	ECHDC1	EPHX2	FBXO25	GAMT	GRB10	HLA-DMB	ID1	KCNA1
CRYZ	DDX18	ECSM2	EPN2	FBXO3	GANAB	GRB2	HLA-DPA1	ID3	KCNA5
CRYZL1	DDX39	EDEM2	ERAL1	FBXO32	GAP43	GRHPR	HLA-DPB1	ID4	KCNK1
CSDE1	DDX5	EDIL3	ERBB2IP	FBXO7	GAPDH	GRIA3	HLA-DQA1	IDE	KCNN2
CSE1L	DECR1	EDN3	ERGIC2	FBXW4	GATAD1	GRIK3	HLA-DQB1	IDH1	KCTD12
CSF1R	DENR	EDNRB	ERH	FBXW8	GATAD2A	GRIN2B	HLA-DRA	IDH2	KCTD3
CSNK1A1	DERL1	EEF1A1	ERMN	FCGR2A	GBA	GRK5	HLA-DRB1	IDH3A	KCTD6
CSNK2A1	DERL2	EEF1B2	ESAM	FCGR3A	GBA2	GSK3B	HLA-E	IDH3B	KCTD7
CSNK2B	DFFA	EEF1E1	ESD	FDFT1	GBAS	GSPT1	HMGA1	IDI1	KDELR1
CSPG5	DGCR2	EEF1G	ESR1	FDPS	GBE1	GSTA4	HMGB1	IDS	KDELR3
CST7	DGKB	EFEMP1	ESR2	FDX1L	GBP1	GSTM1	HMGB2	IER3	KHDRBS3
CSTF1	DGKQ	EFEMP2	ETFA	FEZ1	GBP2	GSTM3	HMGCL	IFI44	KIAA0101
CTBP2	DHPS	EFHA1	ETFB	FGF1	GC	GSTO1	HMGN1	IFI44L	KIAA0174
CTCF	DHRS12	EFNA1	ETNK1	FGF20	GCC2	GSTO2	HMGN2	IFI6	KIAA0196
CTSA	DHRS7	EFR3A	ETNK2	FGFR1OP2	GCH1	GSTP1	HMGN3	IFIT1	KIAA0232
CTSB	DIABLO	EGFLAM	ETV1	FHOD3	GDAP1L1	GSTT1	HMGN4	IFNAR1	KIAA0256
CTSD	DICER1	EGLN1	EVI1	FIBP	GDI1	GSTT2	HMOX1	IFNGR1	KIAA0317
CTSF	DIXDC1	EGLN3	EVI2A	FIG4	GEMIN8	GSTZ1	HMOX2	IFRD1	KIAA0391
CTSS	DKK3	EI24	EWSR1	FKBP3	GFAP	GTF2B	HMP19	IFT20	KIAA0427
CTTNBP2NL	DLD	EID1	EXOC4	FKBPL	GFOD2	GTF2F2	HN1	IFT88	KIAA0430
CTXN3	DLG2	EIF1	EXOC6B	FKSG24	GGH	GTF2I	HNRNPA1	IGBP1	KIAA0652
CUEDC2	DLG4	EIF1AP1	EXOSC2	FLJ11506	GGNBP2	GTF3A	HNRNPA2B1	IGFBP6	KIAA0776
CUL2	DLGAP4	EIF1AY	EXTL2	FLJ20021	GGPS1	GTF3C6	HNRNPC	IGSF8	KIAA0907
CUTC	DMAP1	EIF1B	EZH1	FLJ23834	GGTA1	GTPBP6	HNRPDL	IK	KIAA0913
CXorf21	DMD	EIF2AK1	FADD	FLJ25076	GHITM	GUCY1A3	HOMER1	IKBKG	KIAA1147
CXorf36	DNAJA1	EIF2S2	FADS2	FLJ32065	GIGYF2	GYG1	HOMER3	IL10RB	KIAA1219
CXorf40A	DNAJA3	EIF3B	FAHD1	FLJ35220	GIMAP4	GYPC	HOPX	IL17RC	KIAA1279
CXorf40B	DNAJA4	EIF3D	FAM102A	FLJ37464	GIMAP7	GZF1	HPCAL1	IL1B	KIAA1467
CYB561D2	DNAJB6	EIF3E	FAM107A	FLJ40142	GIPC1	GZMK	HPCAL4	IL2	KIAA1598

KIDINS220	LMO3	MAGI1	MFSD1	MRPS9	NDUFAF1	NSF	PARK12	PICALM	PPIA
KIF13B	LMO4	MAGOHB	MFSD2	MRRF	NDUFB11	NSFL1C	PARK2	PIGC	PPIF
KIF17	LOC116349	MAL	MFSD7	MSRB3	NDUFS1	NSL1	PARK3	PIGH	PPIG
KIF1A	LOC145757	MALAT1	MFSD8	MST150	NDUFS2	NSMCE1	PARK4	PIGL	PPIL1
KIF1B	LOC148189	MALT1	MGAT1	MT1X	NDUFS3	NSMCE4A	PARK7	PIGM	PPM1A
KIF25	LOC148413	MANBAL	MGC16703	MT3	NDUFV1	NSUN5	PARP1	PIGS	PPM1B
KIF2A	LOC202451	MAOA	MGC21881	MTA2	NDUFV2	NT5C	PBX3	PIGY	PPM1F
KIF3A	LOC203274	MAOB	MGC2752	MTA3	NEBL	NT5C3	PCBD1	PIH1D1	PPM2C
KIF3C	LOC220930	MAP1A	MGC5370	MTCH1	NECAP1	NTRK2	PCBP1	PIK3C2A	PPME1
KIF5C	LOC254559	MAP1B	MGEA5	MTCH2	NEFL	NTS	PCBP4	PIK3CB	PPOX
KIFAP3	LOC283070	MAP1LC3B	MGST3	MTDH	NEFM	NTSR2	PCDH17	PIK3IP1	PPP1CB
KIFC3	LOC283089	MAP2	MICA	MTERFD2	NEIL1	NUBP2	PCDH9	PIK3R3	PPP1R13B
KIRREL3	LOC283547	MAP2K3	MICAL3	MTERFD3	NELF	NUCKS1	PCGF5	PINK1	PPP1R15A
KLC1	LOC283951	MAP2K5	MID1IP1	MTG1	NELL2	NUDT1	PCMT1	PIP4K2A	PPP1R7
KLF6	LOC285281	MAP2K6	MIS12	MTHFR	NFASC	NUDT16	PCMTD1	PIP4K2B	PPP1R8
KLF7	LOC286189	MAP3K7	MKX	MTMR1	NFIB	NUDT4	PCNA	PIR	PPP2CA
KLHDC3	LOC344595	MAP4	MLF2	MTMR12	NFKB1	NUDT4P1	PCNP	PIWIL4	PPP2R1A
KLHDC4	LOC388524	MAP4K4	MLL3	MTMR2	NFKBIA	NUDT5	PCNX	PKM2	PPP2R3C
KLHDC5	LOC389203	MAPK1	MLLT11	MTMR9	NGDN	NUDT7	PCOLCE	PKP4	PPP2R4
KLHDC8A	LOC389833	MAPK14	MMAB	MTP18	NHEDC2	NUDT9	PCSK1N	PLA2G5	PPP2R5C
KLHL12	LOC389901	MAPK3	MMP1	MTRF1L	NIF3L1	NUP85	PDCD10	PLCB1	PPP3CB
KLHL24	LOC399959	MAPK8IP1	MMP3	MTSS1	NINJ2	NUPL1	PDCD6	PLCB4	PPP3CC
KLHL4	LOC440104	MAPK9	MMS19	MTUS1	NIP30	NUPL2	PDE10A	PLCG2	PPP6C
KLHL7	LOC440248	MAPRE1	MNDA	MTX1	NIPA1	NUTF2	PDE4DIP	PLCL2	PPT1
KLKB1	LOC493754	MAPRE2	MNT	MTX2	NIPA2	OAS1	PDGFA	PLD5	PPWD1
KLRG1	LOC541471	MAPRE3	MOBKL1B	MUT	NIPSNAP3A	OAZ2	PDHA1	PLEKHB1	PRAF2
KPNA2	LOC642350	MAPT	MOBKL3	MVK	NIT1	OBFC2A	PDHB	PLEKHB2	PRCC
KPNA3	LOC643327	MARCH5	MOBP	MXD4	NKAIN4	OCIAD1	PDHX	PLEKHG5	PRDM4
KRCC1	LOC645212	MARCKSL1	MOCS1	MXRA7	NKAP	OCRL	PDIA3	PLEKHH1	PRDX1
KRIT1	LOC646719	MARK1	MOCS2	MYBPC1	NKPD1	OFD1	PDIA6	PLEKHJ1	PRDX3
KRT18	LOC652968	MARS	MOG	MYCBP2	NLN	OLFM1	PDK2	PLLP	PRDX5
KRT222P	LOC678655	MAT2A	MON2	MYCN	NLRP1	OLIG2	PDLIM3	PLOD3	PRDX6
KRT86	LOC727993	MATN1	MORF4L1	MYLK	NLRP2	OMA1	PDRG1	PLP1	PREB
KTN1	LOC729082	MATR3	MORF4L2	MYO10	NME5	OMG	PDXK	PLSCR1	PREP
LAIR1	LOC729678	MAX	MOV10	MYO6	NOL3	OPRL1	PEA15	PLXNA2	PREPL
LAMA2	LOC730092	MBD4	MPDU1	MYOM2	NOL5A	ORC3L	PEBP1	PMF1	PREX1
LAMP2	LOC91431	MBNL1	MPI	NACA	NOLC1	ORC4L	PECI	PMM1	PRKACA
LANCL1	LOC92270	MBNL2	MPP1	NAE1	NOMO3	ORMDL3	PEG10	PMP2	PRKAG1
LAP3	LOC92973	MBOAT7	MPPE1	NAGK	NOS1	OSBPL1A	PEG3	PNN	PRKAG2
LAPTM4A	LOH12CR1	MBP	MRAS	NANS	NOS2A	OSBPL5	PELO	PNPLA4	PRKAR1A
LAPTM4B	LONP2	MBTPS1	MRCL3	NAP1L1	NOS3	OSBPL6	PELP1	PNPLA8	PRKAR1B
LAPTM5	LONRF1	MCFD2	MRFAP1	NAP1L3	NOSIP	OSGEP	PENK	PNPT1	PRKAR2A
LARP6	LOXL3	MCM3AP	MRFAP1L1	NAP1L5	NOSTRIN	OTUB1	PEPD	PNRC1	PRKCZ
LARP7	LPGAT1	MCM4	MRLC2	NAPA	NOTCH1	OTUD4	PER1	PNRC2	PRKRA
LAT2	LRDD	MCOLN1	MRPL1	NARS	NOTCH2	OXA1L	PEX11B	POGK	PRLHR
LBH	LRP2	MDH1	MRPL10	NASP	NOTCH4	OXNAD1	PEX14	POLB	PRNP
LCMT1	LRP3	MDH2	MRPL15	NAT2	NP	P2RY5	PEX19	POLD2	PROSC
LDB3	LRP4	MDK	MRPL16	NAV3	NPAL3	P4HB	PFDN1	POLG	PRPF3
LDHA	LRRC23	MDN1	MRPL28	NBEA	NPC1	PA2G4	PFKL	POLL	PRPF38A
LDHB	LRRC40	ME2	MRPL3	NBPF12	NPC1	PAAF1	PFKM	POLR1D	PRPF40A
LEPROTL1	LRRC49	MEA1	MRPL32	NCAPG	NPDC1	PACRG	PFN2	POLR1E	PRPS1
LGALS8	LRRK1	MED10	MRPL37	NCKAP1	NPM1	PADI2	PFTK1	POLR2E	PSD3
LGALS9	LRRK2	MED13L	MRPL38	NCKIPSD	NPTXR	PAFAH1B1	PGK1	POLR2F	PSIP1
LHFP	LSM1	MED6	MRPL40	NCOA4	NQO1	PAFAH1B2	PGP	POLR2J2	PSMA1
LIAS	LSM6	MED8	MRPL44	NDFIP1	NQO2	PAICS	PGPEP1	POLR3H	PSMA2
LILRB4	LTC4S	MEF2A	MRPS12	NDN	NR1H2	PAIP2B	PGRMC1	POMC	PSMA3
LIMK2	LYL1	MEMO1	MRPS14	NDP	NR2C1	PALLD	PHACTR3	POMP	PSMA4
LIMS2	LYRM4	MEMO1	MRPS15	NDRG1	NR2C2	PAM	PHB	PON1	PSMA5
LIPA	LZIC	METAP2	MRPS18A	NDRG2	NR2F1	PAN2	PHB2	PON2	PSMB4
LITAF	M6PRBP1	METTL3	MRPS18B	NDRG4	NR2F2	PANK2	PHF3	PON3	PSMB5
LMBR1	MADD	METTL8	MRPS21	NDST1	NR3C1	PANK4	PHF5A	POP4	PSMB8
LMBR1L	MAEA	METTL9	MRPS22	NDUFA4	NR4A2	PAQR4	PHGDH	PPA1	PSMC1
LMBRD1	MAG	MFAP1	MRPS23	NDUFA6	NRBP2	PAQR6	PHLDB1	PPAP2B	PSMC2
LMF1	MAGED1	MFHAS1	MRPS34	NDUFA7	NRD1	PAQR8	PHOX2B	PPARA	PSMC3
LMNA	MAGED2	MFN1	MRPS7	NDUFA9	NRIP3	PARK10	PHYHIPL	PPFIA1	PSMC5

PSMD10	RASL12	RPAIN	SCAMP3	SFRS2	SLMO1	SQLE	SYNGR3	THOC5	TOM1
PSMD11	RBBP6	RPESP	SCARB2	SFRS3	SMAD2	SREBF2	SYNJ1	THTPA	TOMM20
PSMD12	RBM12	RPH3A	SCCPDH	SFRS7	SMAP2	SRGAP3	SYNJ2	THY1	TOMM22
PSMD14	RBM22	RPL10	SCD5	SGCD	SMARCA2	SRP14	SYNJ2BP	TIAM2	TOMM40L
PSMD8	RBM3	RPL12	SCFD2	SGK1	SMARCA4	SRP54	SYPL1	TICAM2	TOMM7
PSME1	RBM39	RPL13	SCG2	SGK2	SMARCAL1	SRP72	SYT1	TIGD5	TOP2B
PSME2	RBM4B	RPL13A	SCG3	SGK269	SMARCB1	SRP9	SYT17	TIMM17A	TOR1A
PSME3	RBM9	RPL15	SCG5	SGPP2	SMARCD3	SRRM2	SYT5	TIMM23B	TP53
PSMF1	RBMX	RPL18A	SCGN	SH2B3	SMARCE1	SS18L1	SYTL4	TIMM8B	TP53I11
PTGES3	RBX1	RPL19	SCHIP1	SH3BGR	SMC1A	SSBP2	TACC1	TIMP2	TP53TG3
PTGS2	RCAN2	RPL23	SCLY	SH3BGRL	SMCR7L	SSBP3	TADA2L	TIMP3	TPD52
PTK2	RCBTB2	RPL28	SCN1A	SH3GL2	SMEK1	SSFA2	TAF11	TINP1	TPD52L1
PTMA	RDH11	RPL3	SCN1B	SH3GL3	SMG1	SSNA1	TAF1C	TJP1	TPI1
PTN	RDX	RPL31	SCN3B	SHARPIN	SMOX	SSR1	TAF3	TLK1	TPM1
PTP4A1	RERGL	RPL35A	SCN4B	SHC4	SMPX	SSR2	TALDO1	TM2D3	TPMT
PTP4A2	REV1	RPL36A	SCPEP1	SHH	SNAP25	SSR4	TAPBPL	TM4SF1	TPP1
PTPLAD1	RFC5	RPL37A	SDAD1	SHMT2	SNAPC2	SSU72	TARSL2	TM4SF18	TPR
PTPN11	RFPL1	RPL4	SDCCAG10	SIAH1	SNAPC5	ST13	TATDN1	TM7SF2	TPT1
PTPRD	RFX5	RPL5	SDF4	SIP1	SNCA	ST3GAL3	TAX1BP3	TM9SF3	TRAF1
PTPRE	RGMA	RPL6	SDHA	SIPA1L1	SNCAIP	ST3GAL5	TBC1D17	TMBIM4	TRAF3IP2
PTPRN2	RGS1	RPL7	SDHC	SIRT2	SNCB	ST3GAL6	TBC1D23	TMCO1	TRAK1
PTTG1IP	RGS3	RPL7A	SEC11C	SIRT5	SNCG	ST5	TBC1D5	TMED10	TRAP1
PXK	RGS5	RPL7L1	SEC13	SKP1	SND1	ST6GALNAC1	TBC1D7	TMED2	TRAPPC4
PXMP3	RGS7	RPL8	SEC14L2	SKP2	SNF1LK2	ST6GALNAC6	TBCA	TMED3	TRIAP1
PXN	RHBDL2	RPL9	SEC22C	SLAIN1	SNN	ST7	TBCB	TMED7	TRIM13
PYCR1	RHEB	RPLP1	SEC31A	SLBP	SNORD22	ST8SIA5	TBCE	TMEM101	TRIM2
PYCRL	RHOA	RPS15A	SEC61A1	SLC13A3	SNPH	STARD3	TBKBP1	TMEM103	TRIM26
PYGL	RHOC	RPS16	SELENBP1	SLC16A1	SNRPA	STARD3NL	TBL1X	TMEM11	TRIM28
ProSAPiP1	RHOF	RPS20	SELM	SLC18A2	SNRPB	STARD4	TBL1XR1	TMEM110	TRIM69
QARS	RHOG	RPS23	SELPLG	SLC1A2	SNRPE	STAT1	TBL2	TMEM111	TRIP10
QDPR	RHOU	RPS25	SELT	SLC22A3	SNRPN	STAU1	TBL3	TMEM119	TRIP12
QKI	RIC8A	RPS27A	SEMA4B	SLC25A1	SNX2	STH	TBP	TMEM123	TRIP6
QRICH1	RIC8B	RPS3	SEMA4D	SLC25A10	SNX3	STIM2	TBRG1	TMEM126B	TRMT1
RAB11A	RILP	RPS3A	SEMA5A	SLC25A11	SNX30	STIP1	TCEA1	TMEM127	TRPC4AP
RAB11B	RIOK3	RPS4X	SENP1	SLC25A14	SNX4	STK19	TCEAL2	TMEM139	TRPC5
RAB13	RIT1	RPS6KA2	SENP6	SLC25A17	SNX6	STK25	TCEAL3	TMEM144	TRUB2
RAB14	RIT2	RPS8	SEP15	SLC25A26	SNX9	STK4	TCEAL4	TMEM14C	TSC22D1
RAB18	RMND5A	RPSA	SEPP1	SLC25A3	SOD1	STMN1	TCEAL7	TMEM151B	TSC22D3
RAB1A	RNASE1	RPUSD3	SEPT11	SLC25A36	SOD2	STMN2	TCEAL8	TMEM159	TSEN34
RAB24	RNASEH2B	RRAGA	SEPT2	SLC25A37	SORT1	STMN3	TCEB2	TMEM165	TSFM
RAB27B	RNASEH2C	RRM1	SEPT4	SLC25A39	SOS1	STMN4	TCF25	TMEM168	TSG101
RAB28	RNASET2	RRS1	SEPT7	SLC25A4	SOX2	STOM	TCF4	TMEM177	TSPAN3
RAB2A	RND2	RSAD1	SEPT8	SLC25A5	SOX2OT	STOML1	TCHP	TMEM183A	TSPAN5
RAB34	RNF10	RSPH1	SEPT9	SLC25A6	SP1	STOML2	TCP1	TMEM184B	TSPAN8
RAB4B	RNF103	RSU1	SEPW1	SLC2A3	SP4	STON2	TDG	TMEM186	TSSC1
RAB5C	RNF11	RTN3	SEPX1	SLC2A5	SPAG9	STRAP	TDGF1	TMEM199	TST
RAB6A	RNF113A	RTN4	SERGEF	SLC2A6	SPARC	STT3B	TEAD4	TMEM204	TSTA3
RAB7A	RNF13	RTP4	SERINC1	SLC30A9	SPARCL1	STX12	TERF1	TMEM33	TTC32
RAB9A	RNF145	RUFY2	SERP1	SLC31A2	SPATA7	STX6	TERF2IP	TMEM35	TTLL3
RABEP1	RNF167	RUFY3	SERP2	SLC35E2	SPATS2	STX7	TESK2	TMEM49	TTR
RABGGTB	RNF175	RUNDC3A	SERPINA1	SLC36A4	SPCS2	SUCLA2	TEX10	TMEM55B	TTRAP
RAC1	RNF180	RUVBL2	SERPINA3	SLC38A2	SPECC1	SUCLG1	TF	TMEM56	TTYH1
RAD21	RNF20	RWDD2A	SERPINB1	SLC39A3	SPG20	SUGT1	TFAM	TMEM59	TUB
RAD23A	RNF26	RWDD2B	SERPINB6	SLC39A9	SPG21	SULT1A1	TFAP2D	TMEM79	TUBA1A
RAD23B	RNF38	RWDD3	SERPINF1	SLC3A2	SPIN1	SULT1A2	TFDP2	TMEM85	TUBA1B
RAD51L3	RNF40	RXRG	SESN1	SLC44A1	SPOCK1	SUMO1	TFG	TMEM9	TUBA1C
RAF1	RNF5	S100A10	SET	SLC46A1	SPOCK3	SUMO3	TFRC	TMOD3	TUBB
RALGPS1	RNMTL1	S100A13	SETMAR	SLC6A13	SPOP	SURF4	TGFB2	TMSB4X	TUBB2A
RALY	ROCK1	SACM1L	SETX	SLC6A3	SPP1	SUSD3	TGFBR1	TNF	TUBB2B
RAN	ROGDI	SALL2	SEZ6L2	SLC6A4	SPR	SUZ12	TGOLN2	TNFAIP8L2	TUBB2C
RANBP2	ROM1	SAMM50	SF3B1	SLC6A8	SPRED1	SV2A	TH	TNFRSF1A	TUBB3
RANBP3	RORA	SAV1	SFPQ	SLC9A3R2	SPRY2	SVIP	THBS2	TNIP1	TUBB4
RAP2A	RP11-35N6.1	SC5DL	SFRS1	SLC9A6	SPSB2	SYF2	THNSL1	TNXB	TUBD1
RAPGEF5	RP5-1077B9.4	SCAMP1	SFRS10	SLCO1A2	SPSB3	SYN1	THNSL2	TOE1	TUBG2
RASGRP3	RPA2	SCAMP2	SFRS18	SLCO2B1	SPTB	SYNCRIP	THOC2	TOLLIP	TUG1

TUSC4	UBE2E3	UFC1	USP40	VPS26A	WDR78	XRCC5	ZBED5	ZFR	ZNF302
TWF1	UBE2F	UFD1L	USP47	VPS28	WDR85	XRCC6	ZBTB33	ZFYVE9	ZNF32
TXNDC13	UBE2G1	UGP2	USP48	VPS29	WFS1	YAF2	ZBTB43	ZHX1	ZNF334
TXNDC14	UBE2J2	UGT8	USP7	VPS35	WHSC1	YIF1A	ZBTB5	ZKSCAN1	ZNF33A
TXNDC9	UBE2L6	UHRF1BP1	USPL1	VPS53	WHSC1L1	YIPF1	ZBTB8OS	ZMAT1	ZNF37B
TXNIP	UBE2M	UMPS	UTP11L	VPS72	WIPI2	YIPF3	ZC3H11A	ZMAT2	ZNF397
TXNL1	UBE2N	UNK	UTP3	VRK3	WNK1	YIPF4	ZC3H15	ZMAT4	ZNF511
TXNRD2	UBE2Q2	UPF3B	VAMP1	VWF	WNT6	YIPF6	ZCCHC12	ZMAT5	ZNF536
TYK2	UBE2R2	UQCC	VAMP3	WAC	WRB	YLPM1	ZCCHC17	ZMIZ1	ZNF569
TYMP	UBE2V1	UQCRC1	VAMP4	WARS2	WSB1	YME1L1	ZDHHC9	ZMPSTE24	ZNF605
TYROBP	UBE2V2	UQCRC2	VAPA	WASF3	WSCD1	YOD1	ZEB2	ZMYM1	ZNF623
U2AF2	UBE2W	URM1	VAV3	WBP1	WTAP	YPEL1	ZFAND1	ZMYND11	ZNF664
UAP1L1	UBE2Z	UROD	VCAN	WBP2	WWC1	YPEL3	ZFAND3	ZMYND8	ZNF673
UBA2	UBE4A	USH1C	VCL	WBSCR22	WWOX	YPEL5	ZFAND5	ZNF134	ZNF692
UBASH3B	UBL3	USP1	VCP	WDR1	XBP1	YTHDF2	ZFAND6	ZNF140	ZNF771
UBB	UBOX5	USP14	VDAC1	WDR33	XPNPEP1	YTHDF3	ZFHX2	ZNF226	ZNF83
UBC	UBQLN1	USP24	VDAC2	WDR42A	XPNPEP2	YWHAB	ZFP36L1	ZNF24	ZNF84
UBE2A	UBQLN2	USP3	VDAC3	WDR45	XPO1	YWHAE	ZFP57	ZNF277	ZNF85
UBE2D3	UBQLN4	USP34	VGLL4	WDR73	XPO5	YWHAH	ZFP91	ZNF282	ZRANB2
UBE2D4	UCHL1	USP36	VIM	WDR74	XPO6	YWHAZ	ZFPL1	ZNF3	ZSCAN29

6.3 Variants checked for segregation with PD

Family	Sex	*Gene*	Mutation	Reason selected	PD	SNP
10	M	*ACTG2*	F263L	Cytoskeleton	Y	N
26	M	*APEX1*	C310Y	Neurodegeneration panel, PDBase SN expression, PD link (DNA repair)	Y	N
28	M	*APEX1*	C310Y		Y	N
6	M	*ARHGEF7*	S771*	PD link (LRRK2 GEF)	Y	N
2	M	*ASAH1*	M226T	PDBase SN expression, PD link (lysosomal storage disorder)	N	N
2	F	*ASAH1*	M226T		N	Y
2	F	*ASAH1*	M226T		Y	N
2	M	*ASAH1*	M226T		Y	Y
2	F	*ASAH1*	M226T		Y	Y
2	M	*ASAH1*	M226T		Y	Y
27	M	*ATP13A2*	K792M	Linkage analysis (Chr 1), PD link (autosomal recessive)	Y	N
4	F	*ATP13A5*	E3K	Linkage analysis (Chr 3), Multiple families, PD link (ATP13A2)	N	N
4	M	*ATP13A5*	E3K		Y	N
4	M	*ATP13A5*	E3K		Y	Y
10	M	*ATP13A5*	G571V		Y	N
1	M	*ATP13A5*	I232T		Y	Y
2	F	*ATP5E*	P18M	Diabetes/Psoriasis/PD (mitochondrial ATP processing)	N	N
2	M	*ATP5E*	P18M		N	N
2	M	*ATP5E*	P18M		N	N
2	M	*ATP5E*	P18M		N	Y
2	M	*ATP5E*	P18M		Y	N
2	F	*ATP5E*	P18M		Y	Y
2	F	*ATP5E*	P18M		Y	Y
2	M	*ATP5E*	P18M		Y	Y
9	M	*ATXN10*	E40*	PDBase SN expression, Neurodegeneration panel, PD link (ataxin genes)	Y	N
10	F	*C10orf112*	R291T	Multiple families	N	N
10	F	*C10orf112*	R291T		N	N
10	F	*C10orf112*	R291T		Y	N
10	M	*C10orf112*	R291T		Y	Y
9	M	*C10orf112*	S858I		Y	N
28	M	*C10orf112*	T1104P		N	N
28	F	*C10orf112*	T1104P		N	N

28	M	*C10orf112*	T1104P		Y	N
28	M	*C10orf112*	T1104P		Y	Y
7	F	*C10orf112*	W836C		Y	N
2	M	*C6*	D336G	Diabetes/Psoriasis/PD – (complement activation increased in PD. Melanin in Psoriasis and diabetes)	Y	N
3	F	*CADPS2*	S326L	PDBase SN expression, PD link (interacts BDNF, vesicle exocytosis)	N	N
3	M	*CADPS2*	S326L		Y	Y
26	M	*CDCP2*	S137F	Linkage analysis (Chr 1), PD link (GWAS)	Y	N
2	M	*CLASP1*	M748T	PDBase SN expression, Neurodegeneration panel, Cytoskeleton	N	N
2	M	*CLASP1*	M748T		N	N
2	M	*CLASP1*	M748T		N	N
2	F	*CLASP1*	M748T		N	Y
2	F	*CLASP1*	M748T		Y	N
2	M	*CLASP1*	M748T		Y	Y
2	F	*CLASP1*	M748T		Y	Y
2	M	*CLASP1*	M748T		Y	Y
4	F	*CLDN20*	A80V	PDBase SN expression, Neurodegeneration panel	N	N
4	M	*CLDN20*	A80V		Y	N
4	M	*CLDN20*	A80V		Y	Y
2	M	*DCTN1*	R361Q	PD link (Perry Syndrome)	Y	Y
2	F	*DCTN1*	R361Q		N	N
2	M	*DCTN1*	R361Q		N	N
2	M	*DCTN1*	R361Q		N	N
2	M	*DCTN1*	R361Q		N	Y
2	F	*DCTN1*	R361Q		Y	N
2	F	*DCTN1*	R361Q		Y	N
2	M	*DCTN1*	R361Q		Y	Y
8	M	*DNAJC14*	Q246K	Dopamine regulation	Y	N
9	M	*DNMT3A*	E865*	Multiple families, PD link (epigenetic modifications alter PD susceptibility?)	Y	N
28	M	*DNMT3A*	G381R		Y	N
4	M	*DNMT3A*	SS		Y	N
5	F	*DNMT3A*	SS		Y	N
9	M	*DNMT3A*	SS		Y	N
9	M	*DYNC1H1*	D1933Y	Multiple families, Cytoskeleton, Neurodegeneration panel,	Y	N
27	M	*DYNC1H1*	E1274*		Y	N
8	M	*DYNC1H1*	E3795*		Y	N
27	M	*DYNC1H1*	K1649E		Y	N
7	F	*DYNC1H1*	N3431K		Y	N
27	M	*EFCAB6*	L1125V	Multiple families, PD link (DJ1 interactor)	Y	N
10	M	*EFCAB6*	M1287R		Y	N
26	M	*EFCAB6*	T940I		N	N
26	M	*EFCAB6*	T940I		N	N
26	M	*EFCAB6*	T940I		N	Y
26	M	*EFCAB6*	T940I		Y	N
26	M	*EFCAB6*	T940I		Y	N
26	M	*EFCAB6*	T940I		Y	Y
26	M	*EFCAB6*	T940I		Y	Y
3	M	*EIF4G3*	N26Y	Multiple families, Linkage analysis (Chr 1), PD link (EIF4G1)	Y	N
5	F	*EIF4G3*	N26Y		Y	N
6	M	*EIF4G3*	N26Y		Y	N
7	F	*EIF4G3*	N26Y		Y	N
28	M	*EIF4G3*	Q1366H		Y	N
1	F	*EPB41L3*	R498Q	PDBase SN expression, Cytoskeleton,	Y	N
2	M	*EPB41L5*	D458V		N	N
2	M	*EPB41L5*	D458V		N	N
2	M	*EPB41L5*	D458V		N	Y
2	F	*EPB41L5*	D458V		N	Y
2	M	*EPB41L5*	D458V		Y	N
2	F	*EPB41L5*	D458V		Y	N
2	F	*EPB41L5*	D458V		Y	N
2	M	*EPB41L5*	D458V		Y	Y
9	F	*ERCC4*	P379S	PDBase SN expression, PD link (DNA repair) (SNP = common)	N	N
9	M	*ERCC4*	P379S		Y	Y

2	M	*ERCC6*	L789V	PDBase SN expression, PD link (DNA repair)	N	N
2	M	*ERCC6*	L789V		N	N
2	F	*ERCC6*	L789V		N	Y
2	M	*ERCC6*	L789V		N	Y
2	M	*ERCC6*	L789V		Y	Y
2	F	*ERCC6*	L789V		Y	Y
2	F	*ERCC6*	L789V		Y	Y
2	M	*ERCC6*	L789V		Y	Y
1	F	*ESR2*	S444N	PDBase SN expression, PD link (Estrogen)	Y	N
1	F	*ESR2*	S444N		Y	N
1	F	*ESR2*	S444N		Y	Y
1	M	*ESR2*	S444N		Y	Y
6	M	*ESRRG*	T144K	Linkage analysis (Chr 1), PD link (Parkin degrades ESRRG to limit MAOA and MAOB expression)	Y	N
2	M	*ETFA*	I276L	PDBase SN expression, PD link (mitochondrial function)	N	N
2	F	*ETFA*	I276L		N	N
2	M	*ETFA*	I276L		N	N
2	M	*ETFA*	I276L		N	Y
2	M	*ETFA*	I276L		Y	N
2	F	*ETFA*	I276L		Y	Y
2	F	*ETFA*	I276L		Y	Y
2	M	*ETFA*	I276L		Y	Y
5	F	*ETNK2*	E303D	Linkage analysis (Chr 1), PDBase SN expression, PD link (ETNK1 interacts with dopamine receptors)	N	N
5	F	*ETNK2*	E303D		N	N
5	M	*ETNK2*	E303D		N	N
5	M	*ETNK2*	E303D		N	N
5	F	*ETNK2*	E303D		Y	Y
5	F	*ETNK2*	E303D		Y	Y
7	F	*FAM104B*	G65S	Multiple families	Y	N
28	M	*FAM104B*	G65S		Y	N
4	M	*FAM104B*	S51N		Y	N
6	M	*FAM104B*	S51N		Y	N
27	M	*FBX07*	F308S	PD link (recessive, early onset *PARK* gene)	Y	N
5	M	*FUCA1*	L134F	Linkage analysis (Chr 1), PDBase SN expression, Neurodegeneration panel, PD link (lysosomal storage disease-fucosidosis)	N	N
5	M	*FUCA1*	L134F		N	N
5	F	*FUCA1*	L134F		N	Y
5	F	*FUCA1*	L134F		N	Y
5	F	*FUCA1*	L134F		Y	Y
5	F	*FUCA1*	L134F		Y	Y
4	M	*FZD4*	R127C	PDBase SN expression, PD link (Wnt signalling)	Y	Y
4	M	*FZD4*	R127C		Y	Y
9	M	*GDNF*	G105V	PD link (neurotrophic factor, dopamine neurons)	Y	N
5	F	*GIGYF2*	N9K	PD link (late-onset PARK gene)	Y	N
5	F	*GPR37*	F536L	PD link (Parkin associated)	Y	N
3	M	*GRN*	R579P	Linkage analysis (Chr 17), Neurodegeneration panel, PD link (suspected PD gene)	Y	N
5	F	*GRN*	T184N		Y	N
28	M	*GRN*	T532A		N	N
28	F	*GRN*	T532A		N	N
28	M	*GRN*	T532A		Y	N
28	M	*GRN*	T532A		Y	Y
27	M	*HPCA*	F72C	Linkage analysis (Chr 1) , Neurodegeneration panel,	Y	N
2	F	*IDH1*	Y183C	PDBase SN expression, PD link (mitochondrial function)	N	N
2	M	*IDH1*	Y183C		N	N
2	M	*IDH1*	Y183C		N	Y
2	M	*IDH1*	Y183C		N	Y
2	F	*IDH1*	Y183C		Y	N
2	F	*IDH1*	Y183C		Y	N
2	M	*IDH1*	Y183C		Y	Y
2	M	*IDH1*	Y183C		Y	Y
8	M	*IGSF10*	A990D	Linkage analysis (Chr 3) Multiple families	Y	?
9	M	*IGSF10*	G1956W		Y	N
27	M	*IGSF10*	T1238A		Y	N

2	M	*IL16*	R889*	Diabetes/psoriasis/PD (Inflammation)	Y	N
8	M	*INSR*	E1206D	Diabetes/psoriasis/PD (Inflammation)	Y	N
27	M	*INSR*	S748T		Y	N
7	F	*IREB2*	P167H	PDBase SN expression, Neurodegeneration panel, PD link (iron accumulation)	Y	N
2	M	*IRF3*	K360N	Diabetes/Psoriasis/PD (CDC4)	Y	N
3	M	*LEPREL1*	P295L	Linkage analysis (Chr 3) Diabetes/Psoriasis/PD (CDC4)	Y	N
6	M	*LEPREL1*	P295L		Y	N
7	F	*LEPREL1*	P295L		Y	N
9	M	*LEPREL1*	P295L		Y	N
9	M	*LINGO2*	S402T	PD link (pubmed 20369371)	Y	N
10	M	*LRP6*	S963I	PDBase SN expression, PD link (Wnt signalling)	Y	N
8	M	*LRRK2*	D2438Y	PD link (Late-onset PD gene)	Y	N
8	M	*LRRK2*	L2062I		Y	N
4	F	*LRRK2*	M1646I		N	Y
4	M	*LRRK2*	M1646I		Y	N
4	M	*LRRK2*	M1646I		Y	Y
9	M	*LRRK2*	M2521I		Y	N
26	M	*LRRK2*	Y1277D		Y	N
8	M	*MAOA*	T512N	Dopamine processing, Neurodegeneration panel	Y	N
4	M	*MAOB*	P234T	Dopamine processing, Neurodegeneration panel	Y	N
28	M	*MAOB*	T241R		Y	N
1	F	*MAP1A*	A1752V	MAP	N	N
1	F	*MAP1A*	A1752V		N	N
1	F	*MAP1A*	A1752V		N	N
1	F	*MAP1A*	A1752V		Y	N
1	F	*MAP1A*	A1752V		Y	Y
1	M	*MAP1A*	A1752V		Y	Y
9	F	*MAP2*	E55K	MAP	N	Y
9	M	*MAP2*	E55K		Y	Yes* but homozygous
10	F	*MAP2*	E55K		N	N
10	F	*MAP2*	E55K		N	Y
10	F	*MAP2*	E55K		Y	Y
10	M	*MAP2*	E55K		Y	Y
2	F	*MGST2*	R109*	Diabetes/psoriasis/PD	N	N
2	M	*MGST2*	R109*		N	Y
2	M	*MGST2*	R109*		N	Y
2	M	*MGST2*	R109*		N	Y
2	M	*MGST2*	R109*		Y	N
2	F	*MGST2*	R109*		Y	Y
2	F	*MGST2*	R109*		Y	Y
2	M	*MGST2*	R109*		Y	Y
2	M	*MYH1*	R1321S	Linkage analysis (Chr 17), Diabetes/psoriasis/PD	N	N
2	F	*MYH1*	R1321S		N	N
2	M	*MYH1*	R1321S		N	N
2	M	*MYH1*	R1321S		N	N
2	M	*MYH1*	R1321S		Y	N
2	F	*MYH1*	R1321S		Y	N
2	F	*MYH1*	R1321S		Y	Y
2	M	*MYH1*	R1321S		Y	Y
2	F	*NDST1*	T210M	Diabetes/psoriasis/PD	N	N
2	M	*NDST1*	T210M		N	N
2	M	*NDST1*	T210M		N	Y
2	M	*NDST1*	T210M		Y	N
2	F	*NDST1*	T210M		Y	N
2	F	*NDST1*	T210M		Y	N
2	M	*NDST1*	T210M		Y	Y
6	M	*NEFH*	D368E	Neurodegeneration panel	Y	N
5	F	*NEGR1*	G199W	Linkage analysis (Chr 1), PD link (neuronal growth factor)	Y	N
26	M	*NEGR1*	K349Q		Y	N
10	F	*NINJ2*	T161I	PDBase SN expression, PD link (neuronal regeneration and	N	N
10	F	*NINJ2*	T161I		N	N

10	F	*NINJ2*	T161I	outgrowth)	Y	N
10	M	*NINJ2*	T161I		Y	Y
6	M	*NPC1*	F760L	Neurodegeneration panel	Y	N
8	M	*PANK2*	P173T	Neurodegeneration panel , PD link (iron accumulation)	Y	?
3	M	*PDE1B*	A349D	Neurodegeneration panel	Y	N
9	M	*PLXND1*	D1816Y	Linkage analysis (Chr 3), Multiple families, PD link (SNARE and SNCA)	Y	?
27	M	*PLXND1*	Q1563L		Y	?
26	M	*PLXND1*	V1835A		Y	?
3	M	*QSER1*	A176S	Multiple families	Y	N
28	M	*QSER1*	N501T		N	N
28	F	*QSER1*	N501T		N	N
28	M	*QSER1*	N501T		Y	N
28	M	*QSER1*	N501T		Y	Y
7	F	*QSER1*	S395*		Y	N
6	F	*QSER1*	V221I		N	N
6	F	*QSER1*	V221I		N	N
6	F	*QSER1*	V221I		N	N
6	F	*QSER1*	V221I		Y	N
6	M	*QSER1*	V221I		Y	Y
1	F	*RDX*	E170K	PDBase SN expression, PD link (ERM protein-LRRK2)	Y	N
1	M	*RDX*	E170K		Y	N
1	F	*RDX*	E170K		Y	N
1	F	*RDX*	E170K		Y	Y
8	M	*RNF19A*	D265Y	PD link (Ubiquitin)	Y	N
1	F	*SELENBP1*	G435E	Linkage analysis (Chr 1), PDBase SN expression,	Y	N
1	F	*SELENBP1*	G435E		Y	Y
1	F	*SELENBP1*	G435E		Y	Y?
1	M	*SELENBP1*	G435E		Y	Y?
2	M	*SEZ6L*	G1015R	Diabetes/Psoriasis/PD (decreased in PD SN, linked ER function)	N	N
2	F	*SEZ6L*	G1015R		N	Y
2	M	*SEZ6L*	G1015R		N	Y
2	M	*SEZ6L*	G1015R		N	Y
2	M	*SEZ6L*	G1015R		Y	Y
2	F	*SEZ6L*	G1015R		Y	Y
2	F	*SEZ6L*	G1015R		Y	Y
2	M	*SEZ6L*	G1015R		Y	Y
9	M	*SEZ6L*	G842V		Y	N
3	F	*SEZ6L*	I916M		N	N
3	M	*SEZ6L*	I916M		Y	Y
2	M	*SH2B1*	R475P	Diabetes/Psoriasis/PD (KO mice glucose intolerance. Role in apoptosis, neuronal differentiation and survival)	N	?
2	M	*SH2B1*	R475P		N	?
2	F	*SH2B1*	R475P		N	N
2	M	*SH2B1*	R475P		N	N
2	M	*SH2B1*	R475P		Y	N
2	F	*SH2B1*	R475P		Y	N
2	F	*SH2B1*	R475P		Y	N
2	M	*SH2B1*	R475P		Y	Y
28	M	*SLC6A3*	K19M	Dopamine processing	Y	N
1	F	*SNCAIP*	M373T	PD link (interacts SNCA)	Y	Y
1	M	*SNCAIP*	M373T		Y	N
1	M	*SNCAIP*	M373T		Y	N
1	M	*SNCAIP*	M373T		N	N
1	F	*SNCAIP*	M373T		Y	N
1	F	*SNCAIP*	M373T		Y	N
9	M	*SNCG*	E35A	Neurodegeneration panel	Y	N
8	M	*SQLE*	G286W	Dopamine processing	Y	N
9	F	*STK4*	T353A	PD link (phosphorylates FOXO transcription factors)	N	N
9	M	*STK4*	T353A		Y	Y
10	M	*STON2*	S540I	PDBase SN expression, PD link (ERM protein-LRRK2)	Y	N
2	F	*TACR3*	N443S	Diabetes/Psoriasis/PD (tachykinin receptor, eg substance P. Tachykinins neuroprotective. Substance P reduced in PD)	N	N
2	M	*TACR3*	N443S		N	N
2	M	*TACR3*	N443S		N	Y
2	M	*TACR3*	N443S		N	Y
2	M	*TACR3*	N443S		Y	N
2	F	*TACR3*	N443S		Y	Y

2	F	*TACR3*	N443S		Y	Y
2	M	*TACR3*	N443S		Y	Y
5	F	*TM7SF2*	P282L	PDBase SN expression, PD link (ERM protein-LRRK2)	N	N
5	M	*TM7SF2*	P282L		N	N
5	F	*TM7SF2*	P282L		Y	N
5	F	*TM7SF2*	P282L		Y	Y
6	M	*TUBB3*	E431K	Cytoskeleton	Y	N
10	M	*TUBB4A*	R359H	Cytoskeleton	Y	N
8	M	*TUBG1*	L398M	Linkage analysis (Chr 17), Cytoskeleton	Y	N
2	M	*TYR*	E4+5	Dopamine processing, PDBase SN expression	Y	Y
2	M	*TYR*	R402Q		Y	Y
5	F	*UBA7*	H304L	Linkage analysis (Chr 3), PD link (ubiquitin)	Y	Y
26	M	*UBA7*	L95S		N	N
26	M	*UBA7*	L95S		N	N
26	M	*UBA7*	L95S		N	N
26	M	*UBA7*	L95S		Y	N
26	M	*UBA7*	L95S		Y	N
26	M	*UBA7*	L95S		Y	N
10	F	*VAPB*	M170I	PDBase SN expression, Neurodegeneration panel	N	N
10	F	*VAPB*	M170I		N	N
10	F	*VAPB*	M170I		Y	N
10	M	*VAPB*	M170I		Y	Y
10	M	*VAPB*	M170I		Y	Y
2	M	*VPS13B*	N2993S	PD link (vaculolar sorting)	Y	Y
2	M	*VPS13B*	V3805L		Y	Y

The chain-termination sequencing results of potentially pathogenic SNPs. Following initial confirmation of the SNP identified by NGS, segregation analyses were performed on family members. Also indicated is the reason the SNP was considered. F/M = sex of individual, Chr = chromosome, KO = knock-out, ER = endoplasmic reticulum. Y/N = yes / no.